Investigating the effect of endurance exercise on mitochondrial function in the ageing heart

Ghazaleh Alimohammadiha

This thesis is submitted for the degree of

Doctor of Philosophy

Wellcome Trust Centre for mitochondrial Research

Institute of Neuroscience

Newcastle University

September 2019

Author's declaration

This thesis is submitted for the degree of Doctor of Philosophy at Newcastle University. The research was conducted by myself at Wellcome Trust centre for mitochondrial research under supervision of Dr Laura Greaves, Dr Djordje Jakovljevic and Dr Fiona Oakley from October 2015 to September 2019.

I certify that none of the material covered in this thesis has previously been submitted/published at any other University/journal by anyone else.

Abstract

Mitochondria are organelles present in most cells of the body responsible for the production of cellular energy in the form of adenosine triphosphate (ATP), through oxidative phosphorylation (OXPHOS). Mitochondrial function is particularly important in the heart due to its high requirement for ATP, and a decline in mitochondrial function with age is implicated in the pathogenesis of age-related cardiovascular disease. Exercise interventions can induce mitochondrial biogenesis and increase OXPHOS capacity; however, it is unknown whether such interventions are successful if started in later life. I wanted to investigate the effect of an endurance exercise intervention in 2 mouse models; 1) a model of accelerated ageing due to enhanced mitochondrial DNA mutagenesis (*PolgA$^{mut/mut}$* mice); 2) C57Bl6/J mouse model of physiological age at 14 months of age.

Study 1: Following baseline characterisation of *PolgA$^{mut/mut}$* mice compared with age-matched controls, male *PolgA$^{mut/mut}$* mice underwent a 6-month endurance exercise programme from 16 weeks of age to investigate the effects of exercise on physiological phenotype, behavioural activity, and cardiac mitochondrial function. I found no improvement in clinical score, locomotor activity, cardiac hypertrophy and fibrosis and mitochondrial function in the exercised mice. This suggests that six months of endurance exercise is unable to improve the clinical phenotype and cardiac mitochondrial function in *PolgA$^{mut/mut}$* mice due to the severity of the genetic defect.

Study 2: To investigate whether starting an exercise programme in later life is beneficial, I first characterised the effect of age on cardiac function in sedentary mice. Between 14 and 22 months of age, I found a significant decline in neuromuscular coordination, decreased cardiac function (measured by cardiac MRI), and diminished aerobic capacity. Six months of endurance exercise improved physiological function and neuromuscular coordination, decreased cardiac fibrosis and apoptosis and improved mitochondrial OXPHOS activity. This suggests that starting an exercise programme later in life can still have beneficial effects.

Acknowledgements

Table of contents

List of figures

List of tables

Abbreviations

AC	Adenylyl cyclase
ADP	Adenosine diphosphate
ATP	Adenosine triphosphate
AVN	Atrioventricular node
Acetyl Co-A	Acetyl Co-enzyme A
AMPK	Adenosine monophosphate-activated protein kinase
AP	Action potential
AVS	Atrioventricular septum
AVN	Atrioventricular node
ASC	Apoptosis-related speck-like protein caspase
BER	Base excision repair
BMD	Bone mineral density
B-AR	B-adrenergic receptor
BSA	Bovine Serum Albumin
BW	Body weight
C3	Pyruvate
C6	Glucose
Ca^{2+}	Calcium ion
cAMP	Cyclic adenosine monophosphate
CC3	Cleaved caspase-3
CHD	Coronary heart disease
CI	Complex I
CM	Cristae membrane

cMRI	Cardiac Magnetic Resonance Imaging
CO	Cardiac output
CoA	Co-enzyme A
CoQ10	Co-enzyme Q10
CICR	Ca^{2+} induced Ca^{2+} release
COX	Cytochrome c oxidase
CX/SDH	Cytochrome c oxidase/succinate dehydrogenase
CRP	C-reactive protein
CMT	Charcot-Marie-Tooth disease
CNS	Central nervous system
CT	Cycle threshold
Cyt C	Cytochrome C
CuZnSOD	Copper-zinc-superoxide dismutase
CVD	Cardiovascular disease
CVS	Cardiovascular system
DAB	3,3'-diaminobenzidine
DBP	Diastolic blood pressure
DISC	Death inducing signal complex
D-loop	Displacement-loop
DNA	Deoxyribonucleic acid
Drp1	Dynamin related protein 1
DHPs	Dihydropyridines
dRP	Deoxyribose phosphate residue
ECG	Electrocardiogram
ED	End-diastole
EDV	End-diastolic volume

ESV	End-systolic volume
EF	Ejection fraction
EF-Tu	Mitochondrial elongation factor
EPCs	Endothelial progenitor cells
ERR	Oestrogen related receptor
ES	End-systole
ETC	Electron transport chain
EtOH	Ethanol
FAD	Flavin adenine dinucleotide
FADH	Reduced flavin adenine dinucleotide
Fe-S	Ion/Sulphur
gDNA	Genomic DNA
GH	Group-housed
GP_x	Glutathione
GSH	Glutathione peroxidase
GTP	Guanosine triphosphate
GTPases	Guanosine triphosphate hydrolase enzyme
H&E	Haematoxylin and Eosin
HCl	Hydrochloric acid
HMG	High mobility group
HR	Heart rate
HRP	*horseradish peroxidase*
HSP	Origin of heavy strand
IBM	Inner boundary membrane
Ig	Immunoglobulin
IGF-1	Insulin like growth factor-1

IL-6	Interleukin-6
IMM	Inner mitochondrial membrane
IMS	Intermembrane space
IFM	Interfibrillar mitochondria
Int +	Intermediate positive
Int -	Intermediate negative
KSS	Kearns-Sayre Syndrome
ISC	Ion-sulphur cluster
LDL	Low density lipoprotein
LSP	Origin of light strand
LVM	Left ventricular mass
L-VDCC	L-type voltage dependent Ca^{2+} channel
LP-BER	Long-patch base excision repair
MABP	Mean arterial blood pressure
MAP	Mitogen activated protein
mCAT	Mitochondrial targeted catalase
miRNA	Micro-RNA
Mfn1	Mitofusin 1
Mfn2	Mitofusin 2
MFTA	Mitochondrial free radical theory of ageing
MMEJ	Microhomology-mediated end joining
MMR	Mismatch repair
mPTP	Mitochondrial pore transition membrane
MRC	Mitochondrial respiratory chain
MELAS	Mitochondrial encephalopathy with lactic acidosis and stroke-like episodes

mRNA	Messenger ribonucleic acid
mtDNA	Mitochondrial DNA
MTERF-1	Mitochondrial Transcription Termination Factor 1
Mt-IF-2	Mitochondrial initiation factor-2
Mt-IF-3	Mitochondrial initiation factor-3
mtSSB	Mitochondrial DNA single-stranded binding protein
MTCOI	Cytochrome c oxidase subunit 1
NaCl	Sodium Chloride
NAD	Nicotinamide adenine dinucleotide
NADH	Reduced nicotinamide adenine dinucleotide
Neg	Negative
NBT	Nitroblue tetrazolium
NCR	Non coding region
nDNA	Nuclear DNA
NDUFB8	Ubiquinone Oxidoreductase Subunit B8
NCX	Na^+/Ca^{2+} exchanger
NF-B	Nuclear-factor B
NGS	Normal goat serum
NIBP	Non-invasive blood pressure
NHEJ	Non-homologous end joining
NIS	Nikon imaging software
NPC	No primary control
NRF-1	Nuclear receptor factor-1

NMRS	Nuclear magnetic resonance spectroscopy
NTC	No template control
NO	Nitric oxide
OSCP	Oligomycin sensitivity conferring protein
OD	Optical density
OFT	Open field testing
OMM	Outer mitochondrial membrane
OPA1	Optic atrophy 1
OXPHOS	Oxidative phosphorylation
O_H	Origin of heavy strand
O_L	Origin of light strand
PBS	Phosphate buffered saline
PDC	Pyruvate dehydrogenase complex
PCR	Polymerase chain reaction
PCr	Phosphocreatine
Pos	Positive
PFA	Paraformaldehyde
PGC1-α	Peroxisome proliferator-activated receptor gamma *coactivator 1-alpha*
P_i	Inorganic phosphate
PI3	phosphatidylinositol 3-kinase
PKA	Protein kinase A
PMS	Phenazine methosulfate
POLG/Polγ	Polymerase gamma
PolgA $^{mut/mut}$ mouse	Homozygous polymerase gamma mutator mouse

POLRMT	mitochondrial RNA polymerase
PPARα	Peroxisome proliferator-activated receptor alpha
Q	Ubiquinone
RER	Respiratory exchange ratio
RNA	Ribonucleic acid
ROS	Reactive Oxygen Species
rRNA	Ribosomal ribonucleic acid
RT-PCR	Real time-PCR
RGB	Red Green Blue
RV	Right ventricle
SAN	Sinoatrial node
SBP	Systolic blood pressure
SDH	Succinate dehydrogenase
SERCA2a	Sarcoplasmic/endoplasmic reticulum calcium ATPase 2a
SH	Singly-housed
SkQ1	10-(6′-plastoquinonyl) decyltriphenyl phosphonium cation
SOD	Superoxide dismutase
SR	Sarcoplasmic reticulum
SV	Stroke volume
SS	Single stranded
SSM	Subsarcolemmal mitochondria
TBS	Tris-buffered saline
TEFM	Transcription elongation factor for mitochondrial genome

TNF-α	*Tumor necrosis factor-α*
TCA	Tricarboxylic acid cycle
TFAM	Mitochondrial transcription factor A
Tfam $^{-/-}$	Homozygous knockout of TFAM gene
TNFR1	*Tumor necrosis factor receptor 1*
TFBM1	Mitochondrial transcription factor B1
TFBM2	Mitochondrial transcription factor B2
TIM	Translocase of the inner membrane
TIMP-1	metallopeptidase inhibitor *1*
TOM	Translocase of the outer membrane
TWINKLE	mtDNA helicase enzyme
tRNA	Transfer ribonucleic acid
UPR ^{mt}	Mitochondrial unfolded protein response
VAP-1	Vascular adhesion pritein-1
VCO_2	Maximum carbon dioxide production
VDAC	Voltage-gated anion channel
VLDL	Very low density lipoprotein
VO_2	Maximum oxygen generation

Chapter 1

Chapter 1. Introduction

1.1 Mitochondria

Mitochondria are rod-shaped intracellular organelles thought to be descended from a symbiotic relationship with α-proteobacterium (Margulis and Bermudes, 1985). Mitochondria exist in most eukaryotic cells and are known as the 'power generators' of cells (Detmer and Chan, 2007). The number of mitochondria varies widely by organism, tissue and cell type depending on the energy demand of the system. The mitochondrial size and shape also varies between cell types depending on their stage of development (Welchen *et al,* 2014). Like many other organelles, the morphology of mitochondria is crucial for its integrity and physiology, and is controlled by fission and fusion processes (Scott and Youle, 2010). Mitochondria are involved in a range of complex cellular interactions such as; cytoplasmic calcium homeostasis (Giorgi *et al*, 2012), cell growth and development (Arciuch *et al*, 2012), programmed cell death (Bras, Queenan and Susin, 2005), generation of reactive oxygen species (ROS) (Murphy, 2009), regulation of innate immunity (West, Shadel and Ghosh, 2011), stem cell regulation (Xu *et al*, 2013), the urea cycle, and ATP production through oxidative phosphorylation (OXPHOS) (Bergman and Ben-Shachar, 2016). Mitochondria have an outer and inner membrane, enclosing the matrix which houses the Krebs cycle and is the main site of fatty acid oxidation. The inner membrane contains the respiratory chain enzymes that reduce molecular oxygen to water by utilising electrons passed on from a series of electron carriers. The redox-driven respiratory chain enzymes pump protons from the matrix to the inner mitochondrial membrane to establish an electrochemical gradient of protons to synthesise ATP from ADP and P_i (Chaban, Boekema and Dudkina, 2012). Mitochondria are the only organelles apart from the nuclei that contain their own genome, which is much smaller (~16.5Kb) than the nuclear genome. Mitochondria are inherited maternally and encode for 13 proteins of the electron transport chain (Sato and Sato, 2013).

1.1.1 *Mitochondrial structure*

Mitochondria have two phospholipid bilayer membranes separated by the intermembrane space (IMS), which encloses the mitochondrial matrix. The outer

mitochondrial membrane (OMM) encloses the organelle and allows for the transport of molecules smaller than 500Da into the IMS through integral membrane proteins (Flis and Daum, 2013). The OMM faces the cytosol and the IMM extends into the matrix which contains mitochondrial DNA (mtDNA). The IMS is the compartment enclosed by the IMM and the OMM (Bornhovd *et al*, 2006). The voltage-dependent anion channel (VDAC) is an outer membrane protein that facilitates the transport of nucleotides, ions and other metabolites from the cytosol to the IMS (Yeagle, 2016).

The inner mitochondrial membrane (IMM) is less permeable and encloses the matrix with a series of invaginations on its surface called cristae (Kuhlbrandt, 2015). The IMM was originally believed to be a continuous membrane enclosing the cristae inside the matrix. However, it's now accepted that the IMM is comprised of two compartments, the inner boundary membrane (IBM) and cristae membrane (CM) (Frey and Manella, 2000). The IMM contains four complexes of the electron transport chain and ATP synthase as well as proteins necessary for fission and fusion processes, metabolite transport proteins, redox carrying proteins and protein import machinery (Alberts *et al*, 1994). The IMM is also home to a high proportion of cardiolipins that make the IMM almost impermeable (Paradies *et al*, 2014). Unlike the outer membrane, the IMM does not contain porins and so molecules and ions are transported into the matrix via the translocase of the inner membrane (TIM) complex (Herrmann and Neupert, 2000). There is also a membrane potential formed across the IMM by the enzymes of the OXPHOS system. Invaginations of the IMM known as cristae expand the surface area of the IMM for greater ATP production. Cells with higher energy demand require a higher density of cristae to facilitate the movement of ions down the electrochemical gradient. A schematic diagram showing the structural organisation of a mitochondrion is shown in figure 1.1.
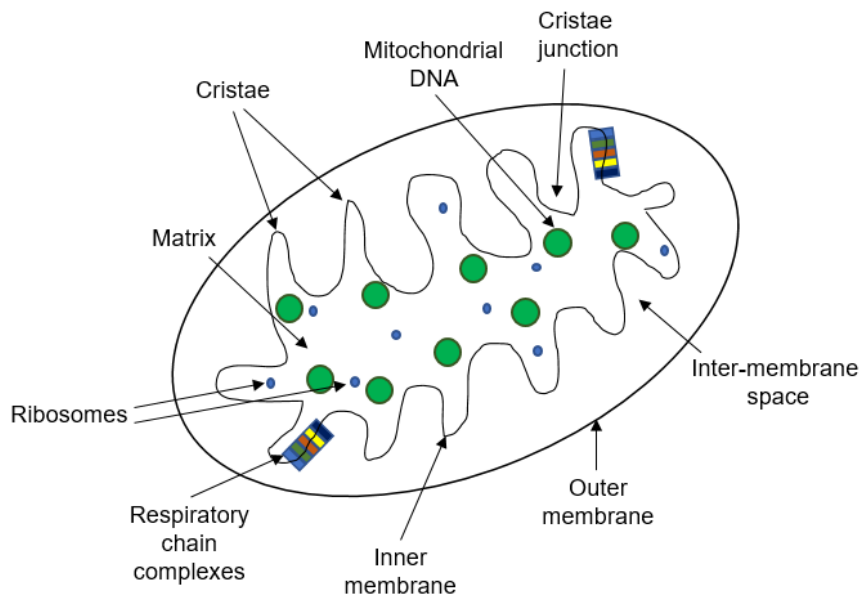
Figure 1.1. Representation of mitochondrion structure. Key features include mitochondrial outer and inner membrane, cristae, mitochondrial DNA and matrix.

1.1.2 *Mitochondrial function*

1.1.2.1 *Mitochondrial OXPHOS system and ATP synthesis*

ATP synthesis through OXPHOS relies on the structural integrity of the mitochondrion. Cellular respiration also known as aerobic respiration (in the presence of oxygen) is the process by which the preferred biochemical energy source, glucose, is converted into ATP. Glucose (C6) is broken down through the process of glycolysis and is converted into pyruvate (C3) generating two molecules of ATP in the process (Figure 1.2). Two molecules of pyruvate per glucose molecule are then transferred to the mitochondria and feed into the Krebs cycle or citric acid cycle where they are oxidised to Acetyl-Coenzyme A (Acetyl Co-A) and CO_2 by the pyruvate dehydrogenase complex (PDC) inside the mitochondrial matrix. NAD^+ is reduced to NADH throughout the citric acid cycle and is used as an energy source in the electron transport chain to generate ATP. In fact, six NADH molecules, two $FADH_2$ molecules and two ATP molecules as well as two molecules of H_2O and CO_2 as waste products are produced per molecule of glucose (equivalent to two molecules of pyruvate and two molecules of Acetyl-CoA) (Alberts *et al,* 2002). Glycolysis takes

3

place inside the cytoplasm and the citric acid cycle occurs in mitochondria as shown in figure 1.2.
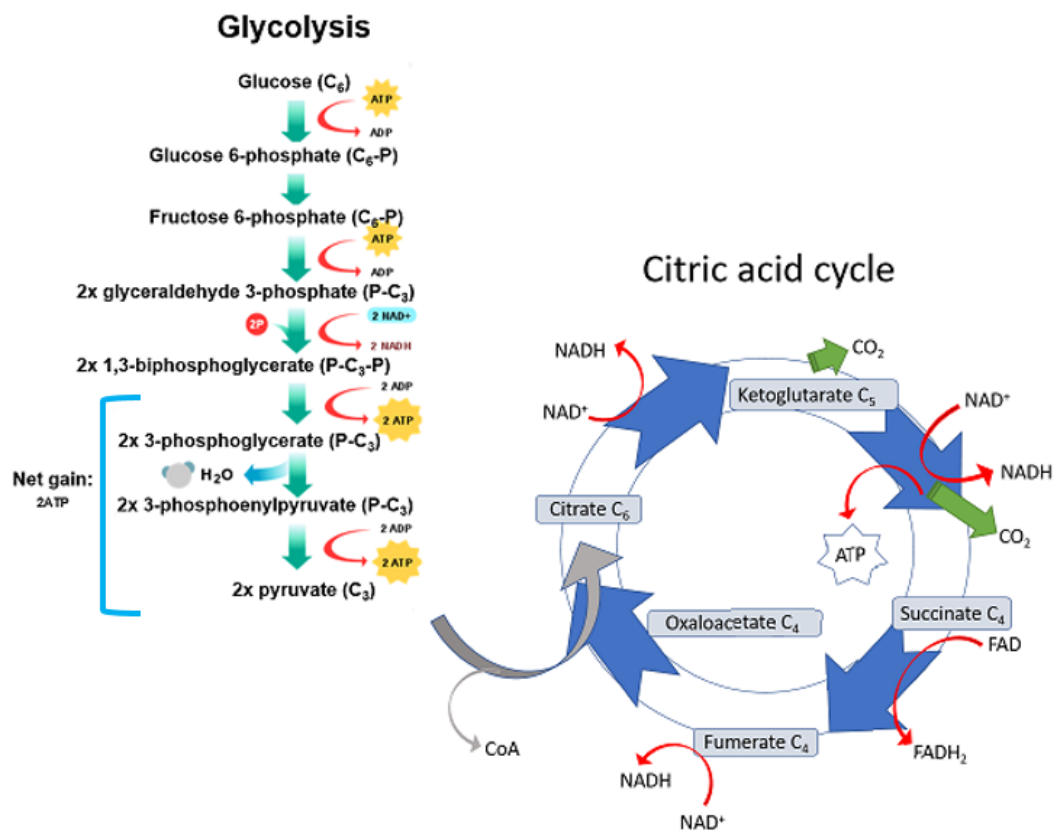
Figure 1.2. Glycolysis and citric acid cycle are linked by their end products.
Glycolysis generates two ATP and two pyruvate molecules which are then fed into the citric acid cycle where pyruvate is converted to Acetyl-CoA and other metabolises to produce NADH and FADH substrates for the electron transport chain.

NADH and $FADH_2$ (reduced forms of electron carriers) from the citric acid cycle and fatty acid β-oxidation are fed into the electron transport chain (ETC) and their electrons are transferred to ETC complexes. The ETC comprises a set of four multi-protein complexes (complexes I-IV) while the OXPHOS machinery comprises of complexes I-V. The complex series of redox reactions create an electrochemical proton gradient across the IMM that drives ATP synthesis as shown in figure 1.3. NADH is able to donate its electrons to complex I in a redox reaction to form NAD^+ and release ATP in order to pump protons (H^+) along the electrochemical gradient from the matrix to the IMS (Hatefi, 1985). $FADH_2$ however isn't as efficient at transferring electrons so bypasses complex I and donates electrons to complex II

4

instead. Electrons are passed from complex I and complex II to an electron carrier called ubiquinone (Q) which carries electrons to complex III, pumping more protons across the membrane (figure 1.3). Electrons are then passed to another electron carrier known as cytochrome *c* (Cyt C) to transfer electrons to complex IV where four electrons then reduce molecular oxygen to form two molecules of H_2O. The flow of electrons enables ATP synthase to catalyse the phosphorylation of ADP to form ATP with P_i by harnessing the flow of protons. One ATP molecule is produced in return for three H^+ that pass through the ATP synthase (Alberts *et al*, 2002). Hundreds of ATP molecules are produced by ATP synthase in one second and these are exported via the adenine nucleotide translocase (ANT) to the rest of the cell (Bonora *et al*, 2012).
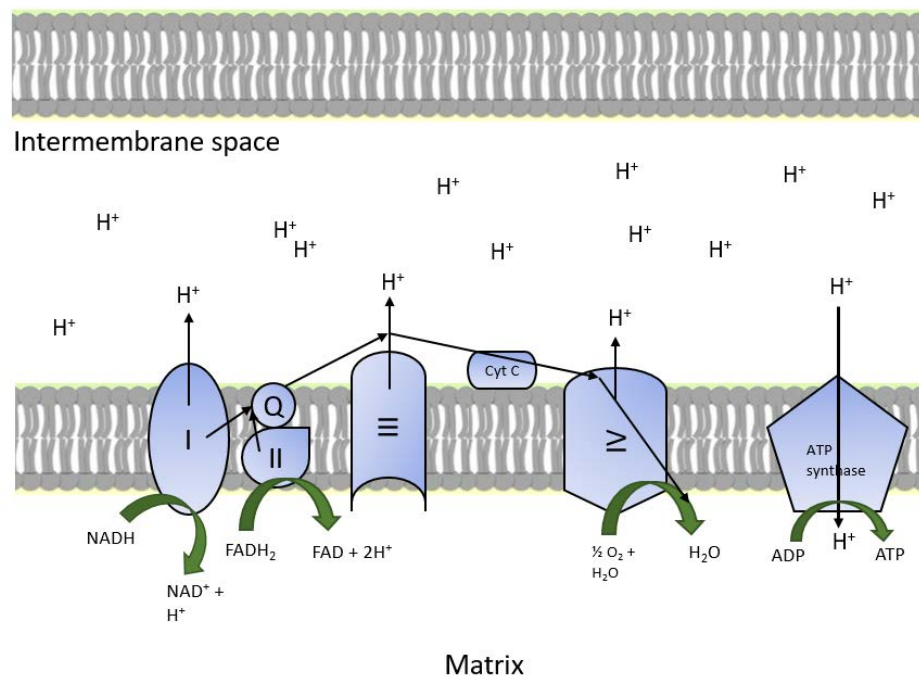
Figure 1.3. Oxidative phosphorylation. Electrons move from complex I to complex IV to create energy for the transfer of protons from the matrix to the intermembrane space (IMS). The electrochemical gradient created is the energy that is stored for ATP synthesis. The protons flow back to the matrix through the ATP synthase which drives the phosphorylation of ADP to generate ATP.

1.1.2.2 *OXPHOS complexes*

OXPHOS complexes are encoded by both the mitochondrial genome and the nuclear genome. The nuclear encoded subunits are translated and processed in the cytosol

before being transported into the mitochondria (Zimmerman, Von Saint-Andre, McLaughlin, 2011).

Respiratory chain complex I also known as NADH dehydrogenase is the largest protein complex of the respiratory chain consisting of 45 subunits, seven of which are encoded by the mtDNA. Complex I catalyses the transfer of electrons from NADH to a ubiquitous coenzyme known as Coenzyme Q10 (CoQ10). This reaction translocates four protons across the IMM per molecule of oxidised NADH. Due to the inefficiency of electron transport across the IMM and the premature leakage of electrons to oxygen, superoxide can form, making complex I the main site of reactive oxygen species (ROS) production (Sharma, Lu and Bai, 2009).

Respiratory chain complex II otherwise known as succinate dehydrogenase (SDH) consists of four protein subunits, two hydrophilic and two hydrophobic all encoded by the nuclear genome and transported into mitochondria. Complex II contributes fewer electrons to the chain in comparison to complex I and hence less ATP is generated through this pathway (Ganesh, Wong and Gorman, 2012).

Respiratory chain complex III, or ubiquinol-cytochrome c reductase, is encoded by both the mitochondrial DNA and the nuclear genome. Of the 11 subunits (Xia *et al*, 1997; Iwata *et al,* 1998), three are respiratory subunits (Rieske protein, cytochrome b and cytochrome C1), two are core protein subunits and six are low molecular weight protein subunits (Benit, Lebon and Rustin, 2009). Only one subunit is encoded by the mtDNA known as cytochrome *b*, the rest are encoded by the nuclear DNA. Complex III catalyses the transfer of electrons to cytochrome *b* and cytochrome *c*. Overall two electrons pass through complex III, four protons are passed across the IMS to facilitate the transfer of electrons to another electron carrier known as cytochrome *c* which carries electrons to complex IV.

Mitochondrial Complex IV, or cytochrome *c* oxidase, (COX) is encoded by three mitochondrial genes (subunits I, II and III) and ten nuclear genes (subunits IV, Va, Vb, Via-Vic, VIIa-VIIc and VIII). Subunits encoded by the mtDNA form the catalytic core of the enzyme and nuclear-encoded subunits are involved in stability and assembly of the complex. Complex IV receives electrons from cytochrome *c* and transfers them to molecular oxygen to form two H_2O molecules. Four protons are transferred to IMS during the process (Chaban, Boekema and Dudkina, 2012).

Mitochondrial Complex V or ATP synthase is the final complex, which couples ATP synthesis to the electrochemical gradient generated by the proton gradient across the mitochondrial membrane. The result is the formation of ATP by Adenosine diphosphate (ADP) and free phosphates. Complex V consists of 14 nuclear encoded and two mtDNA encoded subunits. It has two functional domains situated on the IMM known as F_o and F_1 which are responsible for hydrolysing ATP and catalysing the reaction between ADP and phosphate respectively (De Meirleir *et al*, 2004). The human mitochondrial ATPase F_1 domain is a soluble region in the mitochondrial matrix, which comprises of three copies of subunits α and β and a copy of subunits γ, δ and ε. The second ATPase domain F_o comprises of a subunit ring (Watt *et al*, 2010) and one copies of subunits a, b, d, F_6 and the oligomycin sensitivity conferring protein (OSCP). Two subunits of F_o domain ('a' and 'A6L') are encoded by mtDNA *ATP6* and *ATP8* genes respectively (Anderson *et al*, 1981).

1.1.2.3   *Mitochondrial calcium homeostasis*

Calcium (Ca^{2+}) is an important modulator of signal transduction in mitochondria and its homeostasis is crucial for the normal functioning of mitochondria. There are several routes by which Ca^{2+} can either enter or exit the mitochondria including Ca^{2+} uniporter, Ca^{2+} rapid uptake mode, Ca^{2+}/Na^+ exchanger, and permeability transition pore (mPTP) all located on the IMM as well as VDAC on the OMM. Ca^{2+} homeostasis is significantly more important in high-energy demanding tissues such as cardiac and skeletal muscle as a slight change in its cytosolic concentration could result in significant changes in the rate of muscle contraction. Ca^{2+} has also a key regulatory role in neuronal development and function as well as cell death (Giorgi *et al,* 2012).

1.1.2.4   *Mitochondrial reactive oxygen species (ROS) generation*

Mitochondria are a major source of ROS generation primarily as a by-product of OXPHOS at complexes I and III (Turrens and Boveris, 1980). Balaban, Nemoto and Finkel (2005) have shown that excessive ROS production contributes to oxidative damage to macromolecular complexes including mtDNA and proteins. These toxic by-products of aerobic metabolism include the superoxide anions ($O_2^{\bullet-}$), hydrogen

peroxide (H_2O_2) and hydroxyl radicals (OH^-). H_2O_2 is generated through dismutation of $O_2^{\bullet-}$ and catalysed by superoxide dismutase (SOD) within mitochondria (Fukai and Ushio-Fukai, 2011). The most aggressive form of oxidative stress is through hydroxyl radicals due to their short half-life. OH^- is generated through H_2O_2 and $O_2^{\bullet-}$ and is catalysed through the Haber-Weiss reaction by Fe^{2+}. Figure 1.4 illustrates the production and removal of $O_2^{\bullet-}$ through an enzymatic pathway.
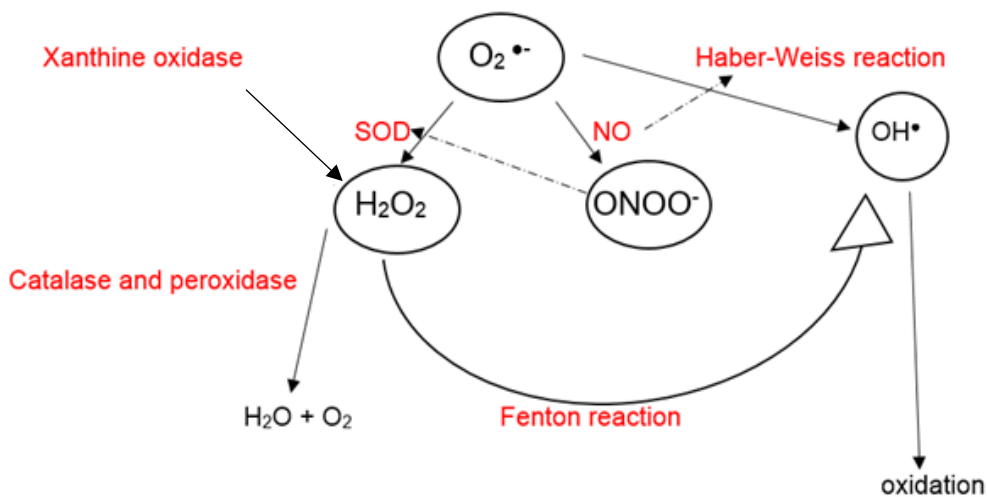
Figure 1.4. ROS generation and removal. $O_2^{-\bullet}$ dismutation is catalysed by superoxide dismutase (SOD) to H_2O_2 or through nitric oxide (NO) to form peroxynitrite ($ONOO^-$) or through Haber-Weiss reaction to form hydroxyl radicals ($OH^\bullet$). H_2O_2 is formed directly from xanthine oxidase and reduced further to H_2O and O_2 by catalase and peroxidase. Dashed lines represent inhibition states where $ONOO^-$ inhibits SOD and NO inhibits $OH^\bullet$.

Maintaining a basal level of ROS is also essential as they act as signalling molecules to activate biological pathways and regulate physiological functions (Mittler, 2017). Manivannan, Soundararajan and Jeong (2017) documented that ROS are vital components in regulating cellular proliferation and differentiation by modulating the redox status of cell components and regulating the transcription of genes associated with cellular proliferation. Similarly, Yarosz and Chang (2018) reported that ROS derived from OXPHOS, regulate T cell-mediated immunity through the AMPK pathway. The AMPK pathway is activated after stimulation of T-cell receptor leading

to activation of cellular transcription factors crucial for promoting T-cell growth (Zhu *et al*, 1999).

In order to regulate cellular redox homeostasis and prevent damage to macromolecules, a network of antioxidants are employed by cells to scavenge excessive ROS. The antioxidant defense system comprises of enzymes such as superoxide dismutase (SOD), catalase, glutathione (GSH) and glutathione peroxidase (GP_X) (Poljsak, Suput and Milisav, 2013). This complex defense mechanism against exessive ROS should be balanced to allow cell signalling and redox regulation. The balance however is slightly in favour of the ROS, allowing continuous low-level ROS formation and damage to human body with age (Cheeseman and Slater, 1993). The failure of antioxidant repair mechanisms contributes to the accumulation of cell damage, for example lysosomal accummulation of lipofuscin (Terman and Brunk, 2006), ageing and age-realted diseases (Gems and Doonan, 2009). Non-proliferative cells such as cardiac myocytes are more affected by age-related oxidative damage since there is no opportunity to dilute the damaged structures via cell division (Terman and Brunk, 2006). As oxidative cellular damage increases with age, an exogenous intake of antioxidants from the diet such as vitamins C and E as well as carotenoids and polyphenols are recommended to support the body's antioxidant defense system (Willett, 2006).

1.1.2.5 *Iron/Sulphur cluster formation*

Mitochondria are also important regulators of iron homeostasis. Fe/S clusters are ubiquitous protein cofactors and contribute to the electron transport chain, redox catalysis, regulation of gene expression and protein translation, mtDNA repair and replication as well as tRNA modification (Johnson *et al*, 2005). Mitochondria contain the iron-sulphur-cluster (ISC) assembly machinery. Over 15 components are required to synthesise Fe/S proteins to be used inside and outside of mitochondria. Fe/S cluster formation and haem biogenesis is carried out in the mitochondrial matrix (Wang and Pantopoulos, 2011). Only 12 Fe/S clusters are involved in the electron transport chain and Fe changes its ionic state between redox reactions (Schultz and Chan, 2001). The ability of the Fe/S protein to adopt to a range of positions suggest

that domain movement is a crucial part of the enzyme reaction mechanism to promote the unidirectional flow of electrons.

1.1.2.6 *Cellular apoptosis*

Programmed cell death or apoptosis is a process of controlled cell death and is important during normal development and for the removal of damaged cells. Factors triggering apoptosis include DNA damage, viral infections, stress and ROS released from mitochondria. During cellular apoptosis, cells shrink in size, the cytoskeleton collapses, and nuclear DNA fragments following nuclear envelope disassembly (Alberts *et al*, 2002). The alteration of the cell surface during apoptosis gives signals to phagocytes and macrophages to initiate the engulfing processes. Apoptosis is mediated by proteolytic enzymes known as caspases that trigger cell death by cleaving proteins in the cytoplasm and nucleus. Cellular apoptosis may be induced by intrinsic (mitochondrial) and extrinsic pathways. In the extrinsic pathway, two direct mechanisms of cell death in mammals are suggested to be involved; TNF-induced and *Fas-Fas* ligand mediated models (Wajant, 2002). In the TNF-induced model, the binding of TNF-α to TNFR-1 activates the caspase pathway whereas in the *Fas-Fas* mediated model, Fas-ligand binds to the Fas (first apoptotic signal) receptor; resulting in formation of the death inducing-signal complex (DISC). This complex contains caspase-8 and caspase-10 which trigger the execution of cellular apoptosis (Gu *et al,* 2011).

Mitochondria play a critical role in initiating apoptosis by making its outer membrane more permeable to proteins especially the Bcl_2 family of proteins, which regulate the permeability of the mitochondrial outer membrane (Wang and Youle, 2009). The two subtypes of this family of proteins, pro-apoptotic and anti-apoptotic, work together to balance the rate of cell death. Under normal healthy circumstances, the balance is in favour of anti-apoptotic proteins to inhibit mitochondria from initiating apoptosis. Once the pro-apoptotic proteins such as cytochrome *c* are released into the cytoplasm by increased permeability of the OMM, a cascade of caspases enzymes are activated. Caspases (family of cysteine-aspartic acid proteases) such as cleaved caspase-3 break down proteins and degrade the large polymers inside the cells, prepare them for phagocytosis and recycle proteins for their own use (Lauber *et al*, 2003).

Caspase-3 is involved in the final execution-phase of cellular apoptosis; hence, its intracellular localisation is commonly used as an immunohistochemical marker of cell death through apoptosis. Fragmentation of DNA is documented during cellular apoptosis as DNase inhibitors are removed by the activity of caspases leading to nuclear DNA fragmentation (Janicke *et al,* 1998).

1.1.3 *Mitochondrial dynamics*

Mitochondria are dynamic organelles and continuously undergo cycles of fission (division) and fusion (connection) to maintain their shape, size, distribution and to meet the energy demands of the cell type in which they reside (Archer, 2013). The structural flexibility of mitochondria allows them to form branches and filaments under various physiological and pathological conditions. Mitochondrial fusion is an integration of two mitochondria to form one mitochondrion. The fusion proteins include two GTPase mitofusins (Mfn1 and Mfn2) that reside on the OMM and OPA1 that exists on IMM (Chen and Chan, 2009). The size and number of mitochondria varies depending on the mitochondrial regulatory fission and fusion proteins. These proteins balance mitochondrial number and morphology depending on the cell type and its function (Jornyvaz and Shulman, 2010). Mitochondrial quality control systems keep mitochondria functional by enabling a stable balance between fission and fusion proteins. Depending on the energetics state of cells, proteins are recruited on the mitochondrial membrane for mitophagy or repair in order to maintain the integrity of mitochondria (Picca *et al*, 2018). OPA1 overexpression leads to mitochondrial elongation and its loss results in mitochondrial fragmentation (Sesaki *et al*, 2003). Mitochondrial fission is defined as the division of a mitochondrion into two daughter mitochondria which allows the damaged mitochondria to be removed by mitophagy (van der Bliek, Shen and Kawajiri, 2013). Fission proteins include a dynamin-related proteins called Drp1 which are recruited to the mitochondrial and peroxisomal membranes. The loss of this cytosolic protein leads to drastic elongation of mitochondria and peroxisome (Koch, 2004). The balance between fission and fusion is an integral component of functional mitochondria. Dysregulation of fission and fusion processes results in a large number of round fragmented mitochondria or an elongated, highly connected, hyper-fused mitochondrial network (Suguira *et al,* 2014). Mfns overexpression results in aggregation of mitochondria around the nuclei

(Eura *et al*, 2003) whereas Mfn-1 knockout results in fragmented mitochondria and Mfn-2 knockout results in enlarged spherical mitochondria (Chen *et al*, 2003).

Baloh *et al* (2007) have reported that a mutant form of Mfn2 induces abnormal clusters of fragmented mitochondria in neuronal cell bodies and axons, causing an impairment of mitochondrial transport in neuronal axons and eventually leading to Charcot-Marie-Tooth disease (CMT) where peripheral sensory and motor axons are degenerated. Similarly, knocking out the *mfn2* gene from mouse dopaminergic neurons result in marked mitochondrial fragmentation in neuronal cell body, reduction of mitochondrial mass and transport in neurons that led to reduced activity and rearing in mice resembling CMT type 2A disease in mice (Pham *et al,* 2012).

Similarly, in a mouse model where mitochondrial fission protein Drp1 was knocked out in embryonic cardiomyocytes, mice displayed neonatal lethargy due to dilated heart, thinned heart wall and premature death (Ishihara *et al*, 2009). The brain specific knockout of Drp1 resulted in a cerebellar developmental defect, with few enlarged mitochondria within Purkinje cells instead of numerous tubular mitochondria. Knockout of Drp1 caused death within 24 hours of birth suggesting that Drp1 is essential for embryonic development of organs with high endogenous levels of Drp1 present in the heart and brain (Wakabayashi *et al*, 2009).

1.1.4 *The mitochondrial Genome*

Mitochondria are the only organelles except the nucleus that contain their own DNA that is located within the mitochondrial matrix. MtDNA is a double stranded ~16.5 kb circular molecule (figure 1.5) and each strand has different base compositions (Chial and Craig, 2008). It consists of the heavy strand, which is a guanine rich strand, a light strand which is rich in cytosine, and a noncoding region of approx. 1100 bp known as the D-loop. MtDNA encodes 37 genes; 13 of which are subunits of the OXPHOS complexes I, III, IV and V. 22 transfer RNAs (tRNAs) and two ribosomal RNAs (rRNA) (12s and 16s) are also encoded by mtDNA and are responsible for the correct translation of the OXPHOS subunit mRNAs within the mitochondria. The other 1000-1500 proteins necessary for the correct functioning of mitochondria are encoded by the nuclear DNA and are imported into mitochondria (Calvo, Calauser and Mootha, 2015). MtDNA is a multi-copy genome packaged into nucleoids, and is

strictly maternally inherited. It has a close proximity to the site of energy production and oxidative stress. MtDNA does not contain any introns and the non-coding regions (D-loop and associated promoters) are highly involved in mtDNA replication and transcription (Shadel and Clayton, 1997). The human mitochondrial genome carries a 5-10 times higher mutation load than the nuclear genome (Siguroardottir *et al,* 2000).

The mouse mtDNA is greatly homologous to human mtDNA in location, sequence and organisation of genes. The conserved regions of mouse mtDNA in descending order is tRNA regions, origins of replication of heavy and light strands (O_H and O_L respectively), rRNA genes protein encoding regions and finally the displacement D-loop (Bibb *et al,* 1981). The mouse mtDNA is also smaller in size (16.295 kb) in comparison to human mtDNA, mainly due to its smaller D-loop region with 879 base pairs (Bibb *et al,* 1981). The mouse and human mitochondrial genome are economically organised by having their tRNA genes between rRNA and protein coding regions. The lack of introns in genes, absence of intergenic sequences excluding one regulatory region and small sizes of rRNA and tRNA molecules makes mtDNA economical in organisation.
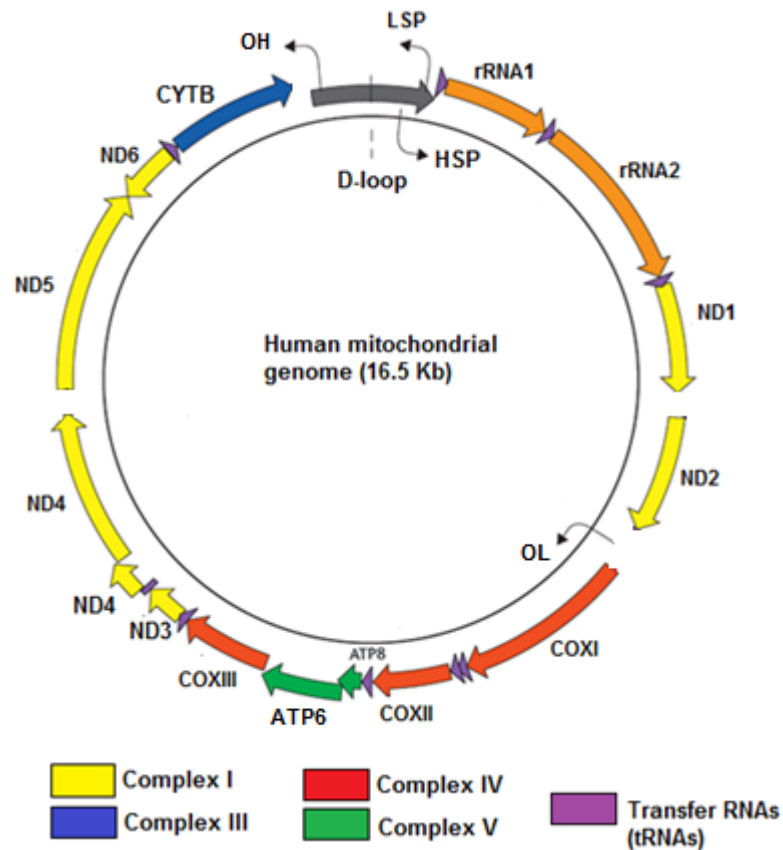
Figure 1.5. The human mitochondrial genome. The human mtDNA encodes for 15 proteins of respiratory chain. Origin of heavy (O_H) strand and origin of light (O_L) strand are involved in mtDNA replication process. The genes encoding for subunits of each complex are colour coded according to the complex group they belong to.

1.1.5 *Mitochondrial DNA transcription and translation*

The mitochondrial genome is very compact in size and is present in numerous copies per cell. The transcription of human mtDNA is polycistronic and occurs on both strands to produce genome-long transcripts of mRNA and rRNA (Ojala, Montoya and Attardi, 1981). For successful mtDNA transcription, a number of proteins come together to initiate, elongate and terminate transcription of mtDNA. Initiation of mitochondrial transcription begins at two main transcription initiation sites within the D-loop; the origin of heavy strand promoter (HSP) and the origin of light strand promoter (LSP) which are 150 base pairs away from one another and are completely functionally independent. A 15 bp consensus sequence envelops the initiation sites assisting the transcription of mtDNA (Chang and Clayton, 1984). The initiation of

transcription of H-strand commences at nucleotide 561 inside the HSP and the initiation of L-strand transcription commences at position 407 within the LSP. H-strand transcription is initiated from two promoter regions; HSP1 and HSP2 which are approximately 100bp apart from one another in the non-coding region (NCR) (Montoya *et al,* 1982). Transcription of the L-strand is initiated from a single site that creates a long transcript encoding the ND6 gene and eight tRNAs. Transcription initiating at HSP1 results in a short transcript containing tRNA^{Phe}, tRNA^{Val}, 12S and 16S rRNAs whereas transcription from HSP2 produces a near genome-length polycistronic RNA strand. (Dalla Rosa *et al,* 2017).

Proteins essential for mtDNA transcription include the non-selective DNA-dependent mitochondrial RNA polymerase known as POLRMT (Fisher and Clayton, 1988) Milenkovic *et al*, 2013) which possesses a high sequence homology at the C-terminus catalytic domain and two pentatricopeptide repeat (PPR) domains required for site-specific protein interactions (Ringel *et al,* 2011). Initiation of transcription also requires association of POLRMT with mitochondrial transcription factor A (TFAM), mitochondrial hexameric TWINKLE helicase, mitochondrial transcription factor B1 (TFB1M) and transcription factor B2 (TFB2M). TFB2M is responsible for DNA melting during the initiation event and is thought to be at least twice as active in promoting transcription with POLRMT *in vitro* than TFB1M (Falkenberg *et al,* 2002).

TFAM is a DNA-binding protein of 25kDa in size and is crucial for initiation of transcription and packaging of mtDNA in nucleoids (Kanki *et al,* 2004). It is made up of two high mobility group (HMG) domains separated by a 27 amino acid residue linker led by a 25 amino acid residue C-terminal tail (Taanman, 1999). The C-terminal tail is crucial for DNA recognition and high level specificity of transcription initiation (Dairaghi, Shadel and Clayton, 1995). At the upstream of HSP and LSP, TFAM forms a protein-DNA complex in order to recruit the modified version of POLRMT to the promoter via its N-terminal (Posse and Gustafsson, 2016). This also allows the mtDNA to form an arrangement that permits selective binding of the POLRMT.

Mitochondrial elongation then occurs and is mediated by mitochondrial transcription elongation factor (TEFM) and POLRMT (Minczuk *et al,* 2011). Transcription termination occurs through mitochondrial transcription termination factor 1 (MTERF1) by bending the mtDNA at the junction between the HSP and tRNA $^{Leu (UUR)}$ terminal region (Jimenes-Menendez *et al*, 2010). MTERF1 then induces termination by base

flipping and DNA unwinding (Martin *et al,* 2005). This was originally believed to explain the 50-fold increase in MTERF1-mediated rRNA synthesis. More recent evidence however suggest that increased rRNA abundance may be a product of increased stability (Terzioglu *et al,* 2013). MTERF1 is also documented to terminate LSP prematurely at 3'-end of the rRNA coding region to prevent the replication fork progressing into mitochondrial rRNA transcription while inhibiting rRNA antisense sequence transcription (Shi *et al,* 2016).

Mammalian mtDNA translation take place on mitochondrial ribosomes (mitoribosomes) with 39S and 28S subunits plus two mitochondrially encoded rRNAs located inside the matrix (Smith, Smeitink and van den Heuvel, 2010). The mitochondrial translation machinery fully relies on nuclear-encoded regulatory proteins such as the initiation factor proteins mtIF2 and mtIF3 (Gaur *et al,* 2008). Initiation codons such as AUG or AUA are placed at the peptidyl site by mtIF3, while mtIF2 guides the assembly of the monosomes and the initiation of translation (Liao and Spremulli, 1990). Similar to mtDNA transcription, translation elongation follows the initiation event. Mitochondrial translation elongation factor EF-Tu forms a complex with Guanosine triphosphate (GTP) to direct the aminoacyl tRNA to base pair with the mRNA causing it to move along each codon (Cai *et al,* 2000). Termination of translation occurs at the A site in the presence of a stop codon (Frolova *et al,* 1999). Richter *et al* (2010) have shown that a -1 base frameshift in mammalian mitoribosomes at the AGA and AGG codons terminate the two open reading frames (ORFs) in *MTCO1* and *MTND6* genes respectively leading to termination of synthesis of 13 polypeptides at standard UAA and UAG stop codons.

1.1.6 *MtDNA replication*

Mitochondrial DNA replication occurs autonomously independently of the cell cycle (Bogenhagen and Clayton, 1997). The proteins involved in mtDNA replication are nuclear encoded and replication is controlled at the D-loop. The replication machinery is called the replisome and is made up of mitochondrial TWINKLE DNA helicase, mitochondrial DNA single-stranded binding protein (mtSSB) (13-16 kDa) (Falkenberg, Larsson and Gustafsson, 2007) and mtDNA polymerase γ (Polγ) which are all encoded by the nuclear DNA and transported into the mitochondria. The RNA-

dependent mtDNA polymerase γ is essential for mtDNA replication, repair and recombination (Kaguni, 2004). Pol γ consists of a catalytic (PolγA) and two homodimeric accessory subunits (PolγB). PolγA has a 3'-5' exonuclease activity and is 140 kDa in size, whereas PolγB is a 55kDa protein necessary for tight mtDNA binding and synthesis (Lim, Longley and Copeland, 1999). PolγA is responsible for proofreading of a newly synthesised mtDNA strand, and PolγB increases the activity, processivity and interaction of PolγA with the DNA template (Hudson and Chinery, 2006). During initiation of DNA replication the double-stranded (ds) mtDNA is unwound to two complementary single-strands (ss) by TWINKLE in an ATP dependent manner in the 5'-3' direction (Korhonen, Gaspari and Falkenberg, 2003). MtSSB is then used to stabilise the ssDNA, enhance the sensitivity of TWINKLE and trigger the activity of Polγ to initiate mtDNA synthesis (Korhonen, Gaspari and Falkenberg, 2003). Other enzymes required for mtDNA replication include ribonuclease H1 which actively removes primers from the O_H and O_L strands as well as mitochondrial topoisomerase to mitigate tension generated during replication of the mtDNA.

MtDNA replication has been proposed to occur via two main mechanisms; the asynchronous (strand-coupled bidirectional replication model or strand displacement model) (Clayton,1982) and the synchronous strand coupled model (Holt, Lorimer and Jacobs, 2000). In the asynchronous strand displacement model mtDNA is replicated asymmetrically. MtDNA replication is initiated from the O_H region in the D-loop and progresses clockwise around the two thirds of the genome until it displaces the origin of light strand replication (O_L). Once the O_L is exposed, lagging light strand synthesis is initiated and proceeds in the opposite direction (Clayton, 1982). A closed circular molecule is then formed as mtDNA daughter molecules ligate and generate a super helical structure known as mtDNA (Clayton, 1982). This method of mtDNA replication is documented to be a relatively slow process.

In 2000, 2D gel electrophoresis analysis revealed that in addition to replication intermediates from the asynchronous mechanism of mtDNA replication, a second class of replication intermediates resistant to single-stranded nuclease degradation were present. These intermediates are consistent with conventional coupled leading and lagging strand DNA synthesis (Holt, Lorimer and Jacobs, 2000). In this model, replication occurs symmetrically and bi-directionally from multiple replication forks across a broad zone encompassing regions of the genome that encode for

cytochrome b subunit of complex III and subunits 5 and 6 of NADH-ubiquinone oxidoreductase (Bowmaker *et al,* 2003).

A more recent mtDNA replication mechanism in vertebrates was proposed by Yasukawa *et al* (2006) known as RNA-incorporation during mtDNA replication (RITOLS). In this model, RNAs are integrated into the lagging strand during the replication process leaving a time lapse between the synthesis of the leading and lagging strand. This model is very similar to the asynchronous replication model. Although the mechanisms determining which mode of replication a cell employs are not yet fully understood, it is thought to be dependent upon the cell type and required rate of mtDNA biogenesis. (Holt Lorimer and Jacobs, 2000; Reyes *et al,* 2004).

1.1.7 *Mammalian mtDNA repair mechanisms*

Mammalian mtDNA is protected from damage such as mutagenic insults to some extent due to the fact that is it packaged into nucleoids containing TFAM (Gouliaeva, Kuznestsova and Gaziev, 2006). Initially mtDNA was considered to not possess DNA repair capacity since alkylation damage (Miyaki, Yatagoi and Ono, 1977) and generation of pyrimidine dimers by UV damage (Clayton *et al,* 1974) were not removed from the mtDNA. MtDNA repair is crucial in preventing the accumulation of damage such as alkylation damage, hydrolytic and oxidative damage, formation of adducts such as photodimers, mismatches such as insertion-deletion loops (IDLs) and DNA strand breaks. More recent experimental evidence has revealed that mtDNA shares many repair mechanisms with nDNA (Blasiak *et al,* 2013). Development of techniques such as sequencing, microscopy and other molecular approaches have greatly advanced our knowledge of mtDNA repair over the last decade.

Mammalian mtDNA repair mechanisms include base excision repair (BER) (Short-patch and long-patch) as well as microhomology-mediated end joining (MMEJ) mechanisms (Zinovkina, 2018). BER pathway corrects the damaged base pairs, removes single base lesions and modifies nucleotides that occur with oxidative damage and alkylation (Bogenhagen and Clayton, 1977). BER occurs by initiation of specific DNA glycosylases and hydrolysis of the glycoside bond at the sugar phosphate backbone of the mtDNA to remove the altered basic site by

Apurinic/apyrimidinic endonuclease enzyme (Tomkinson and Mackey, 1998). Polγ breaks and mtDNA ligase III seals and repairs the mtDNA. (Bogenhagen and Clayton, 1977). There are two classes of mtDNA BER glycosylases enzyme; mono-functional and bi-functional enzymes. Mono-functional enzymes have only glycosylase activity, whereas bi-functional enzymes have both glycosylase and Apurinic/apyrimidinic lyase activity. Long-patch BER (LP-BER) is another category of BER for the removal of oxidised lesions of more than two nucleotides (Liu *et al*, 2008). LP-BER occurs when DNA Polγ initiates polymerisation from 3'-OH adjacent to the deoxyribose phosphate residue (dRP) following Apurinic/apyrimidinic endonuclease activity. (Zheng *et al*, 2008).

Other mtDNA repair mechanisms include correction of lesions on single-stranded mtDNA known as single-strand break repair (SSBR), mismatch repair (MMR) for the removal of unpaired nucleotides and repair of ds-DNA breaks by homologous recombination (HRR) as well as non-homologous end joining (NHEJ) as explained further in (Liu and Demple. 2010; Zinovkina, 2018).

1.1.8 *Heteroplasmy and the threshold effect*

Mitochondrial Heteroplasmy is the term given to a state in which a mix of both wild type mtDNA and mutant mtDNA coexist within an individual cell (Larsson and Calyton, 1995). Similarly, when all the mtDNA inside a cell is identical whether WT or mutant, this is termed homoplasmy. The level of heteroplasmy can vary between cells and is associated with the mosaic pattern of cells with defects in the electron transport chain observed in tissues in patients with mtDNA disease (Dufour *et al*, 2008). The level of heteroplasmy is normally given as the percentage of mtDNA molecules within a cell or tissue that are mutated and indirectly determines the clinical phenotypes of mtDNA disease. A study on isolated skeletal muscle fibres in patients with 8344A>G mutation in the tRNA[Lys] gene revealed that the proportion of mtDNA mutation should exceed a critical threshold before a biochemical defect manifestation, which is typically around 60-80 percent (Boulet, Kapati and Shoubridge, 1992).

MtDNA heteroplasmy levels can also shift over time by relaxed replication and random segregation processes. This is because mtDNA is continuously replicating,

even in non-dividing cells, and if a particular mtDNA variant is replicated more frequently than others, then the proportion of mutated and wild type mtDNA would vary over time. Figure 1.6 demonstrates mtDNA heteroplasmy and the threshold effect.
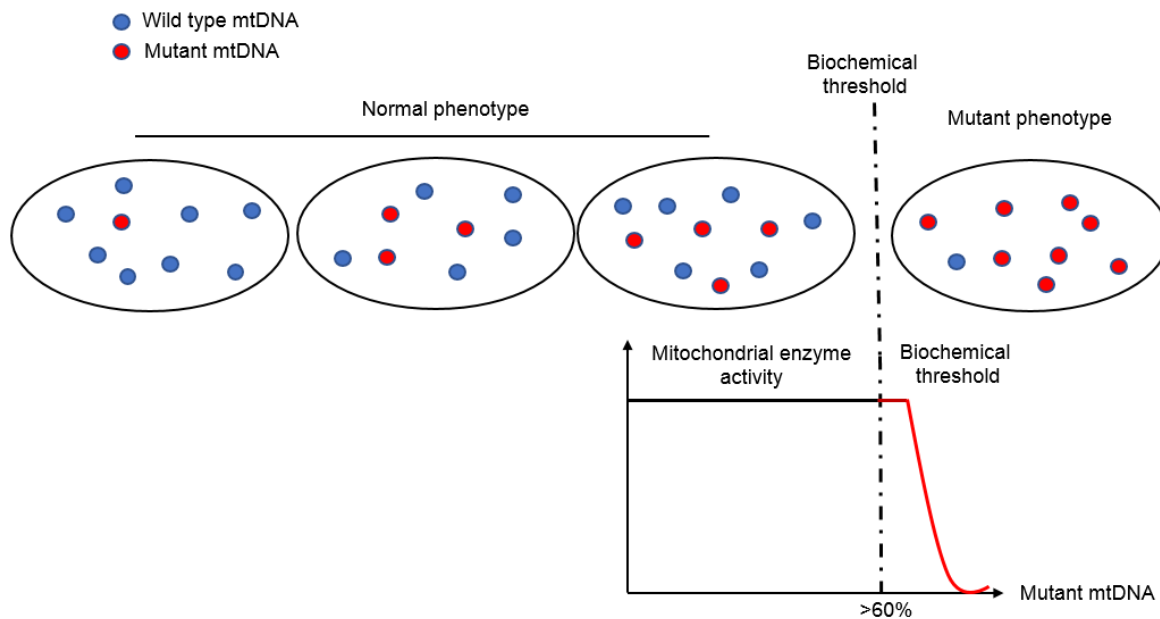
Figure 1.6. MtDNA heteroplasmy and threshold effect. Low levels of mtDNA mutations is tolerated inside a single cell due to the multi-copy nature of the mtDNA. Defect in respiratory chain are detected when the biochemical threshold is exceeded a critical biochemical threshold.

1.1.9 *Mitochondrial DNA inheritance*

The mitochondrial genome is strictly maternally inherited and the transmission of maternal clinical phenotypes to the subsequent generations was also exhibited (Case and Wallace, 1981). During fertilisation, mixing of maternal and paternal mitochondria is averted by several mechanisms including ubiquitination modification (Sutovski *et al*, 2000), proteosomal degradation (Zhou, Li and Xue, 2011) and mitophagy (Al Rawi *et al*, 2011). The underlying mechanism for this uniparental transmission of

mitochondria still remains unclear, however it may partly be due to the higher population of mtDNA oocyte compared to the sperm. Paternal mtDNA however was observed in different species at different stages of embryogenesis, indicating the species-specific mechanism of eliminating sperm mitochondria (Kaneda *et al,* 1995). For example in *C.elegans* spermatozoon selectively prompts the recruitment of autophagosomes to degrade paternal mitochondria during early embryogenesis (Al Rawi *et al*, 2011). This evolutionarily conserved event also prevents the establishment of heteroplasmy by avoiding the paternal mtDNA transmission. Luo *et al* (2013) have reported that sperm mitochondria in mouse persisted unevenly in several cells until the morula stages of embryogenesis but lacked the genetic material, indicating that post-fertilisation elimination of sperm mitochondria in mouse did not occur through autophagy.

The first human paternal transmission of mtDNA was reported in 2002 by Schwartz and Vissing where they have observed an existence of two various mtDNA haplotypes one from the mother and another from the father in the patient. The single male investigated had mitochondrial myopathy and exercise intolerance associated with a 2bp deletion in mitochondrial *ND2* gene. Extensive investigation of the patient and his parents revealed that patient's skeletal muscle tissue had 90% identical mtDNA sequence to the paternal haplotype and only 10% identical to the maternal mtDNA sequence. Studies by Taylor *et al* (2003) and Filosto *et al* (2003) reported a lack of paternal involvement in mtDNA transmission which highlights the rarity of paternal mtDNA inheritance and importance of inherited mtDNA disease diagnosis and counselling. A more comprehensive study was carried out by Luo *et al* (2018) on three unrelated multi-generation families with high levels of mtDNA heteroplasmy. They revealed bi-parental mtDNA inheritance in 17 members of all families. They have proposed that paternal mtDNA transmission was caused by a mutation in nuclear gene associated with paternal mtDNA elimination.

1.1.10 *Mitochondrial DNA bottleneck*

Rapid changes in the level of heteroplasmy were initially detected in pedigree of Holstein cows (1982) where a founder mother with no mtDNA polymorphism produced offsprings with two mitochondrial genotypes causing an mtDNA

polymorphism (Hauswirth and Laipis, 1982). The observations led to the idea that genetic bottlenecking took place during the maternal transmission of mtDNA at oocyte maturation stage. The genetic bottleneck theory suggests that variation in heteroplasmy levels of offspring could be a result of reduction in mtDNA number during oogenesis which in turn forces rapid segregation of mtDNA heteroplasmy leading to high levels of variants (Zhang, Burr and Chinnery, 2018). The mitochondrial bottlenecks were thought to occur during oogenesis and in embryonic primordial germ cells (PGCs) (Jenuth *et al*, 1996).

There is a strong evidence that the genetic bottleneck occurs to allow purifying selection throughout evolution. Muller in 1964 postulated that deleterious mutations accumulate over generations in asexual organism without recombination which ultimately leads to mutational genome meltdown. This process was termed as Muller's ratchet. The mitochondrial genetic bottleneck allows purification selection against rapid advancement of Muller's ratchet (Rand, 2008). Depending on the size of the mtDNA pool, the genetic bottleneck may allow loss or formation of homoplasmic mutation in the process of random and rapid genetic drift. The smaller the selected mtDNA pool, the higher the chances of heteroplasmy would be in a population of mutated and wild type alleles (Zhang, Burr and Chinnery, 2018).

1.1.11 *Clonal expansion*

Clonal expansion is a term used to describe the accumulation of a particular mutated mtDNA species within an individual cell until it reaches the threshold causing a mosaic pattern of respiratory chain defect (Krishnan *et al*, 2007; Larsson, 2010). Clonally expanded mtDNA deletions were initially detected biochemically in human muscle fibres of mitochondrial myopathy patients (Holt, Harding and Morgan-Hughes, 1988).

Müller-Höcker (1990) documented that clonal expansion of mtDNA mutations with increasing age lead to COX deficient muscle fibres. They revealed different patterns of mtDNA *in situ* hybridisation signals in ageing COX-deficient muscle fibres; a normal hybridisation signal, reduced signal as a result of mtDNA depletion and selective hybridisation as a result of a large-scale mtDNA deletion. This was the first documentation of an age-related mosaic pattern of respiratory chain deficiency in

skeletal muscle. Later on it was revealed that clonally expanded mtDNA deletions are also present in muscle fibres of healthy aged humans (Bua *et al*, 2006) and in Parkinson's disease patients (Bender *et al,* 2006). Clonal expansion occurs in post-mitotic tissues however it was also detected in colonic epithelium and crypt stem cells (Baines, Turnbull and Greaves, 2014) highlighting the importance of mtDNA mutations in functional decline during ageing. Sequential cytochrome c oxidase (COX)/ sodium dehydrogenase (SDH) histochemistry is used as a surrogate marker to detect intracellular clonally expanded mtDNA mutations. The mechanism by which a mutated mtDNA species clonally expands to become the dominant species within a cell is unknown. A number of theories to explain this have been proposed.

In 1989, Wallace suggested the first molecular theory to explain the clonal expansion of mtDNA mutations with age; the survival of the smallest hypothesis. This theory suggests that smaller mtDNA molecules replicate faster than larger mtDNA molecules. Large-scale mtDNA deletions would result in smaller molecules that would have a replicative advantage over larger full-length wild-type mtDNA leading to accumulation and the spread of the deleted mtDNA in individual cells. Similarly the larger the deletion, the smaller the remaining genome would be and the greater replicative advantage it will have (Wallace, 1992). In 2014 however, Campbell *et al* demonstrated that mtDNA deletions of various sizes undergo clonal expansion in human skeletal muscle, suggesting that there is no replicative advantage for smaller genomes. In addition, point mutations that do not alter the size of the mtDNA molecule expand to high levels by clonal expansion confirming that clonal expansion isn't driven by genome size (Picard, Vincent and Turnbull, 2016).

A second hypothesis, the survival of the slowest theory (de Grey, 1997), postulates that the slower the rate of mitochondrial turnover, the higher the chances that dysfunctional mitochondria will persist. De Grey suggested that mitochondria with dysfunctional OXPHOS would actually produce fewer ROS, and have lower levels of ROS induced membrane damage. This would result in those mitochondria not being recognised as damaged and therefore degraded, allowing them to preferentially accumulate. However this hypothesis does not take into account the dynamic nature of the reticular mitochondrial network through processes of fission and fusion (Kowald and Kirkwood, 2011). In addition, it has been shown that dysfunctional mitochondria are actually preferentially degraded (Twig *et al*, 2008). Recently multiple studies have reported that a selective advantage is not required for clonal

expansion of mtDNA deletions (Kowald and Kirkwood, 2018). The underlying mechanism of clonal expansion of mtDNA mutations is still largely unknown, although relaxed mtDNA replication can also cause intracellular random genetic drift in post-mitotic tissue leading to clonal expansion of single mtDNA mutation inside a single cell (Elson *et al*, 2001; Coller *et al*, 2002). As an example a stochastic model of mtDNA mutations in stem cells was developed to demonstrate random genetic drift (Stamp *et al*, 2018) and this could explain the pattern of OXPHOS defects present in ageing human colonic crypts.

1.2 Ageing

Ageing is an inevitable slow deterioration of body condition which is characterised by cumulative somatic damage and diminished cellular capacity for repair. The transition through the physiological decline in function with age is associated with dysregulation of gene expression, oxidative damage, increased mutation load, altered metabolite levels and increased susceptibility for developing disease, all of which are suggested to limit human lifespan (Gems and Partridge, 2013). In order to increase the quality of life with age, it's crucial to understand the mechanisms underlying the ageing process. Early studies on ageing suggest that the ageing process is malleable since a single gene was discovered which could extend lifespan in *Caenorhabditis elegans.* Genetic manipulation of the gene *daf-2* in *C.Elegans* result in three mutant strains of which had a doubling of lifespan. These mutants had reduced calorie intake and paralysis suggesting that ageing appeared to be controlled in a polygenic manner (Klass, 1983; Kenyon, 2005). Other altered pathways such as the insulin-like growth factor (IGF-1) pathway and protein translation modulation were identified to increase longevity in model organisms including nematodes, yeast, fruit-flies and mice in an evolutionary conserved manner (Vijg and Campisi, 2008). Hansen *et al (*2007) have shown that reducing the ribosomal protein levels known as the S6 kinase or translation initiation factors increases the lifespan in *C.elegans* by shifting the cell's health state to favour maintenance, longevity and repair.

The experimental evidence to date suggest that ageing is a multi-factorial process which stems from a combination of different mechanisms. Different theories of ageing will be discussed further in this chapter.

1.2.1 *Evolutionary theories of ageing*

Evolutionary theories of ageing and longevity are based on the remarkable differences in lifespan across different biological species which evolved from the interplay between mutation and natural selection. Almost a century after Darwin's theory of biological evolution by natural selection, evolutionary theories of ageing were proposed. August Weismann in 1882 envisioned 'Programmed Death' which suggests that ageing is an advantageous process to replace the older population with younger organisms by programmed death in order to maintain population size (Weismann, 1882). Later Peter Medawar, in 1952, proposed the 'accumulation of somatic mutation' theory of ageing which suggests that accumulation of random unrepaired somatic mutations is detrimental, drives the ageing process and limits one's lifespan by reducing the level of maintenance in function. George Williams hypothesised another theory of ageing in 1957, which suggested that natural selection favours the accumulation of deleterious genes in an older population that once had reproductive benefits early in life. This theory was known as the antagonistic pleiotropy theory of ageing from which the disposable soma theory of ageing was developed by Thomas Kirkwood in 1977. The disposable soma theory of ageing postulates that a gene could have both deleterious and advantageous effects. The initial idea arose from a hypothetical genetic mutation that led to reduced proofreading accuracy in somatic cells but saved and invested energy for reproduction and development instead, which resulted in inevitable ageing process (Gavrilov and Gavrilova, 2002).

Evolutionary theories of ageing are mainly focused on the diminished force of selection and accumulation of mutation as a function of age whereas molecular theories of ageing emphasise the complexity of ageing that is influenced by genetic and environmental factors which is explained further in the subchapter below.

1.2.2 *Modern biological and molecular theories of ageing*

Modern biological theories of ageing fall into two categories which include the programmed and damaged theories of ageing. The programmed theory hypothesises

that gene expression regulates the process of ageing by switching age-associated genes on/off sequentially (Davidovic *et al,* 2010). A sub-group of the programmed theory includes the endocrine theory where hormones act to control the pace of ageing (Heemst, 2010). The observation comes from the single mutation that diminishes the evolutionarily conserved insulin/IGF-1 signalling pathway in *C.elegans* that resulted in their extended lifespan. Another theory was the immunological hypothesis (Fulop *et al,* 2014), where the immune system is programmed to decline with advancing age leading to increase vulnerability to infections, ageing and death. This theory was proposed following the observation that the immune system loses its effectiveness in combating disease as we age (Cornelius, 1972).

Due to extensive unsatisfactory theories of ageing postulated in late 1990s, Kowald and Kirkwood (1996) considered interactions of different hypothesised mechanisms of ageing such as unrepaired damage accumulation in somatic cells, telomeres shortening and mitochondrial dysfunction. In 2005, Kirkwood suggested that ageing occurs as a result of random unrepaired molecular damage to somatic cells that accumulates with age. The efficiency of DNA repair mechanisms and removal of damage also declines with increasing age leading to tissue dysfunction (Mc Auley *et al,* 2017). Telomeres as biological clocks of the cell are neuroprotein structures that protect chromosomal ends against degradation except in cells with infinite proliferative capacity (Olovnikov, 1996). Telomeres progressively shorten with each cell cycle therefore reducing the amount of protection it provides to the genome with age (Campisi, 2000). When telomeres reach a critical length, cells stop replicating and enter a replicative senescence stage (Levy, 1992). Germ cells have telomerases to restore telomere length to the end of chromosomes ensuring cells continue to reproduce and promote their survival cycle. Telomere maintenance through telomerase is absolutely crucial to organs of extensive cell turnover such as stem cells (Flores, Cayuela and Blasco*,* 2005). Mikhelson and Gamley (2013) have suggested that telomere shortening is a sole mechanism of mammalian ageing. They have postulated that if oxidative stress was non-existent then telomeres would still shorten with each mitotic cell cycle due to mtDNA replication and ageing would still occur. DNA damage with age can also arise from post-translational and chemical cross-linking of proteins to intrude the normal functioning of cells (Bjorksten and Tenhu, 1990). Interfering with protein homeostasis and decreased protein biogenesis

within cells (Cuervo and Dice, 2000) may also cause the accumulation of DNA damage in ageing tissues.

1.2.3 *Mitochondrial free radical theory of ageing*

The mitochondrial free radical theory of ageing (MFTA) integrates the contributions of dysfunctional mitochondria, reactive oxygen species and defective proteins and macromolecules in the process of ageing. Denham Harman (1956) suggested that superoxide and hydroxyl radicals and other free radicals generated during cellular respiration in mitochondria can damage macromolecules such as nucleic acids, proteins and lipids inside cells. Since cells posses their own ROS scavenging system to convert harmful superoxides to a less reactive hydrogen peroxide by superoxide dismutase (SOD), the likelihood of damage at lower level is low (Skulachev, 2007). Hydrogen peroxide is usually broken down by catalase, peroxiredoxin or glutathione peroxide to H_2O but can react with ferrous iron to form highly reactive hydrogen radicals which cause damage to cellular components. The body's natural oxidative scavenging system declines with age, which therefore increases the risk of the accumulation of cellular damage. Promoting the body's natural defence system by increasing anti-oxidant levels in rodents has been shown to increase longevity (Schulz *et al,* 2007).

There is conflicting evidence regarding the role of ROS in the ageing process. For example, there is evidence to suggest that an endogenous increase in ROS is positively correlated with lifespan. In a study by Andziak and Buffenstein (2006) naked mole-rats demonstrate exceptional longevity despite extremely high levels of ROS. This led to further research on the role of ROS as cellular signalling mediator in immune and stress response (Labunskyy and Gladyshev, 2013). However, conversely it has been shown that protection against cellular ROS by ROS metabolising enzymes such as mitochondrial catalase (MCAT) results in increased longevity in mice, with delayed cardiac pathology and cataract development and reduced mitochondrial deletion events (Schriner and Linford, 2006). Overexpression of other ROS scavenging enzymes such as CuZnSOD have also been shown to increase longevity in *Drosophila melanogaster* (Sun and Tower, 1999).

During cellular respiration, oxygen can occasionally form superoxide by reacting with reduced components of the electron transport chain (ETC). This normally occurs at complexes I and III of the oxidative phosphorylation (OXPHOS) system (Giorgio *et al*, 2005). Hiona and Leewenburgh (2008) reported that accumulation of mtDNA mutations caused by oxidative damage impairs the function of respiratory chain proteins and triggers further ROS generation and ever-increasing oxidative stress. This leads to a defects in mitochondrial OXPHOS capacity and eventually cell death. This may result in vicious cycle of mitochondrial damage known as the mitochondrial 'vicious cycle' theory of ageing (Miquel *et al,* 1980). Supporting the mitochondrial theory of ageing, somatic mtDNA mutations leading to defects in OXPHOS have been detected in multiple mitotic (colon, stomach, small intestine, liver, oesophagus) and post-mitotic (skeletal muscle, brain, heart) tissues with age (Müller-Höcker, 1990, Cottrell *et al*, 2001, Taylor *et al,* 2003, McDonald *et al*, 2008, Bender *et al*, 2006, Fellous *et al*, 2009, Greaves *et al,* 2012).

In order to test the vicious cycle theory of ageing, Greaves *et al* (2014) examined colorectal epithelium samples from young adult (<25) and aged (>70) humans using a methodology to quantify low level mtDNA mutations (proxy for mtDNA mutation rate) and clonally expanded mtDNA mutations. They showed that non-pathogenic mtDNA mutations exist from embryonic stages and are transmitted through the germline. Pathogenic mtDNA mutations are selected against in the germline, yet occur somatically throughout development and childhood and are detectable at low levels from early adulthood. They did not see any evidence of an increase in the frequency of low-level mtDNA mutations with age, indicating that there was no significant increase in basal mtDNA mutation rate. However, the frequency of cells with clonally expanded mtDNA mutations increased significantly over time. These data provided evidence refuting the vicious cycle hypothesis of ageing (Miquel *et al,* 1980) and instead suggested that clonal expansion by random genetic drift was the driving force underlying the accumulation of mitochondrial dysfunction with age.

Szczepanowska and Trifunovic (2017) suggested that the main source of mtDNA point mutation accumulation with age is the imperfect replication process mainly due to impaired mtDNA polymerase γ (POLG). MtDNA polymerase γ is the main protein involved in mtDNA synthesis. Error rates for proofreading deficient polymerase γ in humans is at 5.6 x10^{-7} (zheng *et al*, 2005). The high accuracy and low error rate of polymerase γ is due to its accurate selection of the correct nucleotide in DNA

synthesis, selective extension of 3'-terminal and accurate excision of false nucleotide pair during a 3'-5' exonuclease activity (Echols and Goodman, 1991; Johnson, 1993).

There are many other studies implicating mitochondrial dysfunction in the ageing processes e.g. a knockout mutation in the p66Shc adaptor protein enhances resistance to apoptotic cell death induced by ROS. P66Shc is a cytoplasmic signal transducer in the transmission of mitogenic signals from activated receptors to ROS (Skulachev, 2000). ROS generated were thought to oxidise phosphatidyl serine in the inner cell membrane and cause phosphorylation of p66shc at a serine residue. Galomov (2010) showed that knockout mice harbouring the mutated form of this protein have a 30% increase in lifespan and resistance to stress apoptotic responses. Another example is a mutation in mitochondrial COX5 gene which encodes for the final subunit V of the cytochrome *c* oxidase complex in a filamentous fungus species known as *Podospora anserine*. The resultant mutation lead to inactivation of the nuclear encoded gene, multiple phenotypic properties such as severe malfunction in germinating mycelium and female sterility as well as a significant decrease in production of ROS enabling an increase in lifespan by ten-fold associated with stabilisation of mitochondrial chromosome (Dufour *et al,* 2000).

1.3 Mouse models of age-related mitochondrial dysfunction

1.3.1 *TFAM knockout mouse*

A mouse model of mitochondrial diabetes was generated by knocking out TFAM in pancreatic beta-cells (Silva *et al,* 2000). TFAM knockout mice developed diabetes from as early as 5 weeks of age, displayed OXPHOS deficiency and mtDNA depletion from 7-9 weeks of age. As a result, the beta-cell population was lower, mitochondrial membrane potential hyperpolarisation threshold was reduced, Ca^{2+} signalling was impaired and insulin secretion was diminished upon stimulation with glucose, highlighting the importance of mitochondria in insulin secretion. Similarly a study by Sorensen *et al* (2001) showed that a neuron-specific TFAM knockout in the mitochondrial late-onset neurodegeneration mouse model (MILON) developed 50% reduction in mtDNA number, progressive neuronal cell loss, apoptosis and gliosis in their neocortex and hippocampus. Wredenberg *et al* (2006) conducted another study revealing the role of respiratory chain dysfunction in skeletal muscle of TFAM

knockout mice. The mice were subjected to glucose tolerance tests but were found to not have diabetes indicating that mitochondrial OXPHOS dysfunction in skeletal muscle is not a primary defect inducing insulin resistance and development of diabetes. In 2007, Ekstrand *et al* have investigated the role of respiratory chain defects on dopaminergic (DA) neurons by creating a DA neuron specific TFAM knockout mouse known as MitoPark mouse. These mice developed a slow progressive motor function impairment, DA neuron cell death and Parkinsonism phenotype in adulthood highlighting the fact that respiratory chain dysfunction may play a critical role in pathophysiology of Parkinson's disease.

1.3.2 *Mitochondrial mutator mouse*

In 2004, Trifunovic *et al* (2004) were the first to develop a mouse model that accumulates high levels of mtDNA mutations in all tissues of the body and shows an accelerated ageing phenotype. This mouse has a knock-in missense mutation causing a substitution of a critical amino acid Aspartate (D257A) to alanine in the proof-reading catalytic core of heterodimeric enzyme (*PolgA*). This amino acid substitution abolishes the 3'-5' POLG exonuclease activity of the protein leading to progressive random somatic mtDNA mutation accumulation by 3-5 fold in a linear fashion with age. This leads to the development of a mosaic pattern of respiratory chain deficiency in tissues of high energy demand such as the heart, skeletal muscle and brain (Trifunovic *et al*, 2004).

From 16 weeks of age the, *PolgA* $^{mut/mut}$ mice developed premature ageing phenotypes such as cardiac hypertrophy, kyphosis, hair loss, anaemia, osteoprosis, reduced fertility and reduced subcutaneous fat as well as reduced lifespan to an average of 48 weeks resembling normal human ageing. Kujoth *et al* (2005) reported that these mice do not develop increased ROS generation and oxidative damage at the tissue level providing evidence against the mitochondrial vicious cycle theory. In contrast with this study, more recent technological advances have shown evidence of elevated hydrogen peroxide levels in the muscle of aged *PolgA$^{mut/mut}$* mice, suggesting that there is a role of oxidative damage in the phenotype of these mice at older age (Kolesar, 2014). Also Niu *et al* (2007) showed that accelerated and progressive degeneration of the auditory system in mutator mice began from as early

as 6 months of age equivalent to wild type mice of 25 months of age. The hearing loss was associated with cell death in the inner ear with the highest density of mitochondrial accumulation. Interestingly, analysis of isolated mitochondria from both spleen and livers of *PolgA* ^{*mut/mut*} mice revealed age-dependent development of abnormal erythroid maturation, macrocytic anaemia and megaloblastic anaemia which resulted in morphological abnormalities in erythroblasts followed by death at 15-16 months of age. Mitochondrial dysfunction therefore plays a significant role in cell-intrinsic haematopoiesis (Chen *et al*, 2009). Ahlqvist *et al* (2012) reported that *PolgA* ^{*mut/mut*} mice had neural and haematopoietic progenitor cell dysfunction from embryogenesis that underlies progeroid phenotype manifestation and respiratory chain dysfunction in non-dividing tissues in older age in these mice.

Another study showed accelerated ageing phenotypes of *PolgA* ^{*mut/mut*} mice associated with increased mitochondrial hydrogen peroxide levels supporting the oxidative damage theory of ageing (Logan *et al,* 2014). They have suggested that prolonged persistent of mtDNA mutations may have activated the ROS production in redox signalling or have modified the response of the immune system to generate an array of pro-inflammatory cytokines contributing to progeroid phenotypes.

Shabalina *et al* (2017) have documented that treating *PolgA* ^{*mut/mut*} mice for ~100 days with mitochondrial targeted antioxidant 10-(6′-plastoquinonyl) decyltri-phenylphosphonium cation (SkQ1) delayed the appearance of age-related features such as kyphosis, weight loss, alopecia and cardiac pathologies in this mouse model. Other antioxidants such as catalase and N-acetyl-L-cysteine (Dai *et al,* 2010; Ahlqvist *et al,* 2012), have also shown lifespan extension in *PolgA* ^{*mut/mut*} mice indicating ROS damage and oxidative stress play a major role in development of ageing characteristics of this mouse model.

1.4 The cardiovascular system

1.4.1 *The heart*

The human heart is located medially inside the thoracic cavity between the left and right lung in a way that the apex of the heart is pointing towards the left lung. A typical weight of an adult heart is about 250-300g in females and 300-350 in males

(Molina and DiMario, 2015). The heart is made of two upper (the atria) and two lower (ventricles) chambers to circulate blood through the pulmonary and systemic circuit as shown in Figure 1.7A. The atrioventricular septum (AVS) separates the right and left side of the heart. Deoxygenated blood is pumped from the right ventricle through the left and right pulmonary arteries into the lungs for gas exchange and the oxygenated blood then returns back to the left atrium through the pulmonary vein. Oxygenated blood is pumped into the left ventricle and then into the systemic circulation through the aorta. The deoxygenated blood then returns back to the right atrium through the superior and inferior vena cava. The valves are to prevent the backflow of blood in the opposite direction. The valves between the atria and the ventricles are called AV valves (tricuspid valves between the right atria and ventricle, mitral valve between the left atria and ventricle). The valves leading to the aorta and pulmonary trunk are known as semilunar valves (left: aortic value and right: pulmonary valve). The valves work in conjunction with the pumping action of the myocardium and are attached to the papillary muscles by chordae tendineae to prevent the backflow of blood, however semilunar valves lack chordae tendineae and papillary muscles. They instead have folds of endocardium made up of connective tissue to seal the valves when the ventricles are filled with blood and the pressure is high (BHF, 2019). Cardiac muscle is encased with pericardial membrane as well as a pericardium bilayer which consists of three layers, epicardium which is the inner wall of the pericardium, myocardium which is the middle layer of pericardium and endocardium which is the inner lining layer in contact with the blood (Figure 1.7B).

The human and mouse heart have exceptional anatomical similarities during development and postnatally. The mouse AVS is however more muscular due to delayed delamination of the tricuspid valve (Webb, Brown and Anderson, 1996) and myocardialisation of the mesenchymal tissue between atria and ventricles (Kruithof *et al,* 2003). In the mouse heart, the tendinous chords (chordae tendineae) are less prominent than in humans. Trabeculae carneae are protrusions in the inner lining of the ventricles. These protrusions vary between the right and left ventricle of human heart, but not in the mouse heart. In the left ventricle, these trabeculae are thin whereas in the right they're being described as coarse (Wessels and Sedmera, 2003). Morphological differences which exist between the human and mouse heart include the size and shape of the muscular AVS and the location of the aortic outlet relative to the AVS. Other anatomical differences exist between the two species

mainly in the venous pool. Mice also demonstrate a significantly higher heart rate than humans. Despite these differences, mice serve a valuable model for the study of the heart due to the similar anatomy.
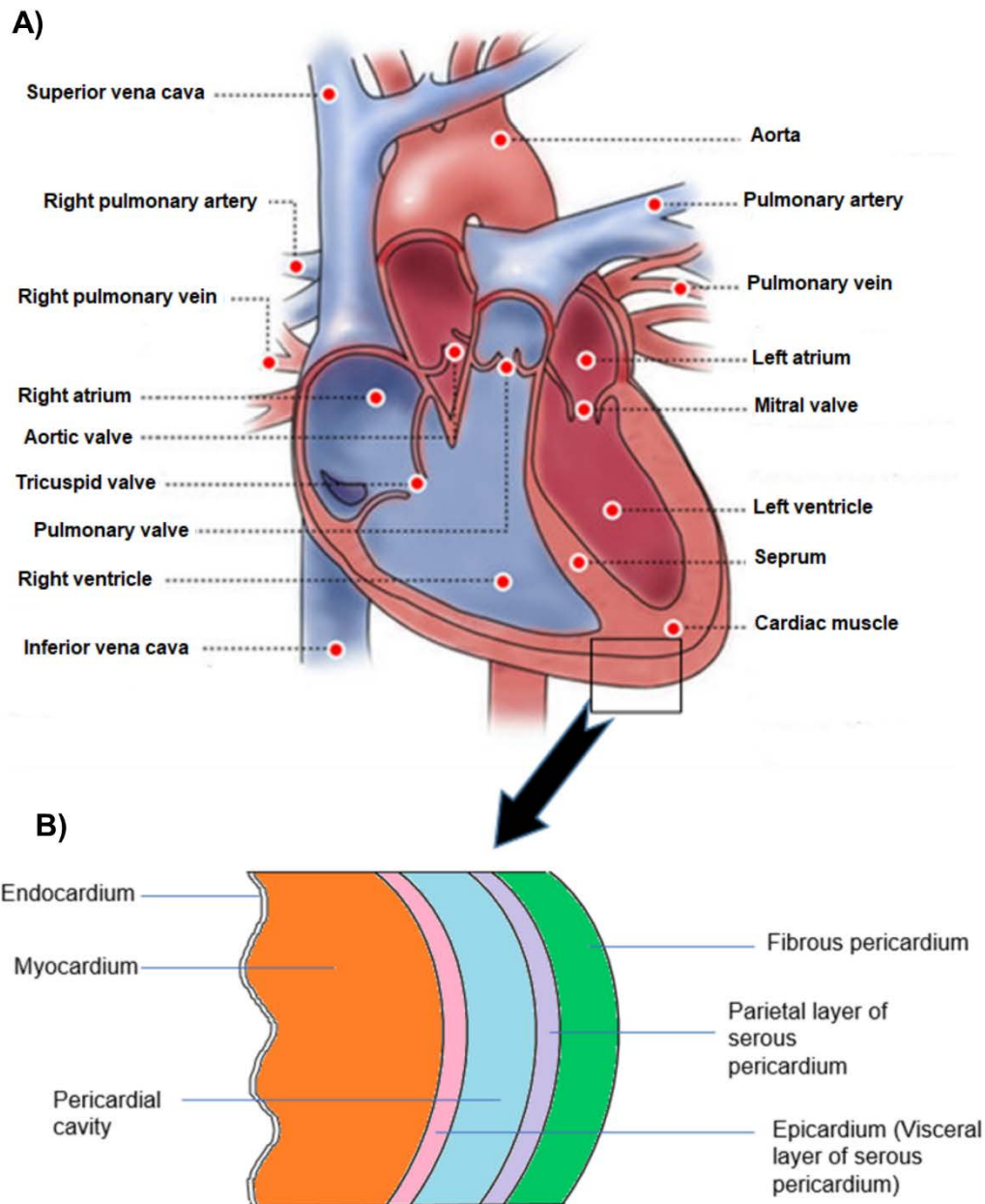
Figure 1.7. The human heart structure. A) Anterior view of the heart. Deoxygenated blood enters the right atrium through superior and inferior vena cava and becomes oxygenated by passing through the lungs through pulmonary artery. Image adapted from OpenStax (2019). B) The epicardial membrane and heart wall layers share epicardium as shown in pale pink.

1.4.2 *The vasculature*

Arteries carry oxygenated blood away from the heart through systemic circulation except the pulmonary and umbilical arteries which carry deoxygenated blood for oxygenation. Coronary arteries supply blood to the cardiac muscle and branch off from the base of the aorta to the right coronary artery and left main coronary artery as well as descending artery and circumflex artery. Blockage in any of these arteries may cause heart diseases, known as coronary artery disease. Arteries have elastic properties and are able to expand and withstand changes in blood pressure (American Heart Association, 2019). The arterial wall consists of the tunica intima which is the outermost squamous epithelium layer surrounded by a connective tissue layer known as the basement membrane (Taki *et al,* 2017). The basement membrane is made of elastic fibres to provide malleability with blood pressure changes. Tunica media is the next upper layer mainly made of thicker smooth muscle to support diameter changes within the blood vessel and regulates blood flow. The final connective tissue layer is the tunica externa which contains varying proportions of elastic and collagenous tissue at different ends of the vessel.

Capillaries are the smallest blood vessels present in abundance that carry out the exchange of O_2, CO_2, nutrients and waste materials between the blood and the tissue (Natural crest cells, 2014). On the other hand, veins carry deoxygenated blood from the rest of the body to the heart apart from the pulmonary and umbilical veins. They are smaller in diameter and do not contain any elastic fibres in the tunica intima layer. The smooth muscle component of veins facilitate contraction and dilation of veins to accommodate blood volume changes (Pinnell, Turner and Howell, 2007).

1.4.3 *Cardiac muscle structure*

Cardiac muscle is a myogenic, involuntary and striated muscle that usually contains one central nuclei in each cardiomyocyte. Individual cardiomyocytes are shorter in length and smaller in diameter than skeletal muscle fibres, however they are organised into sarcomeres and share the same banding organisation as skeletal muscle. On average, human adult cardiomyocytes are about 0.1mm in length and 0.02mm in width (Ward, 2001). Two major types of cardiac muscle cells exist, the first

are myocardial contractile cells which reside predominantly in the atria and ventricles and are responsible for myocardial contraction. The second type are myocardial conducting cells which constitute a very small proportion of cells responsible for conduction and propagation of the action potential (Saxton and Bordoni, 2018). Each cardiomyocyte is surrounded with sarcolemma and is packed with mitochondria for continuous supply of ATP during cardiac contractions. Myofilaments are encased by sarcoplasmic reticulum and t-tubules at the level of Z-line cross the cell to allow rapid transmission of action potentials into the cell (Pinnell, Turner and Howell, 2007). Cardiomyocytes are extensively branched and are connected by double-membraned intercalated discs where individual cells are bound by desmosomes and connected through gap junctions to allow easy conduction of impulses between cells (figure 1.8). Intercalated discs connect two adjacent cardiomyocytes together where two sarcolemma join to support the synchronised contraction of the cardiac muscle (Hong and Shaw, 2016). Desmosomes anchor cardiomyocyte ends together to maintain the integrity of muscle.
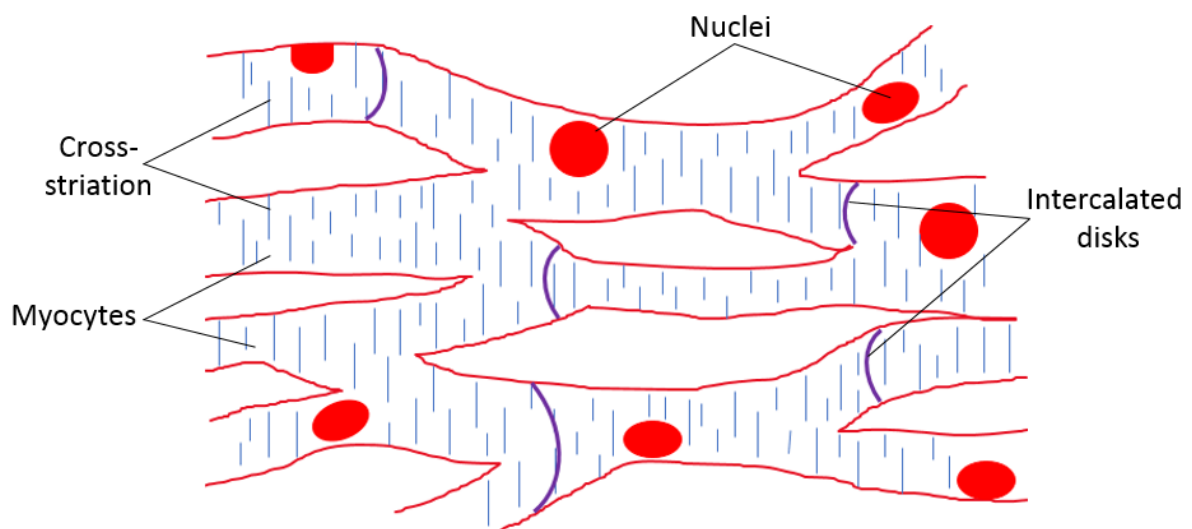
Figure 1.8. Cardiac muscle structure. Structural arrangement of striated cardiac muscle which are connected by intercalated discs to allow for a wave-like pattern of contraction during the pumping action of the heart.

1.4.4 *Cardiac muscle function*

The primary function of heart muscle is to contract and pump oxygenated blood into the circulatory system. The heart thus requires a continuous supply of energy in a

form of ATP which is provided by oxidative phosphorylation in mitochondria. The functional adaptations of cardiomyocytes include their branched structure for faster signal transduction. However due to the low capacity of cardiac muscle to store energy, a constant energy influx in the form of ATP is required (Attansio and Netti, 2017). Cardiac muscle also has longer contraction and refractory periods to maintain a viable heartbeat. External hormonal and nervous system stimulation of the heart muscle enables cardiac muscle to adapt to situations of different energy demand. Also the inherent contractile activity of cardiac muscle is controlled by the autonomic nervous system. Any disruption to the synchronous contraction of cardiac muscle may lead to uncontrolled pumping action of the heart muscle and conditions such as ventricular fibrillation.

Cardiac function responds to meet the metabolic demand of the body by regulating either the stroke volume or respiratory rate. Increasing the respiratory rate increases the rate of oxygen perfusion to the working tissue. Similarly increasing the stroke volume will increase the volume of blood ejected from the ventricle during systole to the working tissue leading to regulated cardiac function. Cardiac function and vascular resistance can be measured by cardiac catheterisation directly or indirectly through thermodilution, cardiac MRI and exercise testing (Carreiro, 2009).

It is widely reported that ageing and heart failure significantly reduce cardiac performance and left ventricular (LV) cardiac output when compared to younger and healthy individuals (Strait and Lakatta, 2012). Reduction in myocardial energetics such as cytoplasmic adenine nucleotide, phosphates and creatine pool with age and in heart failure partly influence the reduction in cardiac output (Wu, Zhang and Beard, 2009; Gao, Jakovljevic and Beard, 2019).

1.4.5 *The cardiac muscle action potential*

Cardiac impulses that facilitate the heartbeat originate from the sinoatrial (SA) node also known as the pacemaker cells of the heart. The SA node is located on the right atrial muscle causing the atria to contract following depolarisation of the atria and release blood into the right ventricle through the tricuspid valve. The heart rate is controlled through the electrical activity of the heart since the SA node responds to

signals from the central nervous system (CNS) and various hormones that modulate heart rate and regulate blood pressure (Hedegard, 2019).

Ventricular contraction (systole) is controlled by the atrioventricular (AV) node which is located on the IVS septum between the two ventricles. The cardiac action potential originates from the spontaneous depolarisation of the SA node which generates the intrinsic electrical activity of the heart. The action potential in the cardiac muscle is more prolonged (about 300ms) than in nerve cells. During this time no further action potential can take place which is known as an absolute refractory period. The sarcoplasmic reticulum (SR) releases Ca^{2+} from internal stores to activate cardiac muscle contraction. During cardiac depolarisation, membrane permeability to K^+ decreases and Na^+ channels open resulting in membrane voltage changes from -90 mV to +10 mV. Once the action potential reaches a plateau, membrane permeability to Ca^{2+} increases to prolong the action potential. The Na^+/Ca^{2+} ATPase pump allows for the influx of Na^+ and produces a net inward of positive current during the plateau phase. Repolarisation takes place soon after Ca^{2+} channels inactivate by an outward flux of K^+ ions and the membrane potential falls back to -90mV (resting membrane potential). The mechanical pumping action of the heart is followed by the electrical activity of pacemaker cells located on the SA node. Once pressure within the heart drops, the contraction of the atria enters a diastole phase which is longer in duration than systole. The cardiac cycle is the process of one heartbeat comprising of a complete relaxation and contraction which lasts about 0.8 seconds in human adults (Malanga, 2007).

1.4.6 *Excitation-contraction coupling*

The auto-rhythmic ability of the heart muscle enables rapid movement of action potentials across gap junctions. The pacemaker activity of the cardiac muscle directly controls the heart rate. This action potential triggers the release of calcium from the sarcoplasmic reticulum and other internal calcium stores causing myofilaments to contract in a process called excitation-contraction coupling (Bers, 2002) (Figure 1.9).

The two main categories of Ca^{2+} currents (I_{Ca}) in cardiac myocytes are L-type and T-type Ca^{2+} currents. The L-type channel activates and deactivates (more slowly) at positive membrane potentials. During the upstroke of the action potential (AP), L-type

voltage dependent Ca^{2+} channels (L-VDCC) open. Unlike skeletal muscle, cardiac muscle relies on a constant heart beat for Ca^{2+} release from SR via Ca^{2+} release channels i.e. ryanodine receptors. This Ca^{2+} -induced Ca^{2+} -release process (CICR) causes a rapid increase in intracellular Ca^{2+} concentrations for optimal binding of Ca^{2+} to troponin C and contraction induction. Troponin C then releases the Ca^{2+} for reuptake by SR by activating SR Ca^{2+} ATPase 2a (SERCA2a) pump and through the Na^+/ Ca^{2+} exchanger (NCX). At resting conditions, a cardiomyocyte takes ~600ms to contract, relax and recover. Ca^{2+} is essential for cellular integrity, cardiac gene expression (Finkbeiner and Greenberg, 1998) and the development of the embyonic heart (Rottbauer *et al*, 2001). T-type Ca^{2+} channels on the other hand are low-voltage activated channels and are relatively insensitive to dihydropyridines (DHPs). T-type Ca^{2+} channels are abundant in sinoatrial node (SAN) and purkinje fibres and are essential for establishing the frequency of AP firing (Ono and Lijima, 2010).
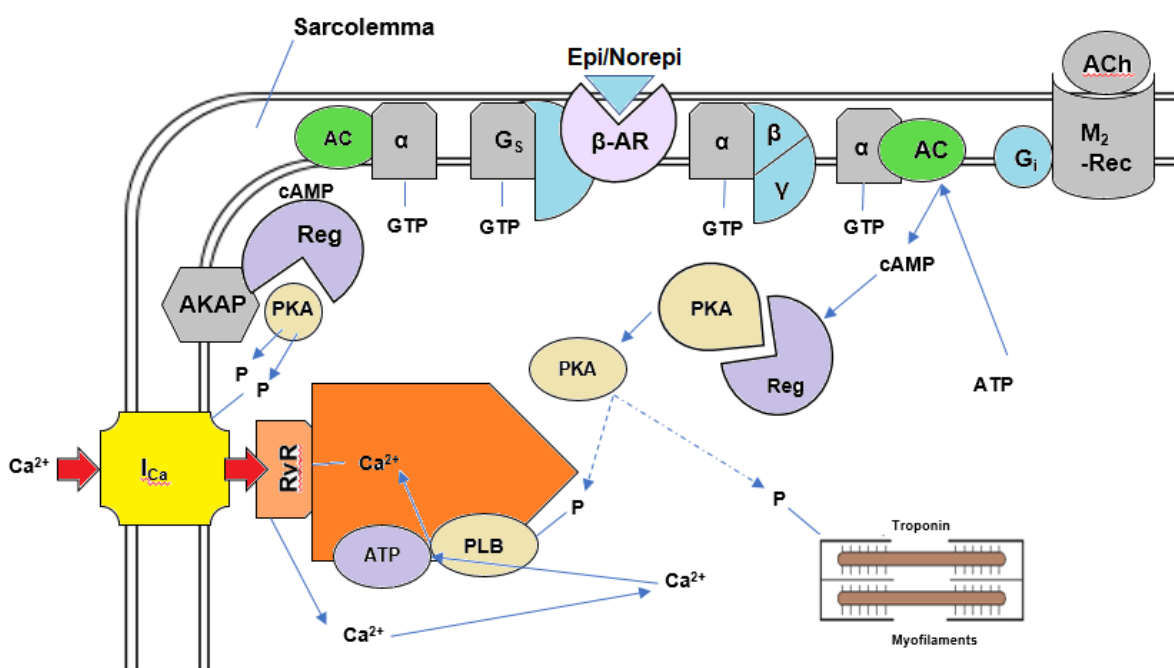
Figure 1.9. Excitation-contraction coupling (ECC). ECC is accompanied by Ca^{2+} transport in the ventricular myocyte. β-adrenergic stimulation and activation by epinephrine or noradrenaline leads to activation pf GTP-binding protein (Gs) which activates adenylyl cyclase (AC) to produce cyclic AMP (cAMP) which in turn activates protein kinase A (PKA). PKA has both positive inotropic (contraction) and lusitropic (relaxation) effects on the muscle. If Phospholamban (PLB) and troponin I are phosphorylated, SR uptake of Ca^{2+} increases and Ca^{2+} dissociates from the myofilaments leading to lusitropic effects on the muscle.

1.4.7 *Mitochondria within the heart muscle*

Cardiomyocytes possess multiple mitochondria and myoglobin since ATP is generated through aerobic metabolism in the heart. In fact, an adult human heart synthesises approximately 30kg of ATP everyday (Ferrari, Cargoni and Ceconi, 2006).

Fatty acids are the preferred energy supply for mitochondria (Murphy *et al,* 2017), however, they are able to convert different substrates into ATP in order to respond to changes in environment such as during exercise or at different altitudes. The fatty acid β-oxylic pathway and tricarboxylic acid cycle (TCA) are described in more detail in section 1.1.2.1. Once fatty acids are broken down into Acetyl-CoA, they enter the TCA cycle, also known as Kreb's cycle. Electron carriers (NADH and $FADH_2$) produced during TCA cycle, are fed into the electron transport chain (ETC) to create an electrochemical gradient across the intermembrane space to activate ATP synthase to produce ATP in the presence of O_2 (Brown *et al*, 2017).

Two types of mitochondria were observed in the ultrastructure of cardiac muscle including subsarcolemmal mitochondria (SSM) and interfibrillar mitochondria (IFM) (Palmer, Tandler and Hoppel, 1985). Interfibrillar mitochondria are located between myofibrils and subsarcolemmal mitochondria are located beneath the plasma membrane. The two mitochondrial types differ in structure, location and their biochemical properties. Interfibrillar mitochondria utilise substrates 1.5 times faster than subsarcolemmal mitochondria and have higher activities of SDH and citrate synthase. These differences make the two populations of mitochondria energetically different but very difficult in isolation (Lenaz *et al*, 2006). For instance, dysfunction of cardiac SSM was reported in a murine model of type 2 diabetes mellitus (Dabkowski *et al*, 2010). Also human studies revealed a significant reduction in complex I and fatty acid-mediated respiration rate in SSM population of type 2 diabetes patients with no changes in IFM population (Croston *et al,* 2014).

It's documented that the failing human heart undergoes significant depletion of energy reserves as evident by low phosphocreatine to ATP ratio (PCr: ATP) through phosphorous-31 NMR spectroscopy (Beer *et al*, 2002). The energy deficit in cardiac

muscle is reported to be correlated with clinical symptoms and is thought to be a better predictor of mortality than EF alone (Neubauer *et al,* 1997).

To understand mitochondrial function in the human heart better, measurements of mitochondrial enzyme activities from cardiac muscle homogenates provided valuable information about the capacity of different steps involved in mitochondrial metabolism. It's difficult to measure the capacity of ATP production by the whole system since functional impairment occurs when OXPHOS enzymatic activities are reduced below a threshold level (Rossignol *et al*, 2003), however complexes III and IV are present in amounts larger than needed to aid maximal electron transport in human cells (Villani and Attardi, 1997), therefore a reduction in the activity of one complex in the ETC may not impact the whole process.

Gellerich *et al*, 1994 have shown that the rate of respiration in the human left atrial appendage is lower than in the left ventricle. In contrast to skeletal muscle, the number of mitochondria and ETC activity is higher in cardiac muscle, but the OXPHOS capacity is limited in cardiac muscle. In fact, respiration coupled to ATP generation is about 40% of the maximal capacity of the heart muscle (Lemieux and Hoppel, 2009), in comparison to 80% in skeletal muscle (Boushel et al, 2007).

In rodent models however the OXPHOS capacity of cardiac muscle is much higher than skeletal muscle and the OXPHOS system does not apply any limitation on the maximal OXPHOS capacity of the cardiac and skeletal muscle (Aragones *et al,* 2008). Calcium accumulation capacity in human cardiac muscle is also much lower than in the hearts of a variety of animals (Lindenmayer *et al*, 1971). The particularities of human heart mitochondria reinforces the importance of understanding mitochondrial metabolism specifically in human heart.

1.4.8 *Cardiac muscle oxidative stress*

Reactive oxygen species (ROS) are generated through aerobic metabolism as a by-product of OXPHOS in mitochondria and are normally regulated by antioxidants (Chen *et al*, 2003). Excessive production of ROS or antioxidant deficiency can cause ROS damage to the proteins and lipids within mitochondria. Oxidation of proteins changes their structure and function leading to their inactivity. ROS play an important

role in cellular homeostasis (Droge, 2002) and are a major source of superoxide radicals (Turrens, 2003). Low concentrations of ROS inside a cell maintains its role as a signal transducer, however its excessive production and redox imbalance leads to oxidative stress and increases the risk of cardiovascular disease. ROS include hydroxyl radicals, superoxide anions, H_2O_2 and peroxynitrite. Those that contain free radicals such as superoxide anions have oxidising effects.

1.4.9 *ROS in cardiac disease*

Excessive ROS have a direct effect on the arterial wall by activating second messenger systems in vascular signalling (Taverne *et al,* 2013). Tunica intima is affected mainly by ROS scavenging system. The imbalance in cell proliferation and growth inhibition is also controlled by cellular ROS state which will cause extreme biogenesis or depletion of endothelial cells respectively (Papaharalambus and Griendling, 2007). Hattouri *et al* (2001) have documented that the ROS produced during ischaemia reperfusion injury activates apoptosis, and during pre-conditioning inhibits apoptosis by regulating expression of Bcl-2 family of proteins.

1.4.10 *Cardiovascular disease*

Cardiovascular disease (CVD) is the leading cause of mortality and hospitalisation worldwide. The prognosis in CVD is still very poor causing 17.9 million deaths annually which accounts for 35% of all deaths globally (WHO, 2019). The risk factors identified in epidemiological studies include hypertension, smoking, inactivity and high cholesterol (Thanassoulis and Vasan, 2010). There are multiple genetic and environmental factors that contribute towards developing cardiovascular disease. Development of CVD is initiated by molecular and cellular changes followed by cardiac pathophysiological remodelling. It is documented that changes in energy metabolism of cells activate profibrotic signalling cascades as well as a hypertrophic response resulting in cellular death and cardiomyocyte loss (Frangogiannis, 2012).

The development of cardiac hypertrophy is a multi-step process beginning with an extracellular hypertrophic stimulus, activation of early response genes and increased production of contractile proteins into sarcoplasmic units. The next step transduces

the hypertrophic signal by activating the mitogen-activated protein (MAP) kinase cascade and finally there is recruitment of nuclear transcription factors, triggering events for cellular hypertrophy (Glennon, Sugden and Poole-Wilson, 1995). Alterations in Ca^{2+} homeostasis and proteins involved in Ca^{2+} transport also leads to impairment of contractility and relaxation by diminishing systolic function of the heart (Lehnart *et al*, 2003).

1.4.11 *Exercise-induced cellular adaptation*

Exercise as a physiological stress requires a synchronised response from both the cardiovascular, pulmonary and nervous system. The increase in blood flow to the working muscle during exercise is a multi-system process and an impairment to any of these systems may lead to decreased exercise capacity. The heart's ability to augment cardiac output (CO) during the enhanced metabolic demand of exercise depends on the heart rate (HR) and stroke volume (SV). Exercise induced adrenergic stimulation enhances both the HR and SV proportional to the exercise intensity up to about 40-50% of maximal capacity. Once the maximal capacity is reached, the SV plateaus despite a further increase in HR and cardiac output (CO) (Tegtbur, Busse and Kubis, 2009).

Many researches have documented the beneficial effects of exercise in humans and rodent models. In cardiac muscle, exercise promotes mitochondrial biogenesis by increasing the expression of PGC-1α (Tadaishi *et al*, 2011). Cardio-protection was also achieved with exercise by enhancing the activity of β-adrenergic signalling as well as SERCA2a expression and activity and increased Ca^{2+} handling which is linked to optimal contractility of cardiac muscle (Calvert and Lefer, 2012). Physiological cardiac hypertrophy is largely observed with exercise training (Fernandes, Soci and Oliveira, 2011). The increase in the size of the LV muscle and decrease in the LV chamber size, enhances the ejection fraction and cardiac output and provides beneficial protective mechanisms with age (Lowery and King, 2019).

1.4.12 *Exercise in mice*

Treadmill running in mice has been a subject of investigations since the 1970s and most of the work was carried out discerning its role and effects on cardiac and skeletal muscle (Avila, Kim and Massett, 2017), (Kemi et al., 2002). Researchers have looked into the effect of different modes of exercise in mice i.e. forced (treadmill) and voluntary (flywheel).

Forced treadmill running has been associated with exacerbation of systemic inflammation in a mouse model of colitis (Cook *et al*,. 2014), induction of stress in a mouse model of cerebral ischaemia (Svensson *et al*, 2016) and promoter of osteoarthritis in a mouse model of decorin-deficiency (Gronau *et al*, 2017). These findings clearly demonstrate that mice with a predisposed disease burden may suffer following the added pressure of forced exercise. On the other hand, Luccetti *et al* (2017) have documented that moderate forced treadmill running provides better cardiac function and resistance against the parasitic infection causing Chagas disease. The findings of all the previous research highlights the fact that type of exercise, intensity, frequency and duration play an essential role in the outcome of results.

A study by Narath, Skalicky and Viidik (2001) reported that voluntary running in rats increases their survival rate and reduces body fat to muscle ratio. As highlighted by the authors, there has been a large variation with respect to how much animals would voluntarily run, therefore inevitably skewing the distribution of data.

Mitochondria play an important role in providing the enhanced ATP source to the working muscle during exercise, hence cardiomyocytes are packed full of mitochondria. It is clear that only healthy mitochondria can contribute to this increased energy demand. The cellular adaptations induced by exercise include physiological cardiac hypertrophy to accommodate the increased reliance on the cardiac muscle for oxygen supply to organs with high energy demand and to meet the increased basal metabolic rate (De Biase *et al*, 2014).

Mitochondrial DNA *PolgA* deficient mouse (*PolgA* *mut/mut* mice) display marked systolic and diastolic dysfunction, cardiac hypertrophy and dilation from the age of 14 months as well as a significant age-related decline in cytochrome-c oxidase activity (Dai *et al,* 2010). It is unlikely that dysfunctional mitochondria could contribute much

in terms of ATP to the cardiac muscle under stress. In fact, Yan *et al* (2017) demonstrated that endurance exercise in obese mice lead to unfavourable cardiac remodelling through initiation of autophagy. Davies *et al* (1982) also reported that strenuous acute exercise increased oxidative stress and led to tissue damage as a result of enhanced tissue oxygen consumption by 3.6 fold in the heart. In comparison, Venditti *et al* (2013) have reported that 10 weeks of swimming training significantly reduce basal H_2O_2 levels in rat skeletal muscle.

1.4.13 *Cardiac mitochondrial adaptations to exercise*

During exercise, cardiac mitochondrial oxygen consumption increases by at least 10 fold in order to accommodate the greater energy demand of working muscles (Olver, Ferguson and Laughlin, 2015). The remarkable metabolic flexibility of cardiac muscle during exercise is the process known as remodelling. Since cardiac muscle is a post mitotic tissue, the growth in the size of cardiomyocytes is more likely to occur than cellular proliferation (Poole *et al,* 2012). This physiological growth is accompanied by increases in mitochondrial number and energy production capacity.

During physiological cardiac remodelling the rate of mitochondrial biogenesis and fatty acid oxidation increases. PGC-1α expression in cardiac muscle is increased significantly by exercise (Pilegaard, Saltin and Neufer, 2003). Enhanced PGC1-α binds to PPARα (peroxisome proliferator activated receptor α) to increase fatty acid oxidation and storage in the heart (Gilde and Van Bilsen, 2003). Aubert, Vega and Kelly (2013) have reported that augmented PGC1-α and PPARα expression in the cardiac muscle during exercise inhibits pathological cardiac growth and heart failure. In 2012, Scarpulla, Vega and Kelly added to the function of increased PGC-1α expression in the cardiac muscle by observing that PGC-1α promotes mitochondrial biogenic response by interacting with oestrogen-related receptor (ERR) and nuclear receptor factor 1 (NRF-1). Notably ERR is required for maximal ATP production and pressure overload adaptations during exercise (Huss *et al*, 2007).

1.4.14 *Age related cardiovascular disease*

Age is the major risk factor for the development of a cardiovascular disease (CVD) (Rosenzweig, 2016). CVDs are leading cause of morbidity and mortality worldwide costing the National Health Service £9 billion each year (WHO, 2019). The most common type of CVD is Coronary Heart Disease (CHD) killing 22,000 individuals under the age of 75 in the UK every year (BHF, 2019). Currently 2.3 million people live with CHD in the UK meaning the prevention and management of the disease with medication is inevitably difficult. Lifestyle changes such as exercise, healthy diet, weight management, limiting alcohol intake and smoking are important contributors of CVD both in prevention and treatment. The underlying cause of CHD is the formation and accumulation of cholesterol plaques (atheroma) on the arterial walls. Over time, the main artery supplying the cardiac muscle becomes restricted, limiting the amount of oxygen and nutrients supplied to the heart especially under high demand situations such as during exercise (Roh *et al,* 2016).

Evidence suggests that events leading to the onset of atherosclerosis begin decades before the clinical symptoms of the disease become apparent (Singh *et al*, 2002). The underlying etiology of this this complex and slow progressing inflammatory disease is still largely unknown. Berliner *et al* (1995) investigated the atherogenic properties of oxidised low density lipoproteins (LDL) cholesterol and other oxidised lipoproteins in cellular oxidative stress. They have confirmed the interaction between mitochondrial redox state within the vascular wall as targets of oxidative induced-damage and initiation of CVD. This is due to the properties of plasma which contains high concentrations of antioxidants and metal ions to provide the best environment for arterial wall to accelerate LDL oxidation by reactive oxygen and nitro-species from various sources such as mitochondria, NADPH or Xanthine oxidase (Berliner *et al*, 1995).

The regulatory links between ETC complexes and the normal functioning of cardiac muscle has been debated for many years. Researchers have argued that ADP and inorganic phosphate (P_i) availability for ATP generation during increased cardiac workload are associated with changes in cardiac function (Balaban, 2012). Others have suggested that regulation of cytosolic Ca^{2+} released from the SR and used by mitochondria in response to increased cardiac workload are tightly modulating the cardiac function (Tarasov, Griffiths and Rutter, 2012).

It's clear that mitochondrial dynamics controlled by fission and fusion processes play a critical role in the normal functioning of cardiac tissue since more than 35% of cardiomyocyte volume is packed with mitochondria necessary for the normal excitation-contraction coupling process.

Another significant risk factor for CVD and mitochondrial dysfunction is age which is accompanied with a general decrease in cellular energy capacity and reduced OXPHOS efficiency (Dhingra and Vasan, 2012). Since mitochondria play a critical role in cardiomyocytes cell signalling, cell death and growth, any alteration in mitochondrial performance due to CVD risk factors will disturb its normal functioning and lead to bioenergetic dysfunction and redox imbalance in cardiac tissue (Dai, Rabinovitch and Ungvari, 2012).

1.4.15 *The effect of age on cardiac responses to exercise*

Cardiovascular conditioning with exercise (i.e. improving cardiovascular function / cardiorespiratory fitness) has been documented previously (Mihl, Dassen and Kuipers, 2008). One way to improve the cardiorespiratory fitness is by regular exercise training (Lin *et al,* 2015).

PolgA$^{mut/mut}$ mice suffer from respiratory chain dysfunction meaning that some essential organs such as skeletal and cardiac muscle are compromised as early as 6 months of age (Trifunovic *et al*, 2004). It's still largely unknown whether endurance exercise would mitigate the phenotypic changes and recover the decline in mitochondrial dysfunction observed in *PolgA$^{mut/mut}$* mice before the manifestation of premature ageing phenotypes and cellular dysfunction.

Fatigue and exercise intolerance are the most common characteristics of patients with mitochondrial dysfunction (Filler *et al,* 2014). Exercise intolerance is directly correlated with the severity of impaired OXPHOS in cardiac muscle, meaning that with age, exercise intolerance will increase as the rate of mtDNA point mutations increase causing lower OXPHOS rate (Taivassalo, 2003).

One way to measure exercise intolerance is by performing a graded exercise treadmill test where peak exercise oxygen consumption is assessed. Taivassalo (2003) carried out a study to measure peak work capacity in patients with severe

mitochondrial respiratory chain defects and found that the capacity of muscle to increase oxygen utilisation is blunted in relation to increased circulatory and ventilatory responses with exercise. A recent study by Safdar *et al* (2011) has shown that 5 months of treadmill running in *PolgA^{mut/mut}* mice have mitigated stress intolerance as evidenced by a reduction in the degree of exhaustion during the stress test. They also observed an increased lifespan, activation of mtDNA mutation repair mechanisms by p53 enzyme, increased mitochondrial biogenesis, preserved mitochondrial morphology as well as reduced systemic multi-organ failure.

The development of cardiac hypertrophy is a multi-step process beginning with an extracellular hypertrophic stimulus, activation of early response genes and increased production of contractile proteins into sarcoplasmic units. The next step is the transduction of hypertrophic signal through activatin of the mitogen-activated protein (MAP) kinase cascade and finally recruitment of nuclear transcription factors, triggering events for cellular hypertrophy (Glennon, sugden and Poole-Wilson, 1995). Cardiac remodelling and physiological hypertrophy are accompanied by ventricular wall thickening with or without changes in ventricular chamber volume (Mihl, Dassen and Kuipers, 2008). Cardiac adaptations to exercise include a 12-15% increase in overall heart weight in both eccentric and concentric growth patterns (Blomqvist and Saltin, 1983; Scheuer and Tipton, 1977).

The reduction in the maximal HR with age also known as chronotropic incompetence is a key factor determining cardiac response to exercise. The age associated reduction in HR with exercise is thought to be due to an impaired autonomic regulation of the heart and changes in the conducting system (Brubaker and Kitzman, 2011). These changes are strong predictors of increased mortality and increased cardiovascular events (Higginbotham *et al,* 1986).

The heart's responsiveness to exercise and autonomic stimuli decreases significantly with age. The diminished autonomic stimuli mainly rises from dysregulation of the sympathetic nervous system through β-adrenergic receptor (β-AR) desensitisation on the cardiac muscle. This in turn reduces cardiac reserve and exercise capacity with age. The diminished β-AR activity with age is complex and is partly due to 10-15% increase per decade in total circulatory norepinephrine levels with age (Roh *et al,* 2016). This will result in greater occupancy of β-AR and diminished reuptake of the neurotransmitter leading to desensitisation of post synaptic machinery and impaired

contraction and relaxation of cardiac muscle and reduced Ca^{2+} transients due to further β-AR stimulation. Multiple proposals by which cardiac responses to exercise diminishes with age exist (Figure 1.10).
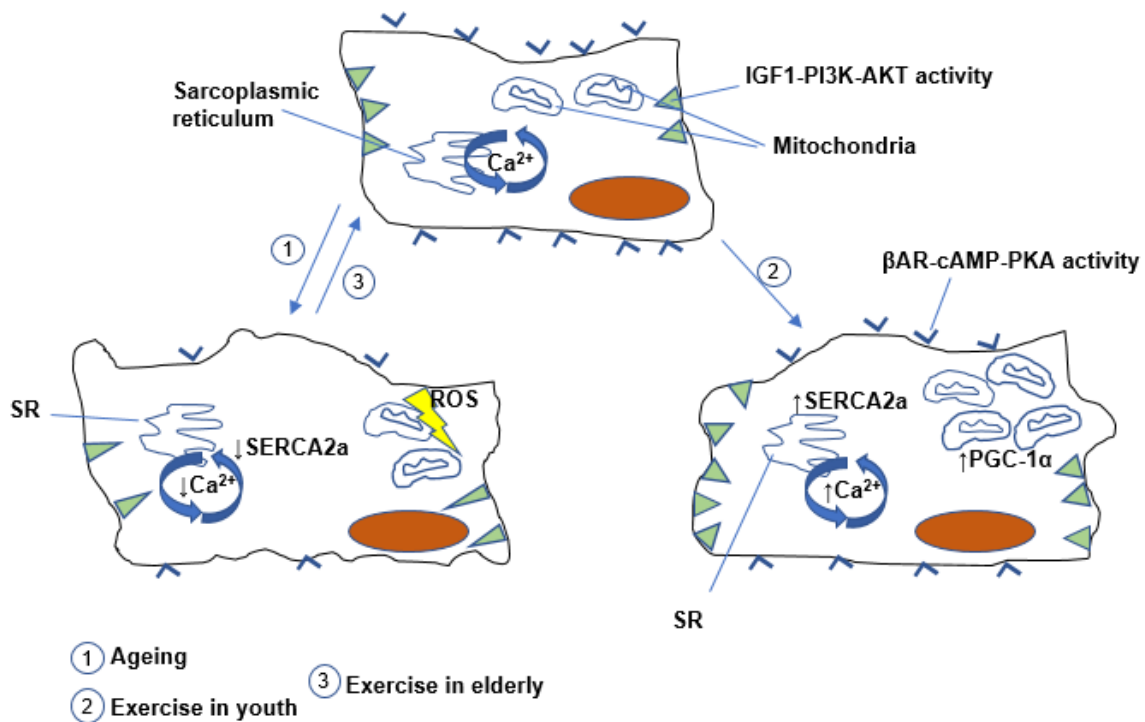
Figure 1.10. Cellular changes in cardiac responses to exercise in young and old. 1) With age, IGF-I-PI3K-AKT activity as well as β-AR-cAMP-PKA activity is reduced leading to diminished SERCA2a expression and activity and so inefficient handling of Ca^{2+}. 2) Impact of exercise in youth. 3) Exercise is thought to reverse the effects of aging seen in the cardiac muscle.

1.5 Aims and objectives

What is the role of endurance exercise on ageing cardiac muscle and mitochondrial function investigated using mouse models of accelerated and physiological ageing?

In order to observe exercise-associated changes in cardiac and mitochondrial function, two established mouse models of ageing known as the C57BL6/J mice and *PolgA$^{mut/mut}$* mice were used to answer the following questions:

- Does endurance exercise alleviate premature, accelerated ageing phenotypes as well as cardiac mitochondrial dysfunction in *PolgA$^{mut/mut}$* mice?

- Does late-life endurance exercise alleviate the decline in aerobic capacity, cardiac function and cardiac mitochondrial function that normally occurs with age?

Chapter 2

Chapter 2. Materials and methods

2.1 Consumables

General consumables	Supplier
0.2ml, 0.5ml PCR tubes	Star Lab
96 well reaction plates	Fisher Scientific
Avidin/Biotin blocking kit	Vector Laboratories
Coverslips (22x22mm, 22x40mm, 22x50mm)	MSD
Falcon tubes (15ml, 50ml)	BD Biosciences
Gilson pipettes (P2, P10, P20, P100, P200, P1000)	Star Lab
Gloves	Star Lab
Hydrophobic pen	Abcam
Microfuge tubes (0.6ml, 1.5ml, 2.0ml)	Star Lab
Microvette	Sarstedt
Mouse cytokine array kit	MSD
Mouse dissection kit	VWR
Multi-channel pipettes	Star Lab
Pipette tips (10µl, 20µl, 200µl, 1000µl)	Star Lab
QIAmp DNA mini kit (50)	Qiagen
Reagent reservoirs	Fisher Scientific
Scalpels	Swann Morton
Slide mailers	Cell path
Solution reservoir	Green Bioresearch
Superfrost glass slides	MSD
Tissue cassettes	Cell path

Weight boats	VWR
Whatman filter paper	Fisher Scientific
Stainless steel beads (5mm)	Qiagen
DNeasy blood and tissue kit	Qiagen

2.2 Antibodies

List of antibodies	Supplier
Active cleaved caspase-3	Abcam
Donkey anti-rabbit IgG-Alexa Fluor ®750	Abcam
Goat anti-mouse IgG1-Alexa Fluor ®647	Thermo Fisher
Goat anti-mouse IgG2a-Alexa Fluor ®546	Life technologies
Goat anti-mouse IgG2b-Alexa Fluor®488	Life technologies
Goat anti-rabbit IgG-Alexa Fluor ®405	Thermo Fisher
Goat-anti-rabbit IgG-Alexa Fluor ®488	Life technologies
Mouse anti-MTCO1 IgG2a	Abcam
Mouse anti-NDUFB8 IgG1	Abcam
Mouse anti-VDAC1 IgG2b	Abcam
Rabbit anti-Laminin (Polyclonal)	Sigma-Aldrich

2.3 Reagents

Reagents	Supplier
Acetic acid	VWR
4% Paraformaldehyde (PFA) in PBS	Santa Cruz Biotechnology
Avidin/Biotin kit	Vector Laboratories

Bovine Serum Albumin (BSA)	Sigma-Aldrich
Catalase	Sigma-Aldrich
Cytochrome c	Sigma-Aldrich
3,3'-diaminobenzidine (DAB)	Sigma-Aldrich
DEPC treated water	Ambion
DPX ™	Merck
Eosin	Cell Path
Ethanol (AnalR)	MSD
Haematoxylin	TCS Biosciences Ltd
Histoclear ™	National Diagnostics
Hydrochloric acid (HCl)	VWR International Ltd,
Isopentane	Merck
Liquid nitrogen	BOC
Methanol (AnalR)	MSD
MSD cytokine immunoassay kit	MSD
Nito Blue Tetrazolium (NBT)	Sigma-Aldrich
Normal Goat Serum (NGS)	Sigma-Aldrich
Nuclease-Free water	Fisher Scientific
OCT mounting media	Pyramid innovation
PBS tablets	OXOID
Phosphate buffer Saline (PBS) tablets	Sigma-Aldrich
Phosphotungstic acid	Sigma-Aldrich
Prolong gold mounting media	Fisher Scientific
Proteinase K	Invitrogen
Real time PCR primers	Eurofins Genomics

Scot's tap water	Leica Biosystems
Sodium Azide	Sigma-Aldrich
Sodium Chloride (NaCl)	Sigma-Aldrich
Sodium succinate	Sigma-Aldrich
SYBR Green	Fisher Scientific
Trizma base	Sigma-Aldrich
Tween-20	Sigma-Aldrich

2.4 Solutions

Solutions	**Recipe**
TBST (pH 7.4)	100mM NaCl
	5 mM Trizma base
	0.1% (v/v) Tween 20%
EDTA antigen retrieval buffer (pH 8)	1mM EDTA
PBS (pH 7.4)	1 tablet in 100ml dH_2O
RIPA buffer	1M Tris-HCl pH 7.6
	SDS 10%
	5M NaCl
	Sodium deoxycholate 10%
	1% IPEGAL
	Protein inhibitor cocktail (1 tablet)
Sodium citrate antigen retrieval buffer (pH 6.0)	10mM Tri-sodium citrate
0.1M Phosphate buffer solution (pH 7)	0.4M sodium dihydrogen orthophosphate
	0.06M disodium hydrogen orthophosphate
NBTx solution	130mM sodium succinate
	2mM NBT

	0.2mM PMS
	In 0.1M phosphate buffer
Tris Lysis buffer	150 mM NaCl
	20mM Tris, pH 7.5
	1mM EDTA
	1mM EGTA
	1% Triton-X-100

2.5 Equipment and computer software

Equipment	Supplier
TissueLyser II	Qiagen
ABI Verti 96 well plate Thermal Cycler	Applied Biosystems
Antigen retrieval unit	2100 Retriever
Aperio Scanner	Leica Biosystems
Autoclave	Prior Clave
Zeiss Axioimager fluorescence microscope with apotome (widefield upright)	Zeiss
Benchtop Micro Centrifuge	Fisher Scientific
Eppendorf thermo-shaker	Eppendorf
Microtome	Leica
MSD SECTOR	MSD
Nanodrop ND-1000 spectrophotometer	Labtech International
Nano-Pure water purification system	Barnstead
OFT 5000 Cryostat	Bright
UV hood (PCR clean room)	Astec
Spectrophotometer	Tecan

Magnetic stirrer	IKA
Nikon A1R scanning confocal microscope	Nikon
Zeiss AxioObserver/SD1 (inverted)/AirScan	Zeiss
Nikon Tie fluorescence widefield microscope (inverted)	Nikon
Oxymax metabolic treadmill	Columbus instruments
NIBP	Columbus instruments
Rotarod	Ugo Basile

Computer software	Supplier
Segment v2.0 R5165	Medvision
Aperio Image Scope analyser	Leica Biosystems
NIBP software	Columbus instruments
Vnmrj Cardiac MR software	Agilent technologies
Image J, Fiji	NIH
Matlab R2015a	Math Works
Oxymax treadmill software	Columbus instruments
Treadmill software	PanLab
Minitab 17	Minitab
ND-1000 software	Labtech International
NIS Elements	Nikon
Prism v7.0 and v8.0	Graph Pad
Quadruple immune-analyser	Mathworks

Step-One Plus Real time PCR	Applied Biosystems
ZEN blue version	Zeiss
Mousetrap	GitHub

2.6 Mouse models

2.6.1 *C57BL/6J mouse*

C57BL/6J male mice aged to 59 weeks were purchased from Charles River Laboratory (Kent). Each mouse was identified by a unique ear notch. Mice were housed in cages of 2, 3 and 4 and those from the same litter were kept in the same cage.

2.6.2 *PolgA$^{mut/mut}$ mouse*

PolgA$^{mut/mut}$ male and female mice were kindly donated by Tomas Prolla (University of Wisconsin, Washington, USA) and a breeding colony was subsequently established at the Wellcome Centre for Mitochondrial Research (Newcastle University). Each mouse was accurately genotyped and an RFID microchip (Destron Fearing, USA) implanted under the skin which was used for both identification and temperature monitoring purposes. *PolgA$^{mut/mut}$* male mice were housed with their heterozygous and wild type littermates in cages of 3-5.

2.7 Mouse husbandry and monitoring

Mice were kept at a temperature controlled room (25°C) and cages (25°C) with 12hrs light/dark cycle. They had ad libitum access to expanded RM3 chow diet (Special Diet Services, LSB Biotech) as detailed in appendix 3 and dH$_2$O. Enrichment materials such as pieces of wood and cardboard tunnels were placed in the cages. Mouse monitoring criteria (table 2.1) and a recording table were used to assess the health of mice on a weekly basis (Appendix section 1 and section 2).

2.8 Ethical considerations

All animal work was approved by the animal welfare and ethical review board-Newcastle University (reference BH136648) in compliance with the UK Home Office under project licence numbers P3F79C606 and P76987201.

2.9 Statistical analysis

Statistical analysis used to compare two groups at one time-point was an unpaired t-test. When the effect of age at two time-points were taken into account in one group a paired t-test was used. A one-way ANOVA (repeated measures) was implemented when one group was compared at three time-points and a two way ANOVA (repeated measures) was implemented when two groups were tested at more than two time-points. Graphpad Prism (v.8) was used to carry out statistical analysis and graphs were generated through this statistical package. The biological significance was determined as the p-value of below 0.05.

2.10 Mouse clinical scoring and monitoring

Clinical scoring was performed in order to assess the severity of disease, predict disease progression and implement endpoints in mice. The clinical scoring was designed by Dr Claire Richardson (Named veterinary surgeon, Newcastle University) and Dr Laura Greaves (Newcastle University) in order to evaluate the welfare of mice quantitatively (Table 2.1). The clinical scoring criteria is based on eight characteristics which are further categorised into scores of 0= normal, 1= mild, 2= moderate and 3= substantial. In $PolgA^{mut/mut}$ mice, clinical scoring was carried out at 14 weeks of age (pre-intervention), 29 weeks of age (mid-intervention) and 43 weeks of age (post-intervention) in order to observe any changes in each group of mice with age and/or as a result of the exercise intervention. In C57BL/6J mice clinical scoring was carried out at 14 months of age (pre-intervention), 18 months of age (mid-intervention) and 22 months of age (post-intervention). Body weight was recorded on a weekly basis

on the same day and time in order to eliminate effects of circadian cycle changes as part of the clinical scoring assessment.

Table 2.1. Mouse monitoring criteria. Clinical phenotypes of *PolgA*^{mut/mut} and C57BL/6J mice were assessed based on a scoring system (Richardson and Greaves, 2015).

Characteristic	Score	0- Normal	1- Mild	2- Moderate	3- Substantial
1	Weight	No weight loss / gain	5-15% weight loss	15-20% weight loss	Over 20% weight loss
2	Coat- general	Normal	Slight lack of grooming	Starey	
3	Skin Tone	Normal	Tents, returns to normal in 1-2 seconds	Tents, persists	
4	Behaviour	Normal	Subdued but responsive. Animal shows normal behaviour patterns. Interacts with peers	Subdued- animal shows subdued behaviour. Little peer interaction. May show aggression.	Animal unresponsive to extraneous activity and provocation even when provoked.
5	Posture and mobility	Normal	Transient hunched posture, especially after dosing. Normal mobility	Hunched intermittently. Reduced mobility	Hunched persistently 'frozen'. No spontaneous mobility.
6	Abdominal distension	None	None	Abdominal distension up to the size expected in late pregnancy	Severe abdominal distension beyond that of late pregnancy affecting locomotor and / or breathing patterns.
7	Foot colour	Normal	Whitening of feet due to mild anaemia	Whitening of feet due to moderate anaemia	Feet are completely white due to severe anaemia
8	Faeces	Normal	No diarrhoea or transient diarrhoea	Intermittent or continuous diarrhoea (>72h). No dehydration.	Continuous diarrhoea (>72h) with faecal soiling of perineum and/or dehydration.

2.11 Mouse Cardiac Magnetic Resonance Imaging (cMRI)

2.11.1 *Mouse preparation pre- and post- cMRI*

Cardiac Magnetic Resonance Imaging (cMRI) was carried out on anaesthetised mice (5% isoflurane, 1.5% O_2, 0.3ml/min flow rate) in order to assess cardiac function. Mice were prepared by having their hair removed from the ECG contact regions and eyes lubricated with an ointment prior to the scan. The amount of isoflurane and oxygen flow rate was monitored to ensure that the mice were fully anaesthetised, and their breathing rate was within the normal range (~25-40 breaths/min). Mice were secured inside the MRI machine using a pneumatic pillow and skin tapes (figure 2.1, left image). A rectal thermometer was used to monitor the temperature of mice throughout the scan as this may affect their heart rate. Mice were warmed inside the MRI machine with a heater fan tube to avoid hypothermia. Post-scan, mice were transferred to a heating pad for recovery and were housed individually for an hour before being transferred to their original cages.

2.12 Cardiac MRI

CMRI was carried out using a 7-Tesla horizontal bore microimaging system (Varian Inc, Palo Alto, CA, USA) equipped with a 12cm microimaging gradient insert (40 gauss/cm) (figure 2.1, right image). Mice were scanned in supine position where parameters including heart rate and breathing rate were kept stable to ensure limited respiratory artefacts during the scan. Scout scans were obtained using Vnmrj software to ensure left ventricular (LV) short and long axes were obtained in the correct orientation. Respiratory and ECG-gated cine-MRI images were obtained following a general shimming process to homogenise the MR magnet. A total of 20 phases per cardiac cycle from each mouse was obtained to measure global cardiac function. Sufficient contiguous short axes slides of 1mm thick in plane resolution of ~1mm/pixel and temporal resolution of 40-50ms was obtained to cover the whole LV depending on the size of the LV and the heart rate.
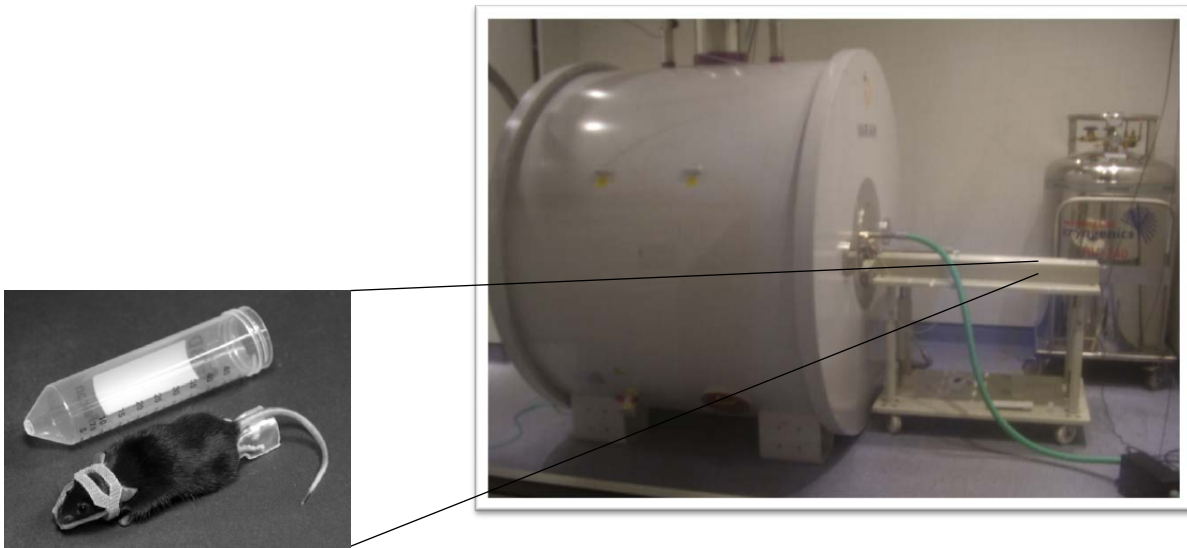
Figure 2.1. MRI system compatible for mice. The mouse was placed on a pneumatic pillow to allow rapid physiological interfacing (left image). Oxygen and isoflurane was delivered through a nosecone throughout the scan.

2.12.1 *MR image analysis*

The obtained cardiac MRI scans were used to track cardiac measures and short-axis images were analysed in Segment v2.0 (http://segment.heiberg.se) by semi-automatically tracing epicardial and endocardial borders as shown in figure 2.2. LV segmentation ensured volume measurements at the end of systole and diastole were accurate. Cardiac function measurements including LV mass (LVM), and the LV functional parameters including the end diastolic volume (LVEDV), end systolic volume (LVESV) as well as stroke volume (SV), ejection fraction (EF) and cardiac output (CO) were analysed by two investigators independently blinded to the experiment design at both time points (pre- and post-intervention). Due to fluctuations in body weights, left ventricular mass, volume measurements and cardiac output were also normalised to body weight for each mouse.
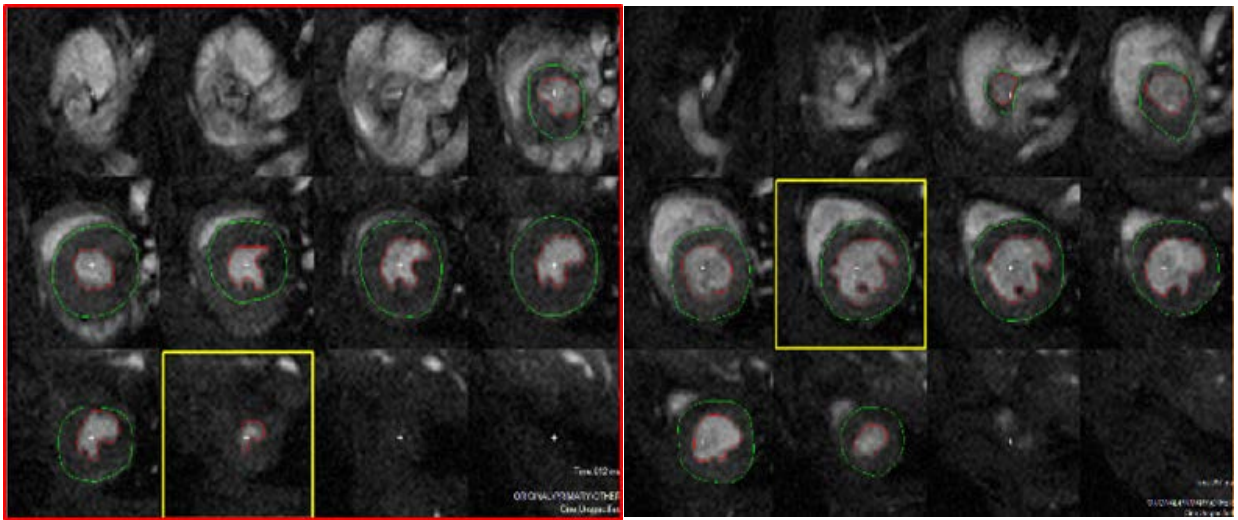
Figure 2.2. ECG-gated cine cMRI images in segment software. A) LV segmentation at the end of systole (ES) where LV is in its smallest form. B) LV segmentation at the end of diastole (ED) where LV is at its largest stage. The volume difference between ED and ES determines the stroke volume (SV).

2.13 Oxymax metabolic treadmill

Oxymax (Columbus instrument, Ohio, USA) is a system designed to monitor oxygen consumption (VO_2) and carbon dioxide production (VCO_2) while the mice are running on the one-lane enclosed metabolic treadmill chamber (figure 2.3). The open system pumped air through the test chamber and gas sensors and then expelled into the atmosphere. The O_2 and CO_2 content of the atmospheric air were tested periodically, and the changes were recorded to compute VO_2 and VCO_2 as well as respiratory exchange ratio (RER) and heat generated at three time points (pre-, mid- and post-exercise intervention). During calibration, the reference air measurements were taken as well as the animal weight to equilibrate the system for each mouse. Sample air flow rate was set to 4-5L/min. Depending on the size of the mouse, gas flow rate changed i.e. for a mouse of up to 40g the flow rate was set to 0.5L/min based on handbook recommendations. The pressure of the gas was set to 800mmHg with tank output pressure of 10psi. Coarse and fine gain knobs were used to adjust room O_2 and CO_2 readings making sure O_2 was within 20.88-20.95% reading and CO_2 was within 0.04-0.06% range. Both sedentary and exercised mice were initially acclimatised to the treadmill lane and running protocol one week prior to the actual measurements by being placed on the motionless treadmill for 5 minutes, followed by a walking speed of 10cm/sec for 5 minutes. For actual test measurements, mice were

subjected to a 20 minute run in an enclosed chamber at 20cm/s which included 5 minute warm-up and 5 minute cool-down. Mice were homed individually for 30 minutes post-testing before returning back to their original cages.
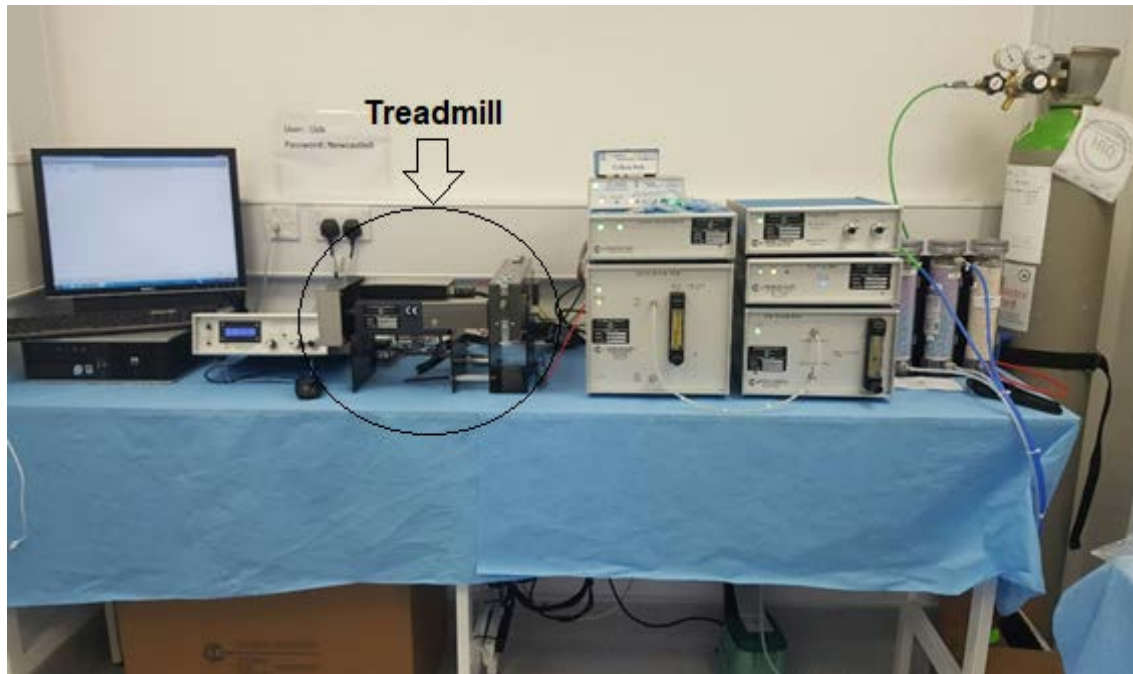
Figure 2.3. Single-lane Oxymax metabolic treadmill system. O_2 and CO_2 gases were calibrated and normalised to room gas content pre-testing.

2.14 Treadmill running protocol

Exercised mice were first acclimatised to the 5-laned treadmill (Panlab, Harvard apparatus, USA) and environment 5 days prior to the start of the intervention for two minutes with the treadmill switched off on day one, at 17cm/s for one minute on day two, at 17cm/s for two minutes on day three, at 17cm/s for seven minutes on day four and 17cm/s for 10 minutes on day five (figure 2.4). In this treadmill protocol, only the exercised mice are subjected to endurance exercise whereas the Oxymax metabolic treadmill is carried out at two time points only (pre- and post-intervention) in exercised and sedentary animals.

Exercise intervention in *PolgA^{mut/mut}* mice commenced at four months of age and terminated at 11 months of age. The speed of treadmill running remained at 20cm/s for 40 minutes from week two onwards for the duration of six months, four

times/week. A five minute warm up and cool down periods were included in each run at 12cm/s. Sedentary mice were allowed to carry on their normal cage activity while exercised mice were running on the treadmill.

Exercise intervention in C57BL/6J mice commenced at 16 months of age and ended at 22 months of age due to the fact that no long term physiological benefits of exercise was seen in *PolgA^{mut/mut}* mice. Mice were acclimatised to the treadmill in the same way as the *PolgA^{mut/mut}* mice. The speed at which mice were running remained at 20cm/s for 30 minutes for the duration of the study three times/week plus five minutes of warm up and cool down at 12cm/s.

Figure 2.4. Multi-lane air-puff equipped treadmill. Mice were allowed to run alongside each other on the 5-laned treadmill.

2.15 Non-invasive blood pressure monitor

Non-invasive blood pressure (NIBP) system (Columbus instrument, Ohio, USA) was used to measure tail arterial blood pressure (figure 2.5). Mice were weighed and placed inside a suitably sized restrainer with a nose cone and had blinded vision to ensure a comfortable fit and limited stress during the test. Mice were acclimatised to the restrainer one week prior to the test for five minutes/day. For the actual

65

measurements, the mouse's tail was warmed in lukewarm water to ensure good circulation. Room temperature was controlled, and the mouse was warmed with a heater fan to avoid hypothermia during the test. The occlusion cuff was placed near the tip of the tail and was set to a maximum of 200mmHg whereas the smaller sensor cuff was placed near the base of the tail proximal to the occlusion cuff. The pressure of the sensor cuff was set to up to 45mmHg depending on the size of the mouse. Both cuffs were tested to ensure no leakage was detected in the system by generating a generic BP curve as demonstrated further in 8-Channel Non-Invasive Blood Pressure Monitor NIBP-8 User's Manual 0219-008M. Blood pressure was taken at two time points pre- and post-intervention to ensure the stress exerted to mice is minimal. Each time three measurements were taken from each mouse leaving a one minute gap between each test to allow full arterial occlusion and expansion. Heart rate (HR) was also measured at the same time in order to calculate blood pressure from mice.
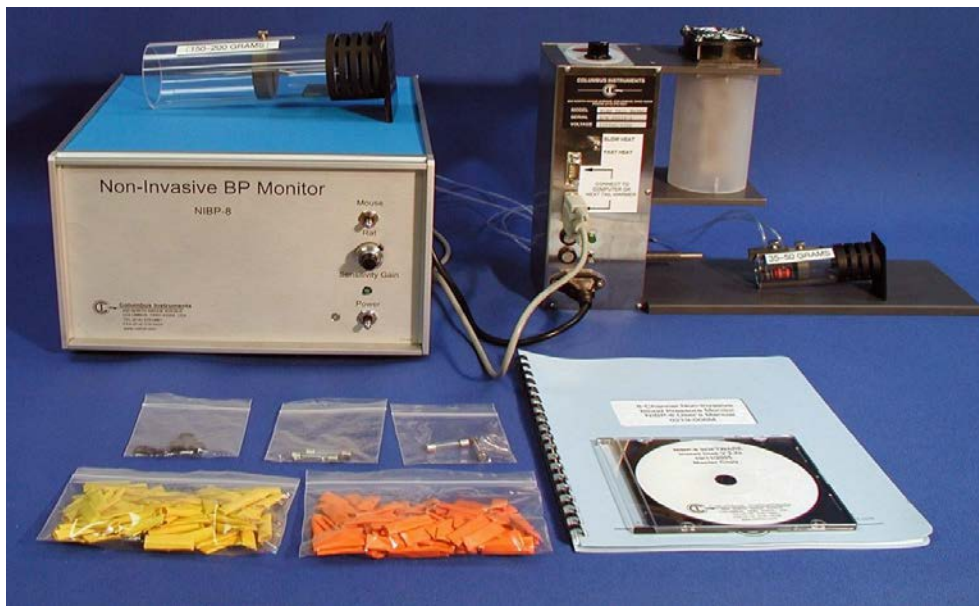
Figure 2.5. Blood pressure monitor system. Mice were restrained secure during BP measurements to eliminate movements and increase sensitivity to noise ratio.

2.16 Mouse behavioural tests

2.16.1 *Open field testing (OFT)*

Open field testing (OFT) was carried out using an enclosed arena with a tablet underneath (figure 2.6) to assess behavioural and locomotor activity of mice using the mousetrap software (Ryanware v4.0). Since the OFT is time, handling and sex dependent, the mice were acclimatised to the testing procedure and environment for two minutes each day for a week prior to the test. The acclimatisation period limits any fear-related behaviour such as stretch attend in which mice elongate their abdomen for any movement, as well as activity in the corners of the open field device. Mice were tested during a five minute period where they were placed inside an enclosed arena on a black background. The quality and quantity of activity and behavioural state was recorded using a series of measures such as rearing frequency, distance travelled, velocity of movements, and number of touches. Step length was calculated as the total distance moved divided by the total number of touches. The apparatus was cleaned after each use to limit inquisitiveness in mice due to unfamiliar smells or situations. The temperature, humidity and lighting remained constant for every single test.
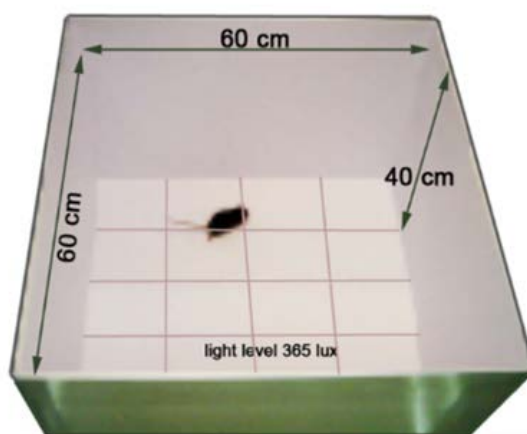
Figure 2.6. Open field testing device to record locomotive and behavioural changes within 5 minutes. Mice were allowed to carry out normal cage activity while in the arena with minimal environmental distractions.

2.16.2 *Rotarod*

The rotarod (Ugo Basile, Italy) is a multi-lane device that measures coordination, endurance, the grip strength and motor activity of mice (figure 2.7). The test was carried out by placing a mouse on a set speed rotating rod and the time it took for the animal to fall was recorded as the latency to fall. Since this is a learnt test, the mice were only acclimatised to the device once prior to the first test. The mice were tested for their balance, grip strength and motor coordination over three trials and the latency (time to fall) to fall was recorded. The ramp speed was set to 5rpm and steadily increased up to 40rpm by 300s.

Figure 2.7. Rotarod device to measure latency to fall. The multi-lane device allowed for grip strength and coordination testing independently over three trials.

2.17 Tissue harvest

Mice were culled by cervical dislocation and organs were harvested, weighed and processed under a sterilised fume hood according to the tissue harvesting protocol in table 1 of appendix 2. Blood was aspirated from the heart by cardiac puncture. The heart, liver, skeletal muscle, urogenitus and the rest of the organs were harvested accordingly.

2.18 Blood and serum collection

Tail vein blood was collected from approx. 1/3 along the length of the tail tip using a sterilised lance to make an incision and blood was collected using a microvette containing lithium heparin. Mice were placed inside a warming cabinet (39°C) for up to 10 minutes to dilate blood vessels prior to sampling. Mice were placed in a suitably sized restrainer with their tail secured with an end cap. A maximum of 10% of total blood volume was taken at any time point according to the license allowance. Serum was obtained by centrifugation of whole blood at 8000rpm for 10 minutes and stored at -80°C for long term.

2.19 Mouse tissue preparation for histochemical analysis

2.19.1 *Fixed cardiac muscle preparation*

Hearts were sectioned longitudinally through the interventricular septum. The right side of the heart was fixed in 4% paraformaldehyde (4% PFA) intra-septal side down inside a tissue cassette for no more than 48 hours. The hearts were then transferred to 70% ethanol solution at room temperature and were processed further first by dehydrating specimen in increasing ethanol gradient to remove water and formalin, next by clearing in histoclear to allow infiltration with paraffin wax and finally embed in paraffin wax at Newcastle University Biobank services. For sectioning, the cooled blocks of fixed right heart were sectioned (4µm) using a microtome (Leica Biosystems, UK) on glass superfrost slides (MSD) and were stored in 37°C oven at least for 48 hours before any histochemical procedure. The slides were then air-dried for one hours at room temperature before long-term storage at 4°C.

2.19.2 *Frozen cardiac muscle preparation*

The left side of the heart was slowly snap frozen in isopentane cooled to -150°C in liquid nitrogen for 15 seconds to maintain the integrity of organelles. The skeletal and cardiac muscle were processed this way to avoid ice crystal formation due to high water content of those tissues. The tissues were temporarily stored in liquid nitrogen

during full tissue harvest and were placed in -80°C freezer for long-term storage. For sectioning, the left side of the heart was mounted intra-septal side down on Whatman filter paper with a small amount of OCT cryo-embedding medium. Once the OCT turned white at -20°C (inside Cryostat), the tissue was submerged in liquid nitrogen until fully frozen using previously cooled forceps and scalpels. Sections were cut at 8μm using an OFT 5000 Cryostat (Bright) on to a polysine slides (Thermofisher, UK) and air-dried at room temperature for an hour before being stored at -80°C freezer in sealed slide mailers. A small chunk from the LV (~25mg) was cut by a cooled sterilised scalpel for tissue homogenisation and subsequent DNA extraction. Similarly a small chunk of quadriceps (~100-200mg) from the right leg was cut for protein extraction from each mouse and stored in a microcentrifuge tubes for future cytokine analysis.

2.20 Histochemistry

2.20.1 *H&E*

Haematoxylin and Eosin (H&E) staining was carried out to assess the morphology and structural integrity of tissues. 4μm paraffin embedded cardiac sections were deparaffinised in Histoclear (2x10 minutes) and rehydrated in an ethanol gradient (100%, 95% and 70%) each for 5 minutes. Slides were then washed in dH_2O for 5-10 minutes and stained in Harris haematoxylin for 8 minutes to stain nuclei blue/black. The slides were washed in running tap water subsequently until ran clear and 'blued' in Scott's tap water for 1 minute to blue the nuclei stain. Slides were washed in running tap water for 5 minutes and counterstained in eosin for 1 minute to stain other basic proteins such as cytoplasm, muscle fibres and the extracellular matrix pink or red. After a brief wash under running tap water, the sections were dehydrated in a graded ethanol series (70%, 95%, and 100%) and cleared in two changes of Histoclear. Sections were mounted in DPX and visualised using Zeiss Axioimager microscope.

2.20.2 *Cardiomyocyte width analysis*

Cardiomyocyte width analysis was performed in Zen 2.5 software (Zeiss) by measuring the shortest cross-sectional width of individual cardiomyocytes from 5 random fields of x20 magnification. 50 cardiomyocytes per field were selected and the average width of cardiomyocytes were calculated. Since cardiomyocytes come in various shapes and sizes, analysis was performed only on transverse cardiomyocytes. The analysis technique was based on the publication by Huynh *et al*, (2010) (figure 2.8).
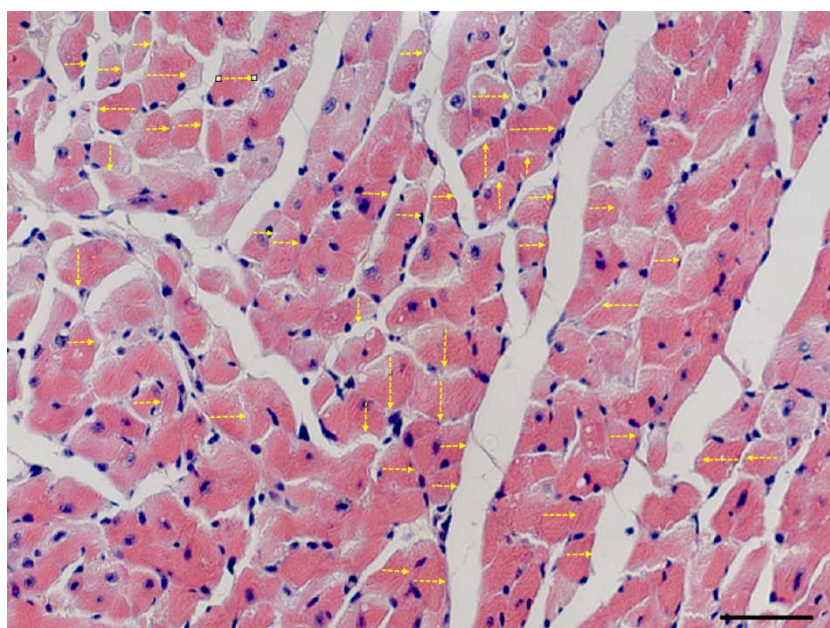
Figure 2.8. Cardiomyocyte width analysis. Representative example of H&E image for cardiomyocyte width analysis. The shortest width of cardiomyocytes were measured as shown by yellow arrows. Cardiomyocytes are shown in dark pink/red; nuclei are shown in blue. Magnification x20. Scale bar=100µm.

2.21 Sequential COX/SDH histochemistry

Cytochrome *c* oxidase/ succinate dehydrogenate (COX/SDH) histochemistry was carried out on 8µm cryo-sectioned mouse hearts. Sections were air-dried for an hour at room temperature and incubated in COX histochemical media (~100µl/section) (100 µM cytochrome c, 4mM DAB and 20µg/ml catalase from bovine liver in 0.2M phosphate buffer, pH 7.0) at room temperature for 20 minutes. Sections were then washed in PBS (3x5 minutes) and incubated in SDH histochemical medium (1.5 mM NBT, 130 mM sodium succinate, 1.0 mM sodium azide and 0.2 mM PMS in 0.2M

phosphate buffer pH 7.0) at room temperature for 10 minutes. Sections were then washed in PBS (3x5mins) and dehydrated through an ethanol gradient (70%, 95%, 100%) for 2 minutes each and cleared in histoclear (National diagnostics, Atlanta, Georgia, USA). Sections were mounted on DPX (BDH laboratory, UK) and stored at room temperature for 24 hours until imaging. To minimise time delay, a maximum of 10 slides were processed at a time, with further staining took place straight after. Two serial sections from each mouse heart were processed to reduce variability between experiments. COX and SDH histochemistry were also performed individually using the same protocol as above but with incubation in COX or SDH histochemical media only.

2.21.1 *Quantification of COX/SDH histochemical analysis*

Sections were imaged using Nikon TiE wide field invert microscope. Five regions at x10 magnification from the left ventricle were randomly picked and imaged. For direct comparison, areas with transverse cardiomyocytes were chosen from each section. An auto-white balance was used across all slides and the same settings i.e. same LED power and gain were used across all sections. Images were analysed using NIS elements software to distinguish between the brown (COX functional) and blue (COX deficient) fibres. The software uses the RGB thresholding method to separate and mask blue COX-deficient fibres from the whole tissue area (figure 2.9). The percentage of COX deficiency is then calculated from the total tissue area versus total blue area. The LED intensity and RGB channel threshold remain constant across all the samples.
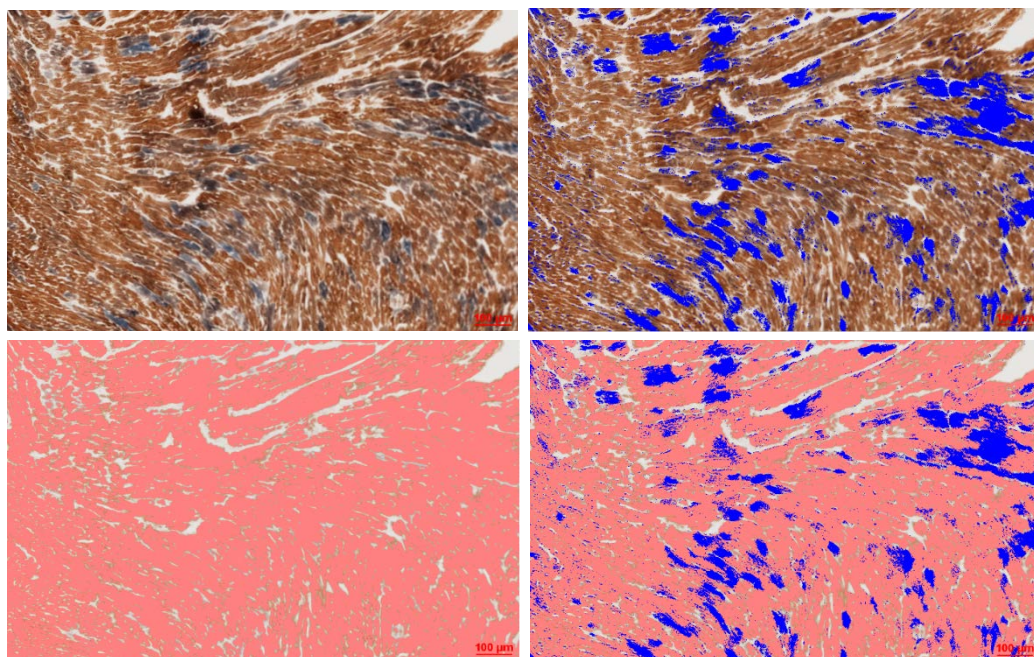
Figure 2.9. COX/SDH analysis. COX deficiency was quantified using NIS elements software RGB general analysis for COX/SDH histochemistry (top left image) by thresholding for COX deficient blue colour (top right image), pink tissue area (bottom left image), and combined merged channels (bottom right image). Magnification x10. Scale bars=100µm.

2.22 Masson Trichrome staining

Masson trichrome stain is a laboratory technique used to distinguish collagen from muscle tissue by utilising dyes that stain cell cytoplasm, collagen and nuclei. Transverse mouse fixed heart sections (4µm) were deparaffinised in 2 changes of Histoclear (2x10 minutes) and rehydrated in ethanol gradient (100%, 95%, 70% and dH$_2$O), each for five minutes. Sections were then incubated in Bouin's solution overnight at room temperature. This fixes the sections slowly allowing for better and crisper nuclear staining. Slides were then cooled in dH$_2$O and incubated in working Wiegert's iron haematoxylin for 5-10 mins to stain the nuclei blue/black followed by a 10 minute wash in deionised H$_2$O. Slides were then stained in Biebrich Scarlet-Acid Fucshin for 5 mins to stain the cytoplasm red and were subsequently rinsed in deionised H$_2$O. Staining was followed by a 5 minute incubation in working Phosphotungstic/Phosphomolybdic acid solution for uptake and incubation of aniline blue solution to stain collagen blue. After a brief washes under running tap water, slides were washed with 1% glacial acetic acid for 2 minutes to remove any excess stain. This is followed by a 2 minute wash in dH$_2$O and dehydration in 70%, 90% and

100% ethanol each for 3 minutes. The slides were cleared in Histoclear for 5 minutes and mounted on DPX. After drying at room temperature, the image acquisition took place using the Nikon Tie widefield microscope and images were analysed in NIS elements software.

2.22.1 *Cardiac fibrosis analysis*

Cardiac fibrosis was carried out using masson trichrome staining and quantified in NIS elements software using the RGB general analysis algorithm. The analysis was carried out by setting a threshold for each channel manually which were differentiated by the different colours (figure 2.10). Manual thresholding remained consistent across all the samples and the percentage of blue collagen accumulation shown in yellow was quantified as the percentage of whole tissue section in green.
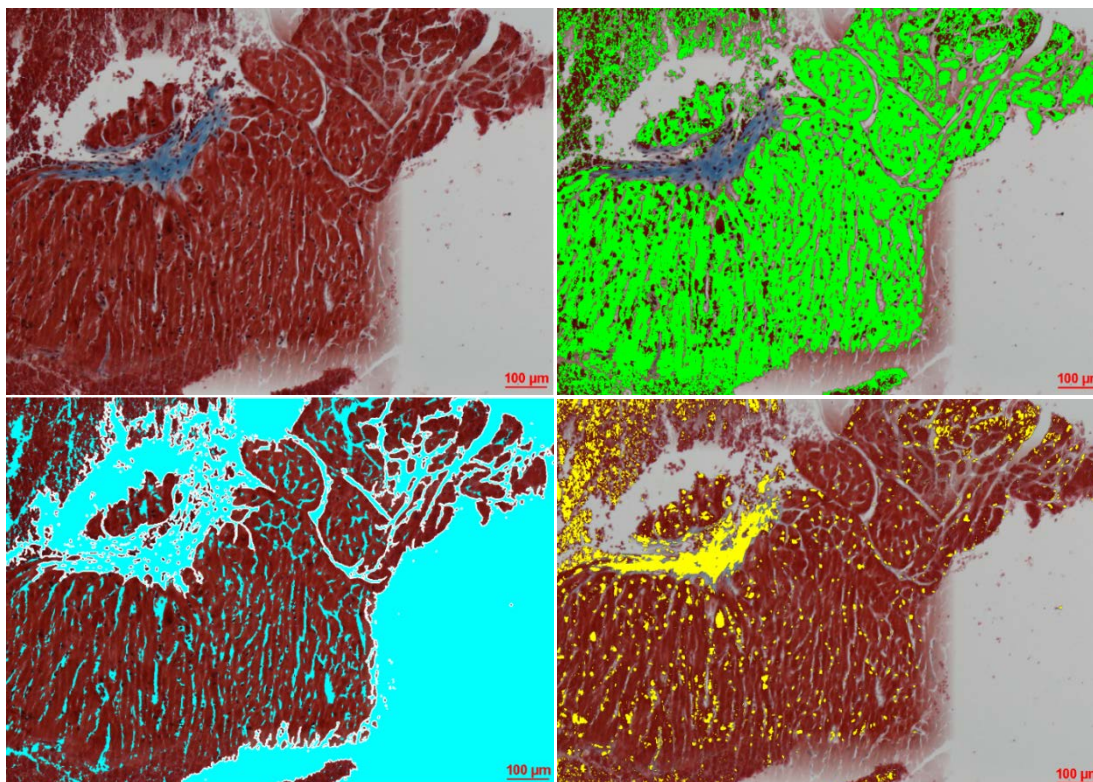
Figure 2.10. Cardiac fibrosis analysis. Fibrosis analysis by NIS elements quantifying the percentage of light blue collagen in the whole tissue section. Top right image represents all cardiomyocytes in green and bottom right image represents the distribution of collagen in yellow. Bottom left image show the background in blue which is subtracted from the total tissue area. Magnification x10. Scale bars=100μm.

2.23 Immunohistochemistry

2.23.1 *Cleaved caspase-3 immunohistochemistry*

Cleaved caspase-3 staining is used to detect apoptotic cells. 4µm mouse cardiac sections were deparaffinised in Histoclear (2x10 minutes) and dehydrated in an ethanol gradient (100%, 95%, 70% and dH$_2$O) for 5 minutes each. Sections were placed in citrate buffer (10mM, pH 6.0) in an antigen retrieval unit to reveal epitopes under a heat and pressure cycle of 20 minutes. Slides were allowed to cool in the unit for 20 minutes and were then washed under running tap H$_2$O and then incubated in 10% normal goat serum (NGS) in TBST for 30 minutes. TBST washes were carried out subsequently (3x5minutes) and primary antibody solution (Rabbit anti-active caspase 3- cleaved (Merck Millipore, Hertfordshire, UK) was diluted in TBS (1:35) and applied to sections overnight at 4°C. TBST washes were carried out (3x5 minutes) and sections were incubated in HRP-labelled polymer (Dako envision kit) for 30 mins. Slides were washed in TBST 3x5 mins followed by incibation on a DAB+ chromogen mixture (100µl DAB in 1ml of substrate buffer) for 10 minutes. Slides were then washed in dH$_2$O briefly and dipped in Haematoxylin (Sigma, Misouri, USA) solution to counterstain nuclei for 10 minutes. Slides were washed in dH$_2$O for 10 minutes and rehydrated by passing through an ethanol gradient (70%, 95% and 100%) for 10 seconds each with two changes of Histoclear. Sections were mounted on DPX and visualised using Image Scope software (Aperio Scanner) in NICR (Newcastle University).

2.23.2 *Cardiac active cleaved-caspase 3 analysis*

Cardiac active cleaved caspase-3 staining (CC3) was quantified by nuclear staining algorithm in Imagescope software (http://aperioscanner.ncl.ac.uk/Login.php) in which active caspase-3 labelled cells were stained brown by HRP-conjugated CC3 antibody and nuclei were stained blue by haematoxylin (figure 2.11). Number of dark brown regions were counted, and the frequency of apoptotic cells was quantified as a percentage of the total count.
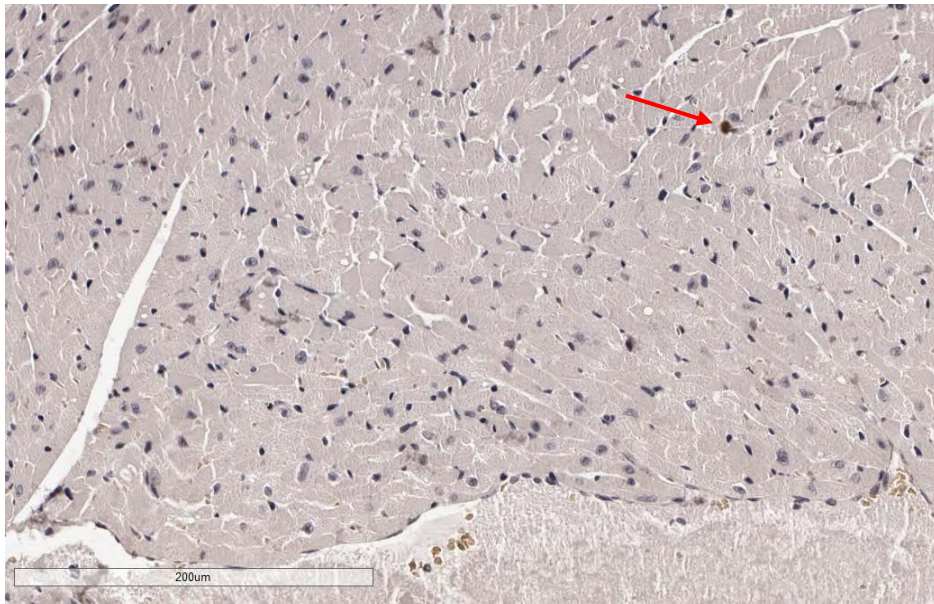
Figure 2.11. Cardiac active cleaved caspase- 3 analysis. Percentage of dark brown apoptotic nuclei (represented with red arrow) was quantified against normal blue nuclei. Magnification x10. Scale car=200µm.

2.24 Immunofluorescence

2.24.1 *NBTx, laminin immunofluorescence assay*

NBTx assay was performed to support the findings of COX/SDH histochemistry and furthermore categorise cardiomyocytes into COX positive, COX intermediate and COX negative activity using a numbering system based on the COX activity of wild-type tissue. This assay reveals the dual affinity of oxidised PMS (electron donor) for molecular oxygen in fully functional OXPHOS system and for NBT in a dysfunctional OXPHOS system. Cardiac cryosections (8µM) were incubated in cytochrome *c* solution (500µM in 0.1M PBS pH 7.0) for 10 minutes at room temperature. Sections were subsequently washed in PBS and incubated with NBTx solution containing 130 mM sodium succinate, 2mM NBT, 0.2 mM PMS in 0.1M phosphate buffer (pH 7.0) for 20 minutes and washed briefly in PBS. Sections were fixed in 4% paraformaldehyde for 10 minutes at room temperature and washed subsequently in TBST for 5 minutes. Sections were then permeabilised in a graded methanol series (70% and 90%) for 10 minutes and 100% for 20 minutes. They were then taken down the methanol gradient (90% and 70%) for 10 minutes each. The slides were washed in TBST for 5 minutes and incubated with 10% Normal Goat Serum (NGS) for 30 minutes at room temperature.

Primary antibody (anti-laminin polyclonal antibody produced in rabbit) diluted in TBS (1:75) was added to the sections and incubated overnight at 4°C. To best detect the cardiomyocyte boundary post NBTx assay, the concentration of laminin primary antibody was first optimised using various dilutions of anti-Laminin antibody (Sigma-Aldrich) in TBS (1:200, 1:100, 1:75 and 1:50). The sections were then washed in TBST (3x5 minutes) and incubated with secondary antibody solution (goat anti-rabbit IgG 488) (1:200) for 2 hours and washed with TBST (3x5 minutes). Sections were rehydrated in ethanol gradient (70%, 95% and 100%) 2 minutes each, cleared in two changes of Histoclear (10 minutes) and mounted on prolong gold. The sections were then left to dry overnight at room temperature and imaged using Zeiss Axioobserver/SDI/LSM800 inverted microscope to take five random snapshots of x10 magnification from LV transverse cardiomyocytes. The sections were analysed using the immunoanalyzer software similar to quadruple OXPHOS immunofluorescence analysis which is explained further in section 2.1.1.2. A numbering system was used to categorise cardiomyocytes into positive (<-3 SD from the mean optical density (OD)), intermediate (-3SD<x>-6SD from the mean OD), negative (<-6SD from the mean OD) based on the activity of NDUFB8 and MTCOI in the wild-type *PolgA* $^{mut/mut}$ mice tissue.

2.24.2 *Quadruple OXPHOS immunofluorescence*

2.1.1.1 *Optimisation*

An array of antibody concentrations were tested for the specific detection of two OXPHOS complexes, Complex I (NDUFB8 subunit) and Complex IV (MTCOI subunit). The optimisation included a series of primary antibody dilutions as described in table 2.2. Each cardiac section was only incubated with one dilution of primary antibody and the same secondary antibody as in table 2.3.

Primary antibody	Primary antibody dilution	Host	Producer (product number)
NDUFB8 (IgG1)	1:30	Mouse	Abcam (Ab110242)
	1:50		
	1:75		
MTCOI (IgG2a)	1:200	Mouse	Abcam (14705)
	1:150		
	1:100		
Laminin	1: 400	Rabbit	Sigma-Aldrich (L9393)
	1: 300		
	1: 200		
	1:100		
	1:75		
	1:50		

Table 2.2. Optimisation of primary antibody concentration for paraffin-embedded cardiac tissue. Secondary antibodies are the same dilution as described in table 2.3.

2.24.2.1 *Final OXPHOS immunofluorescence assay*

Fixed heart sections (4µm) were deparaffinised in Histoclear (2x10 minutes) and rehydrated through an ethanol gradient (100%, 95%, and 70%) each for 5 minutes and washed under tap water for 5 minutes. Antigen retrieval was carried out using EDTA pH 8 in a pressure cooker for 20 minutes and washed subsequently in TBST (3x5 minute). Sections were incubated in 10% NGS solution for 30 minutes and washed in TBST (3 x 5 minutes). The primary antibody cocktail was made (table 2.3) and sections were incubated with the primary antibody overnight at 4ºC. No primary

control (NPC) slides were only incubated with anti-laminin antibody solution (1:50) in TBST. The sections were washed in TBST (3x 5 minutes). Both the test and NPC slides were incubated with the secondary antibody cocktail (table 2.3) for two hours and washed subsequently in TBST in the dark (3x5 minutes). The sections were then mounted in prolong gold to extend their fluorescence life and were left to dry at room temperature overnight. For better retention of fluorescent signal, slides were stored at 4ºC. Sections were then analysed using an inverted microscope (LSM800/SDI) (Zeiss Axio-Observer) against an NPC slide. The monochrome camera used filter cubes for detection of light at 405nm, 488nm, 546nm and 647nm. The smart path was used to select two filters in one track (AF488 and AF647) and (AF405 and AF546) in another track. The pinhole remained consistent across all samples at 34µM, 1AU). Master gain and digital offset also remained consistent for all slides. Images were analysed using an in-house immunoanalyzer software.

Antibody	Host	Dilution	Producer (product number)
Primary antibodies			
Laminin	Rabbit	1:50	Sigma-Aldrich (L9393)
VDAC-I (IgG2b)	Mouse	1:300	Abcam (Ab14734)
MTCOI (IgG2a)	Mouse	1:150	Abcam (14705)
NDUFB8 (IgG1)	Mouse	1:50	Abcam (Ab110242)
Secondary antibodies			
Anti-rabbit IgG Alexa Fluor 405nm	Goat	1:100	Thermofisher Scientific (A-31556)
Anti-mouse IgG2b Alexa Fluor 488nm	Goat	1:200	Thermofisher Scientific (A-31556)
Anti-mouse IgG2a Alexa Fluor 546nm	Goat	1:200	Thermofisher Scientific (A-31556)
Anti-mouse IgG1 Alexa Fluor 647nm	Goat	1:200	Thermofisher Scientific (A-31556)

Table 2.3. Primary and secondary antibodies for immunofluorescent detection of OXPHOS complexes, mitochondrial mass (VDAC-1) and cardiomyocyte boundary marker (Laminin).

2.1.1.2 Densitometry analysis using immunoanalyzer software

Quadruple OXPHOS immunofluorescent images were acquired and .czi files were uploaded on the immunoanalyzer software. Laminin was used to detect cardiomyocytes where possible based on the threshold and size of the fibres (figure 2.12). Manual drawing around the cardiomyocytes outlined by laminin, was

sometimes required if the signal was weaker in some areas. The software used a MATLAB based technique (R2015a) to convert .czi images to low resolution Tiff files for each channel. The mean optical density (OD) of each channel was measured on each section i.e. OD-COXI, OD-NDUFB8 and OD-VDACI. The NPC slides were also analysed to determine the background signal intensity of each channel. Laminin was used in the NPC slides to determine the background channel signal intensity on a fibre by fibre basis. Data were merged and uploaded to R studio Inc. (Version 0.97.551) at (http://research.ncl.ac.uk/mitoresearch/).
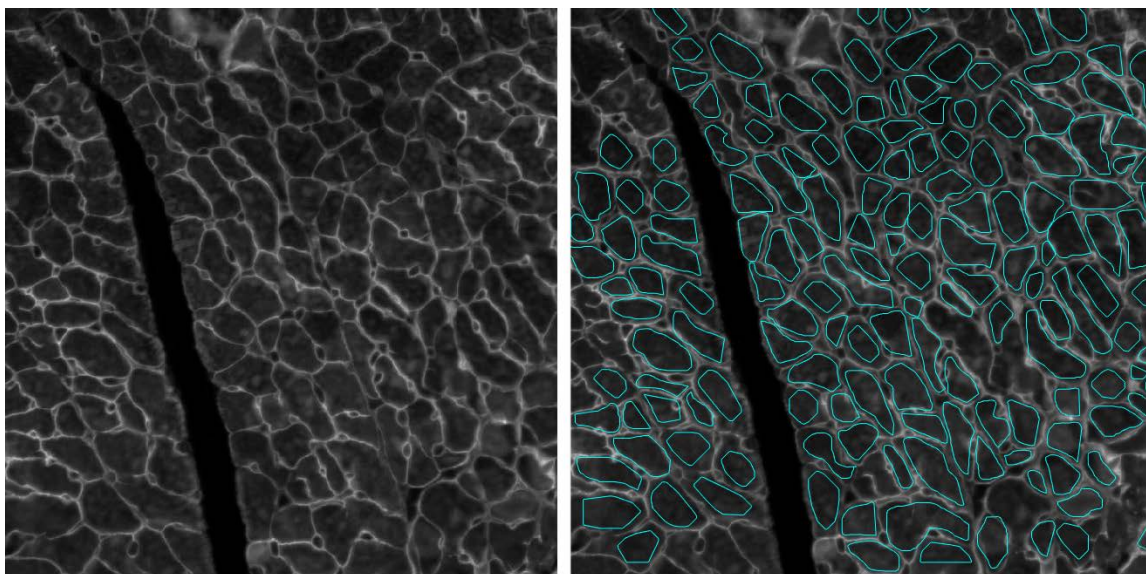
Figure 2.12. Laminin outlining cardiomyocytes. Laminin was detected (left image) and cardiomyocytes were semi-automatically selected through immunoanalyzer software (right image).

2.1.1.3 Quadruple immunofluorescence analysis

Analysis of optical density data that were corrected for background signal was used to normalise the data i.e. OD VDACI, OD NDUFB8, OD MTCOI. A plot of NDUFB8 vs MTCOI was generated by the software for each sample. Linear regression analysis of the data enabled an estimated level of MTCOI and NDUFB8 for each fibre based on porin (VDAC-I) levels. Z-scores are used to describe the deviation of levels in NDUFB8 and MTCOI from the predicted levels described in table 2.4. The classification of fibres this way has been validated, published and used extensively in the past (Rocha *et al,* 2015).

Classification	Z-score boundaries (standard deviation)
Porin (VDAC-I)	
Very low	Z<-3
Low	-3<z<-2
Normal	-2<z<2
High	2<z<3
Very high	z>3
MTCOI and NDUFB8	
Negative	Z<-6
Intermediate negative	-6<z<-4.5
Intermediate positive	-4.5<z<-3
positive	z>-3

Table 2.4.Cardiomyocytes classification based on defined and optimised z-score values.

2.25 DNA extraction form mouse tissues

2.25.1 *DNA homogenisation using pestle and mortar*

Frozen LV cardiac muscle (25mg) was homogenised using a sterilised and autoclaved pestle and mortar. Tissue was broken down carefully by addition of liquid nitrogen and the samples were scraped off with cooled scalpel to a sterile collecting tube for DNA extraction. This method was proven to not be free of contamination which resulted in lower DNA yield and in general is a slower process. Hence a faster,

more consistent method of homogenisation was tried with a TissueLyser II (Qiagen) as listed below.

2.25.2 *DNA homogenisation using TissueLyser II*

Frozen LV cardiac muscle (25mg) was homogenised using TissueLyser II (Qiagen) with 80µl cooled PBS and a sterilised titanium bead (Qiagen) in a sterilised and autoclaved 2mL tube. The tissues were shaken vigorously at a frequency of 20Hz for a total of 4 minutes until all broken down. The beads were taken out carefully and tissues were briefly centrifuged ready for DNA extraction. This method provided a more consistent DNA yield within an efficient time.

2.25.3 *DNA extraction*

Isolation and purification of DNA from homogenised cardiac muscle was carried out using a QIAamp DNA mini kit (Qiagen) according to the manufacturer's instructions in QIAamp DNA mini and blood handbook (fifth edition). DNA extracts were aliquoted in smaller volumes of 20µl and stored in -20°C for future use.

2.25.4 *DNA purification*

DNA concentration was assessed using the NanoDrop 2000 spectrophotometer. The Nanodrop was cleaned initially with 1µl of nuclease free dH_2O. 1µl of ATL buffer was loaded on the Nanodrop to calibrate the system. For measurements, 1µl of each sample DNA was loaded and the absorbance was determined at 260/280nm and 260/230nm range. The initial range determined the purity of DNA. A ratio of ~1.8 is acceptable for pure DNA. The latter 260/230nm range was used as a secondary measure of nucleic acid purity. A ratio of less than ~2.0 indicated a source of contamination. The concentration of DNA obtained was in the units of ng/µl.

2.26 Real-time PCR

2.26.1 *Preparation of reagents*

Primers (table 2.6) were prepared by reconstitution using nuclease-free water under the microflow OMNI PCR workstation (ASTEC). Primers (ND1 and B-actin) were diluted from 100µM to 10µM using nuclease-free water and stored at -20°C. Prior to PCR, all the pipettes including p5,p10,p20,p100, p200 and p1000 as well as annotated 96-well plate, adhesive film, annotated microcentrifuge tubes, pipette tips and autoclaved dH_2O were placed in PCR UV hood (Bio air instruments) for 30 minutes to eliminate contamination rate. Other reagents such as SYBR green, primers and DNA samples were left on ice to thaw. Two x15µl/well PCR-amplification reaction mixtures (master-mixes) were prepared, one for mitochondrial targeted gene (ND1) and one for a housekeeping nuclear-encoded gene (B-actin). Each master-mix consisted of ND1 primers (forward and reverse) (0.6µl/well) or B-actin primers (forward and reverse) (0.6µl/well) as well as SYBR green (10µl/well) and DEPC treated dH_2O (3.8µl/well) (Sigma). The reaction mixture for 20 wells is listed in table 2.5. Primer sequences are outlined in table 2.6.

Master mix	Volume	Supplier
Forward primer (0.6µl/well)	12µl	Eurofins Genomics
Reverse primer (0.6µl/well)	12µl	Eurofins Genomics
DPEC dH$_2$O (3.8µl/well)	76µl	Sigma Aldrich
Platinum SYBR Green (10µl/well)	200µl	Thermofisher

Table 2.5. Reagents used for PCR reaction mixtures for 20 wells. 5µl of sample gDNA is added to each well following master mix addition.

Primers	Sequence
Mouse ND1-F	5'-ACA CTT ATT ACA ACC CAA GAA CAC AT-3'
Mouse ND1-R	5'-TCA TAT TAT GGC TAT GGG TCA GG-3'
Mouse B-actin-F	5'-CCA TCT TGT CTT GCT TTC TTC A-3'
Mouse B-actin-R	5'-CCA CCG ATC CAC ACA GAG TA-3'

Table 2.6. ND1 and B-actin forward and reverse primer sequence. Primer sequences were used to amplify nuclear (β-actin) and mitochondrial DNA (ND1) genes.

The two reaction mixtures were vortexed briefly and 20µl/well of reaction mixture including master mix solution (15µl/well) plus gDNA (5µl/well) was added to each well in triplicate including the standard curve solutions. Three wells for ND1 and three wells for β-actin was left without gDNA sample to act as No Template Controls (NTC). The incubated 96-well plates were vortexed briefly ensuring consistent

mixture without bubbles within wells. DNA was amplified over 30 cycles according to the listed cycling conditions (table 2.7). The data obtained as CT values were averaged from triplicate results.

Cycling stage	Temperature
Initial denaturation	95°C for 3 minutes
35 cycles of denaturation	95°C for 30 seconds
Annealing	58°C for 35 seconds
Extension	72°C for 30 seconds
Elongation	72°C for 15 minutes

Table 2.7. Thermal cycling conditions for quantitative real time-PCR.

2.26.2 *Standard curve preparation*

Standard curve solutions were prepared using a high concentration DNA samples from mouse. A 10-fold serial dilution of sample DNA was loaded in triplicate on each well. Average CT values for each standard curve value was plotted against the dilution on a base-10 semi logarithmic graph with a line of best-fit. The equation of the line, slope and reaction efficiency of the plot was used to calculate the absolute quantification of gene of interest. The standard curve was acceptable only if R^2 was greater than 0.99.

2.27 Total cytokine Array muscle preparation

Cytokine array utilises a U-PLEX plate to detect the expression of cytokines present in the sample. A multiplex assay kit (MSD) was used to measure 10 analytes including IFN-γ, IL-1β, IL-2, IL-4, IL-5, IL-6, KC/GRO, IL-10, IL-12p70, and TNF-α

from protein extracts of mouse quadriceps. Frozen quadriceps from the left leg were homogenised manually using TissueLyser II as explained in section 2.24.2. Cell lysis and protein extraction was carried out by Tris Lysis buffer where tissue homogenates were incubated with Tris lysis buffer in 1:10 ratio. The resultant mixture was centrifuged at 12,000 rpm for 20 minutes at $4^{\circ}C$. The supernatant was removed and placed on ice-cold clean microcentrifuge tube for protein concentration determination by Bradford assay. Protein extracts was stored for long term in $-80^{\circ}C$ freezer.

2.27.1 *Protein quantification*

The amount of protein in each sample was quantified using Bradford assay. A standard curve solution is made using serial dilution of 1µg/ml Bovine Serum Albumin (BSA) to cover the range of protein values obtained from the sample, i.e. standards of 0, 2, 5, 10, 15 and 20µl were produced as shown in table 2.8.

BSA (µl)	dH$_2$O (µl)	Bradford reagent (µl)
0	800	200
2	798	200
5	795	200
10	790	200
15	785	200
20	780	200

Table 2.8.Bradford reagents for standard curve set up.

1µg/mL of each sample was added to 200µl Bradford reagent and 799µl of dH$_2$O. The higher the amount of protein present in the sample, the bluer the solution, the less protein available the browner the solution will turn. 250µl of each sample was loaded on a 96 well Bradford plates in duplicate and measured on a plate reader (Elx800) at 595nm. The concentration of standard curve samples were recorded and the concentration of proteins in samples were extrapolated from the linear graph generated.

2.27.2 *Cytokine analysis of mouse skeletal muscle*

A 10 spot/well multi-array 96-well plate uses antibodies to detect cytokines that are labelled with an electro-chemiluminescent compound (MSD SULFO-TAG). When a voltage is applied to the plate electrodes inside the MSD Sector instrument, the SULFO-TAG label binds to the electrode surface to emit light and determine the concentration of cytokines inside samples. Calibrators, buffers and control solutions were prepared according to the Mouse cytokine assay (multi-array system)

handbook. The concentration of cytokines were normalised to protein concentration measured using Bradford assay. Initially the U-plex plate is prepared by addition of 200μL of each biotinylated antibody to 300μl of assigned linker, centrifuged briefly and incubated at room temperature for 30 minutes. The multiplex coating solution is then prepared by addition of 600μl of prepared U-plex coupled antibody into a 15ml tube and vortexed briefly. 50μl of each multiplex coating solution is then added to each well using a multi-channel pipette. The plates were then sealed and incubated at room temperature on the plate shaker for one hour. The plate was then washed with MSD wash buffer or PBST for at least three times.

An 8-point standard curve solutions were prepared from 1μg/mL of calibrator stock solution (50μl) in diluent 41 by adding 200μl of diluent 41 to 50μl calibrator stock. 75μL of the diluted stock calibrator was then added to 225μl diluent 41 to generate the rest of the calibrator standard solution. The recommended 8th standard is diluent 41 only (zero calibrator) (table 2.9). Calibrators were run in duplicate for standard curve generation.

Tube #	Source of calibrator	Volume of reconstituted calibrator (μl)	Assay diluent (μl)	Total volume (μl)
1	calibrator standard 1		225	300
2	From tube 1	75	225	300
3	From tube 2	75	225	300
4	From tube 3	75	225	300
5	From tube 4	75	225	300
6	From tube 5	75	225	300
7	From tube 6	75	225	300
8 (zero calibrator)	-	0	300	300

Table 2.9. Dilution of calibrator for standard curve (tubes 1-7) and control solution (8th tube).

25μl of diluent 4 was dispensed into each well and the sealed plate was incubated for 30 minutes over a plate shaker (1000rpm) at room temperature. 25μl of calibrator solution for standard curve wells and 25μl of sample was added to test wells of the MSD plate, sealed and incubated at room temperature on a shaker (1000rpm) for two hours. Plate was washed with PBST three times. 25μl of detection antibody solution was added to each well, plate was sealed and incubated at room temperature for two hours on a shaker (1000rpm). Plates were washed three times with PBST. 150μl of 2x read buffer T was added to each well and plates were analysed on SECTOR imager (MSD) immediately. Standard curve graphs were generated by plotting the concentration of cytokines (pg/mL) over the signal intensity.

Chapter 3

Chapter 3. The role of mtDNA mutation in ageing mouse cardiac muscle

3.1 Introduction

3.1.1 *Mitochondria and ageing*

Ageing is defined as a progressive and time-related deterioration in physiological functions with an ever increasing risk of death. Mitochondria are thought to be involved in the ageing process as an accumulation of cells with mitochondrial dysfunction due to mutations of mitochondrial DNA (mtDNA) have been documented in a number of ageing tissues such as the heart (Müller-Höcker *et al,* 1986) brain (Cottrell *et al*, 2001), skeletal muscle (Fayet *et al*, 2002), colon (Greaves *et al*, 2014) and liver (Yen *et al*, 1989). The mitochondrial free radical theory of ageing was proposed in the 1950s (Harman, 1956) and refined in the early 1980s (Miquel *et al,* 1980). The theory predicts that reactive oxygen species (ROS) generated through premature electron leakage in the respiratory chain, mainly at Complexes I and III, (Lenaz, 2001) can directly target and damage mtDNA. This damage can result in mtDNA mutations which cause dysfunction of the oxidative phosphorylation (OXPHOS) system which can impair ATP production. It was further proposed that dysfunctional OXPHOS could then induce further ROS production and further mutation resulting in a vicious cycle (Bandy and Davison, 1990). More recent studies have refuted both the vicious cycle and free radical theory of ageing. MtDNA has been shown to be densely and efficiently packaged (Jiang *et al*, 2017) and is well protected with the vast majority of repair mechanisms present in the nucleus also present in the mitochondrial (Gredilla, Garm and Stevnsner, 2012). In addition, mitochondria have multiple antioxidant defence mechanisms to maintain the physiologically required ROS levels (Poljsak, Suput and Milisav, 2013), and the mtDNA mutational spectrum present in ageing cells does not show the predicted ROS-damage signature (Kauppila and Stewart, 2015). Two mouse models which accumulate high levels of mtDNA mutations due to a loss of the proof-reading capability of the mtDNA polymerase gamma (PolgA) do not show evidence of increased ROS related cellular damage at young ages (Dai *et al,* 2014), and only mild increases in H_2O_2 production at older ages (Logan *et al*, 2014). Since mitochondria exist in thousands of copies per cell, the mutant mtDNA load must exceed a threshold value for the biochemical defect to be visible (Rossignol *et al*,

2003). The level of heteroplasmy indicates the proportion of mutant and wild type mtDNA in a cell and the biochemical threshold is determined by the percentage of mtDNA heteroplasmy. Shoffner *et al* (1993) first reported that the phenotypic threshold is around 60% for mtDNA deletions and around 90% for other mtDNA mutations depending on the type of mutation and the tissue affected. As the biochemical defect doesn't become apparent until the clonal expansion has occurred, if ROS are playing a role in ageing, it may only be at this point that their levels begin to change due to OXPHOS dysfunction. Greaves *et al* (2014) used aged human colorectal epithelium as an example of a well-defined stem cell population to assess the age-related decline in mitochondrial function. They found that clonally expanded mtDNA point mutations within individual cells were responsible for the decline in mitochondrial function during ageing, rather than an ever increasing rate of mtDNA mutation occurrence.

3.1.2 *PolgA$^{mut/mut}$ mouse model*

A direct causal role for mtDNA mutations in the ageing process was established by studies in mice expressing a proof-reading deficient mtDNA polymerase gamma (*PolgA*) (Trifunovic *et al*, 2004, Kujoth *et al,* 2005). The mice have a knock-in mutation causing an aspartate to alanine amino acid change (D257A) in the second exonuclease domain of the catalytic (*PolgA*) subunit of the mtDNA polymerase (Polγ). The mice harbouring the homozygous *PolgA* mutation (*PolgA$^{mut/mut}$* mouse, also known as the mitochondrial mutator mouse) have a 3-5 fold increase in the number of point mutations and large scale deletions compared with WT control mice. The *PolgA$^{mut/mut}$* mice show a premature ageing phenotype with phenotypic characteristics including: loss of muscle mass, cardiac enlargement, alopecia, kyphosis, reduced subcutaneous fat, weight loss, osteoporosis, reduced fertility and anaemia from as early as 25 weeks of age. The median lifespan of the *PolgA$^{mut/mut}$* mice was reduced to 48 weeks of age and the premature signs of ageing accelerated from 7-9 months of age resembling human ageing. Safdar *et al* (2011) have documented that 5 months of endurance exercise rescues the progeroid phenotypes of *PolgA $^{mut/mut}$* mice and mitigates systemic mitochondrial dysfunction from 8 months of age.

3.1.3 *PolgA^{mut/mut} mouse cardiovascular phenotypes*

Due to the inherent dependency of normal cardiac physiology on mitochondria, Trifunovic *et al* (2004) investigated the cardiovascular phenotypes of *PolgA^{mut/mut}* mice. They reported significant cardiac remodelling including cardiac hypertrophy as evident by enlarged cardiomyocyte width, heart size and a marked increase in left ventricular mass index compared to wild type littermates. Cardiomyocyte mitochondrial complex IV deficiency and enlarged mitochondria were also characteristic of *PolgA^{mut/mut}* mouse hearts. A second study by Dai *et al* (2010) reported age-related changes in *PolgA^{mut/mut}* mouse hearts including increased levels of mtDNA deletions and protein oxidative damage as well as increased expression of apoptotic and senescence markers, and a decline in mitochondrial biogenesis signalling. Other phenotypic features of *PolgA^{mut/mut}* mouse hearts were depressed cardiac fractional shortening which determines myocardial performance, as well as systolic dysfunction, diastolic dysfunction, ventricular interstitial and perivascular cardiomyocyte fibrosis (Dai *et al*, 2010).

3.2 Aims of study

The focus of this chapter was to characterise the *PolgA^{mut/mut}* mice phenotypes compared with wild-type *PolgA^{+/+}* mice at the physiological and cellular level to establish baseline characteristics prior to the exercise intervention. Specifically, I aimed to characterise the following:

1. Clinical phenotype of the *PolgA^{mut/mut}* vs *PolgA^{+/+}* mice from 3 to 11 months of age

2. Behavioural characteristics of *PolgA^{mut/mut}* vs *PolgA^{+/+}* mice from 3 to 11 months of age

3. Cardiac structure, histology and mitochondrial function in *PolgA^{mut/mut}* vs *PolgA^{+/+}* mice from 3 to 11 months of age

3.3 Results

3.3.1 *Survival curve, Clinical scoring and Body weight of PolgA$^{+/+}$ mice and PolgA$^{mut/mut}$ mice*

Clinical scoring is a measure of health span and is a determinant of the severity of disease and the clinical end point for this study. The phenotypic features rate the health condition of mice and include weight, coat condition, skin tone, behaviour, posture and mobility, abdominal distension, foot colour and hydration of mice (table 2.1). The clinical scoring criteria and an example of monitoring sheet are detailed in the appendix 1 tables 8.1 and 8.2. Clinical scoring was performed on n=5 *PolgA$^{+/+}$* mice and n=10 *PolgA$^{mut/mut}$* mice on a weekly basis from 14 weeks of age (baseline) up to 43 weeks of age. Animals were scored from 0 to 3 for each characteristic, 0 being normal and 3 being substantial worsening of the animal's condition for each characteristic. All 8 characteristics were assessed during each monitoring session and the final total score was recorded. The higher the total clinical score value, the worse body condition was deemed to be. If a mouse received one score of 3, three scores of 2, over 20% weight loss or temperatures below 30ºC, the animal was humanely killed by cervical dislocation.

The survival curve in Figure 3.1A shows that 100% of *PolgA$^{+/+}$* mice lived until the end of the study (46 weeks) whereas only 53.85% of *PolgA$^{mut/mut}$* mice survived to the end of the study. Mice that died prematurely from prolapse or fight wounds were excluded from the survival curve. Since only 53.85% of *PolgA$^{mut/mut}$* mice lived until the 46 week endpoint, all the *in vivo* measurements including the body weight, temperature, open field testing and clinical scoring were taken from 43 weeks of age in both groups for reliable statistical analysis.

Figure 3.1B shows the body weights of *PolgA$^{+/+}$* mice from 14-43 weeks of age (up to 40.52g± 2.26g at 43 weeks of age). This is within the normal range when compared a database of the expected body weight of C57Bl6/J mice body at the same age (39g±4.5g) (The Jackson Laboratory, 2019). At 43 weeks of age, the body weight of *PolgA$^{+/+}$* mice was significantly higher than 14 weeks ($p<0.001$). In comparison, *PolgA$^{mut/mut}$* mice also showed a steady but significant ($p<0.01$) weight gain (up to 32.5g±1g at 43 weeks of age) which was significantly lower than *PolgA$^{+/+}$* mice at the same time point ($p<0.001$) (Two-way repeated measure ANOVA).

Figure 3.1C shows that at 14 weeks of age there were no significant differences in the total clinical scores between $PolgA^{mut/mut}$ and $PolgA^{+/+}$ mice. However, by 46 weeks of age $PolgA^{mut/mut}$ had a significantly higher clinical score as a result of a decline in their body condition compared to their total score at 14 weeks (p=0.0003) and a significantly higher total clinical score compared with $PolgA^{+/+}$ mice at 43 weeks (p=0.0013) (two-way repeated measure ANOVA). At 43 weeks of age 85% of $PolgA^{mut/mut}$ mice showed significant piloerection, 14.3% demonstrated hunched posture and reduced mobility, 57.1% had paling of the feet due to anaemia, 14.3% showed behavioural changes such as lack of social interaction and 14.3% experienced up to 20% weight loss (all with a total score of ≥2). In addition, 100% of age-matched $PolgA^{+/+}$ mice showed normal body weight, 100% with no signs of piloerection, 100% with normal posture and mobility and 100% with behavioural engagement during monitoring at 43 weeks of age (all with the score of <2).
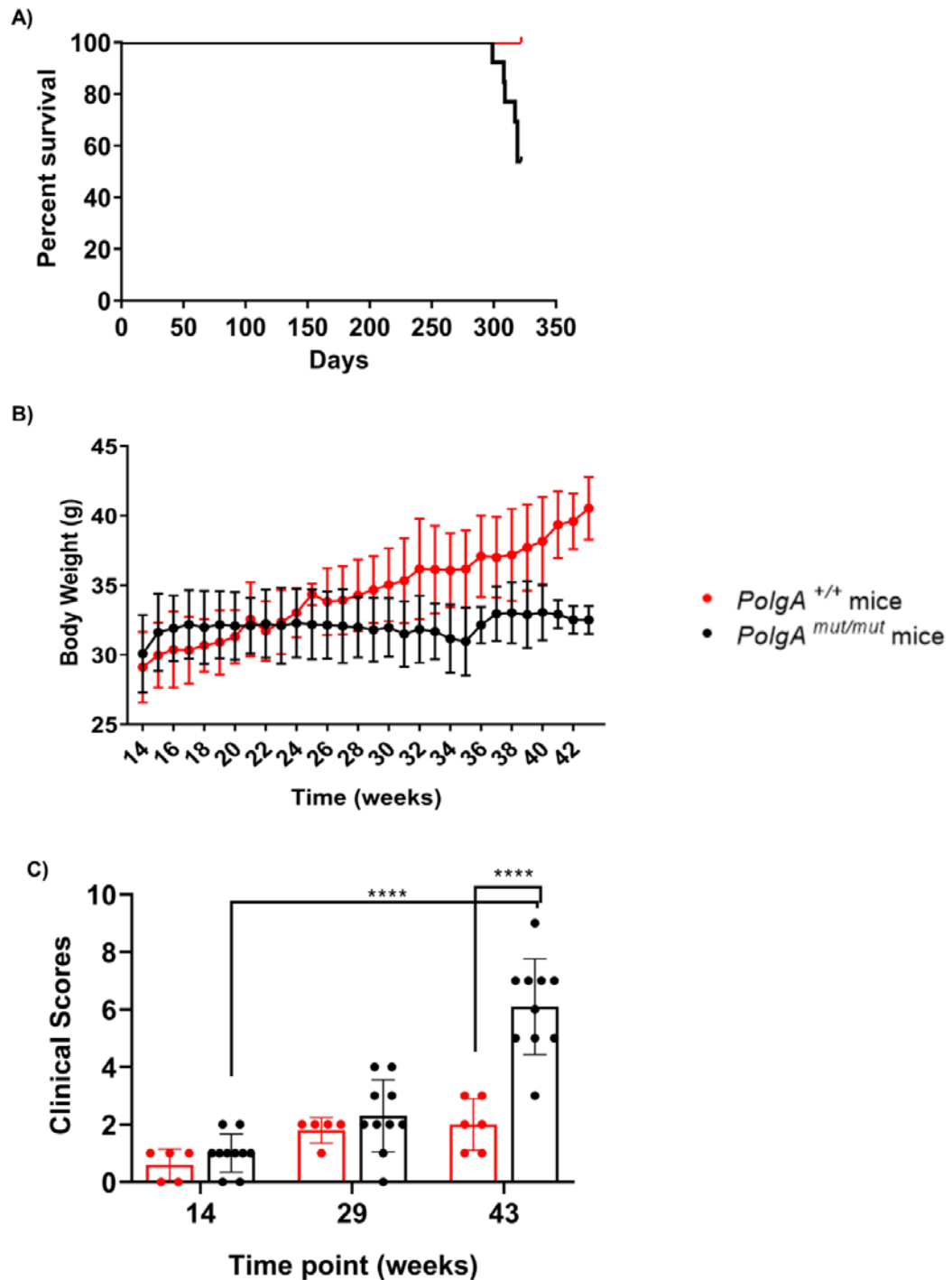
Figure 3.1. Comparison of *PolgA+/+* mice and *PolgAmut/mut* mice survival curve, clinical scoring and body weight. A) 100% of *PolgA+/+* mouse survived to the end of the study in comparison to 53.85% *PolgAmut/mut* mice. B) *PolgA+/+* mice showed a significant increase in body weight with increasing age (p<0.001). Body weight from 14 weeks to 43 weeks in *PolgAmut/mut* mice (p<0.01). *PolgA+/+* and *PolgAmut/mut* mice at 14 weeks (p>0.05), *PolgA+/+* and *PolgAmut/mut* mice at 43 weeks (****p<0.0001). C) Clinical scoring at 14 weeks was not significant different between the two cohorts (p=0.422). *PolgAmut/mut* mice had significant decline in body condition at 43 weeks in comparison to *PolgA+/+* mice (****p=0.0003) and with increasing age (****p=0.0013, Two-way repeated measures ANOVA). Error bars represent mean ±SD.

3.3.2 Body temperature in *PolgA*$^{+/+}$ mice and *PolgA*$^{mut/mut}$ mice

The body temperature of individual mice was recorded from a subcutaneous RFID chip implanted under the skin on the top of the mouse's neck using a chip reader four times per week from 14 weeks onwards for the duration of the study. *PolgA*$^{mut/mut}$ mice were group-housed with *PolgA*$^{+/+}$ mice and *PolgA*$^{mut/+}$ mice in cages of 2, 3 or 4. Figure 3.2 demonstrates the mean body temperature of *PolgA*$^{+/+}$ mice (n=5) and *PolgA*$^{mut/mut}$ mice (n=10) at the age of 14 weeks, 29 weeks and 43 weeks. There was no significant difference between the body temperatures of *PolgA*$^{+/+}$ mice and *PolgA*$^{mut/mut}$ mice at 14 weeks and 29 weeks of age (p>0.05). At 43 weeks of age the mean body temperature of *PolgA*$^{mut/mut}$ mice (35.1°C ±0.2) was significantly lower than *PolgA*$^{+/+}$ mice (36.47°C ±0.58) (p<0.001, two way repeated measures ANOVA). The body temperature of *PolgA*$^{+/+}$ mice increased significantly from 14 weeks (35.3°C±0.9) to 43 weeks (36.5°C±0.6) of age (p<0.01, two way repeated measures ANOVA). The body temperature of *PolgA*$^{mut/mut}$ mice did not change significantly with advancing age from 14 weeks to 43 weeks (p>0.05). Although the cages were temperature regulated, the ability to control core body temperature is down to the basal metabolic activity of each mouse. Temperature regulation also depends on external factors such as living in groups, diet and levels of exercise (Marriott and Carlson-Newberry, 1996).
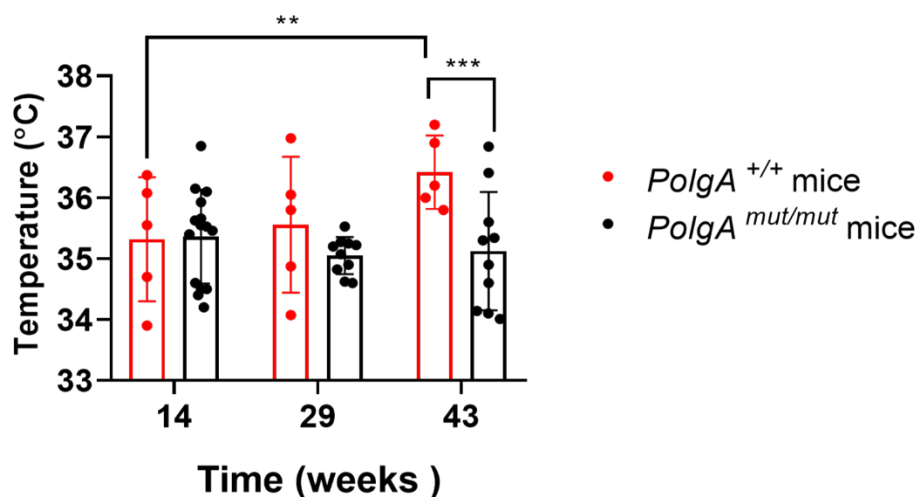
Figure 3.2. Body temperature of *PolgA+/+* mice and *PolgA^mut/mut^* mice at 14, 29 and 43 weeks of age. *PolgA+/+* vs *PolgA^mut/mut^* mice at 14 weeks and 29 weeks of age (p>0.05), *PolgA+/+* vs *PolgA^mut/mut^* mice at 43 weeks (***p<0.001), *PolgA+/+* mice 14 weeks vs 43 weeks (**p<0.01). *PolgA^mut/mut^* mice 14 weeks vs 43 weeks (p>0.05), (Two-way repeated measures ANOVA). Error bars represent mean ±SD.

3.3.3 *Open Field Testing (OFT) of PolgA+/+ mice and PolgA^mut/mut^ mice*

In order to understand and characterise the locomotive and behavioural characteristics of the two groups of mice, open field testing (OFT) was carried out over a 5 minute period at 15 weeks, 29 weeks and 43 weeks of age in *PolgA+/+* mice (n=5) and *PolgA^mut/mut^* mice (n=10). The method by which OFT was carried out detailed in chapter 2 section 2.16.1. The graphs shown in figure 3.3 indicate a range of quantitative measures from the emotional and behavioural state of mice to ambulatory ability using the mousetrap software (Ryanware v4.0). The total distance moved indicates the locomotive state of mice. The velocity at which mice travel may indicate responsiveness and assesses reaction time to an unknown stimuli or situation. Rearing behaviour is described as a position where the mouse is standing on both hind limbs in an upright position and its frequency is a measure of inquisitiveness and exploratory behaviour in mice. Total number of touches is the number of times the animal's forelimbs touched the arena which sometimes gives an indication of fear-related behaviours such as when the sum of touches were high and the total distance travelled by the mice is low. It also indirectly assesses the balance

and coordination of animals as a higher number of touches; lower travelling distance and shorter step length indicate a state of impaired coordination. Step length was calculated manually by dividing the total distance moved over total number of touches.
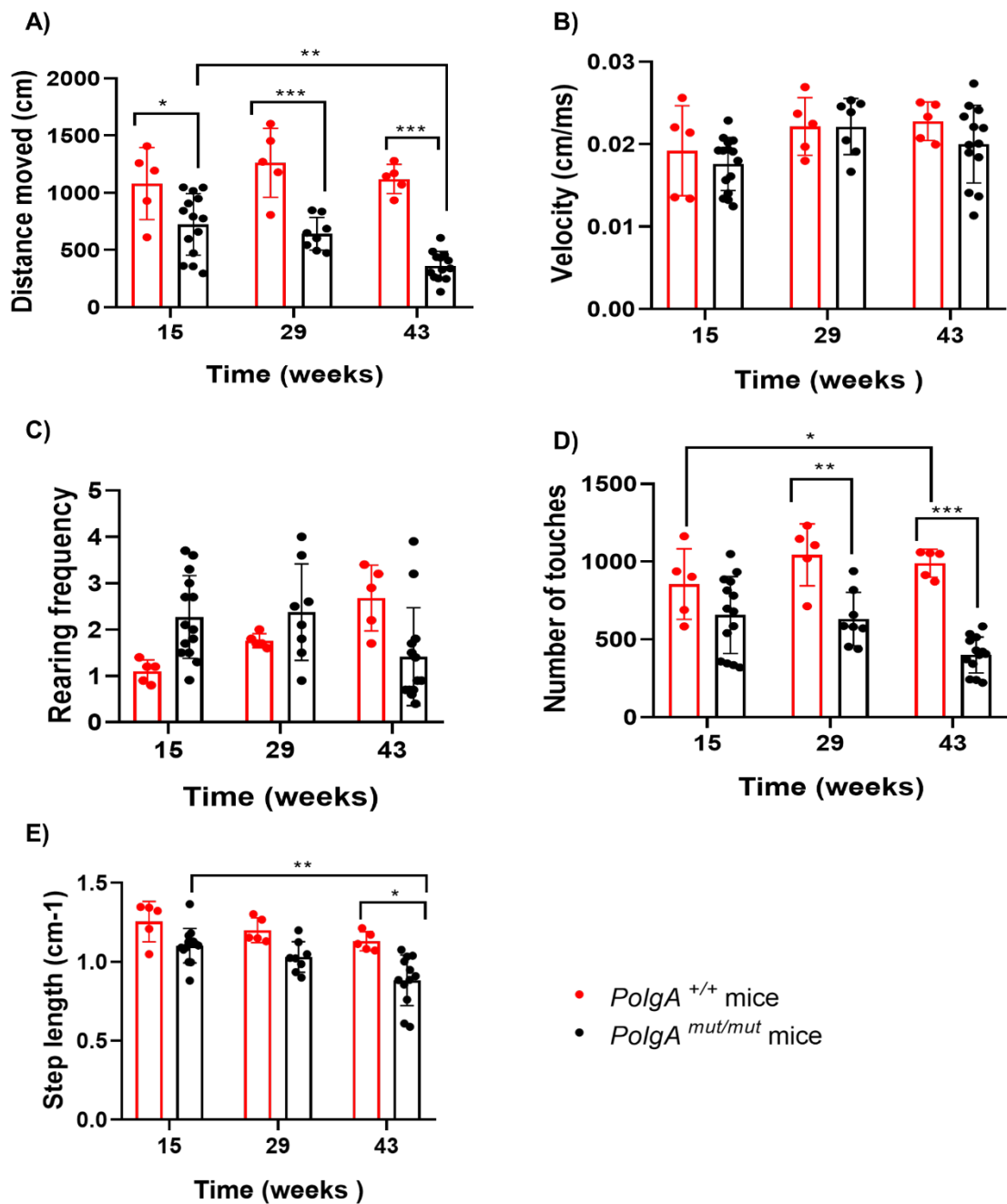
Figure 3.3.Open Field Testing at 15, 29 and 43 weeks of age in *PolgA+/+* vs *PolgAmut/mut* mice. A) Total distance moved significantly reduced with advancing age in *PolgAmut/mut* mice (**$p<0.01$) and was significantly lower in *PolgAmut/mut* at 15 weeks (*$p<0.05$), 29 weeks, (**$p<0.01$) and 43 weeks (***$p<0.001$) of age in comparison to *PolgA+/+* mice. B) No significant changes in the velocity of movements and C) rearing frequency of both cohorts were seen. D) Number of touches were significantly higher in *PolgA+/+* mice at 29 weeks (**$p<0.01$) and 43 weeks (***$p<0.001$) in comparison to *PolgAmut/mut* mice and decreased significantly in *PolgAmut/mut* mice with age (*$p<0.05$). E) Step length significantly reduced in *PolgAmut/mut* mice with age (**$p<0.01$) and is significantly lower in *PolgAmut/mut* mice at 43 weeks (*$p<0.05$) in comparison to *PolgA+/+* mice (Two-way repeated measures ANOVA). Error bars represent mean ±SD.

The total distance moved in *PolgA^mut/mut* mice was significantly lower in comparison to *PolgA^+/+* mice at 15 weeks (p<0.05), 29 weeks (p<0.001) and 43 weeks (p<0.001) of age. There was however no age-associated changes in the total distance travelled of *PolgA^+/+* mice but a significant decline in *Polg^mut/mut* mice with age (p<0.01). There was no significant difference in velocity of movement and the rearing frequency between the two groups and within groups at any time points as shown in figures 3.3B and 3.3C. In general, the less contact the mouse has with the arena, the lower the locomotive activity of the mouse is considered to be. At 15 weeks of age, no significant differences in the number of touches were seen between the cohorts. A significantly lower number of touches were observed in *PolgA^mut/mut* mice in comparison to *PolgA^+/+* mice at 29 weeks (p<0.01) and 43 weeks (p<0.001) of age (figure 3.3D). The number of touches did not significantly change with age in *PolgA^+/+* mice but was significantly reduced in *PolgA^mut/mut* mice from 15 weeks to 43 weeks of age (p<0.05). *PolgA^mut/mut* mice showed a significant decline in their step length by 43 weeks of age in comparison to *PolgA^+/+* mice (p<0.05). Step length in *PolgA^+/+* mice did not change significantly with age (figure 3.3E). *PolgA^mut/mut* mice showed a state of imbalance with age progression indicated by significant decline in step length at 43 weeks of age (p<0.01) (Two-way repeated measures ANOVA).

Incorporating all the OFT parameters measured to assess the state of locomotion and physical capacity of mice, it is evident that *PolgA^mut/mut* mice have significantly less movement and therefore less contact with the arena as shown by the lower frequency of touches and significantly lower step length that indicate an overall musculoskeletal weakness and coordination imbalance in comparison to *PolgA^+/+* mice at 43 weeks of age (Seibenhener and Wooten, 2015).

3.3.4 *Organs weights in PolgA$^{+/+}$ mice and PolgA$^{mut/mut}$ mice*

Organs were harvested according to the mouse organ harvesting sheet in appendix 2. Organ weight was recorded immediately following cervical dislocation at the end of the study or when the clinical endpoint was reached. Organ weight data are presented as both the actual organ weights (Figure 3.4A) and organ to body weight ratios (Figure 3.4B) in *PolgA* $^{+/+}$ mice (n=5) and *PolgA$^{mut/mut}$* mice (n=10). Figure 3.4A demonstrates that the weight of; liver (p<0.001), spleen (p<0.01) and heart (p<0.05) was significantly higher in *PolgA$^{mut/mut}$* mice and the weight of pancreas (p<0.001) was significantly higher in *PolgA* $^{+/+}$ mice (unpaired t-test). The liver (p<0.01), spleen (p<0.01), right kidney (p<0.05), left kidney (p<0.01), heart (p<0.01), lungs (p<0.05) and brain (p<0.05) weight when normalised to body weight was significantly higher in *PolgA$^{mut/mut}$* mice in comparison to *PolgA* $^{+/+}$ mice using an unpaired t-test. The weight of pancreas was non-significantly different between the two cohorts when the body weight was taken into consideration. As body weight was significantly reduced in *PolgA$^{mut/mut}$* mice compared with *PolgA$^{+/+}$* mice at endpoint, it is difficult to determine whether organ to bodyweight ratio is a good measure in these mice.
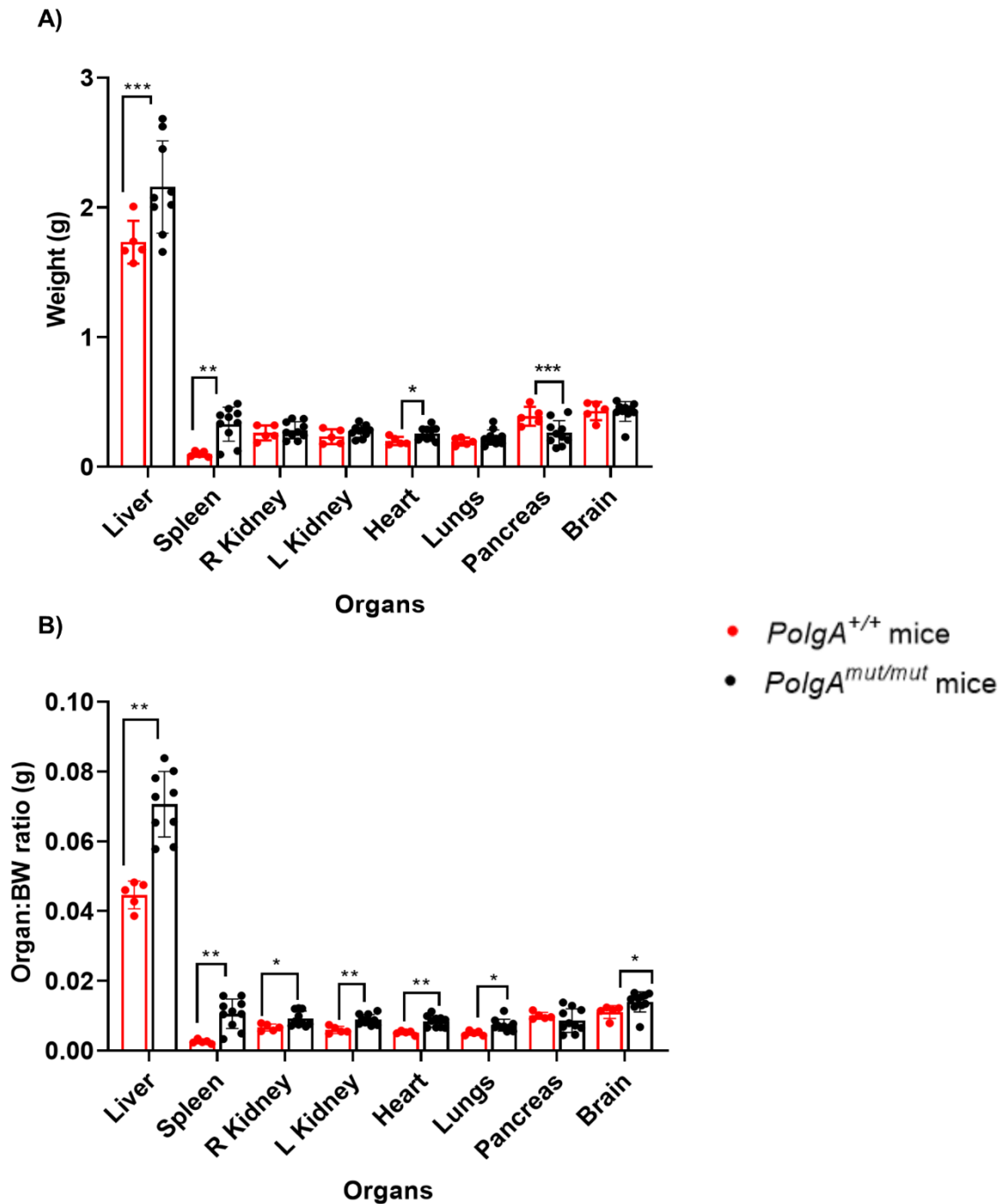
Figure 3.4.Organ weights. A) Liver, spleen and heart weight was significantly higher in *PolgA^mut/mut^* mice in comparison to *PolgA^+/+^* mice. B) Normalised organ weight in *PolgA^+/+^* mice and *PolgA^mut/mut^* mice. Liver, spleen, left kidney and heart (**p<0.01), lungs, right kidney and brain (*p<0.05) were significantly bigger in *PolgA^mut/mut^* mice in comparison to *PolgA^+/+^* mice (unpaired t-test). Error bars represent mean ±SD.

3.3.5 *Cellular and molecular analysis of the heart in PolgA$^{mut/mut}$ and PolgA$^{+/+}$ mice at 46 weeks of age*

Since the heart was the organ of interest in this study, I harvested and longitudinally dissected the hearts and froze the left side in isopentane, and fixed and embedded the right side in paraffin for further analysis.

Histological and molecular techniques such as COX/SDH histochemistry, NBTx analysis and mitochondrial DNA copy number analysis were carried out on the frozen left ventricular tissue. Haematoxylin and Eosin stain, Masson trichrome cardiac fibrosis analysis, cleaved-caspase 3 immunohistochemistry (apoptotic marker) and mitochondrial complexes I and IV immunofluorescence was carried out on the right fixed ventricular tissue.

3.3.6 *Histological analysis of PolgA$^{+/+}$ mice and PolgA$^{mut/mut}$ right ventricle at endpoint*

Haematoxylin and Eosin (H&E) staining was carried out to visualise cardiomyocyte morphology and assess cardiomyocyte width (Figure 3.5A). The nuclei were stained blue and cardiomyocytes were stained various shades of pink. 4µm paraffin embedded cardiac tissue from (n=10) *PolgA$^{mut/mut}$* mice and (n=5) *PolgA$^{+/+}$* mice were subjected to H&E staining and visualised using the Zeiss light microscope. Five random snapshots from the RV were taken at x20 magnification and the width of 50 cardiomyocytes per image were measured using Zen image analysis software. Figure 3.5B shows that the width of cardiomyocytes in *PolgA$^{mut/mut}$* mice was significantly larger in comparison to *PolgA$^{+/+}$* mice (p=0.0001, unpaired t-test)

Cardiac fibrosis was assessed in n=10 *PolgA$^{mut/mut}$* mice and n=5 *PolgA$^{+/+}$* mice hearts by Masson's trichrome staining. This technique uses three dyes to detect cardiac myopathies such as scarring and accumulation of excess collagen during pathological cardiac hypertrophy and fibrosis. The histochemical technique stains cell nuclei purple by Haematoxylin, cytoplasm and cardiomyocytes red by Biebrich scarlet solution and collagenous connective tissue blue by Aniline blue solution. 4µm paraffin embedded cardiac sections were subjected to Masson's trichrome staining and visualised using Nikon Tie widefield invert microscope. X10 magnification RV

105

sections were analysed in NIS elements software using RGB general analysis algorithm by creating RGB channels and setting the threshold for the intensity of each colour ensuring no under/over saturated regions remained. The LED intensity and analysis settings remained constant throughout. Areas of interstitial and perivascular fibrosis were identified and analysed per mouse cardiac section, and the percentage of tissue fibrosis was quantified. The percentage of collagenous connective tissue (tissue fibrosis) was significantly higher in the cardiac tissue of *PolgA^{mut/mut}* mice in comparison with *PolgA^{+/+}* mice (p=0.01) (figure 3.5C). Collagen accumulation is evident as the area of blue collagen aggregation and the myocardium is stained in red as shown in figure 3.5A bottom images.
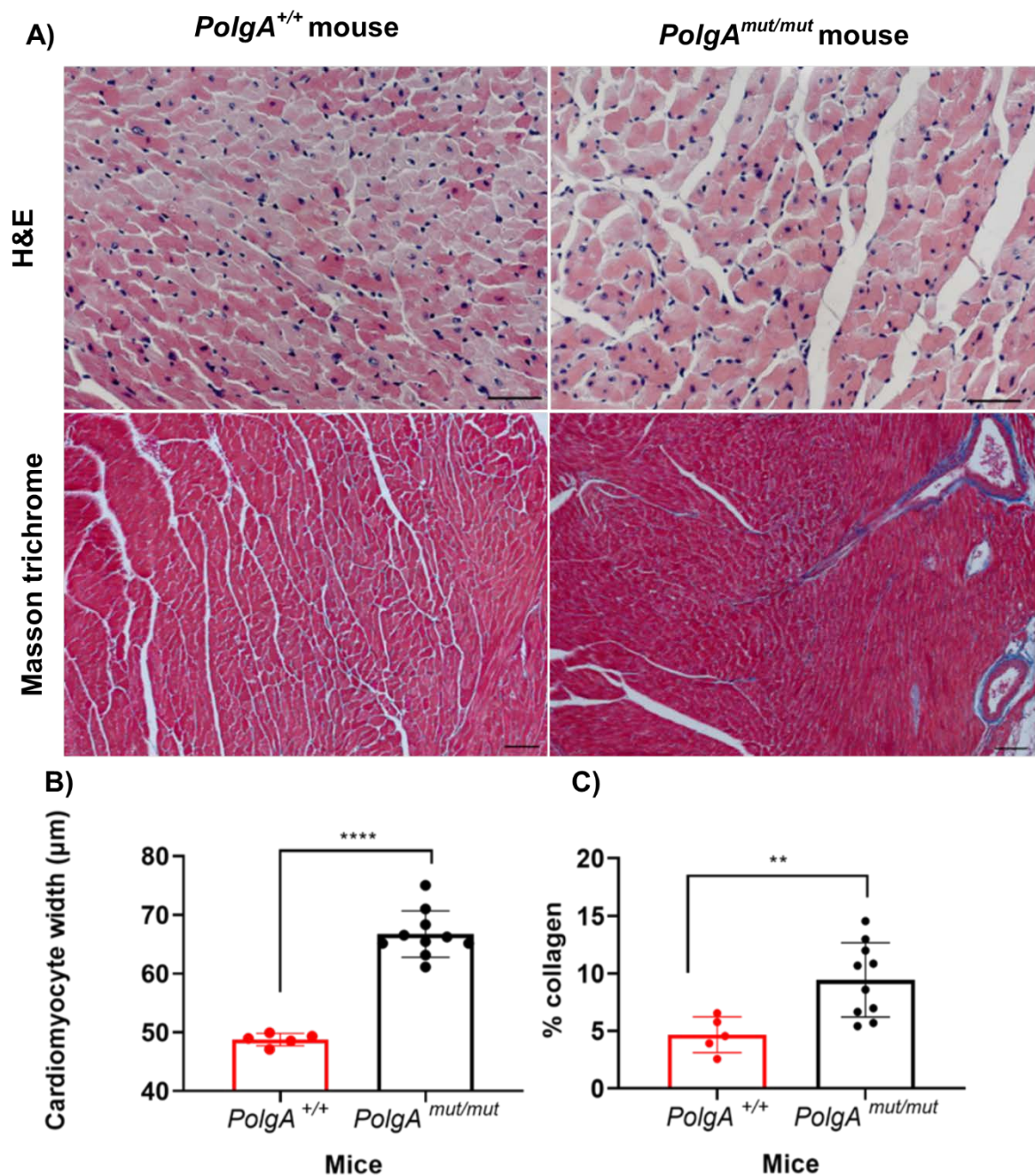
Figure 3.5. Cardiac fibrosis and cardiomyocyte width in *PolgA^{mut/mut}* and *PolgA^{+/+}* mice. A) Representative x20 H&E and trichrome images of *PolgA^{mut/mut}* and *PolgA^{+/+}* mice cardiac tissue. H&E images were used to measure cardiomyocyte width (scale bars=100µm). Masson trichrome images (x10) represent collagenous connective tissue in blue and cardiomyocytes in red (scale bars=200µm). B) There is a significant increase in *PolgA^{mut/mut}* mice cardiomyocyte width (****$p<0.0001$) in comparison to *PolgA^{+/+}* mice. C) Percentage of fibrosis in *PolgA^{mut/mut}* mice cardiac tissue is significantly higher than *PolgA^{+/+}* hearts (**$p=0.01$) (unpaired t-test). Error bars represent mean ±SD.

3.3.7 *Apoptosis*

Caspases are a family of peptides that cleave their target substrates proteolytically in the process of apoptotic cell death. Cleaved caspase-3 (CC-3) is an executioner caspase and becomes activated by an apoptotic signalling event responsible for chromatic condensation and DNA fragmentation (Bressenot *et al*, 2008). Activated-cleaved caspase 3 (CC3) immunohistochemistry was carried out in order to visualise and quantify apoptotic nuclei in cells by targeting CC3 as a critical executioner of apoptosis in *PolgA$^{+/+}$* mice (n=5) and *PolgA$^{mut/mut}$* mice hearts (n=10). Five random fields were taken and the frequency of CC3 positive nuclei shown as dark brown staining was quantified (Figure 3.6). Images were obtained using Aperio-scanner and analysed using Image-scope software nuclear staining algorithm (Leica Biosystems). The total number of nuclei and the total number of apoptotic nuclei were counted, and the percentage of apoptotic nuclei was calculated. The percentage of CC3 nuclei was significantly higher in the cardiac muscle in *PolgA$^{mut/mut}$* mice compared with *PolgA$^{+/+}$* mice at 46 weeks of age (p=0.001, unpaired t-test).
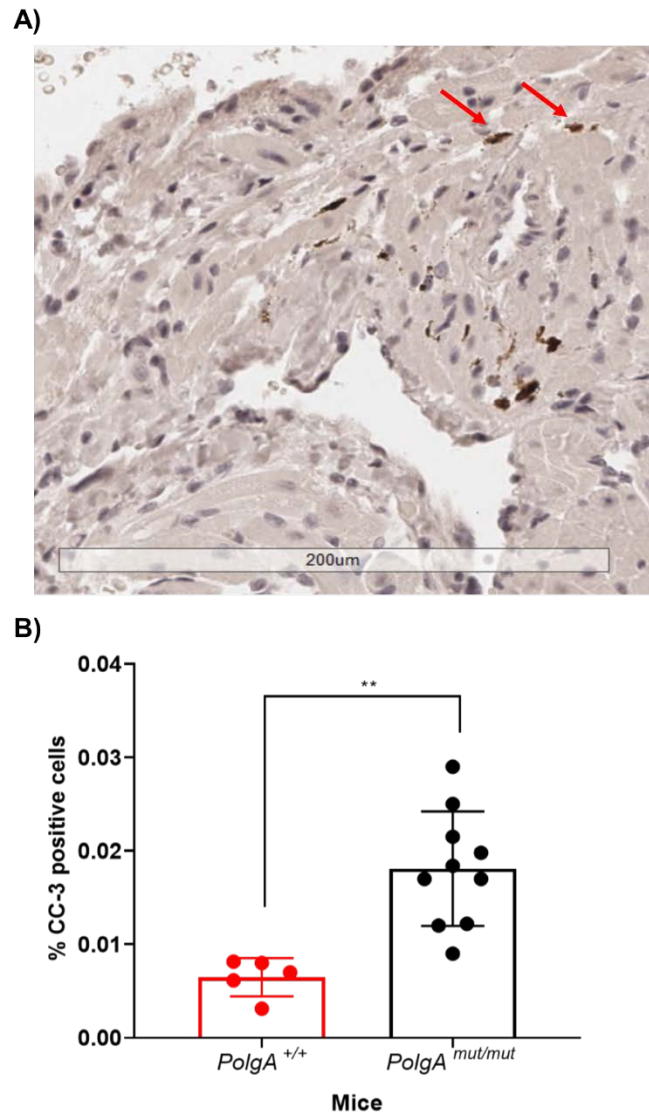
Figure 3.6. Percentage of apoptosis. A) Apoptosis measured by CC3 histochemistry in *PolgA^mut/mut^* mouse heart. CC3-positive cells are shown with red arrows. B) The percentage of cell death was quantified as the frequency of cleaved caspase-3 positive cells ratio to normal nuclei count which is significantly higher in cardiac muscle of *PolgA^mut/mut^* mice in comparison to *PolgA^+/+^* mice (**p=0.001). Error bars represent mean ±SD.

3.3.8 *Mitochondrial Complex I and Complex IV expression levels in PolgA^{+/+}*

mice and PolgA^{mut/mut} mice hearts

Mitochondrial OXPHOS complex I and complex IV expression levels were quantified in transverse fixed RV cardiac muscle by immunofluorescence assay using antibodies against MTCOI subunit of complex IV and NDUFB8 subunit of complex I. The optical density (OD) values of each enzyme is quantified from each cardiomyocyte through the fluorescence signal arising from the secondary antibody binding to the antigen of interest marked by the primary antibody. Mitochondrial mass was detected using an antibody against VDAC1 (Porin). Cardiomyocytes were differentiated from one another by an anti-laminin antibody that outlines each cardiomyocyte for easier differentiation and quantification. Five random snapshots of x10 magnification from 4µm paraffin embedded cardiac muscle were randomly selected and images were acquired using Zeiss AxioObserver LS800/SD/Airscan inverted microscope. The final .czi images were uploaded on to in-house analysis software known as the Quadruple Immuno-analyser created by Dr John Grady (Wellcome Centre for Mitochondrial Research, Newcastle University). The semi-automated software allows for the detection of individual cardiomyocytes visualised by laminin labelling. No primary control sections were used to remove background signal and set the exposure times accurate to visualise genuine signal with the right brightness. Merged files were uploaded on (http://research.ncl.ac.uk/mitoresearch/) for further analysis using *PolgA^{+/+}* mice as reference value for normality. The mitochondrial complex I and complex IV OD values were normalised to Porin levels by the software, z-scores were generated and used to classify fibres into negative, intermediate negative, intermediate positive and positive complex I and complex IV expression levels (Rocha *et al*, 2015). Mitochondrial respiratory chain (MRC) plots were created for each subject to showcase the distribution of cardiomyocytes with different complex I and complex IV expression levels.

Mitochondrial Complex I subunit (NDUFB8) and Complex IV subunit (MTCOI) expression levels were quantified in the RV cardiac muscle of *PolgA^{+/+}* mice (n=5) and *PolgA^{mut/mut}* mice (n=10). Figure 3.7A shows micrographs from the RV cardiac muscle. Expression of both complexes were obtained from individual transverse cardiomyocytes using quadruple immune-analyser software which is based on MATLAB. The OD values obtained were averaged for each cardiomyocytes, omitting the heterogeneity of each fibre.
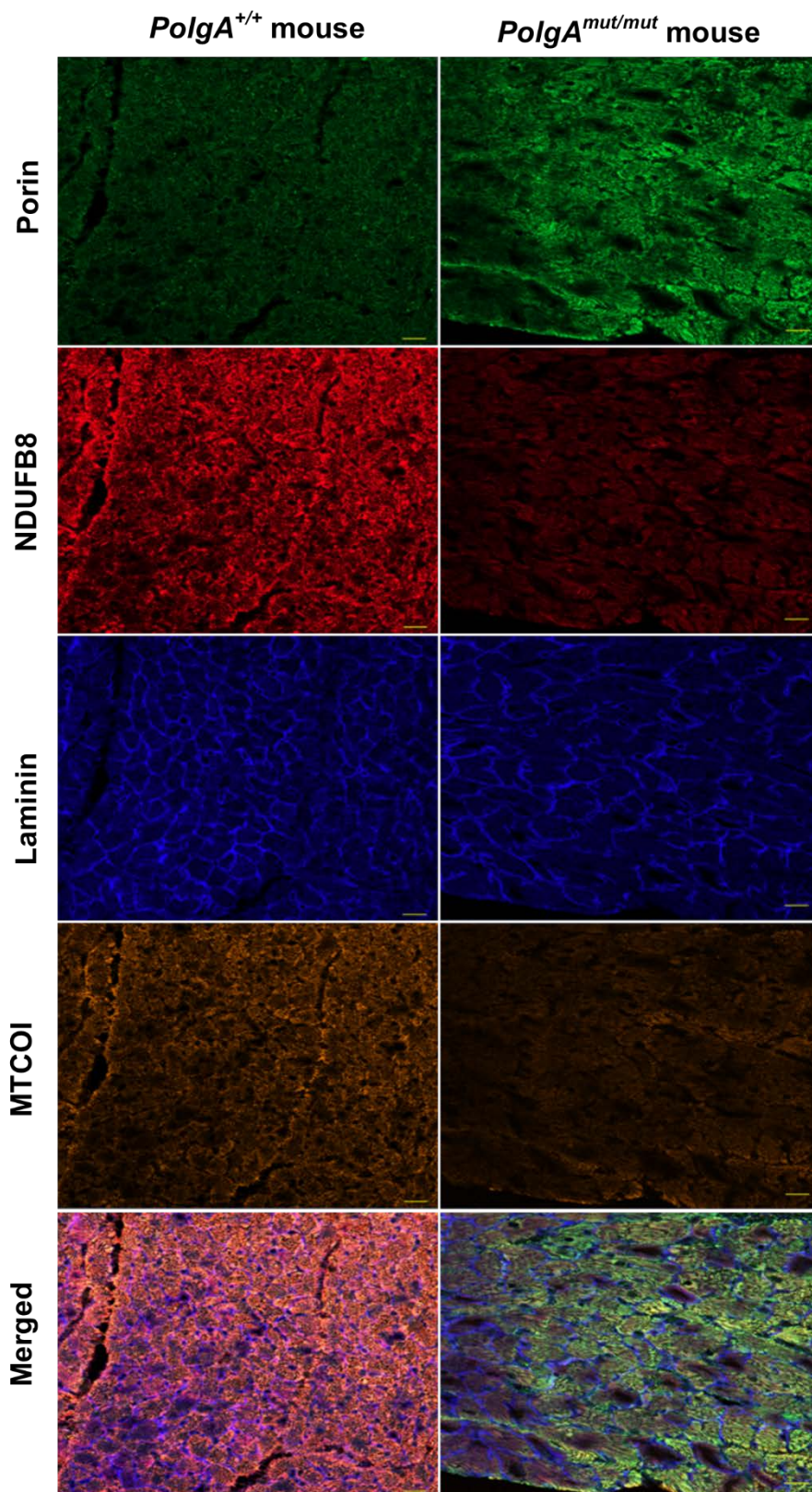
Figure 3.7.Mitochondrial Complex I (CI) and Complex IV (CIV) subunits expression levels in *PolgA+/+* mouse and *PolgAmut/mut* mouse hearts. CI was detected using an antibody against NDUFB8 and CIV was detected using an antibody against MTCOI. Mitochondrial mass was visualised using an antibody against Porin. Cardiomyocytes boundary was marked using an antibody against Laminin protein. Magnification x10. Scale bars= 100μm.

Cardiac muscle from all *PolgA+/+* mice showed 100% positive NDUFB8 (Complex I) and MTCOI (Complex IV) expression levels since the software used OD values obtained from *PolgA+/+* mice as a control to compare the *PolgAmut/mut* mice data against it. Therefore figure 3.8 represents the percentage of cardiomyocytes with categories of NDUFB8 and MTCOI in *PolgAmut/mut* mice relative to *PolgA+/+* cardiomyocytes as well as the MRC graphs. An example from each cohort is shown (figures 3.8A and 3.8B). Each dot on the graphs represents a cardiomyocyte which is colour coded by the levels of mitochondrial mass (porin) (blue=very low, light blue= low, beige=normal, orange=high, red=very high). In addition, dashed lines represent the standard deviation limits for the classification deficiency of complexes I and IV in individual cardiomyocytes.

Figure 3.8 (C-D) shows the variation in optical density of NDUFB8 and MTCO1 in cardiomyocytes; ranging from negative to positive covering intermediate positive and intermediate negative levels in the middle. In *PolgAmut/mut* mice hearts, relative to age-matched *PolgA+/+* hearts, 23.79% of cardiomyocytes were NDUFB8 positive, 42.8% were intermediate positive, 25.1% were intermediate negative and 8.1% negative. 30.13% of cardiomyocytes were MTCOI positive, 65.1% were intermediate positive, 4.6% intermediate negative, and 0.12% negative in *PolgAmut/mut* mice relative to age-matched *PolgA+/+* mice. The significant reduction in the percentage of complex I and complex IV positive cardiomyocytes and significant increase in the percentage of negative complex I and intermediate negative complex IV levels in *PolgAmut/mut* mice hearts is the result of increased mtDNA mutagenesis. This could limit the capacity of cardiac tissue for efficient ATP generation since the NDUFB8 subunit of complex I and MTCOI subunit of complex IV are crucial for correct functioning of the electron transport chain. Figure 3.8E demonstrates porin expression levels as z-score values (detailed chapter 2 talbe 2.4) where values between -2 and 2 represent normal porin levels. Each dot represent an average of porin z-scores in each mouse.
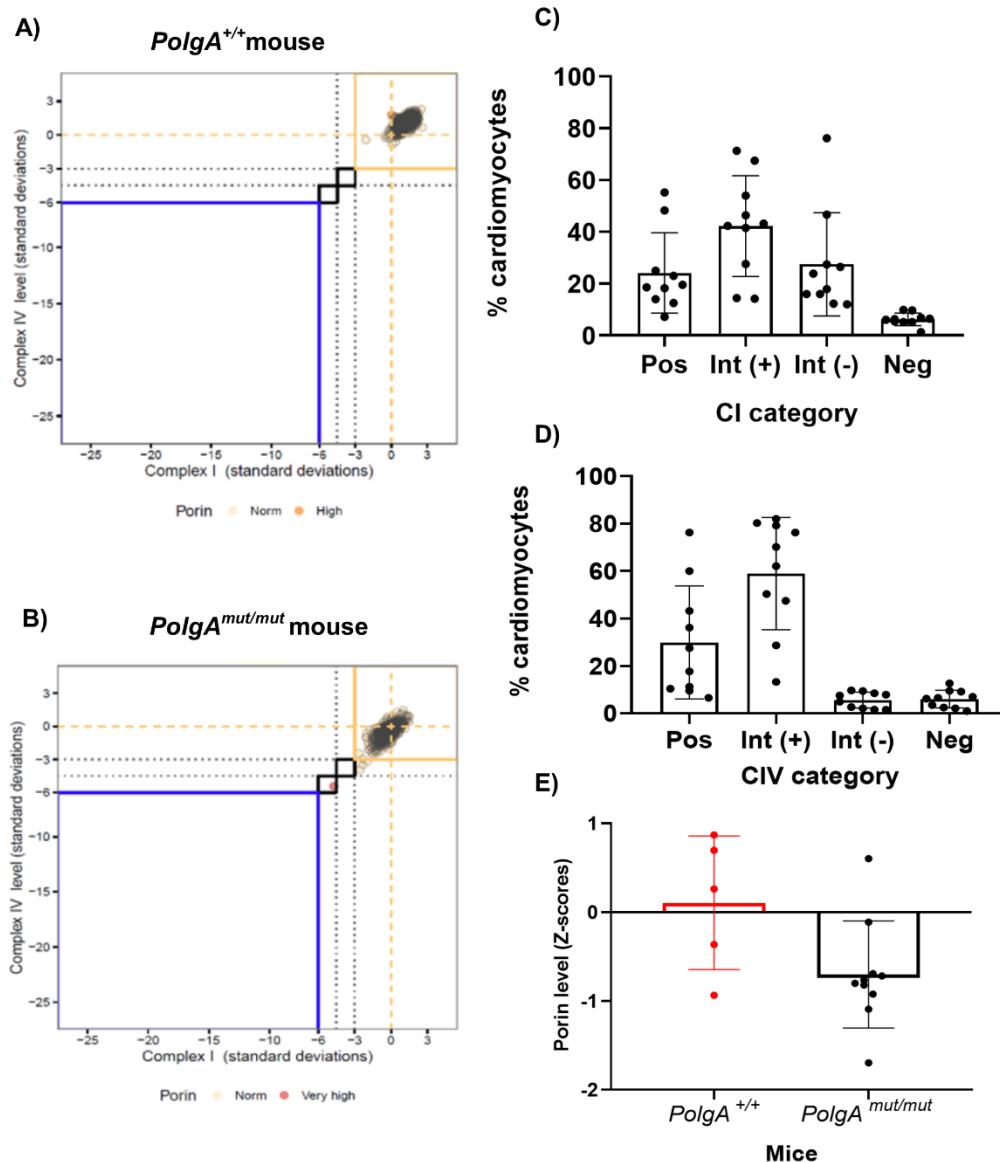
Figure 3.8. Mitochondrial NDUFB8 (Complex I) and MTCOI (Complex IV) immunoreactivity levels in *PolgA+/+* mice and *PolgAmut/mut* right ventricular cardiac muscle. A) Mitochondrial Respiratory Chain (MRC) plot obtained from a *PolgA+/+* mouse heart showing the categorisation of each cardiomyocyte for CI and CIV. B) MRC plot from a *PolgAmut/mut* mouse heart. C) Percentage of cardiomyocytes with positive, intermediate positive, intermediate negative and negative NDUFB8 expression in *PolgAmut/mut* mice hearts. D) Percentage of cardiomyocytes with positive, intermediate positive, intermediate negative and negative MTCOI expression in *PolgAmut/mut* mice hearts. E) Mitochondrial mass marker (porin) levels expressed as z-scores. Error bars represent mean ±SD.

3.3.9 *Complex IV activity in PolgA⁺/⁺ mice and PolgAmut/mut mice*

Mitochondrial complex IV (cytochrome *c* oxidase or COX) activity was investigated by sequential cytochrome *c* oxidase/succinate dehydrogenase (COX/SDH) histochemistry. Complex IV is the only complex of the OXPHOS system in which enzyme activity (rather than protein levels) can be demonstrated histochemically. SDH is entirely encoded by nuclear DNA and is unaffected by mtDNA mutations. The sequential COX/SDH histochemical assay allows for the visualisation of COX positive cardiomyocytes by localisation of the brown indamine polymer DAB (electron donor) in mitochondrial cristae in the presence of functional COX. Cardiomyocytes with dysfunctional COX do not saturate with DAB. Following incubation in media to demonstrate SDH activity, in those cells with no DAB precipitate there is the formation of a blue formazan end product due to the reduction of NBT by SDH in COX negative fibres (figure 3.9). 8µm cryosections of LV cardiac tissue from *PolgAmut/mut* mice (n=10) and *PolgA⁺/⁺* mice (n=5) underwent COX/SDH histochemistry and were imaged using a Nikon widefield Tie microscope. Five random snapshots were taken at x10 magnification from each LV mouse heart and COX deficiency was quantified in cardiomyocytes using NIS elements software. The software categorised the cardiomyocytes according to their colour using RGB general analysis algorithm. Since a mosaic pattern of COX deficiency is documented in *PolgAmut/mut* mouse heart, this three colour analysis software was used to extract most of the pigments with combination of red, green and blue for each fibre. The manual thresholding was kept constant for all the samples. The percentage of COX deficiency is quantified based on differentiating and subtracting the percentage of deficient SDH blue staining from the whole tissue area. There was a significant increase in COX deficiency in the LV tissue of *PolgAmut/mut* mice at 46 week of age compared with age-matched *PolgA⁺/⁺* mice following a two-tailed unpaired t-test analysis (p=0.0027) (Figure 3.10).
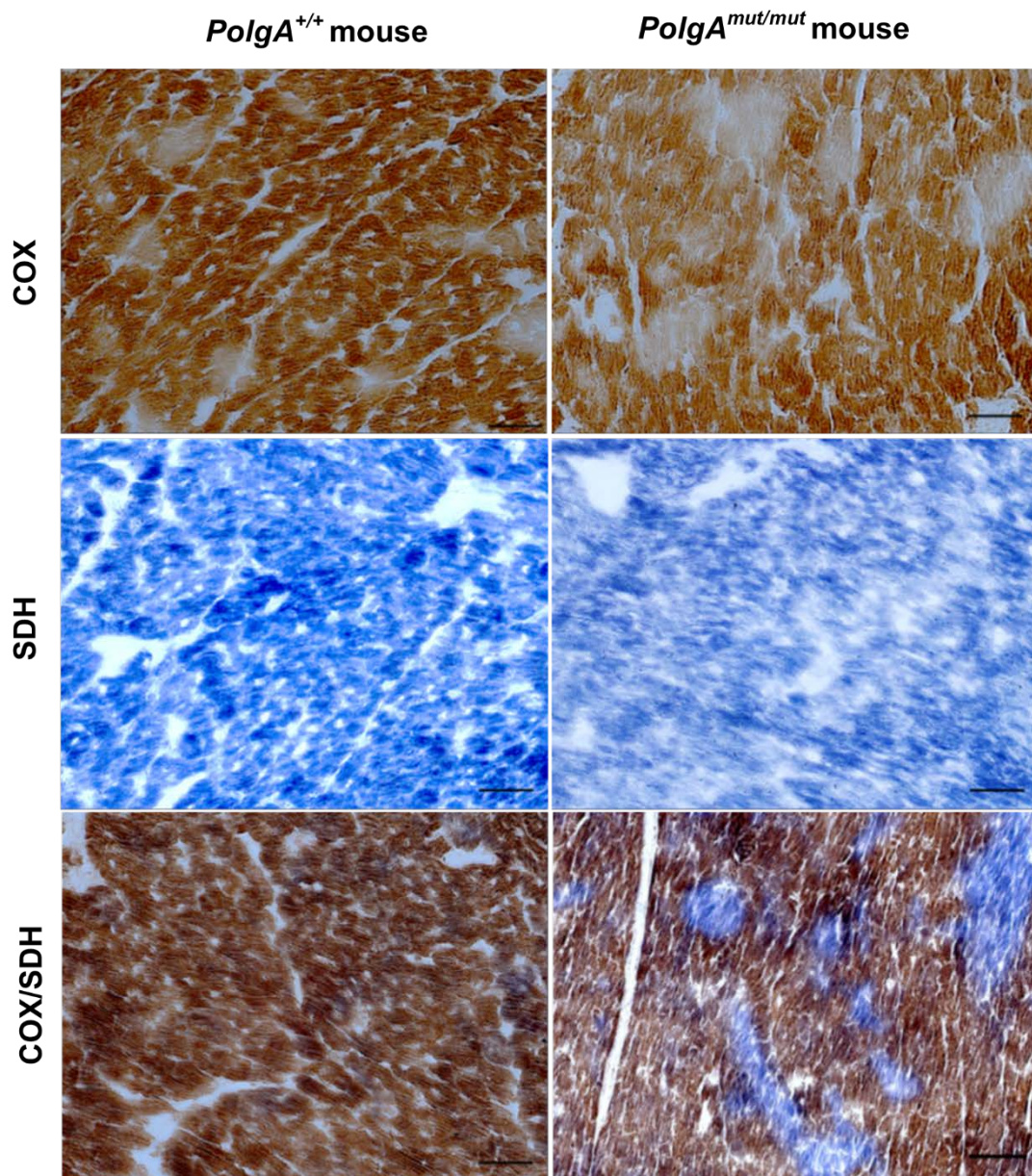
Figure 3.9.COX/SDH imaging and analysis. Representative serial sections of COX, SDH histochemistry and sequential COX/SDH from *PolgA⁺/⁺* mice and *PolgAᵐᵘᵗ/ᵐᵘᵗ* mice hearts. COX/SDH analysis was carried out using NIS elements by creating surfaces to mask and distinguish cardiomyocytes with respiratory chain deficiency (COX negative area) from the blue region to COX normal brown area. Magnification x10. Scale bars=100μm.
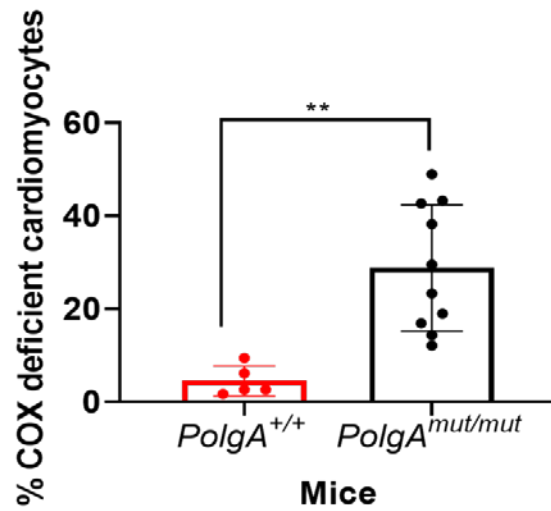
Figure 3.10. COX deficiency in the LV cardiac muscle of *PolgA+/+* and *PolgAmut/mut* mice. The percentage of total COX deficient blue regions were significantly higher in *PolgAmut/mut* mice hearts in comparison to *PolgA+/+* mice hearts (**p=0.0027) (unpaired t-test). Error bars represent mean ±SD.

3.3.10 *NBTx and laminin immunofluorescence in PolgA$^{+/+}$ mice and PolgA$^{mut/mut}$ mice hearts*

A disadvantage of the COX/SDH histochemical assay is that this dual colour test may hinder the detection of low or intermediate deficiency levels since the prominent brown colour may obstruct the light blue colour. Therefore, a more sophisticated histochemical assay known as the NBTx assay (Simard *et al*, 2018) was carried out to determine the intermediate COX level fibres. The NBTx assay exploits the competing redox reactions between electron carrier PMS, complex IV and NBT as explained in detail in chapter 2 section 2.24.1. Figure 3.11 shows a simplified diagram of how the assay works.
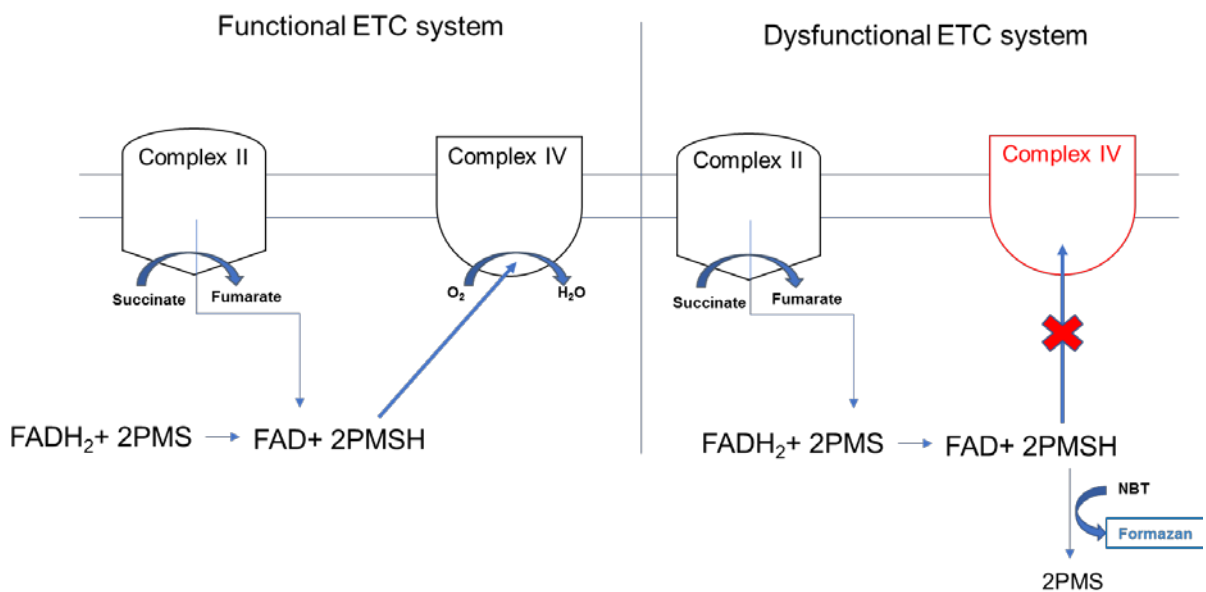
Figure 3.11. NBTx assay. Oxidised PMS has a dual affinity for COX and NBT.
PMSH passes on electrons to molecular oxygen via electron acceptors in COX in a fully functional system (left image) resulting in no colour change. When COX is dysfunctional, PMS preferentially passes electrons to NBT for reduction to a blue formazan end product (right image).

An advantage of NBTx assay over COX/SDH histochemistry is that the pathogenic loss of COX is distinguishable from lower levels of COX activity in cells with heterogeneous mitochondrial activity. Since the amount of NBT deposition in cells is directly proportional to the degree of COX deficiency, the darker the blue, the more COX negative the cardiomyocytes were.

NBTx histochemistry was performed in combination with laminin immunofluorescence (to demarcate the outline of individual cardiomyocytes) on 8µm LV cryosections of *PolgA$^{mut/mut}$* mice (n=10) and *PolgA$^{+/+}$* mice (n=5) hearts. Five random snapshots were taken at x10 magnification and a minimum of 500 LV transverse cardiomyocytes were investigated per mouse. Figure 3.12 shows laminin outlining the cardiomyocytes and NBTx image outlining the COX deficient fibres in blue. Images were acquired using Zeiss LSM800/SDI inverted microscope and analysed using quadruple immunoanalyser software**.**
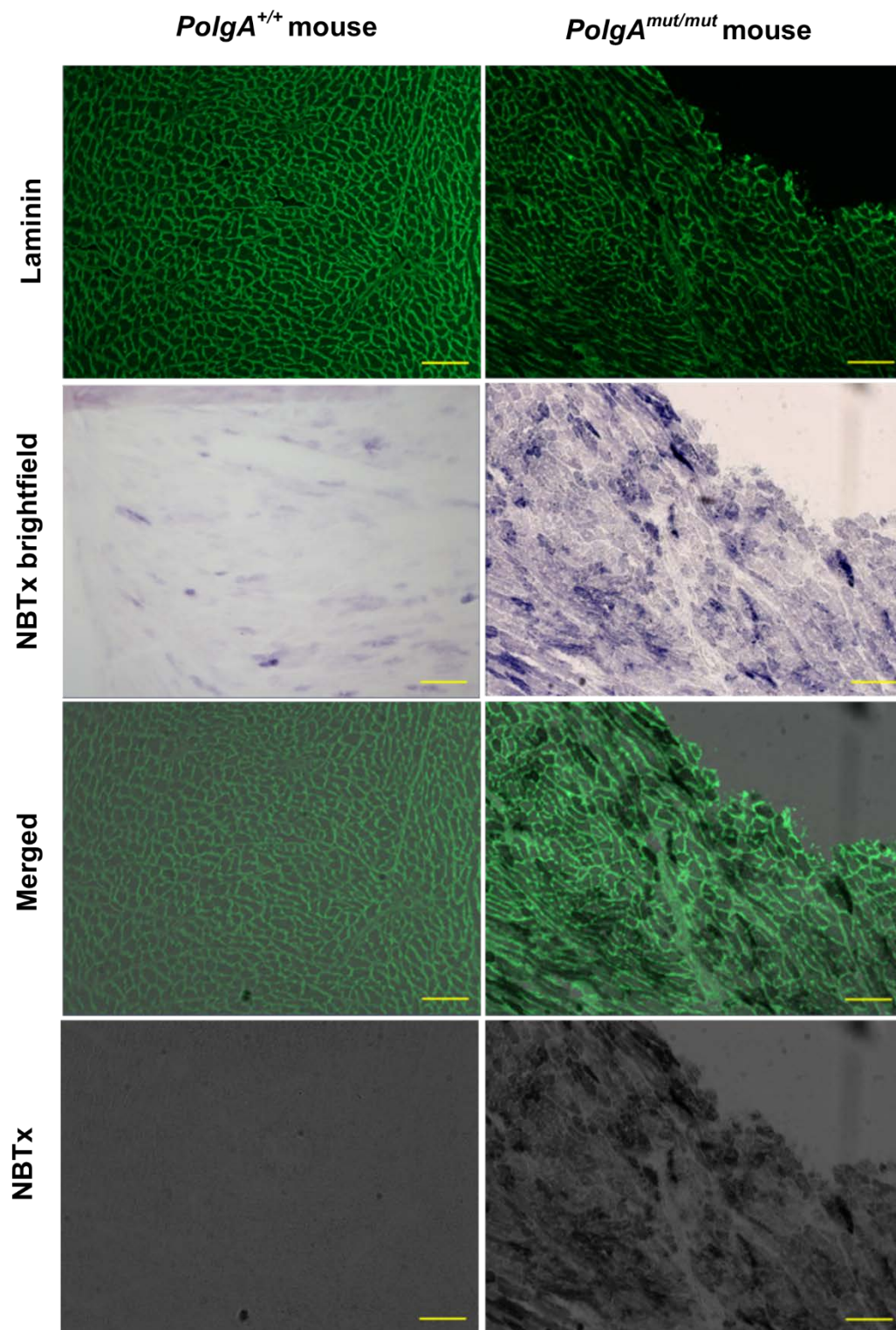
Figure 3.12. NBTx and laminin immunofluorescence. Laminin is used to outline cardiomyocytes. The images obtained from NBTx brightfield colour camera highlights the various degree of COX deficiency in blue in *PolgA$^{+/+}$* mice and *PolgA$^{mut/mut}$* mice LV tissue. Images from NBTx monochrome camera are uploaded on the quadruple immuno-analyser software. Magnification x10. Scale bars=100μm.

The analysis software measures the optical density (OD) of each individual cardiomyocytes. OD is a measure of how slowly light can travel through an object, therefore the higher the OD value, the slower the light travels and the darker the object is. The higher the optical density values, the darker the pixels and the more COX deficient the fibres are. The lower the optical density value, the lighter the pixels and the higher the COX activity is. An arbitrary numbering system was used to categorise COX levels into: positive (anything below -3SD from the mean OD of the cardiomyocytes in *PolgA*^{+/+} mice hearts), intermediate (between -3SD and -6SD from the mean OD cardiomyocytes in *PolgA*^{+/+} mice hearts) and negative (anything below -6SD from the mean of the cardiomyocytes of *PolgA*^{+/+} mice hearts). The mean OD of the no primary control sections (NPC) were measured to determine the levels of non-specific fluorescent signal which was subtracted from each value. Figure 3.13 shows the percentage of cardiomyocytes with positive, intermediate and negative COX activity in *PolgA*^{mut/mut} mice hearts relative to *PolgA*^{+/+} mice hearts. Eat dot represent average of all OD values that fall within the positive, intermediate and negative category.
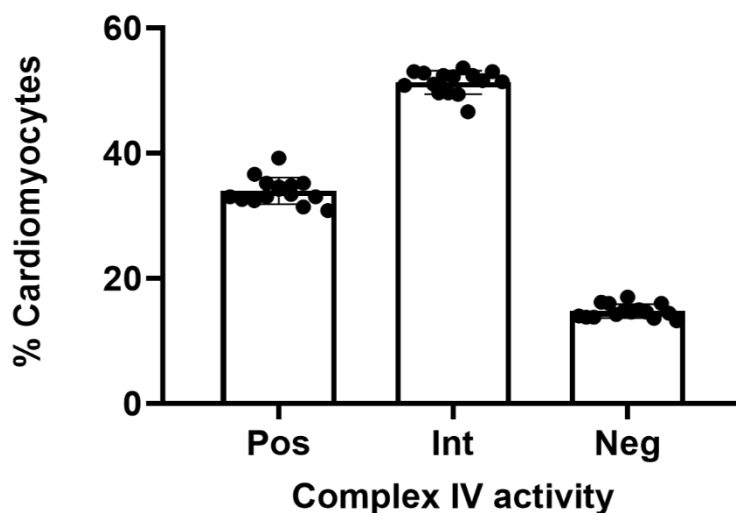
Figure 3.13. Category of COX activity levels. The percentage of COX positive, intermediate and negative cardiomyocytes in *PolgA*^{mut/mut} mice hearts relative to *PolgA*^{+/+} mice hearts. Error bars represent mean ±SD.

3.3.11 *Mitochondrial DNA copy number in PolgA$^{+/+}$ mice and PolgA$^{mut/mut}$ mice*

To assess whether the observed OXPHOS defects were only due to mtDNA mutations or whether there was any change in mtDNA copy number, real-time quantitative PCR was carried out to quantify mtDNA copy number in left ventricular (LV) cardiac muscle of *PolgA$^{mut/mut}$* mice (n=10) and *PolgA$^{+/+}$* mice (n=5). LV tissue was homogenised at the end of the study and the total genomic DNA was obtained. ND1 and β-actin primers were used to detect mtDNA and nuclear DNA respectively using relative standard curve method for three replicates per mouse. The ratio of ND1 to B-actin determined the relative mtDNA copy number frequency. There is no significant difference in mtDNA copy number in the cardiac muscle of *PolgA$^{mut/mut}$* and *PolgA$^{+/+}$* mice as shown in figure 3.14.
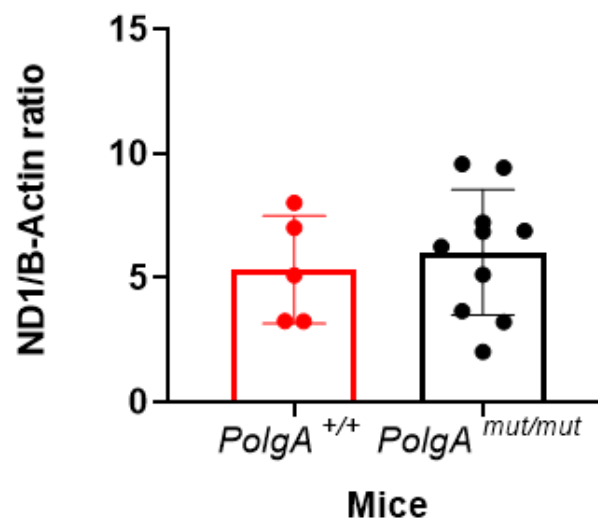
Figure 3.14. Mitochondrial DNA copy number as the ratio of ND1 to B-actin in *PolgA$^{+/+}$* mice and *PolgA$^{mut/mut}$* mice LV homogenates. There is no significant difference between the mtDNA copy number in the LV cardiac muscle of both cohorts (p=0.8) (unpaired t-test). Error bars represent mean ±SD.

3.4 Discussion

The aim of this study was to characterise the *PolgA$^{mut/mut}$* mice phenotypes and cardiac features in comparison to *PolgA$^{+/+}$* mice from the age of 14 weeks to 43 weeks. *PolgA$^{mut/mut}$* mice have shown an overall decreased lifespan with only 53.85%

reaching the end of the study while 100% of $PolgA^{+/+}$ mice survived to the endpoint. These data are in agreement with previous studies using the $PolgA^{mut/mut}$ mice. Kujoth et al (2005) demonstrated a significant reduction in lifespan of at least 230 $PolgA^{mut/mut}$ mice (p<0.0001) in comparison to wild-type littermates. A significant deterioration in health span of $PolgA^{mut/mut}$ mice was also evident with advancing age in comparison to $PolgA^{+/+}$ mice shown by the clinical scoring data. Similarly, Kujoth et al (2005) also identified an age-related decline in $PolgA^{mut/mut}$ mice including weight loss, loss of bone density, loss of intestinal crypts and testicular atrophy. They investigated the role of oxidative stress caused by mitochondrial ROS generation in isolated $PolgA^{mut/mut}$ mice hearts and livers to identify sources of increased mtDNA mutation load and found that the levels of mitochondrial H_2O_2, F2-isoprostanes and protein carbonyls (marker of ROS-induced damage) were not significantly different between the young and old $PolgA^{mut/mut}$ and $PolgA^{+/+}$ mice. Parallel with our findings of cellular apoptosis, Kujoth et al (2005) showed that $PolgA^{mut/mut}$ mice display early onset of caspase-3 mediated apoptotic pathway in their liver, testes, thymus and duodenum. They concluded that post-mitotic tissues such as skeletal muscle and brain are more resistant to the induction of apoptosis mediated mtDNA mutations in $PolgA^{mut/mut}$ mice. They suggested that phenotypic features of these mice were due to a depletion of oxidative capacity of tissues which is not as severe in normal ageing mice.

Trifunovic et al (2004) first identified the defects in the oxidative phosphorylation capacity of $PolgA^{mut/mut}$ mice in various tissues and correlated the phenotypic premature ageing phenotypes to the accumulation of somatic mtDNA mutation and clonal expansion of point mutations and deletions when $PolgA^{mut/mut}$ mice reach about 48 weeks of age. The phenotypic data presented in this chapter were supported by biochemical defects in oxidative phosphorylation capacity of cardiac muscle shown as the patchy pattern of respiratory chain deficiency in $PolgA^{mut/mut}$ mice confirming the findings of previous studies. Trifunovic et al (2004) reported significant levels of COX deficiency in the hearts of $PolgA^{mut/mut}$ mice as well as cardiac hypertrophy and development of cardiomyopathy at 40 weeks of age in comparison to their WT counterparts, similar to findings in ageing human studies (Muller-Hocker, 1990) and findings of this study. They confirmed the presence of abnormal vacuolated mitochondria in the cardiac muscle of $PolgA^{mut/mut}$ mice by electron microscopy. The frequency of full-length mtDNA copy number was also assessed by Trifunovic et al

(2004). They found that the number of full length mtDNA copy number in $PolgA^{mut/mut}$ mice was only 70% of the level in WT mice, however this observation did not alter the mtDNA expression levels. Consistent with the findings of this study, changes in the mtDNA copy number of $PolgA^{mut/mut}$ mice hearts was not associated with respiratory chain function, since significant COX deficiency with no change in mtDNA copy number was evident.

Safdar *et al* (2011) also highlighted the decline in clinical phenotypes of $PolgA^{mut/mut}$ mice from as early as 6 months of age, confirming the baseline characteristics of these mice. They have shown that $PolgA^{mut/mut}$ mice had significant loss of body fat, muscle mass and brain atrophy, anaemia as well as cardiac hypertrophy and cardiomyopathy compared with WT mice. They concluded that COX deficiency, reduction in electron transport chain protein subunits and nuclear DNA fragmentation as a measure of apoptosis were also significantly diminished in the hearts of $PolgA^{mut/mut}$ mice. The link between sustained mitochondrial dysfunction and activation of caspase 3 in DNA fragmentation of aged tissues and neurometabolic disorders were investigated by many other researchers (Hiona *et al,* 2010, Wohlgemuth *et al*, 2010, Wasilewski and Scorrano, 2009). One group showed that suppression of apoptosis prevented cardiomyopathy in the cardiac mitochondria of $PolgA^{mut/mut}$ mice (Mott *et al*, 2004). A study by the same group of scientists proposed that somatic mtDNA mutation-driven generation of misfolded mitochondrial proteins bind to pro-apoptotic enzymes to activate systemic apoptosis (Mott *et al*, 2004). Here we have shown that $PolgA^{mut/mut}$ mice hearts developed significant complex I and complex IV deficiency along with observations in increased cardiac muscle apoptosis.

Body energy stores such as fat are regulated by many factors in mice and have a direct effect on body temperature regulation. The changes in the mental behaviour and vegetative state of mice as well as disease state control energy expenditure and potentially body temperature. Since $PolgA^{mut/mut}$ mice do not show significant weight gain after 24 weeks of age, it's not surprising to see lower core body temperatures in $PolgA^{mut/mut}$ mice. The thermogenic capacity of $PolgA^{mut/mut}$ mice is partly diminished according to Shabalina *et al* (2017). We have not observed any body temperatures below 34°C in $PolgA^{mut/mut}$ mice. It's assumed that living in groups may hinder any fluctuations that would have been visible if animals were housed in individual cages.

The link between the level of activity and emotional state of mice was first observed by Costall *et al* (1989). Seibenhener and Wooten (2015) also documented that significant reduction in ambulatory ability of mice may be as a result of disturbed emotional state. My study showed that *PolgA*^{mut/mut} mice had a significant reduction in their total distance moved from the age of 15 weeks onwards which is a determinant of their overall level of activity. A reduction in the total number of touches and shorter step lengths were also characteristic of *PolgA*^{mut/mut} mice with advancing age in comparison to *PolgA* ^{+/+} mice at 43 weeks of age. Step length is a measure of gait and balance according to Lakes and Allen (2016) in a way that smaller step length indicates disturbed balance and coordination. Viveros *et al* (2007) documented that the intensity of behavioural responses to stressful conditions are inversely related to their lifespan. They assessed BALB/c mice in a T-maze test and concluded that those that slowly explore the maze are biologically similar to observations seen in prematurely aged mice. They have impaired neuromuscular ability and coordination as well as decreased locomotor activity, increased levels of anxiety and reduced lifespan. Dai *et al* (2013) have also shown that *PolgA*^{mut/mut} mice showed a significant decline in the locomotor activity at the age of 52 weeks in comparison to *PolgA*^{+/+} mice counterparts.

Pathological organ hypertrophy in *PolgA*^{mut/mut} mice is documented by many studies (Trifunovic *et al*, 2004, Dai *et al*, 2010) and is correlated with increased mtDNA point mutations and deletions and OXPHOS protein dysfunction. In this study cardiac hypertrophy was detected in the form of increased heart weight and increased cardiomyocyte width in *PolgA*^{mut/mut} mice. Organ weights are excellent screening tool to compare intervention-related effects which will be looked into more detail in chapters 4 and 5. Kujoth *et al* (2005) and Trifunovic *et al* (2004) have previously shown that there is a significant decline in subcutaneous fat and muscle mass as well as development of osteoporosis at around the age of 7-9 months in *PolgA*^{mut/mut} mice. The increase in organ size and decrease in body weight could mean a reduction in muscle mass, adipose tissue and/or bone density as these were the only tissues not weighed in this study. Others have previously shown that there is a significant reduction in adiposity, muscle mass and osteoporosis in the *PolgA*^{mut/mut} mice (Trifunovic *et al*, 2004). It was noted during the dissections that there was very little subcutaneous and visceral fat in the *PolgA*^{mut/mut} mice compared with the *PolgA*^{+/+} mice however it was not formally measured. In addition, data on bone mineral density

(BMD) on *PolgA^{mut/mut}* mice from this colony was generated in our lab showing significant loss of BMD by micro CT at 11 months of age compared with *PolgA^{+/+}* mice (Philip Dobson, PhD Thesis).

Cardiac tissue is a highly metabolic organ and is rich in mitochondria (Boengler *et al*, 2017). As *PolgA^{mut/mut}* mice accumulate mtDNA mutations at a faster rate than *PolgA^{+/+}* mice, highly active organs such as the heart work under pressure to supply other bodily organs with oxygenated blood. Due to the fact that adult cardiomyocytes are terminally differentiated and are highly specialised cells, the hypertrophic response is predominantly observed as increased cardiomyocyte size, rather than number as confirmed by the significant increase in cardiomyocyte width in this study. Myocardial hypertrophy is divided into physiological and pathological categories. Vanempel and Windt (2005) have demonstrated that when cardiac muscle experiences increased biochemical stress, individual cardiomyocytes grow in size to normalise wall tension by activating G-protein coupled receptors ($G\alpha_q$) and the downstream signalling cascade leading to normal cardiac function in mice. The hypertrophic signalling cascade is linked to cellular apoptosis in such a way that over-expression of $G\alpha_q$ by 25 fold, leads to a significant chamber dilation and a higher percentage of myocyte apoptosis eventually leading to heart failure. The molecular mechanism underlying this phenomenon is explained in the ability of $G\alpha_q$ to cause mitochondrial membrane potential loss and cytoplasmic release of cytochrome c when overexpressed in the cardiac muscle. Cytochrome c activation in turn initiates a cascade of events leading to activation of pro-apoptotic Bcl-2 family members and initiates proteolytic activity of caspase-3. The outcomes of this study are in agreement with the current research confirming the correlation between cardiac hypertrophic response and activation of cardiac apoptosis (Mayorga *et al*, 2004).

It's well documented that mitochondrial dynamics, biogenesis and turnover is dysregulated with age resulting in accumulation of damaged and compromised mitochondria (Leeuwenburgh *et al*, 2016). What happens to mtDNA copy number with age in post-mitotic cardiac muscle is however not fully understood. Recent research has shown that altered mtDNA copy number is associated with numerous disorders such as cancer (Xing, 2008), liver disease (Morten *et al*, 2007) developmental delays (Macmillan and Shoubridge, 1996), cardiomyopathies (Bai and Wong, 2005) and diabetes (Choi *et al*, 2001) in which a reduction in the mtDNA copy

number was seen in all cases. Perier *et al* (2013) have reported a significant increase in the mtDNA copy number of *PolgA^{mut/mut}* mice ventral midbrain sections and have suggested that the increase in mtDNA copy number may be a compensatory protective mechanism at older age. They have also confirmed that this compensatory mechanism of increasing the mtDNA copy number were only applicable to neurons with mtDNA deletions of below 60% of total mtDNA when mitochondrial biochemical defects were not detected in the tissue.

3.5 Strengths and limitations of the study

One of the strengths of this study was the establishment of a colony of *PolgA^{mut/mut}* mice over a few years and a large sample size dedicated for this study. Power calculations were carried out to evaluate the sample size according to the aims and objectives of this research and current literature. This gives precision, reliability and direction to the data obtained from a variety of investigations. On the other hand, the *PolgA^{+/+}* mice with smaller sample size may leave a larger margin for error as the level of confidence was lower. However due to extensive research on the *PolgA^{+/+}* mice, as expected we obtained data with a narrow distribution.

3.6 Conclusion

An in-depth investigation of *PolgA^{mut/mut}* mice phenotypes in comparison to *PolgA^{+/+}* mice was carried out in this study. The cardiac mitochondrial function was assessed, and the cardiac muscle pathology was quantified in *PolgA^{mut/mut}* mice. The phenotypic data accompanied the molecular findings of age-dependent decline in *PolgA^{mut/mut}* mice such as diminished locomotive activity, deterioration of body conditioning, weight loss, organ hypertrophy, increased cardiac fibrosis and cardiomyocyte width as well as increased cardiac apoptosis and mitochondrial COX dysfunction. The results of this chapter set the foundation for further investigation of effects of endurance exercise in *PolgA^{mut/mut}* mice cardiac muscle.

Chapter 4

Chapter 4. The effects of moderate to high intensity treadmill running on cardiac mitochondrial function and progeroid ageing phenotypes in *PolgA$^{mut/mut}$* mice

4.1 Introduction

4.1.1 *The impact of endurance exercise on mouse and human studies*

The baseline characteristics of *PolgA$^{mut/mut}$ mice* were established in chapter 3 of this thesis and confirmed the phenotype described in previous studies (Trifunovic *et al*, 2004 and Kujoth *et al*, 2005) which included a premature ageing phenotypes, reduced lifespan, systemic mitochondrial dysfunction and multisystem pathology with advancing age. Safdar *et al* (2011) demonstrated that 5 months of endurance exercise training in *PolgA$^{mut/mut}$* mice prevented the premature mortality rate, reduced pathological levels of apoptosis, mtDNA depletion and mutation rate, induced mitochondrial biogenesis, increased oxidative capacity and restored mitochondrial morphology. Safdar *et al* in 2016 published a follow up study demonstrating a reduction in mitochondrial oxidative stress with endurance exercise. They concluded that alleviation of premature ageing phenotypes in *PolgA$^{mut/mut}$* mice muscle by exercise is not associated with reduction of mtDNA mutation load, but rather with reduction in oxidative stress. Endurance exercise-mediated PGC-1α expression promotes mitochondrial biogenesis and increases the expression of mitochondrial antioxidants hence depressing oxidative stress (St-Pierre *et al*, 2006). Wenz *et al* in 2009 demonstrated that increasing the expression of PGC-1α attenuates age-associated metabolic disorders and sarcopenia. Peroxisome proliferator-activated receptor gamma coactivator 1-alpha (PGC-1α) is a key regulator of energy metabolism in mitochondria acting as a transcriptional coactivator that is central to induction of mitochondrial biogenesis (Austin and St-Pierre, 2012). P53 is a tumour suppressor protein which translocates to the mitochondria during endurance exercise and in response to intra- and extra-cellular insults such as ROS accumulation, to facilitate mtDNA mutation repair mechanisms and mitochondrial biogenesis by interacting with mtDNA, POLG1 and PGC-1α (Safdar *et al*, 2016). In the absence of nuclear p53, PGC1-α should be acting to ameliorate the mutator phenotypes in *PolgA$^{mut/mut}$* mice since nuclear p53 directly represses pro-metabolic activity of

PGC1-α. However biochemical analysis of p53 revealed its inherent 3'-5' exonuclease activity which helps promote mitochondrial genomic stability in *PolgA mut/mut* mice. Also an exercise intervention in muscle-specific p53 knockout *PolgA^mut/mut* mice failed to alleviate oxidative stress and premature signs of ageing. Saleem and Hood (2013) suggested that p53 is working in a PGC-1α independent manner to supress reactive oxygen species (ROS) generation. A study by Meek *et al* (2009) reported that transgenic mice with high endurance capacity run ~3 times more than control mice. They determined that the mechanistic basis of high endurance in these mice appear to be partly due to elevated VO_{2max} levels (Rezende *et al*, 2006), enhanced insulin-triggered glucose in skeletal muscle (Dumke *et al*, 2001) and enhanced ability of lipid oxidation to fuel sustained exercise (Gomes *et al*, 2009).

Endurance exercise is documented to be the most potent inducer of mitochondrial biogenesis in many organs especially those with higher ATP demand (Irrcher *et al*, 2003). Safdar *et al* (2011) reported that endurance exercise rescued mitochondrial depletion, increased mitochondrial abundance, maintained mitochondrial morphology and ETC subunit content and regulated COX activity in the cardiac tissue of exercised *PolgA^mut/mut* mice. They also reported that endurance exercise has systemically abrogated apoptosis and prevented cardiac fibrosis. Although *PolgA^mut/mut* mice do not show increased levels of ROS in cardiac tissue (Kujoth *et al*, 2005 and Trifunovic *et al*, 2005), the expression of mitochondrial-targeted catalase (mCAT), which protects cells from oxidative damage, reverses the accumulation of mtDNA mutations in cardiac tissue of *PolgA mut/mut* mice (Dai *et al*, 2010).

The cardiovascular benefits of exercise have also been widely investigated on humans and on mice studies. Munukka *et al* (2018) published their work indicating that 6 weeks of bicycle endurance training three sessions/week significantly modified the composition and function of gut microbiota without any dietary changes. They observed a reduction in the levels of proteobacteria post exercise by 16s rRNA sequencing. Proteobacteria are involved in gut inflammation while the levels of beneficial bacteria were increased indicating better metabolism with exercise. Pekkala *et al* (2017) investigated the cardiometabolic benefits of endurance exercise and established that endurance training decreased plasma phospholipids and VLDL (very-low density lipoprotein) levels significantly. VLDLs transport lipids from the liver to other organs, converting into bad cholesterol in the circulation, thus has unfavourable cardiovascular effects. They also found that the activity of vascular

adhesion protein-1 (VAP-1) was lowered with endurance training. VAP-1 is involved in lipolysaccharide-induced inflammation and is proven to mediate microenvironment to pro-inflammatory direction hence have detrimental effects on the vasculature (Yu *et al*, 2006).

Human ageing is associated with loss of muscle mass (sarcopenia) and reduced muscle function that results in frailty (Fried *et al,* 2001). At least some of this muscle mass loss has been proven to be linked to reduced physical activity and muscle disuse with age. However, Faulkner *et al* in 2008 reported that life-long exercise cannot fully rescue age-related decline in muscle mass, indicating the multi-factorial process that lead to sarcopenia with age. Lutz and Quinn (2012) have suggested that elevated levels of inflammatory biomarkers may play a role in the pathogenesis of sarcopenia. Mikkelsen *et al,* (2013) have reported that life-long endurance exercise in non-obese individuals was linked to a reduction in the age-associated increase in insulin sensitivity, as well as significant reduction in inflammatory biomarkers such as C-reactive protein (CRP) and Interleukin-6 (IL-6).

The degree of exercise intolerance in patients with mtDNA mutations varies from low to debilitating (Taivassalo, 2003). These exercise-related symptoms inevitably cause a high proportion of patients with mtDNA mutations to lead a sedentary lifestyle (Taivassalo and Haller, 2004). It's also confirmed that inactivity results in deconditioning which is associated with a decrease in functional mitochondrial number and limited capacity of skeletal muscle for oxidative phosphorylation (Gehrig *et al*, 2016) as well as diminished cardiovascular capacity (Martin *et al*, 1986). Patients with mtDNA mutations thus further exacerbate their functional limitations by being inactive. Taivassalo *et al* (2006) have shown that 14 weeks of endurance exercise training improved peak oxygen capacity with no changes in the level of deleted mtDNA.

The gene-shifting theory was established by Crameri *et al* (2004) stating that satellite cells in skeletal muscle become activated and replace the mature post-mitotic myofibrils in response to muscle overload such as during injury or acute muscle resistance overload. Clark *et al* (1997) used a myotoxic agent to induce muscle necrosis and revealed that regenerated muscle fibres had wild-type mtDNA genotype upon induction of satellite cells. Satellite cells have proliferative and regenerative capacity, documented to withstand injury in skeletal muscle. Although further studies

are needed to ascertain the type of muscle contraction required to maximally induce satellite cell activation. Eccentric muscle contraction is proven to provide a more potent stimulus however this is less practical for patients with mtDNA mutation (Franchi, Reeves and Narici, 2017). Therefore, the magnitude of physiological benefits of exercise depend on duration, intensity and frequency of training. Endurance exercise-related increase in mitochondrial biogenesis may cause an increase the proportion of absolute wild-type mtDNA and mutant mtDNA in skeletal muscle below threshold for phenotypic disease expression but enough to confer physiological and biochemical benefits in patients with mtDNA defects (Taivassalo and Haller, 2004).

4.2 Aims of study

The aim of this study was to investigate the effect of 6 months of endurance exercise on the premature age-associated phenotypes in *PolgA$^{mut/mut}$* mice compared to the sedentary *PolgA$^{mut/mut}$* mice characterised in chapter 3 focusing particularly on the cardiac muscle. The data were used in keeping with the 3Rs of animal use (reduction, refinement and replacement). This study used an established treadmill running protocol, previously shown to be well-tolerated and advantageous in *PolgA$^{mut/mut}$* mice (Safdar *et al*, 2011). The central questions, I aimed to answer were to ascertain the following:

1. What is the effect of endurance exercise on the clinical phenotype of sedentary and exercised *PolgA$^{mut/mut}$* mice from 3 to 11 months of age?

2. What is the effect of endurance exercise on the behavioural characteristics of sedentary and exercised *PolgA$^{mut/mut}$* mice from 3 to 11 months of age?

3. What is the effect of endurance exercise on cardiac structure, histology and mitochondrial function in sedentary and exercised *PolgA$^{mut/mut}$* mice from 3 to 11 months of age?

4.3 Results

4.3.1 *Survival curve, Clinical scoring and Body weight of sedentary and exercised PolgA$^{mut/mut}$ mice*

PolgA$^{mut/mut}$ mice were housed with their heterozygous (*PolgA$^{mut/+}$*) and wild type littermates (*PolgA$^{+/+}$)* in cages of 2, 3 or 4. They were randomly divided into groups of (n=10) exercised and (n=10) sedentary mice from the age of 4 months. An endurance exercise intervention programme was performed on exercised *PolgA$^{mut/mut}$* mice according to the protocol documented in chapter 2 section 2.14. The lifespan of mice was recorded and is shown in the survival curve in figure 4.1A. 53.85% of sedentary mice lived to the end of the study and 58.4% of exercised mice made it to the 46 week endpoint. Those that did not survive to the endpoint for reasons such as fight wounds and anal prolapse were not included in the survival curve.

Figure 4.1B shows the body weight of sedentary and exercised *PolgA$^{mut/mut}$* mice from weeks 14 to 43. There was no significant difference between the body weight of sedentary *PolgA$^{mut/mut}$* mice and exercised *PolgA$^{mut/mut}$* mice at 14 weeks (30.07±2.78 and 29.87±3.01 respectively) and at 43 weeks of age (32.5±0.0002 and 30.02±2.15 respectively). There was also no significant age-related weight changes within each group (p>0.05, two-way ANOVA repeated measures).

The clinical scoring of mice was carried out from the age of 14 weeks up to 43 weeks to assess the health span of mice including weight, coat condition, skin tone, behaviour, posture and mobility, abdominal distension, foot colour and the level of hydration of mice. Sedentary (n=10) and exercised (n=10) mice were scored for each characteristic from 0 to 3 which indicate the normal and worsening of specific characteristic respectively. 8 characteristics were rated, and the total score was recorded and plotted in figure 4.1C. Each dot on the graph represent an individual mouse. At 43 weeks 100% of exercised mice showed no evidence of weight loss, 28.6% had piloerection, 14.3% showed behavioural changes such as isolation and avoidance, 14.3% had hunched posture and compromise mobility and 28.6% had pale foot colour (indicative of anaemia). In comparison to sedentary mice in which 14.3% showed weight loss, 85% had piloerection, 14.3% demonstrated behavioural isolation and avoidance, 14.3% had hunched posture and compromised mobility and 57.1% had pale foot colour. The body condition of both sedentary and exercised

PolgA^{mut/mut} mice declined significantly with advancing age shown as the increase in clinical scores (p<0.001 in both cases, Two-way ANOVA repeated measures). There was no significant difference between the body condition of sedentary and exercised *PolgA^{mut/mut}* mice at any time points (p>0.05).
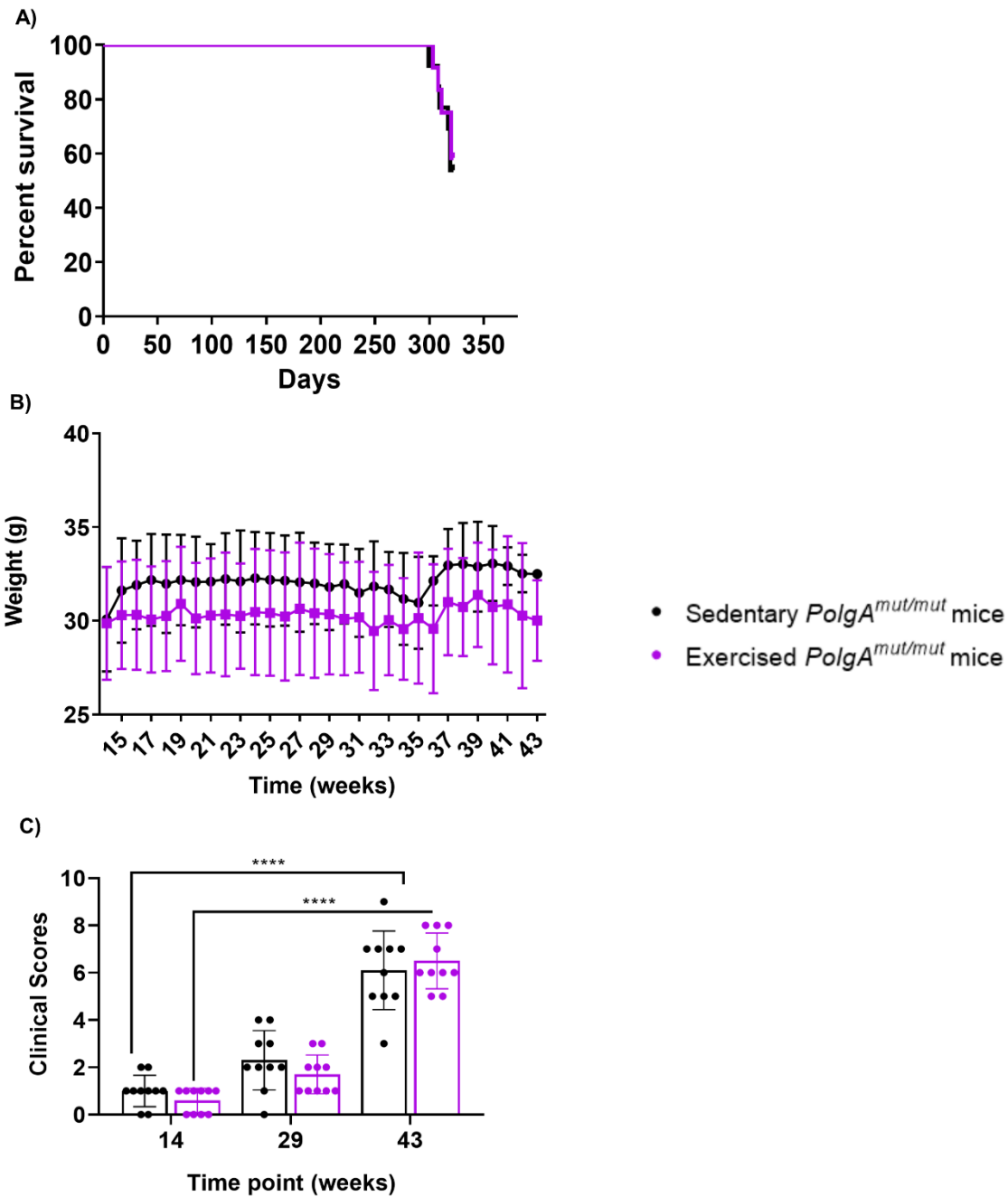
Figure 4.1. Kaplan-Meier survival curve, body weight and clinical scoring in sedentary and exercised *PolgA^mut/mut* mice. A) 53.85% of sedentary mice and 58.4% of exercised mice survived to the end of the study. B) The body weight of sedentary and exercised *PolgA^mut/mut* mice was not significantly different between the two cohorts at any time point. C) Clinical scoring at 14 week, 29 weeks and 43 weeks of age. Both cohorts have shown a significant decline in body condition (****$p<0.001$) (Two-way ANOVA, repeated measures). Error bars represent mean ±SD.

4.3.2 *Body temperature in sedentary and exercised PolgA^mut/mut^ mice*

The body temperature of sedentary and exercised *PolgA^mut/mut^* mice was recorded 4x/week from 14 weeks of age to 43 weeks of age. Figure 4.2 shows the body temperature of both cohorts of mice which was recorded before treadmill running in exercised *PolgA^mut/mut^* mice (n=10) and at the same time from the sedentary *PolgA^mut/mut^* mice (n=10). The room and cage temperatures remained constant at all times. Figure 4.2 shows that the body temperature of sedentary and exercised *PolgA^mut/mut^* mice at 14 weeks (pre-intervention), 29 weeks (mid-intervention) and 43 weeks (post-intervention) did not differ significantly at different time points. At 14 weeks of age, the body temperature of sedentary *PolgA^mut/mut^* mice was 35.36°C±0.74 in comparison to 35.33°C±0.4 in exercised mice (p>0.05). At 29 weeks of age the body temperature of exercised *PolgA^mut/mut^* mice started to go down to 34.79°C±0.7 however this was not significantly different to the sedentary mice at 29 weeks (35.05°C±0.2). Similarly, at 43 weeks, the body temperature of sedentary mice was 35.1°C±0.2 in comparison to exercised mice 34.63°C±0.83 (p>0.05). The exercised mice however seemed to have significantly lower body temperature with advancing age, falling from 35.3°C±0.4 to 34.6°C±0.83 from 14 weeks to 43 weeks of age (p<0.05) as shown in figure 4.2 (Two-way ANOVA repeated measures).
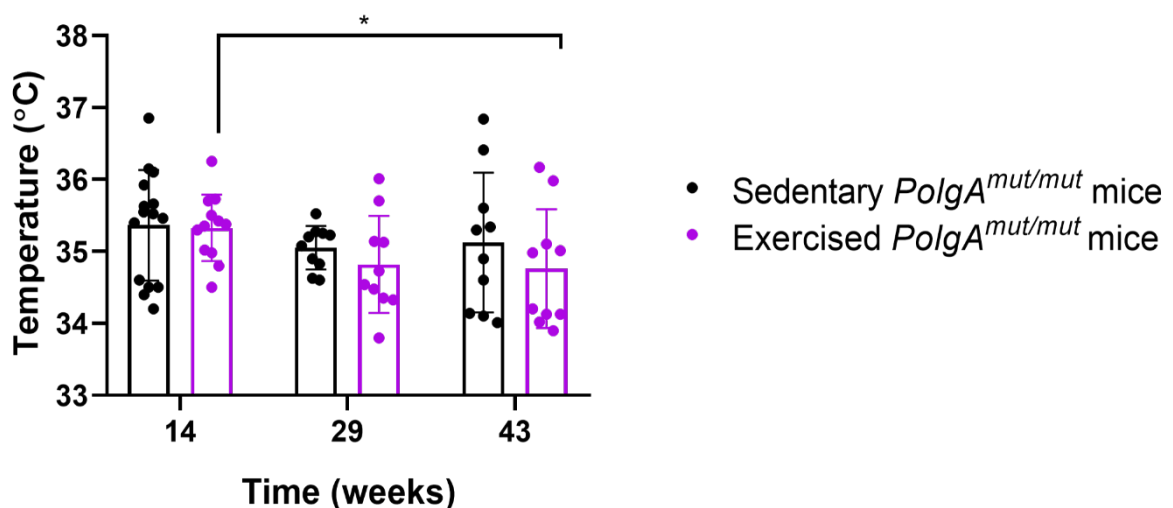
Figure 4.2. Body temperature in sedentary and exercised *PolgA^mut/mut^* mice at 14, 29 and 43 weeks of age. Exercised mice had a significant decrease in body temperature with advancing age, 14 weeks vs 43 weeks (*p<0.05, Two-way ANOVA, repeated measures). Error bars represent mean ±SD.

4.3.3 *Open field testing (OFT) in sedentary and exercised PolgA$^{mut/mut}$ mice*

In order to evaluate motor performance and quantitatively assess gait analysis, open field testing was performed in sedentary (n=10) and exercised (n=10) *PolgA$^{mut/mut}$* mice pre- (15 weeks), mid- (29 weeks) and post- (43 weeks) intervention. The room temperature, humidity and the lighting were kept consistent at all times during the OFT. The parameters measured within a 5 minute period of testing time included the total distance moved, average velocity, rearing frequency, total number of touches and average step length (figure 4.3). A two-way ANOVA repeated measures was carried out in order to see the interaction between and within groups.

Total distance moved by both groups of mice (figure 4.3A) increased significantly with age up to the age of 29 weeks, however exercised mice showed a further increase in distance travelled by 43 weeks of age ($p<0.01$). Sedentary mice showed a significant reduction in their velocity of movement with age up to 43 weeks ($p<0.01$) and exercised mice moved faster at 43 weeks of age in comparison to sedentary mice ($p<0.01$) (figure 4.3B).

Figure 4.3C shows that the number of touches reduced significantly with age in sedentary mice ($p<0.05$) and was significantly lower at 43 weeks in sedentary mice comparison to exercised mice ($p<0.05$). A reduction in the number of touches with age are indicative of less movements or longer step lengths. In general step length was reduced significantly in sedentary cohort at 43 weeks ($p<0.01$) however both groups had significant decline in step length with age. Interestingly exercised mice seem to have a slight but significant decrease in their step length at 29 weeks of age ($p>0.05$) however that increased significantly at 43 weeks of age in comparison to sedentary cohort ($p<0.01$). The final parameter obtained from the OFT device was the rearing frequency in which mice stand on their hind legs and explore their environment as a measure of exploratory and inquisitiveness behaviour. Figure 4.3E shows that rearing frequency has significantly decreased in sedentary mice with advancing age from 29 weeks to 43 weeks of age ($p<0.05$) however there was no significant difference between the rearing frequency of sedentary and exercised mice at different time points. A two-way ANOVA statistical analysis test repeated measures was carried out to extract the interaction between groups and with age.
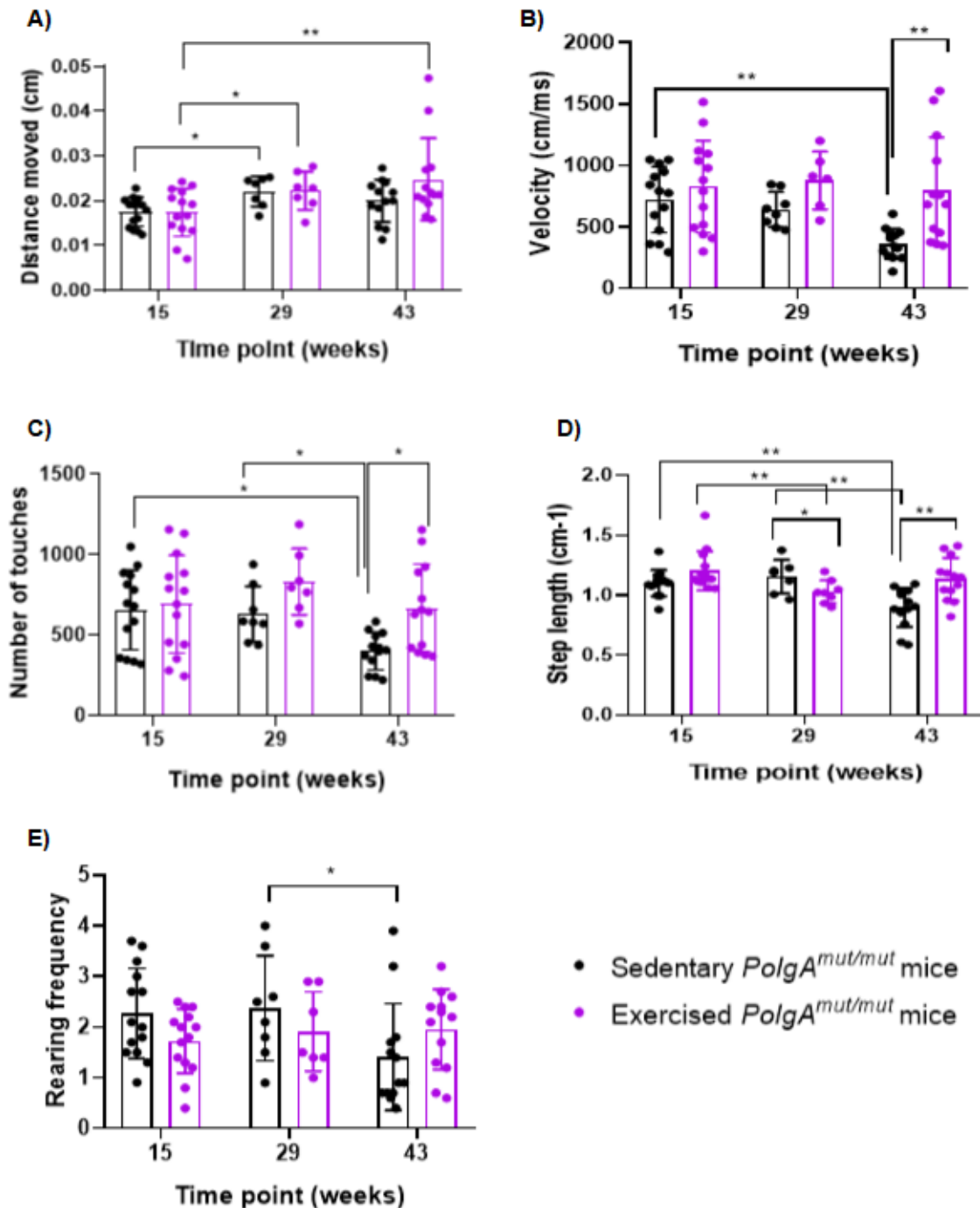
Figure 4.3.Open field testing in sedentary and exercised *PolgA^mut/mut* mice at 15, 29 and 43 weeks of age. A) Total distance moved significantly increased in exercised and sedentary mice with advancing age up to 29 weeks (*$p < 0.05$). B) Average velocity of sedentary mice reduced significantly with advancing age (**$p < 0.01$) and exercised mice had significantly higher velocity at 43 weeks (**$p < 0.01$) in comparison to sedentary mice. C) Total number of touches significantly reduced in sedentary mice with advancing age (*$p < 0.05$) and was significantly higher in exercised mice at 43 weeks of age (*$p < 0.05$). D) Step length has significantly reduced in both groups with advancing age but was significantly higher in exercised mice at 43 weeks of age (**$p < 0.01$). E) Rearing frequency has significantly reduced in sedentary mice with age (*$p < 0.05$) (Two-way ANOVA repeated measures). Error bar represent mean ±SD.

4.3.4 *Organ weights in sedentary and exercised PolgA$^{mut/mut}$ mice*

Organs weights (figure 4.4A) were recorded immediately after harvest in both groups according to the mouse organ harvesting sheet in appendix 2. Normalised organ weights were also calculated by the ratio of organ weight to body weight to observe changes in organ weight in proportion to body weight (figure 4.4B). Since body weights were not significantly different between the groups at any time point throughout the intervention, it's unlikely that organ weights would significantly alter due to body weight fluctuation. There were no significant differences in the weight or organ to body weight ratios in any of the organs analysed in the two groups of mice (unpaired t-test).
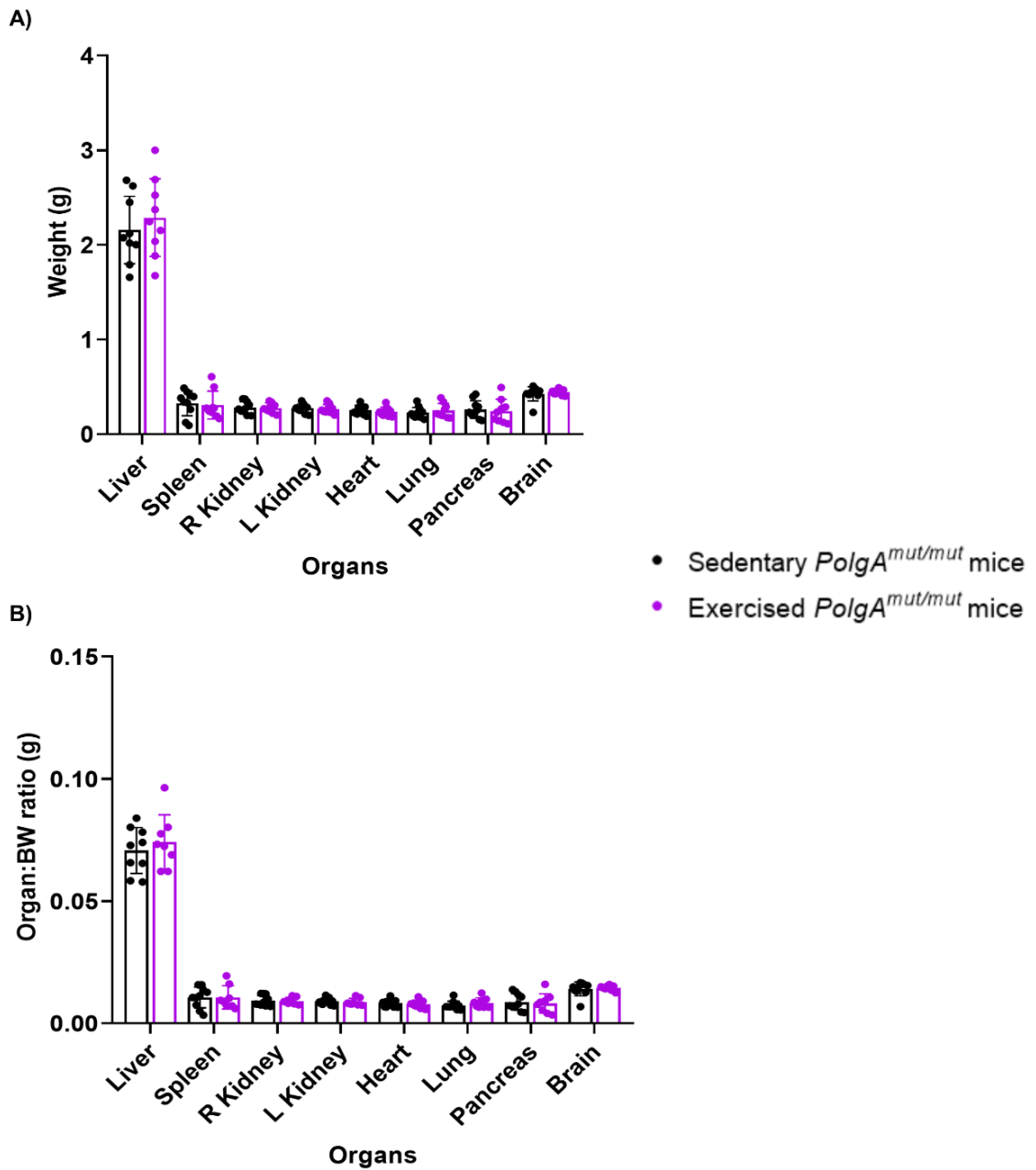
Figure 4.4.Organ weight and normalised organ weights in sedentary and exercised *PolgA^{mut/mut}* mice. A) Organ weights in sedentary and exercised mice were not significantly different. B) None of the organ to body weights ratios of sedentary and exercised mice were significantly different. Error bars represent mean ±SD.

139

4.3.5 . Cellular and molecular analysis of the heart in sedentary and exercised PolgA^{mut/mut} mice

Mouse hearts were harvested and dissected through the interventricular septum longitudinally to divide into left and right sides with one atria and one ventricle on each side.

Histological techniques including COX/SDH histochemistry, NBTx assay and mitochondrial DNA copy number analysis was carried out on the frozen left ventricular tissue as explained in chapter 2 sections 2.21, 2.24.1 and 2.26 respectively. H&E staining, Masson trichrome, cleaved caspase 3 immunohistochemistry as well as mitochondrial OXPHOS complex I and complex IV immunofluorescence was carried out on the fixed RV tissue as detailed in chapter 2 sections 2.20,2.22, 2.23.1 and 2.24.2 respectively.

4.3.6 . Histological analysis of sedentary and exercised PolgA^{mut/mut} mice right ventricle at 46 weeks of age

In order to asses cardiomyocytes size and morphology, Haematoxylin and Eosin (H&E) staining was carried out on 4µm paraffin embedded right ventricular section from sedentary (n=10) and exercised (n=10) *PolgA^{mut/mut}* mice hearts according to protocol detailed in chapter 2 section 2.20. Five random snapshots of x20 magnification images were selected and 50 random transverse cardiomyocytes were analysed per image. Images were acquired using Zeiss Axiomager microscope and analysed in Zen (v2.5) software to record the width of cardiomyocytes. Figure 4.5A top row shows representative H&E images from both cohorts of mice. There was no significant difference between the mean cardiomyocyte width of both groups (p=0.245, unpaired t-test), although the individual mouse data showed more variation in the exercised cohort.

Right ventricular fibrosis was also carried out by Masson trichrome staining in 10 sedentary and 10 exercised *PolgA^{mut/mut}* mice (figure 4.5A bottom row images). 4µm paraffin embedded cardiac sections were stained for the presence of nuclei in purple, collagenous connective tissue in blue and cardiomyocytes in red. Images were obtained using Nikon Tie widefield invert microscope. The percentage of collagen to

total tissue was calculated in NIS elements software by the thresholding method using the RGB general analysis algorithm. The three channel analysis method masks off and measures the percentage of total blue collagen area from total tissue section. The thresholding for each channel and LED light intensity remained constant for all the mice. There was no significant difference in the percentage of fibrosis between the two cohorts (p=0.61, unpaired t-test). The left hand side images presented in figure 4.5A from *PolgA^mut/mut* sedentary cohort were also presented in chapter 3.
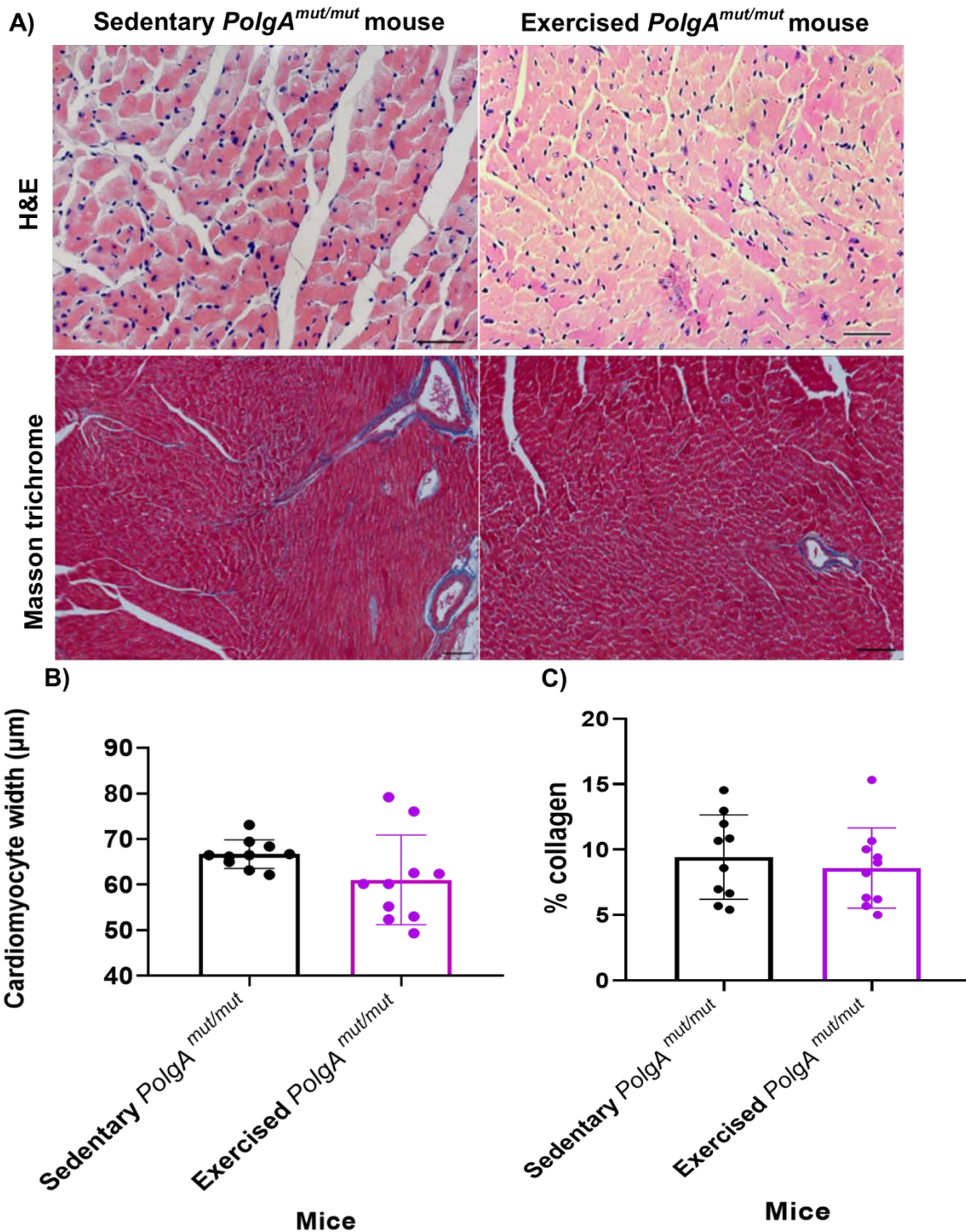
Figure 4.5. Cardiomyocyte width and fibrosis in sedentary and exercised *PolgA^{mut/mut}* hearts. A) Top row: H&E staining showing cardiomyocytes in pink and nuclei in blue, scale bars= 100µm (x20 magnification). Bottom row: Masson trichrome staining (x10 magnification) showing the presence of fibrous tissue in light blue and cardiomyocytes in red. Scale bars=200µm. B) Cardiomyocyte width in sedentary and exercise *PolgA^{mut/mut}* hearts (p=0.245). C) Percentage of collagen in cardiac muscle of sedentary and exercised *PolgA^{mut/mut}* hearts (p=0.61) (unpaired t-test). Error bars represent mean ±SD.

4.3.7 *Cardiac apoptosis in sedentary and exercised PolgA*$^{mut/mut}$ *hearts*

Active-cleaved caspase 3 (CC3) immunohistochemistry was carried out to identify cardiomyocytes with apoptotic nuclei in sedentary (n=10) and exercised (n=10) *PolgA*$^{mut/mut}$ mice according to the protocol stated in chapter 2 section 2.23. Paraffin embedded right ventricular cardiac muscle (4µm) were subjected to CC3 immunohistochemistry to identify apoptotic nuclei. Five random snapshots of x10 magnification images were selected and the frequency of apoptotic nuclei as dark brown circular regions were quantified in comparison to the total number of non-apoptotic nuclei. Images were obtained using Aperio-scanner and analysed using Imagescope nuclear staining algorithm. An unpaired t-test was carried out to statistically compare the percentage of CC3 positive nuclei in the two groups. There was no significant difference in the percentage of CC-3 positive cells in sedentary and exercised mice (p>0.05) as shown in figure 4.6.
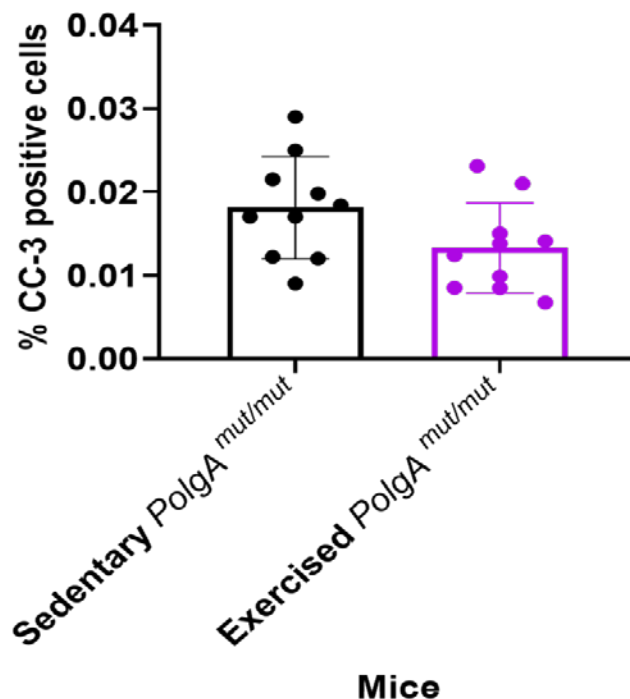
Figure 4.6. Cardiac apoptosis in sedentary and exercised *PolgA*$^{mut/mut}$ mice. Percentage of cardiac apoptosis is not significant different between the two cohorts (p>0.05, unpaired t-test). Error bars represent mean ±SD.

4.3.8 *Mitochondrial complex I and complex IV expression levels in sedentary and exercised PolgA$^{mut/mut}$ hearts*

Mitochondrial OXPHOS complex I (NDUFB8) and complex IV (MTCOI) subunit immunofluorescence was carried out according to the method in chapter 2 section 2.24.2. 4µm fixed right ventricular sections were immunolabelled for detection of complex I (NDUFB8), complex IV (MTCOI), mitochondrial mass marker (Porin) and cardiomyocyte boundary marker (laminin). N=10 mice were analysed per group (exercise or sedentary). Figure 4.7 shows representative images obtained from LSM800 Axio-observer microscope from a sedentary and an exercised *PolgA$^{mut/mut}$* mouse heart. The expression levels of NDUFB8 and MTCOI were quantified relative to mitochondrial mass marker (Porin) levels through immunoanalyzer software. Cardiomyocytes were marked with laminin for easier detection and analysis through immunoanalyzer software which is explained in more detail in chapter 2 section 2.24.2. Cardiomyocytes were categorised into groups of positive (Pos), intermediate positive (Int +), intermediate negative (Int -) and negative (Neg) in both NDUFB8 and MTCOI levels (figure 4.8) according to their z-scores adapted from Rocha *et al* (2015). Mitochondrial respiratory chain plots (MRC) were obtained from the immunoanalyzer software. Representative MRC plots from a sedentary and an exercised mice are shown in figure 8 A-B. These plots show the levels of MTCOI and NDUFB8 proteins in individual cardiomyocytes. The colour of each dot represents the level of Porin, and the category boundaries are marked with yellow and black lines.

As shown in figure 4.8C, the percentage of cardiomyocytes with negative CI levels and negative CIV levels were significantly higher in the sedentary cohort ($p<0.001$ and $p<0.05$ respectively). The percentage of cardiomyocytes with CIV intermediate negative was significantly higher in the exercised cohort ($p<0.001$) through unpaired t-test between categories in comparison to exercised group.
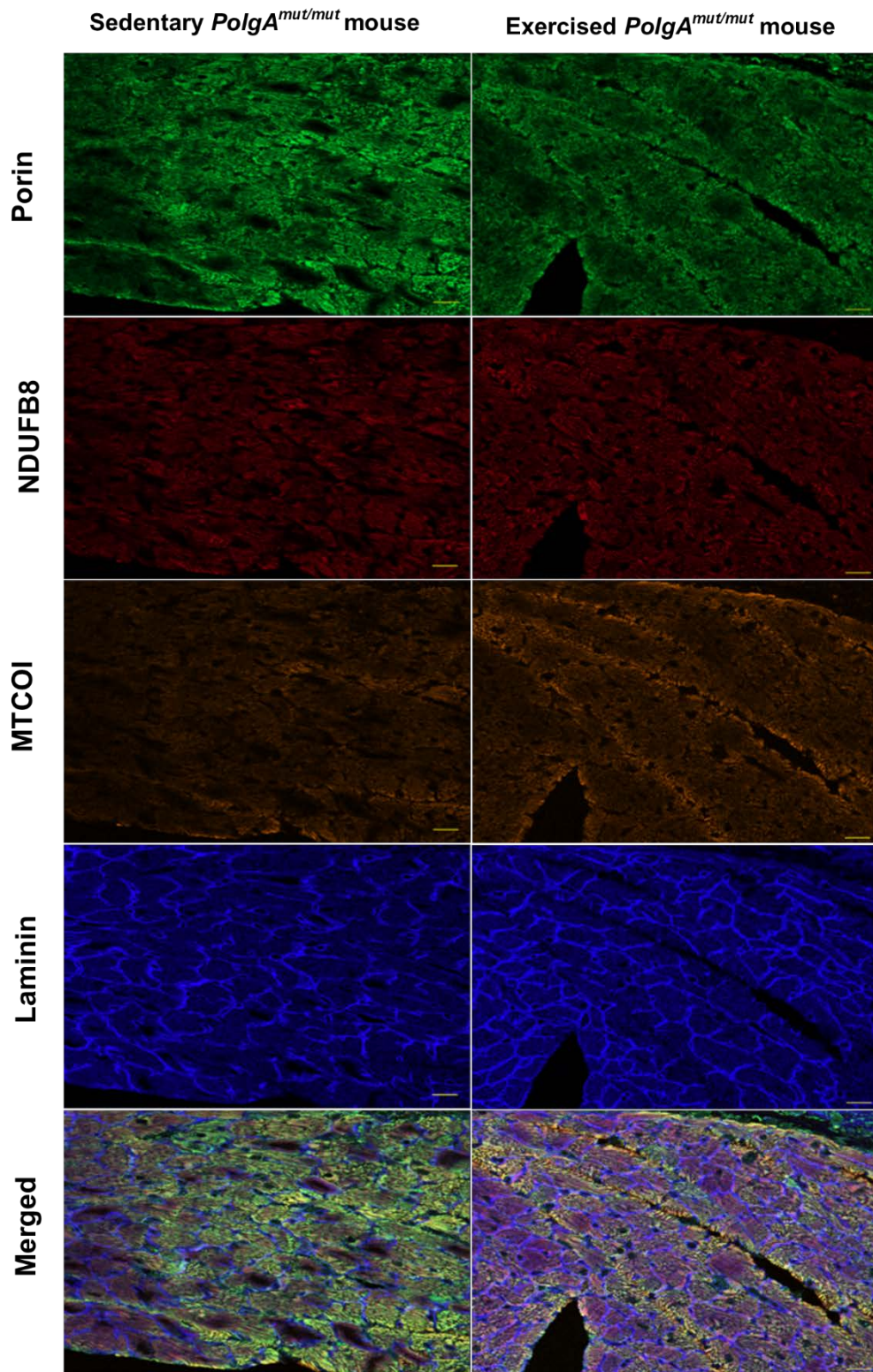
Figure 4.7.Mitochondrial Complex I (CI) and Complex IV (CIV) expression levels. CI was detected using antibody against NDUFB8 subunit and COX was detected using antibody against MTCOI subunit. Porin was used to mark mitochondrial mass and laminin was used to mark myocardial boundaries. Magnification x10. Scale bars=100µm.
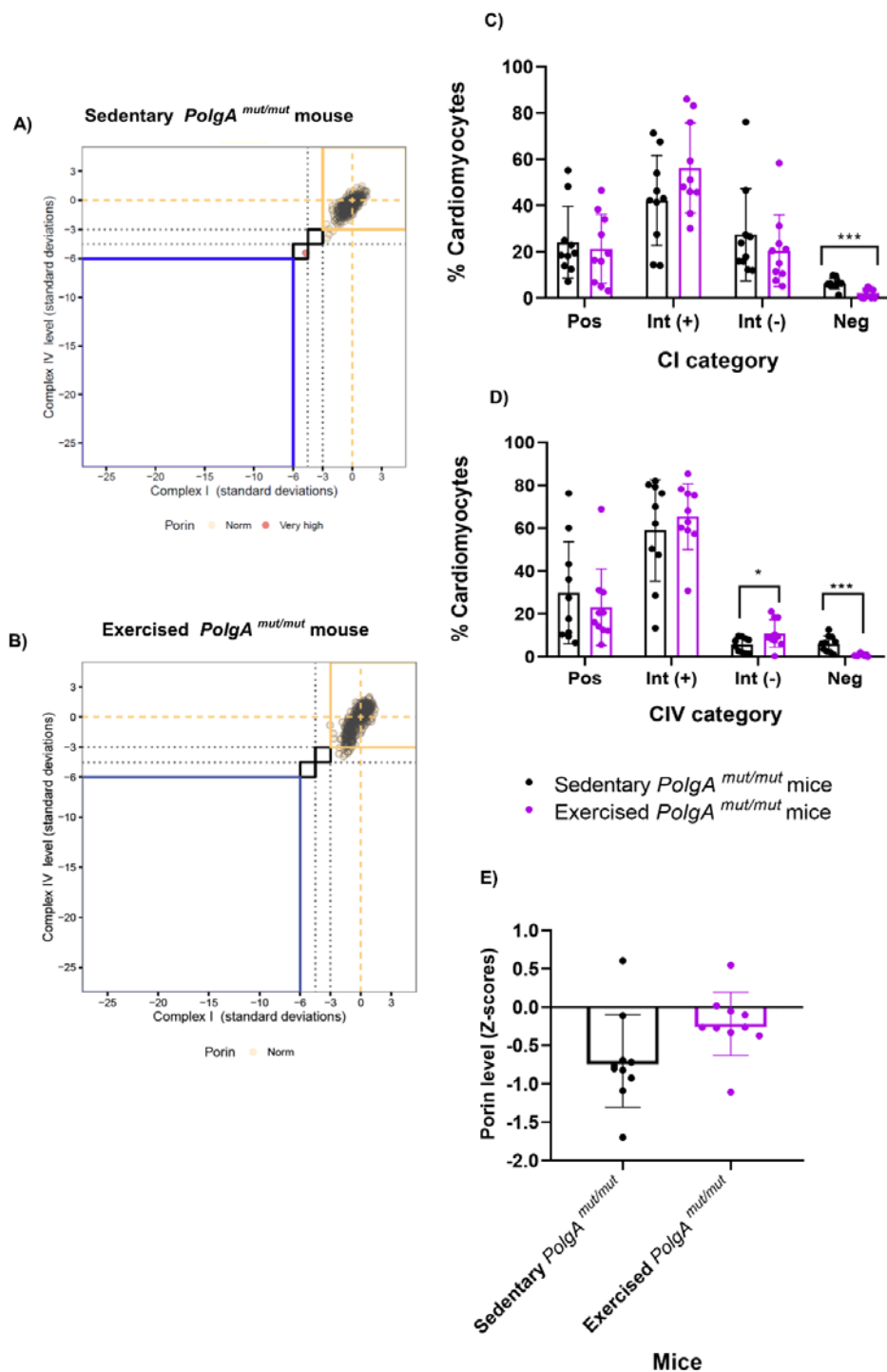
Figure 4.8. Mitochondrial NDUFB8 (CI) and MTCOI (CIV) immunoreactivity in sedentary and exercised *PolgA^mut/mut* mice cardiac muscle. A) MRC plots of sedentary mouse heart. B) MRC plots of exercised mouse heart. C) Percentage of cardiomyocytes with negative NDUFB8 and negative MTCOI levels were significantly higher in the sedentary cohort (***p<0.001 and *p<0.05 respectively). D) Percentage of cardiomyocytes with intermediate negative MTCOI is significantly higher in the exercised cohort (***p<0.001) (unpaired t-test). E) Porin levels in sedentary and exercised mice are within the normal range between 2 and -2SD. Error bars represent mean ±SD.

146

4.3.9 *Complex IV activity in sedentary and exercised PolgA^{mut/mut} mice hearts*

Mitochondrial COX activity was assessed using sequential COX/SDH histochemistry in the cardiac tissue of sedentary (n=10) and exercised (n=10) *PolgA^{mut/mut}* mice as detailed in chapter 2 section 2.21. Cryosections from the left ventricle (8µm) were stained to visualise cytochrome c oxidase and succinate dehydrogenase activity levels by localisation of DAB (electron donor) in COX functional cardiomyocytes and formation of NBT in COX deficient cardiomyocytes. Sections were visualised using Nikon Tie microscope (figure 4.9) and the percentage of blue COX deficient cardiomyocytes were quantified using General analysis RGB algorithm in Nikon imaging software elements programme. Five random snapshots of x10 magnification per mouse heart was selected and the percentage of COX deficiency was calculated from the ratio of total tissue area to COX negative tissue area. The analysis software uses RGB channel intensity to demonstrate the analysis process where total tissue area visualised by pink is differentiated from total COX deficient blue area. There was no significant difference between the cardiac muscle COX activity of both groups of mice (p=0.19, unpaired t-test) as shown in figure 4.10.
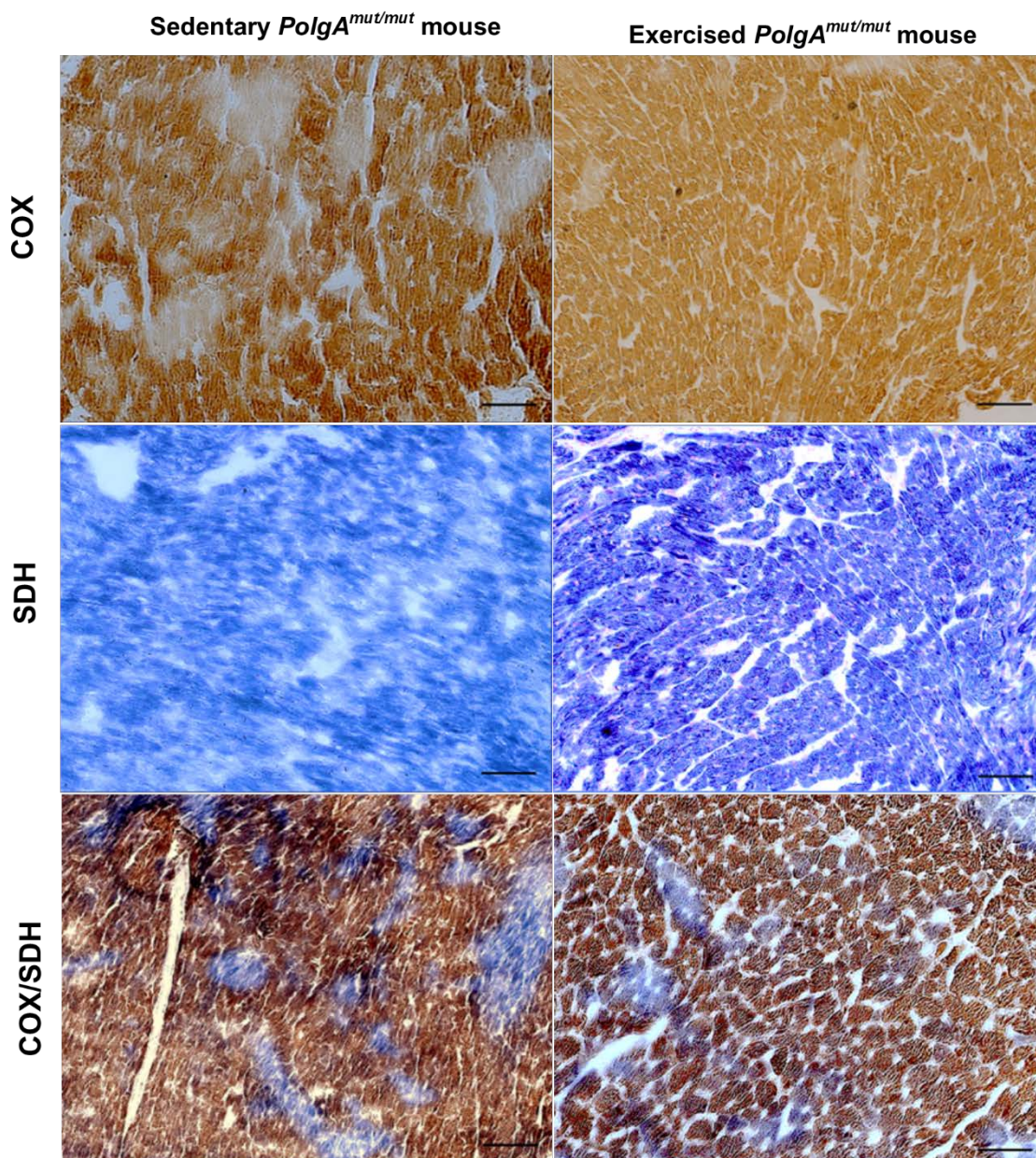
Figure 4.9. Mitochondrial CIV activity in sedentary and exercised mice hearts.
Representative serial sections of COX, SDH, and COX/SDH histochemistry images
of x10 magnification to assess mtDNA encoded COX activity in comparison to
nuclear DNA encoded SDH activity. Merged images (COX/SDH) were used to
quantify COX activity using NIS elements software by thresholding of RGB channel
to obtain the percentage of desired staining i.e. percentage of COX negative blue
region. Scale bars= 100µm.
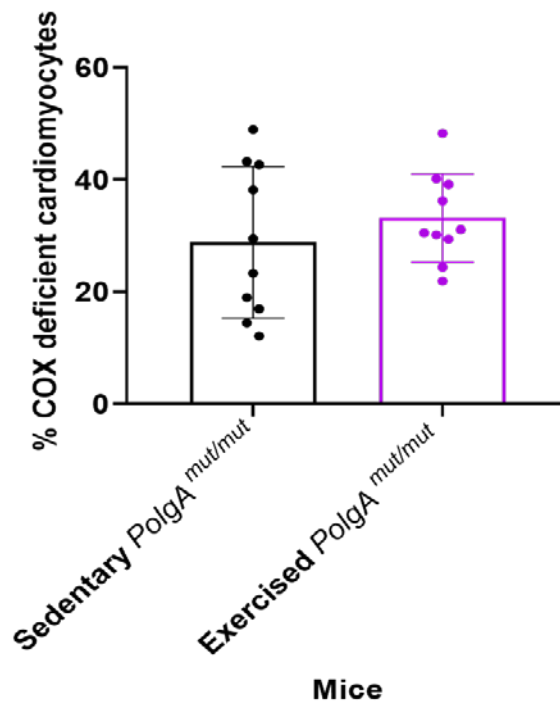
Figure 4.10. COX deficiency in left ventricular cardiac muscle of sedentary and exercised *PolgA^{mut/mut}* mice. There is no significant difference between the COX activity of both groups (p=0.19) (unpaired t-test). Error bars show mean ±SD.

4.4 NBTx and laminin immunohistochemistry in sedentary and exercised *PolgA^{mut/mut}* mice

NBTx assay and laminin immunofluorescence was carried out according to the method explained in chapter 2 section 2.24.1 in order to visualise and quantify COX deficiency based on NBT activity only. Different levels of COX deficiency were detected by quantifying the amount of NBT deposition in cells ranging from light blue to dark blue (detailed in chapter 3 section 3.3.10). Laminin immunofluorescence was carried out to determine cardiomyocyte boundaries for easier detection and analysis. Figure 4.11 shows images obtained from LSM800 microscope. NBTx brightfield images represent only the NBTx assay without laminin to confirm COX deficiency in blue in the absence of fluorescent signal. Merged images from five random snapshots of x10 magnification were uploaded on the immunoanalyzer software for analysis. 500 LV transverse cardiomyocytes from each mouse heart were analysed. The darker the cardiomyocytes, the higher the COX deficiency and the higher the optical density (OD) values were. Data from both groups of animals was compared with that from cardiac muscle from wild-type mice at 12 months of age in order to

149

categorise fibres into COX positive, intermediate and negative fibres as described in chapter 3, section 3.3.10. OD values less than 3SD of the mean was categorised as positive COX fibres, anything between 3SD and 6SD were named as intermediate COX fibres and those more than 6SD were categorised as negative COX fibres (figure 4.11), relative to wild-type mice.
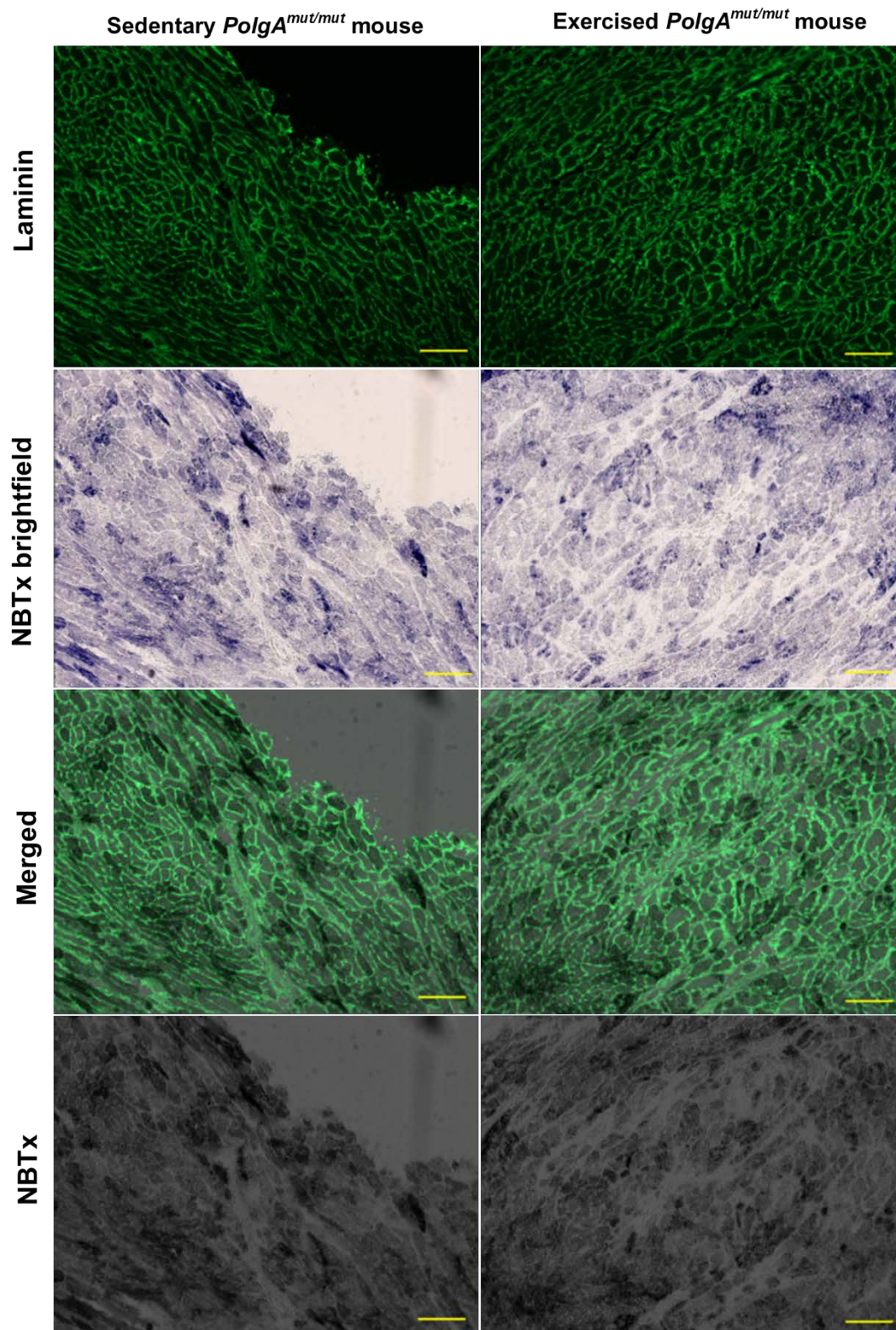
Figure 4.11. NBTx assay and laminin immunofluorescence. Images were obtained from LSM800 microscope. Merged files were used for analysis on immunoanalyzer software by automatically selecting transverse cardiomyocytes for analysis. Magnification x10. Scale bars= 100µm.

Figure 4.12 shows the percentage of cardiomyocytes with positive, intermediate and negative COX activity. There were no significant differences in percentage of COX positive, intermediate or deficiency cardiomyocytes between the exercised and sedentary groups (p>0.05, unpaired t-test).
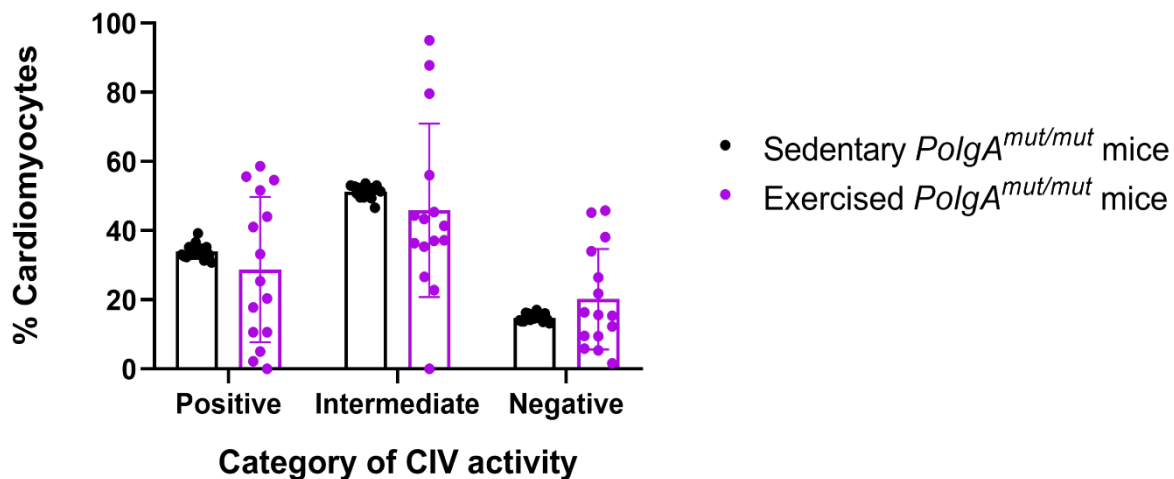
Figure 4.12. CIV activity levels in sedentary and exercised *PolgA*^{mut/mut} mice hearts. The level of CIV activity was not significantly different between the two cohorts (p>0.05) (unpaired t-test). Error bars represent mean ±SD.

4.4.1 *Mitochondrial DNA copy number in sedentary and exercised PolgA*$^{mut/mut}$ *mice hearts*

Mitochondrial DNA copy number was quantified in homogenised left ventricular cardiac muscle using quantitative real-time PCR by amplifying a portion of the gene on the mtDNA known as ND1 and a housekeeping nuclear DNA encoded gene β-actin. The ratio of ND1 to B-actin determines the relative mitochondrial DNA copy number as explained in more detail in chapter 2 section 2.26. There was no significant difference in the mitochondrial copy number in sedentary (n=10) and exercised (n=10) *PolgA*$^{mut/mut}$ mice cardiac muscle (p=0.13) as shown in figure 4.13.
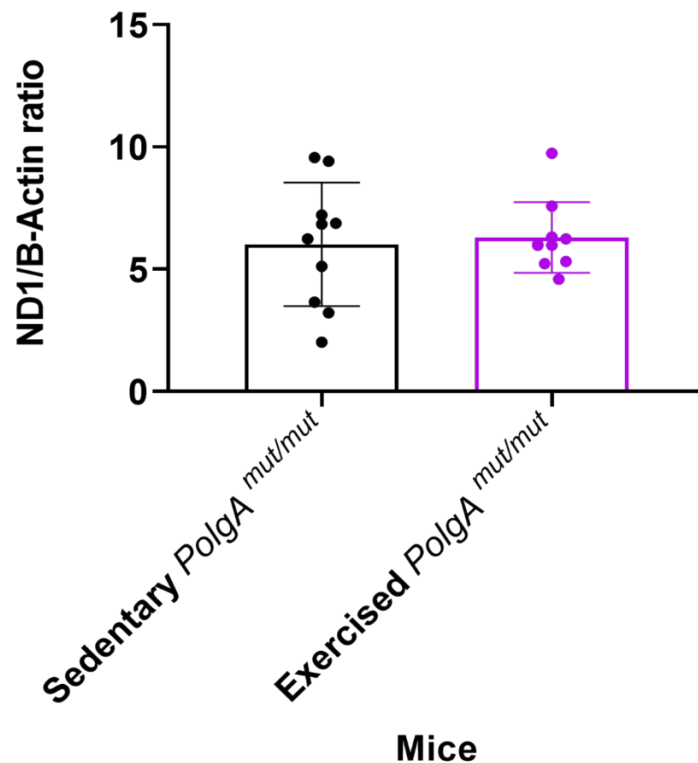
Figure 4.13. MtDNA copy number in sedentary and exercised mice LV. There is no significant difference between the copy number of mtDNA in the two groups (p>0.05).

4.5 Discussion

This study showed that 7 months of treadmill running exercise did not extend the lifespan of *PolgA*^{mut/mut} mice in comparison to non-exercised *PolgA*^{mut/mut} mice. In terms of the clinical phenotype, exercised and sedentary mice both experienced premature aging phenotypes such as hunched posture, weakened mobility, piloerection, and anaemia with advancing age. Both groups showed significantly higher clinical scores with advancing age indicating worsening of the body condition as they age. The body weight of mice did not significantly change with advancing age and with exercise. The body temperature however revealed that exercised mice experienced significantly lower body temperatures with advancing age however this was not significantly different in comparison to the sedentary cohort at any time point. The gradual drop in body temperature of exercised mice may not be biologically significant since regular exercise is proven to regulate the core body temperature

(Okazaki, 2016) and the fact that both cohorts of mice were group housed would help to maintain environmental temperature stable.

From a behavioural point of view, my data revealed that exercised mice experienced a significant increase in their mobility level with advancing age up to 43 weeks of age and sedentary mice only had an increase in their locomotive activity up to 29 weeks of age. Exercised mice also moved a lot faster than sedentary mice at 43 weeks of age and sedentary mice experienced a significant decline in their velocity of movement with advancing age, indicating that sedentary mice may have slower reaction time to any stimuli as they age. Similarly, exercised mice had a significantly higher number of touches at 43 weeks and longer step lengths showing an improvement in locomotive and behavioural phenotypes. Exercised mice took more frequent steps and longer steps at 46 weeks in an attempt to keep their gait balanced. Lemieux *et al* (2016) reported that longer step lengths occur as a consequence to enable postural stability in mice.

I have shown that the degree of cardiac fibrosis, percentage of active CC-3 labelled nuclei, cardiomyocyte width, heart weight and cardiac mtDNA copy number were not significantly different between the two cohorts. Mitochondrial CI and COX expression levels were not significantly different in the cardiac muscle of both cohorts and the level of COX activity was down regulated in both groups to the same extent. Interestingly, exercised mice showed a great variation in COX activity through NBTx assay revealing that mice have responded to exercise differently.

Safdar *et al* in 2011 have reported that 5 months of endurance exercise rescued accelerated aging phenotypes in *PolgA$^{mut/mut}$* mice. They showed that exercise increased the functional capacity of the mice, attenuated cardiac fibrosis, cardiac apoptosis and cardiac hypertrophy in comparison to sedentary mice. Their research also showed that endurance exercise enhanced systemic CIV activity in the heart and skeletal muscle of *PolgA $^{mut/mut}$* mice and attenuated the decline in mtDNA copy number. In 2016 Safdar *et al* went on to demonstrate that the same endurance exercise protocol led to the reduction of non-mutational mtDNA damage in the skeletal muscle of *PolgA$^{mut/mut}$* mice through a p53 mediated mechanism. P53 acts as an accessory fidelity enhancer to the DNA repair mechanism of POLG by localising to the mitochondria and forming a complex with Tfam.

My research has shown that exercise does not extend the lifespan *PolgA* *mut/mut* mice and does not provide physiological benefits to *PolgA* *mut/mut* mice, contrasting with the findings of Safdar *et al* (2011). I have also confirmed that cardiac pathology and cardiac mitochondrial function remain unchanged with exercise in *PolgA* *mut/mut* mice which is controversial to Safdar *et al* (2011) research despite using mice originating from the same colony with the same age and exercise protocol. There were some differences between the two studies. Safdar *et al* (2011, 2016) singly housed their mice in an attempt to keep external factors such as cage fights to minimal level. However, since mice are social animals, they will be affected by living in solitude. They also performed different assays on different numbers of mice. They started with n=18/group with male and female mice however only four from each group were selected to be included on the survival curve plot, 12 from each group were selected for clinical phenotyping and six from each group were selected to be analysed for heart weight. There were no reasoning on the selection process for different assays meaning that further research is needed to affirm conclusions. Safdar *et al* (2011) also used both sexes in their experiments without taking into account the effects of female endocrine system on parameters measured and possible higher physical performance in male mice.

Some possible reasons for discrepancies between the two studies may include differences in husbandry of mice, diet and environmental factors such as lighting, temperature, handling and pathogens present in the cages. Other factors may include different genetic background of mice, despite the same in-bred colonies. Also Safdar *et al* (2011) generated wild-type control mice (*PolgA*$^{+/+}$) from *PolgA*$^{mut/+}$ mice colonies indicating the chances of transmitting mtDNA mutation from the mother to the offspring through the female germline. The smallest difference in the genetic background could have a significant impact on the phenotype and response of individuals to external stimuli such as exercise training (Skinner, 2005). More than 600 genes and chromosomal regions were suggested to be involved in energy metabolism regulation (Deram and Villares, 2009). A review study by Leońska-Duniec, Ahmetov and Zmijewski (2016) investigated the impact of human genetic variants of obesity related genes causing polymorphism on exercise intervention and concluded that some genes play a significant role in determination of individual differences in response to exercise.

Faraci *et al* (2018) investigated the impact of 6 months of treadmill running exercise on oocyte number and yield in *PolgA^mut/mut* mice at 5,7 and 9 months of age. No significant differences were seen in the number of ovulated oocytes between the two groups, however improvements in ovarian follicle reserve and oocyte quality were observed in exercised mice in comparison to sedentary group. Oocyte quality was assessed based on meiotic spindle assembly, chromosomal segregation and mitochondrial distribution at the age of 7 months. They reported a significant decline in the number of ovulated oocytes in *PolgA^mut/mut* mice in comparison to wild type littermates after 9 months of age, but there was no significant difference between the sedentary and exercised cohort. They documented that exercise prevented the decline in the reserve of oocyte containing primordial follicles in the ovaries up to 7 months of age, however the trend was not sustained in 9 month old exercised mice. They suggested that exercise may prevent early loss of follicles in *PolgA^mut/mut* mice but does not sustain the quantity of follicles and the number of ovulated oocytes after 9 months of age. MtDNA mutation load and copy number in the oocytes of *PolgA^mut/mut* mice were also assessed and were not significantly different between the two groups at 9 months of age, suggesting that unlike somatic tissues, exercise does not induce mitochondrial biogenesis in the oocyte. Faraci *et al* (2018) showed that there was no direct effect of exercise on mtDNA repair mechanism unlike in skeletal muscle, however improvements in mitotic spindle and chromosomal alignment were observed.

Salesniemi *et al* (2011) have shown that mice lacking PGC-1α exhibit increased offspring mortality, but females that do survive to 12 months of age demonstrate improved oocyte quality, reduced spindle abnormalities and chromosomal misalignment and a decrease in abnormal mitochondria aggregation with age, showcasing a positive impact of lack of PGC-1α in oocyte quality. Similar to PGC-1α, the role of p53 in the oocyte function is different to those that operate in the soma and so is the mechanism that governs the impact of exercise on oocyte quality.

According to previous research, (Zahn *et al*, 2006, Bua *et al*, 2006, Lynons *et al*, 2006) age-related mitochondrial adaptations include reduction in mitochondrial components, capacity and biogenesis especially in high energy demand organs such as skeletal muscle. Also due to the lack of protective proteins and proximity of mtDNA to free radicals, mtDNA is more prone to replicative error which increases with advancing age. Kim, Triolo and Hood (2017) reported that the decline in

mitochondrial biogenesis with age is initiated through activation of AMPK and subsequent reduction in co-activation of PGC-1α. Since PGC1-α is a master regulator of mtDNA biogenesis through positive feedback, it's over expression was shown to be linked to increased protein content. Therefore, aging muscle is associated with a decline in mtDNA copy number since mitochondrial transcripts reduce in number in less oxidative muscle due to decreased use of muscle with age. Aged muscle is also less able to respond to mitochondrial biogenesis-altering factors such as exercise, nutritional imbalance, ROS and Ca^{2+} changes. A study carried out by Menshikova *et al* (2006) reported that 12 weeks of moderate exercise training significantly increased the ETC protein activity, increased muscle contractile protein synthesis, mitochondrial content and function and mtDNA copy number in subsarcolemmal mitochondria of aged human skeletal muscle. Koltai *et al* (2012) and Kang *et al* (2013) have shown that endurance exercise training in rats reduces age-associated decline in skeletal muscle mitochondrial biogenesis and dysfunction. Rowe *et al* (2012) have investigated the effects of 12 weeks of cycling in the skeletal muscle of elderly women and found that exercise-induced mitochondrial biogenesis is independent of PGC1α expression.

Despite many previous exercise-related studies in *PolgA^{mut/mut}* mice, it's still unclear the exact impact of exercise on cardiac mitochondrial function. Since cardiac muscle is composed of many cell types with different functions and capacities, it's important that similar experiments are carried out on the same region of the muscle to achieve representative results. For example the study carried out by Safdar *et al* (2011) documented that heart mitochondrial abundance and morphology was improved with endurance exercise. They have looked at electron micrographs of cardiac tissue, from six mice/group without further specifying which region of the cardiac muscle they were investigating. They reported improvements in mitochondrial morphology as reversal of enlarged and abnormally shaped mitochondria in exercised mice. Since mitochondrial dynamics in different cells of cardiac muscle is varied, it's crucial to declare which region of cardiac tissue is selected for histological and molecular assays (Piquereau *et al,* 2013). Even though mice with similar genetic background were selected throughout the studies, but the environmental factors such as the amount of food consumed, level of stress due to cage fights, impact of solitary housing, the aerobic capacity of each mouse and the level of mitochondrial

heteroplasmy in the tissues of each mouse differ. These factors inevitably increase data variability and remain a confounding factor in animal studies.

Safdar *et al* (2011) confirmed that sedentary *PolgA^mut/mut* mice lived up to ~240 days (n=4) whereas their exercised mice survived to ~500 days (n=4) similar to their control mice group. Their controversial findings raise questions to why only four mice from the exercised and control group were included in the survival curve assessment.

Unpublished data from our lab showed that the maximum survival of our *PolgA^mut/mut* sedentary mice at the animal facility of Cardiff University was up to 220 days (Ashwin Sachdeva, personal communication) whereas at Newcastle University these mice lived up to 300 days after which they were culled and so could potentially have lived longer. Kujoth *et al* (2005), Trifunovic *et al* (2004) and Vermulst *et al* (2008) documented that the maximum survival rate of *PolgA^mut/mut* mice is 460 days, 427 days and 547 days respectively. Possible reasons for discrepancies in lifespan data could be due to differences in mice husbandry practices, diet, environmental pathogens and genetic background. One difference between Safdar *et al* (2011) study and other studies were the housing condition in mice, in which Safdar *et al* (2011) have singly housed their mice and my study group housed the mice. This seems to have a significant effect on the lifespan of mice and the very early appearance of progeroid phenotypes of *PolgA^mut/mut* mice.

Many factors influence body temperature such as environmental temperature, amount of brown adipose tissue in the body, levels of basal metabolic activity and effects of physical activity or diet. Body temperature of wild type laboratory mice is tightly regulated to around 36-37C° in order to maintain metabolic processes in the body within a normal range (Ades, 2019). *PolgA^mut/mut* mice seem to have an overall lower body temperature in comparison to wild-type mice by the age of 43 weeks as shown in chapter 3 section 3.3.2 due to the effect of a high mtDNA mutation burden. The temperature of mice may have a direct effect on the overall health and general wellbeing especially with advancing age.

4.6 Conclusion and future work

This study has provided an in-depth insight into the role of endurance exercise in cardiac mitochondrial function, general wellbeing and lifespan of $PolgA^{mut/mut}$ mice. Endurance exercise did not seem to alleviate pre-mature signs of aging and did not improve mitochondrial dysfunction. The future work is to identify the maximal aerobic capacity (VO$_2$ max) of each mouse which gives an indication of each subject's aerobic capacity and the degree of conditioning in each mouse. Although it's known that young muscle is able to respond to chronic exercise by undergoing plasticity to increase its oxidative capacity, the aged muscle is already under compromised physiological mechanisms and that strenuous exercise may have an adverse impact on the function of the muscle. Even though, $PolgA^{mut/mut}$ mice have the same genotypes, the level of mtDNA heteroplasmy may differ between animals and so the state of oxidative phosphorylation. For this reason, the aerobic capacity of each mouse will differ. In order to make sure mice benefit from an exercise regime, therefore it's recommended to exercise mice between 60%-80% of individual's VO$_2$ max to improve aerobic fitness levels. Future work would be to assess fat to muscle ratio in these mice and normalise the data for the effects of environmental factors such as food intake, amount of cage activity etc.

Chapter 5

Chapter 5. The effects of single housing and endurance exercise on cardiac mitochondrial function and progeroid ageing phenotypes in *PolgA^{mut/mut}* mice

5.1 Introduction

The discrepancies between this study and that of Safdar *et al* (2011) (discussed in chapter 4) led us to investigate further the possible causes of differences. One major difference was the single housing of experimental animals and so I performed a pilot study to see if this could explain the variation between the two studies.

5.1.1 *Housing conditions in mice*

Housing conditions affect different strains of mice in different ways, meaning that some mice withstand environmental stresses better. Collins and Tabak (2014) have shown that environmental conditions such as diet, housing conditions and exercise play a significant role in the expression of ageing phenotypes in mouse models. Previous research has shown that although younger mice are not used to handling, they are extremely malleable in adjusting to environments, meaning that regular human interactions puts an added stress on mice within tolerated levels. Olsson and Dahlborn (2002) have reported that restrictive housing conditions cause long-term stress and limit the animal's potential for managing their social and physical interactions. This directly affects their reaction to external challenges such as exercise. A study carried out by Kalliokoski *et al* (2014) has provided evidence that male BALB/c immunodeficient mice suffer from marked hypothermia following 3 weeks of solitary housing. They have demonstrated that male mice deprived of social contact respond with altered serotonergic signaling activity. Another study by the same author in 2013 showed that singly housed BALB/c male mice suffer from elevated levels of oxidative stress evident by a significant increase in their urine corticosteroid metabolites. Some researchers on the other hand, argue that more than housing conditions, lack of familiarity of mice with their cage mates triggers social stress. Bartolomucci, Palanza and Parmigiani (2002) suggested that group housing could be stressful only for subordinate male mice. They identified that living

with siblings of the same sex from birth is the ideal social environment for mice. A study carried out by Nagy *et al* (2001) on the effect of group housing on phenotypic variance of C57BL/6J mice revealed that group housing increases the variation in measures such as bone mineral density (BMD) and content as well as tissue and fat mass. They have concluded that singly housing wild type mice provides a more representative genotype effects on body composition than group housing. Although singly housed mice were overall smaller in size and had less soft tissue and body fat when compared to group housed mice.

Since *PolgA^{mut/mut}* mice suffer from pathogenic mtDNA mutations and pre-mature ageing phenotypes, housing conditions and other lifestyle factors have a significant influence on their ageing and potentially on cellular and molecular findings. For this reason, in order to eliminate the influence of external variables in experiments most researchers singly house the mice, however this could be a limiting factor in ageing-related studies especially if combined with another intervention.

5.2 Aims of study

The general aim of this study was to investigate the impact of housing condition on the ageing profile of *PolgA*^{*mut/mut*} mice and in response to exercise.

The objectives of this study were met by investigating the clinical phenotypes, behavioural characteristics, cardiac structure, histology and mitochondrial function of the following mice:

1. Group-housed and singly-housed sedentary *PolgA*^{*mut/mut*} mice from 3 to 11 months of age.

2. Singly-housed sedentary and exercised *PolgA*^{*mut/mut*} mice from 3 to 11 months of age.

3. Group-housed and singly-housed exercised *PolgA*^{*mut/mut*} mice from 3 to 11 months of age.

5.3 Results

PolgA^(mut/mut) mice were randomly assigned to groups of n=5 sedentary, n=5 exercised in single cages and were compared with the data generated from the group-housed animals investigated in chapters 3 and 4 (n=10 sedentary and n=10 exercised). Group-housed mice are referred to as 'GH' and singly-housed mice are referred to as 'SH', throughout this thesis. This study used the same treadmill running protocol as in chapter 4. Exercise regime commenced at 16 weeks of age for the duration of 6 months while sedentary mice kept normal cage activity. Comparisons were made between groups at 14/15 weeks (pre-intervention), 29 weeks (during-intervention) and 43 weeks (post-intervention).

5.3.1 *Survival curve, Clinical scoring and Body weight of PolgA^(mut/mut) mice*

A. Sedentary GH compared with sedentarySH *PolgA^(mut/mut)* mice

The lifespan of sedentary *PolgA^(mut/mut)* GH mice (n=10) and sedentary *PolgA^(mut/mut)* SH mice (n=5) were compared. The end point for the study was 46 weeks (322 days), however those mice that died prior to their culling date for reasons other than fight wounds and prolapse were included in the survival curve. Figure 5.1A demonstrates that only one mouse (20%) from the SH cohort lived to the endpoint (322 days) the other 4 mice died as early as 272 days.

Sedentary SH mice had significantly lower weights in comparison to GH mice at 37 and 39 weeks (p<0.05) as well as 41 (p<0.001), 42 and 43 (p<0.0001) weeks of age. The body weight of sedentary GH mice increased significantly with advancing age (p<0.05) raising from 30.08g±2.78 to 32.5g±0.0002. SH mice showed an overall significant decline in body weight with advancing age from 30.78g±0.61 to 25.97g±0.08 (figure 5.1B) (P<0.01, two-way ANOVA repeated measures).

Clinical scoring was carried out in sedentary *PolgA^(mut/mut)* GH and SH mice on a weekly basis from the age of 14 weeks to 43 weeks. Eight characteristics were assessed in mice and the severity of conditions were scored from 0 (normal) to 3 (worsening of condition). Higher clinical score values indicate worsened body condition. A weight loss of over 10-15% and any characteristic above the score of 2 were considered as severe. Cumulative clinical score values at 14 weeks (start of the

study), 29 weeks (mid-point) and 43 weeks (end point) from the SH and GH mice were compared (two-way ANOVA repeated measures). Body condition assessment through clinical scoring (figure 5.1C) revealed that sedentary GH and SH mice had significant body condition deterioration with advancing age ($p<0.001$, $p<0.01$ respectively). At 14 weeks the average clinical score of SH mice was 2.2 ± 0.97 whereas for GH mice it was 1 ± 0.98 ($p>0.05$). Similarly, the body condition of GH mice at 29 weeks was 2.4 ± 1.7 and of SH mice was 3.4 ± 1.5 ($p>0.05$). Clinical scores increased at 43 weeks in GH mice to 6.16 ± 1.86 and in SH mice to 6 ± 0.054 ($p>0.05$) revealing a trend but with low numbers of SH mice there was no significant difference between the two groups at 14 weeks, 29 weeks and 43 weeks of age. 40% of SH mice suffered from severe weight loss, 100% with piloerection and 20% with anemia. In comparison to GH mice with 14.3% severe weight loss, 85% with piloerection, 14.3% behavioral isolation where mice do not engage in social interaction with other mice, 14.3% with hunched posture and weakened mobility and 57.1% with anemia.
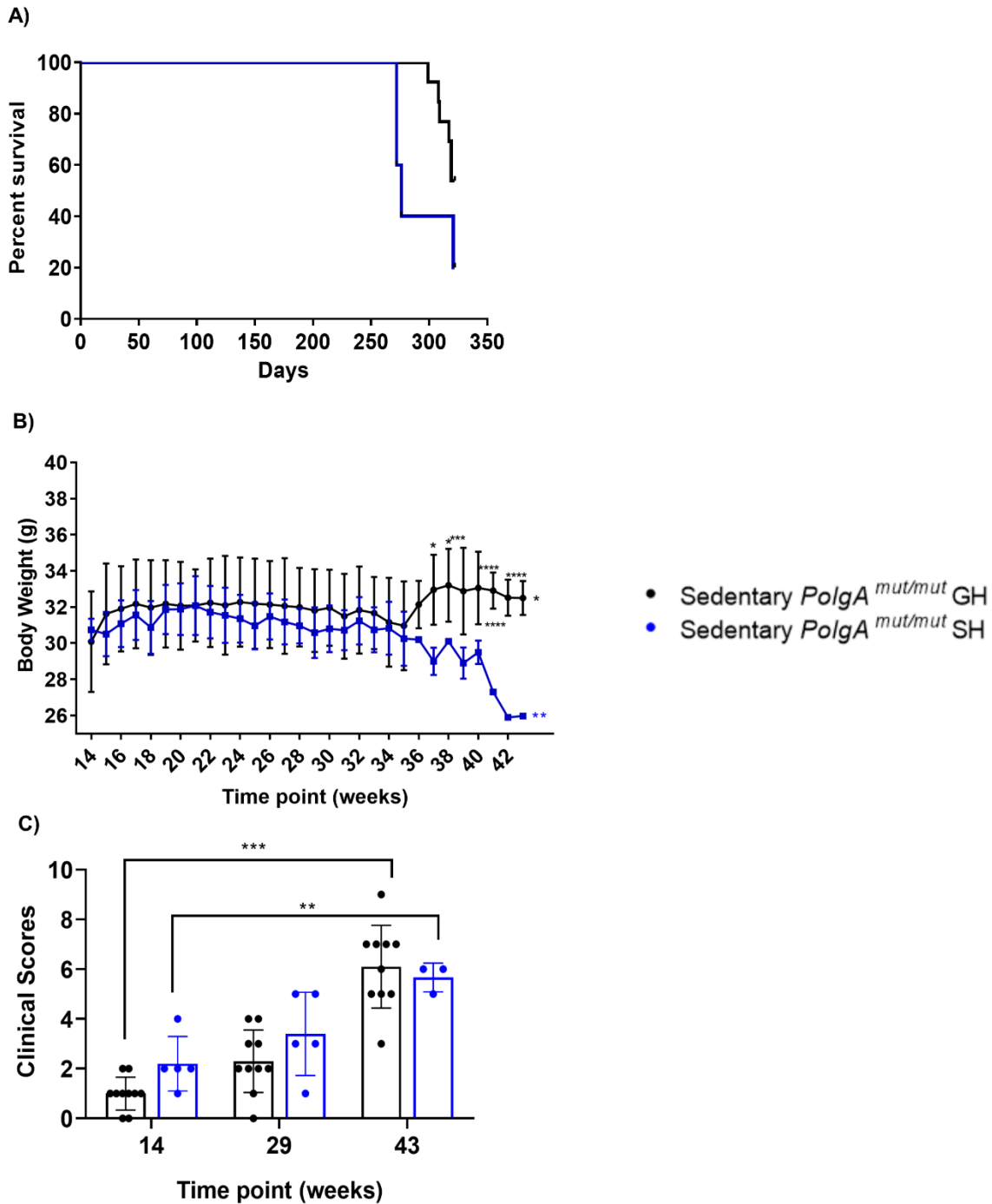
Figure 5.1. Survival curve, Clinical scoring and Body weight of sedentary group-housed and singly-housed *PolgA^mut/mut* mice at 14, 29 and 43 weeks of age (two-way ANOVA repeated measures). A) Survival curve. B) Body weight was significantly reduced in sedentary SH mice in comparison to sedentary GH mice from weeks 27 onwards. C) Clinical scoring was significantly reduced in sedentary GH and sedentary SH mice with advancing age (***$p<0.001$ and **$p<0.01$ respectively). Error bars represent ±SD.

B. Sedentary compared with Exercised SH *PolgA^mut/mut* mice

Figure 5.2.A shows the lifespan of sedentary and exercised *PolgA^mut/mut* SH mice. Only one exercised mouse lived to 316 days, the other 3 died at days 272, 278 and 288. The median survival of the exercised and sedentary cohorts were 283 days and 276 days respectively. Only 1 mouse from the sedentary cohort survived longest to 322 days hence a 20% survival rate, the others died at 321, 272 and 276 days of age.

Figure 5.2B shows that the body weight of sedentary *PolgA^mut/mut* SH mice decreased significantly with advancing age ($p < 0.001$), however exercised *PolgA^mut/mut* SH mice showed no significant age-related change in body weight ($p > 0.05$). At weeks 17, 21 ($p < 0.05$) and 20 ($p < 0.01$) the body weight of sedentary SH mice was significantly higher than exercised mice. Exercised SH mice seemed to be able to maintain their body weight with advancing age, however the body weight of sedentary SH mice declined significantly from 30.74g±0.61 at 14 weeks to 25.98g±0.08 at 43 weeks of age ($p < 0.001$, two-way ANOVA repeated measures).

There was no significant difference between the body conditions of sedentary and exercised *PolgA^mut/mut* SH mice at any time point ($p > 0.05$, two-way ANOVA repeated measures) (figure 5.2C). The body condition of both groups however declined significantly with advancing age as shown as an increase in the clinical scoring graph. The body condition of sedentary mice declined from the score of 2.2±0.9 to 6±0.54 ($p < 0.001$) whereas in exercised mice it changed from 2.2±0.97 to 5±0.98 ($p < 0.01$). At 43 weeks of age 40% of sedentary SH mice suffered from severe weight loss in comparison to 20% of exercised mice. 100% of sedentary and 100% of exercised mice suffered from piloerection and 20% from each sedentary and exercised group experienced anemia.
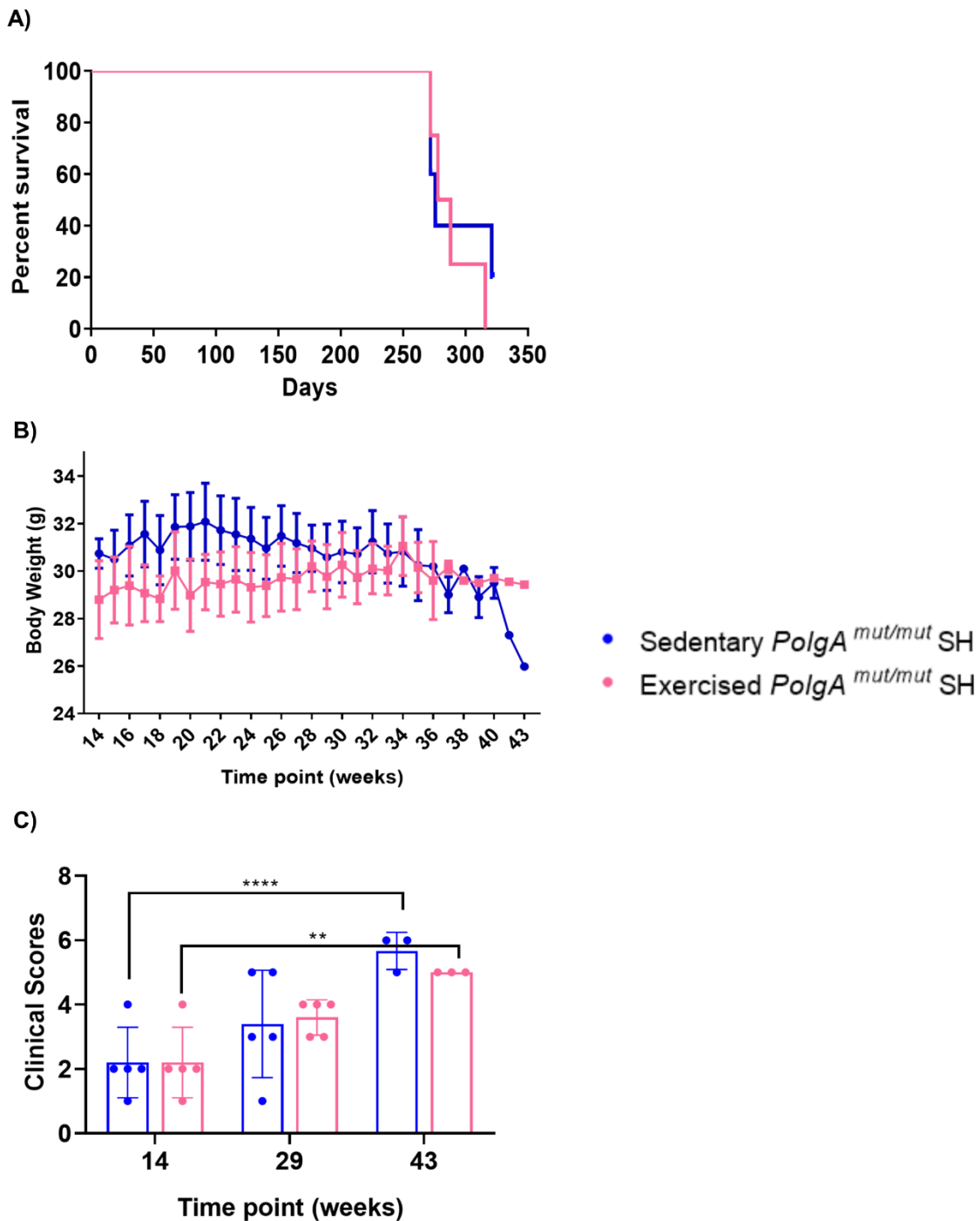
Figure 5.2. Survival curve, Clinical scoring and Body weight of singly-housed sedentary and exercised *PolgA^mut/mut* mice at 14, 29 and 43 weeks of age (two-way ANOVA repeated measures). A) Survival curve. B) Body weight. C) Clinical scoring was significantly increased in sedentary and exercised SH mice with advancing age (****$p<0.0001$ and **$p<0.01$ respectively). Error bars represent ±SD.

C. Exercised GH compared with exercised SH *PolgA^{mut/mut}* mice

The lifespan, body weight and clinical scores of two exercised cohorts from *PolgA^{mut/mut}* mice GH (n=10) and SH (n=5) were compared (two-way ANOVA repeated measures). Figure 5.3A shows that 58.4% of exercised GH mice lived to the endpoint whereas none of the exercised SH mice survived to the endpoint. The longest lived mouse in the SH cohort survived to 316 days. The shorter survival rate of SH mice is reflected in their poor body condition.

Figure 5.3B shows the continuous body weight of exercised GH and SH mice which was not significantly different between the two cohorts at any time point throughout the intervention.

The finding that exercised SH mice had a shorter lifespan was supported by significantly higher clinical scores than the exercised GH mice. Clinical scores at 14 weeks of age were significantly higher in SH mice in comparison to GH mice (p<0.001) (figure 5.3C) as well as 29 weeks (p<0.01) and 43 weeks (p<0.01, two way ANOVA repeated measures). Both groups had a significant decline in their body condition with advancing age. At 43 weeks of age 28.6% of GH mice and 100% of SH mice show signs of piloerection, 14.3% of GH mice and none of SH mice with hunched posture and mobility, 28.6% of GH mice and 20% of SH mice with signs of anemia, 14.3% of GH and 20% of SH mice showed severe weight loss.
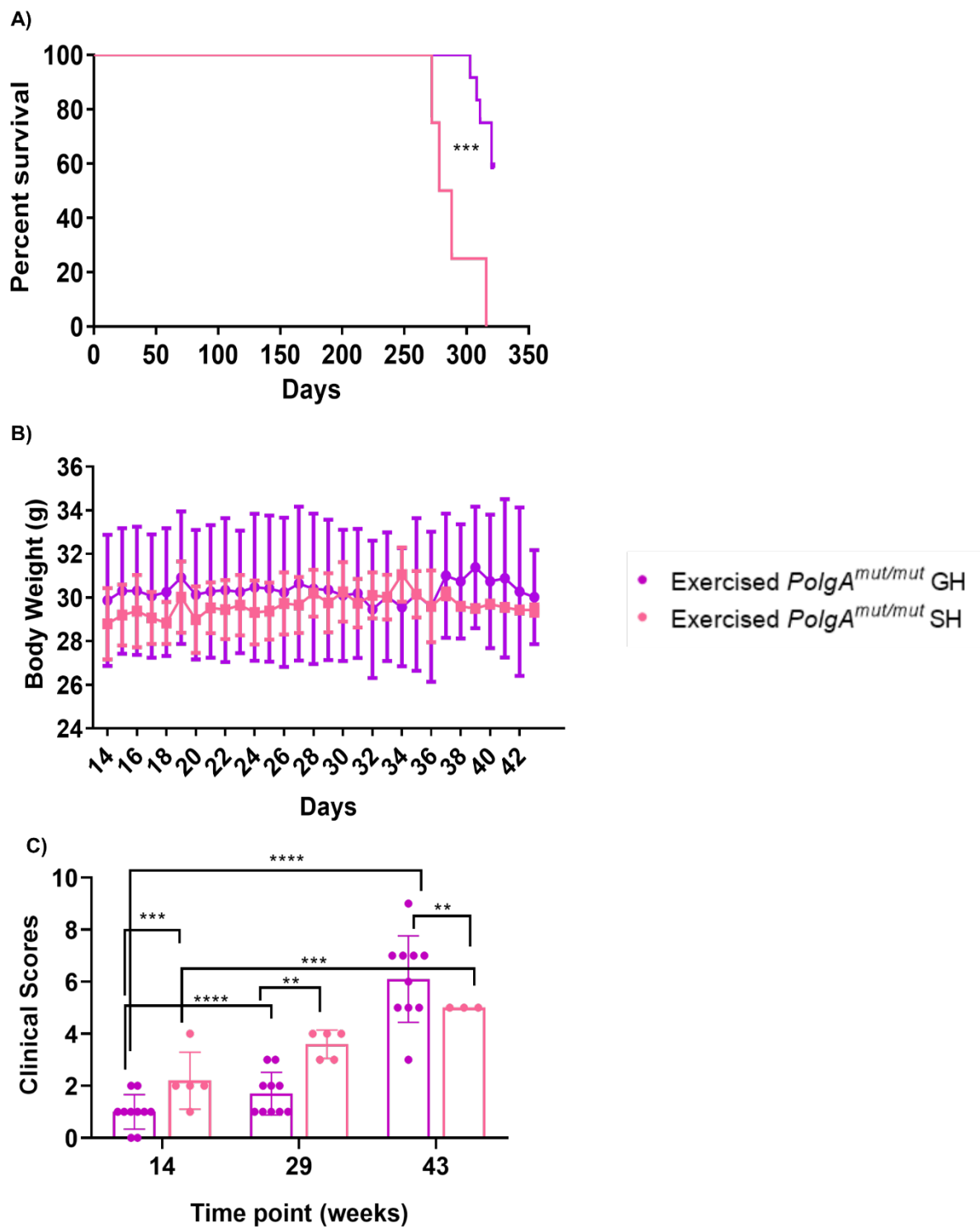
Figure 5.3. Survival curve, Clinical scoring and Body weight of exercised group-housed and singly-housed *PolgA^mut/mut* mice at 14, 29 and 43 weeks of age (two-way ANOVA repeated measures). A) Survival curve. B) Body weight. C) Clinical scoring was significantly increased in exercised GH and exercised SH mice with advancing age (****p<0.0001 and ***p<0.001 respectively). Body condition of exercised GH mice was significaly worse at 43 weeks (**p<0.01) in comparison to exercised SH mice. Error bars represent ±SD.

5.3.2 *Body temperature in PolgA$^{mut/mut}$ mice*

Body temperature from sedentary *PolgA$^{mut/mut}$* GH mice (n=10), sedentary *PolgA$^{mut/mut}$* SH mice (n=5), exercised *PolgA$^{mut/mut}$* GH mice (n=10) and exercised *PolgA$^{mut/mut}$* SH mice (n=5) were recorded at 14 weeks, 29 weeks and 46 weeks of age using a two-way ANOVA repeated measures statistical analysis. Room and cage temperatures were maintained at all times. There was no significant difference between the body temperatures of sedentary GH and SH mice at any time point (figure 5.4A).

The body temperature of exercised SH mice increased briefly from 14 weeks to 29 weeks of age and declined subsequently at 43 weeks of age (p<0.01) (figure 5.4B).

Exercised SH mice showed significantly higher body temperatures in comparison to exercised GH mice during (29 weeks of age) and post-intervention (43 weeks of age) (figure 5.4C). The mechanism by which exercised SH mice regulate their core body temperature seems to be different in those of group-housed mice. Exercise is likely to have an effect since the sedentary SH mice also have significantly lower body temperature mid-intervention at 29 weeks of age.
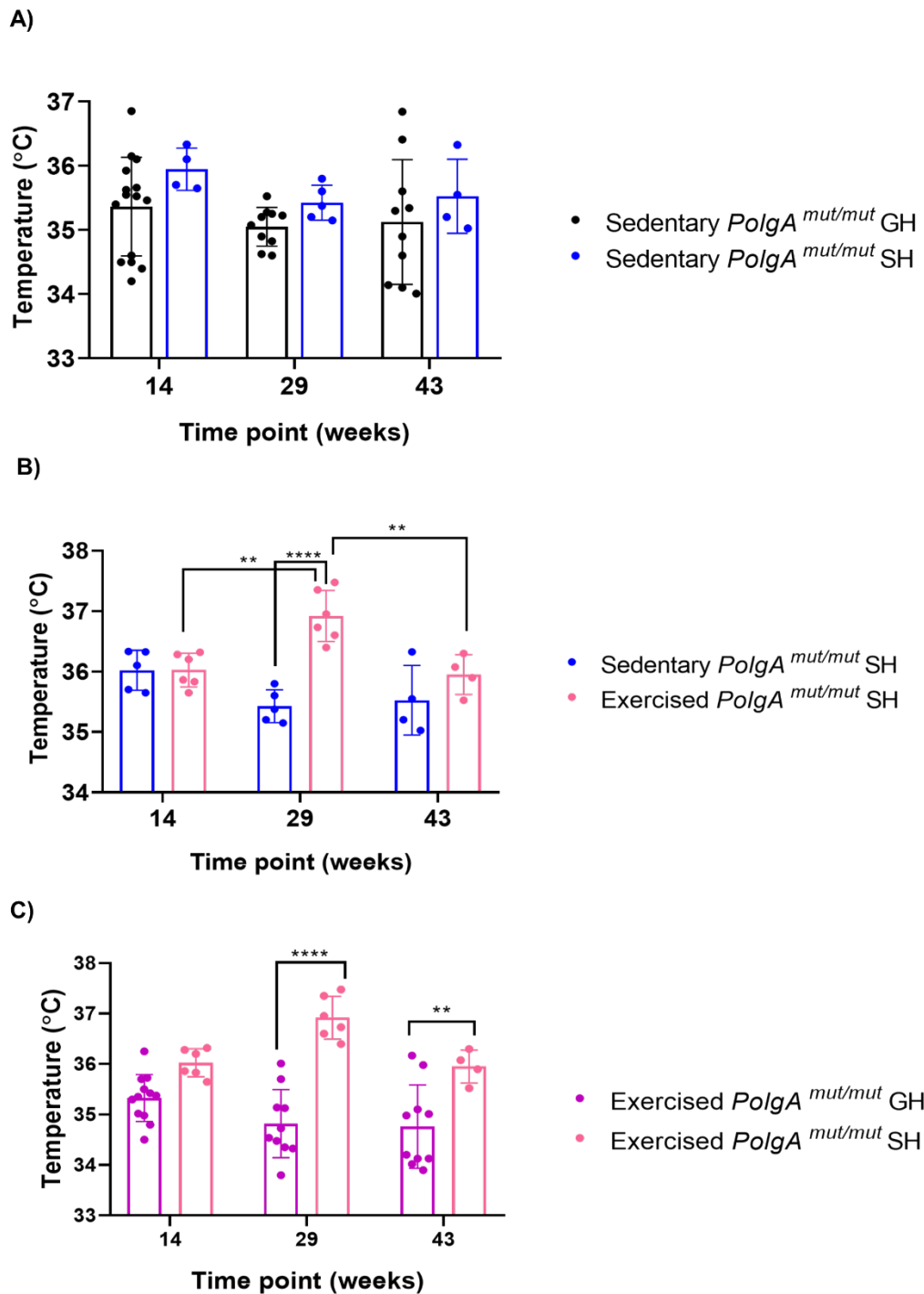
Figure 5.4. Body temperature of mice at 14, 29 and 43 weeks of age. A) No significant changes in the body temperature of sedentary group-housed (GH) and singly-housed (SH) mice were observed. B) Sedentary SH mice showed higher body temperature at 29 weeks (****$p<0.0001$) in comparison to exercised SH mice. C) Exercised SH mice showed significantly higher body temperatures at 29 weeks (****$p<0.0001$) and 43 weeks of age in comparison to exercised GH mice (**$p<0.01$). (Two-way ANOVA repeated measures). Error bars represent mean ±SD.

5.3.3 *Open field testing (OFT) in PolgA^{mut/mut} mice*

OFT was carried out to discern any changes in behaviour and/or locomotive activity within a 5 minute period between different cohorts of mice at three time points (15, 29 and 43 weeks of age). OFT was performed using the open field arena and dark phase programme on Mousetrap software (detailed chapter 2 section 2.16.1). The parameters obtained included the total distance travelled by the mouse, average velocity, average rearing frequency, sum of number of touches and average step length within a 5 minute period of testing time. A two-way ANOVA repeated measures was used to make comparisons between and within groups with age.

A. Sedentary GH compared with SH *PolgA*^{mut/mut} mice

OFT was carried out on sedentary *PolgA*^{mut/mut} GH mice (n=10) and sedentary *PolgA*^{mut/mut} SH mice (n=5) (figure 5.5). The total distance moved was significantly reduced in sedentary GH mice with advancing age ($p < 0.001$). There were no significant changes in the total distance moved with age in sedentary SH cohort (figure 5.5A). The average velocity in 5 minutes in sedentary GH mice increased significantly with advancing age up to 29 weeks ($p < 0.01$). However, there was no significant difference between the velocities of groups at any time point (figure 5.5B). Rearing frequency shown in figure 5.5C also shows that at 15 weeks and 43 weeks of age, SH mice had significantly higher rearing frequency than GH mice ($p < 0.001$, $p < 0.01$ respectively). Also the rearing frequency of GH mice reduced significantly with advancing age ($p < 0.01$) (figure 5.5.C). The total number of touches were also measured in both groups which decreased significantly in sedentary GH mice with advancing age ($p < 0.05$). Also, the total number of touches were significantly higher in the sedentary SH mice in comparison to sedentary GH mice at 15 weeks ($p < 0.05$), 29 weeks ($p < 0.01$) and 43 weeks of age ($p < 0.01$) (figure 5.5D). Step length was measured by dividing the total distance travelled by total number of touches for balance and coordination analysis. The step length of sedentary SH mice was significantly higher at 43 weeks of age ($p < 0.01$) in comparison to sedentary GH mice. The step length of sedentary GH mice decreased significantly with advancing age ($p < 0.001$) (figure 5.5E).

As part of the first aim of this study, it was observed that the total distance moved, total number of touches and step length was significantly higher in sedentary *PolgA^{mut/mut}* SH mice in comparison to sedentary *PolgA^{mut/mut}* GH mice. This could indicate that sedentary *PolgA^{mut/mut}* SH mice are more active within a 5 minute period of testing time from 15 weeks of age and move with longer step length to retain their gait and balance stable. This is interesting because sedentary *PolgA^{mut/mut}* GH mice experience a significant decline in their total distance travelled, total number of touches and step length with advancing age. As animals get older, their locomotive activity reduce proportionally with age. Sedentary *PolgA^{mut/mut}* GH mice showed reduced step length with age ($p < 0.001$). This could mean that GH mice move less but without having to take longer steps or they are more confident and are familiar with the arena during the testing time, since longer step lengths indicate the state of imbalance and unfamiliarity of mice with the apparatus. Reduced number of touches in sedentary GH mice indicate their reduced movement. Interestingly sedentary GH mice showed significantly higher velocity of movements at 29 weeks in comparison to 15 weeks of age indicating that despite less movements, GH mice were faster in moving without having to compensate by taking more frequent steps or longer steps.
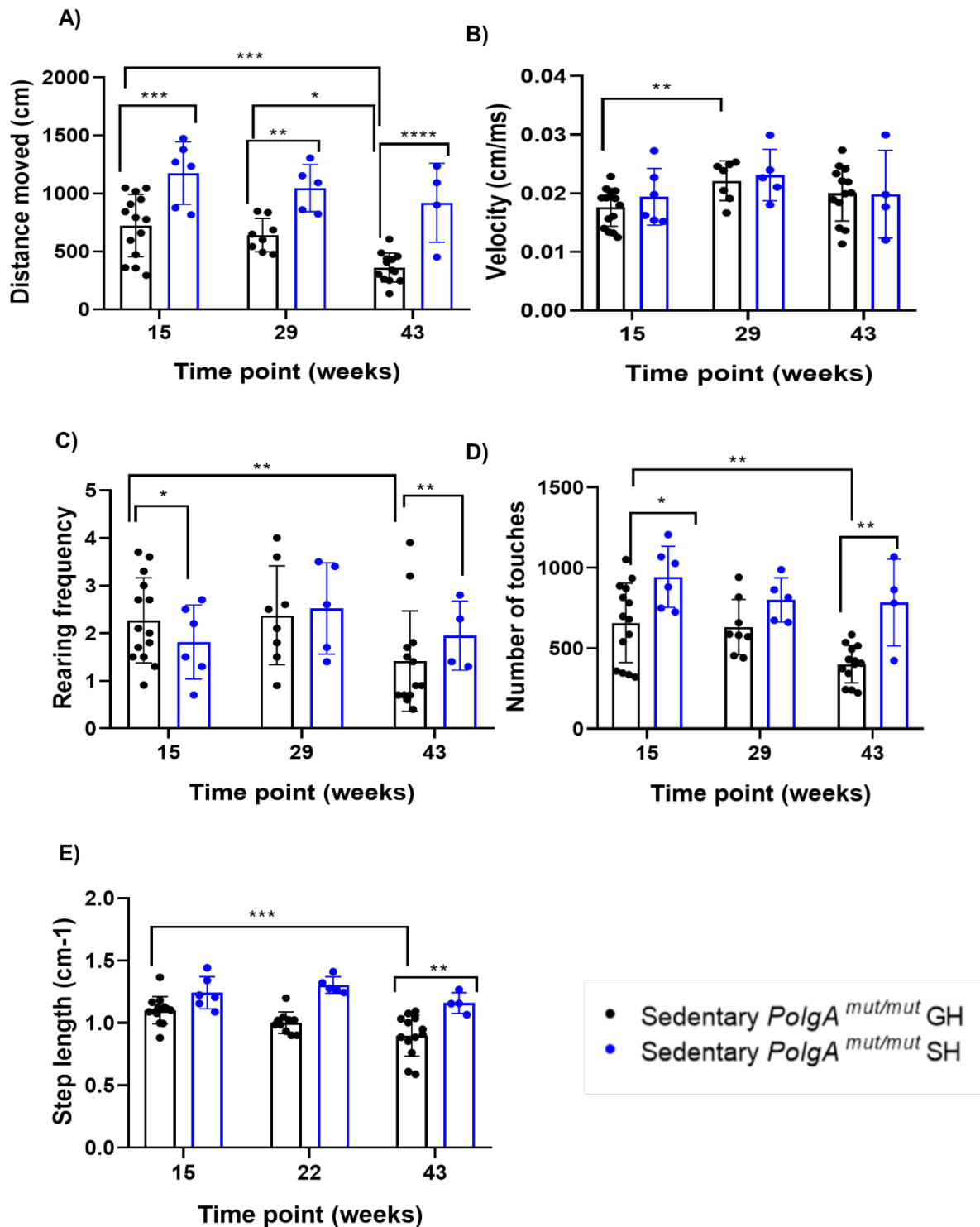
Figure 5.5. Open field testing in sedentary GH and SH *PolgA^mut/mut* mice. A) Total distance moved was significantly higher in sedentary SH mice (****p<0.0001) in comparison to sedentary GH mice at 43 weeks of age. B) Average velocity. C) Rearing frequency was significantly higher in sedentary SH mice (**p<0.01) in comparison to GH mice at 43 weeks of age. D) Total number of touches was significantly greater in sedentary SH mice at 43 weeks (**p<0.01) in comparison to sedentary GH mice. E) Step length was significantly higher in sedentary SH mice in comparison to GH mice at 43 weeks of age (**p<0.01). Error bars represent ±SD.

B. Sedentary compared with Exercised SH *PolgA^mut/mut* mice

OFT was performed on sedentary *PolgA^mut/mut* SH (n=5) and exercised *PolgA^mut/mut* SH mice (n=5) in order to find out whether exercise has any behavioural and locomotive effect on solitary housed mice in comparison to non-exercised solitary housed mice (figure 5.6). The total distance moved in exercised SH mice was significantly reduced with advancing age from 15 weeks to 43 weeks ($p < 0.01$) and from 29 weeks to 43 weeks ($p < 0.0001$). However at 29 weeks of age, exercised SH mice moved significantly further than sedentary SH mice ($p < 0.05$) (figure 5.6A). There was no significant difference between the velocity and rearing frequency of both groups at any time point and with advancing age (figure 5.6B and 5.6C respectively). Total number of touches was reduced significantly in exercised SH group with advancing age ($p < 0.001$). However, in sedentary SH mice this remained unchanged with age (figure 5.6D). The step length was reduced significantly in exercised SH group with advancing age from 29 weeks to 43 weeks ($p < 0.01$), however no significant difference were seen between the groups at any time point as shown by figure 5.6E. As part of the second aim of this study, I have shown that exercised *PolgA^mut/mut* SH mice moved significantly less with advancing age which reflects on their lower overall number of touches. The exercised mice also had significantly lower step length with advancing age.
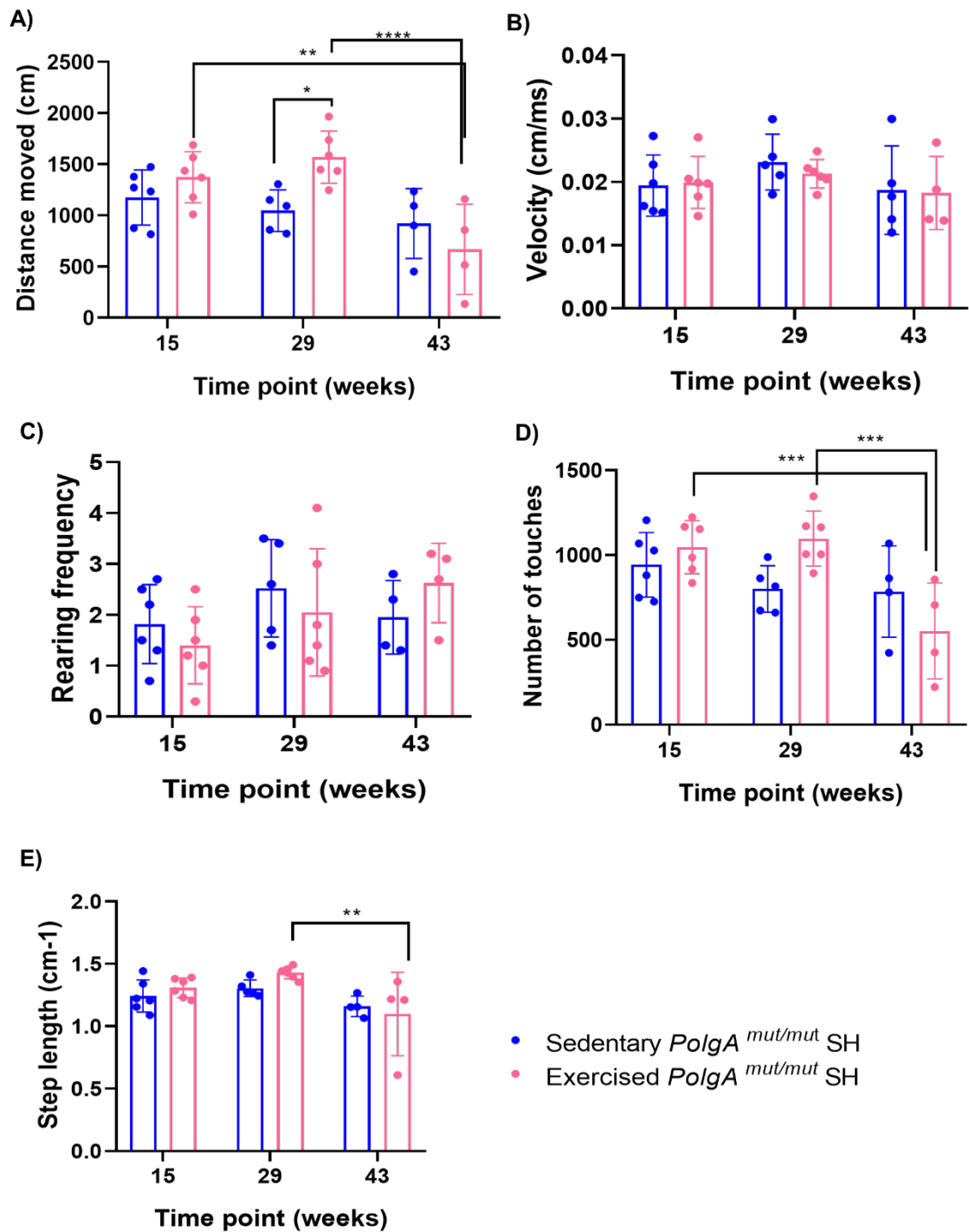
Figure 5.6. Open field testing in exercised GH and SH *PolgA^mut/mut* mice. A) Total distance moved was significantly reduced in exercised SH mice with advancing ggae (**p<0.01). B) Average velocity. C) Rearing frequency. D) Total number of touches were significantly reduced in exercised SH mice with advancing age (***p<0.001). E) Step length. Error bars represent ±SD.

C. Exercised GH compared with SH *PolgA^{mut/mut}* mice

OFT was carried out on exercised *PolgA^{mut/mut}* GH mice (n=10) and exercised *PolgA^{mut/mut}* SH mice (n=5) in order to find out whether housing condition affect behavioural and locomotive activity of exercised *PolgA^{mut/mut}* mice. The total distance moved in exercised SH mice was significantly higher at 15 weeks ($p<0.05$) and 29 weeks of age ($p<0.01$) compared with exercised GH mice (figure 5.7A). Exercised SH mice also showed a significant reduction in distance moved from 15 weeks to 43 weeks ($p<0.01$) and from 29 to 43 weeks of age ($p<0.01$) (figure 5.7A). The average velocity of exercised GH mice was significantly increased with advancing age ($p<0.01$) but was significantly higher at 15 weeks in exercised SH mice ($p<0.05$) (figure 5.7B). The rearing frequency of exercised SH mice increased significantly with advancing age ($p<0.05$) (figure 5.7C). Total number of touches was significantly higher in the exercised SH mice at 15 weeks ($p<0.05$) in comparison to exercised GH mice and decreased significantly with advancing age in exercised SH mice from 15 weeks to 43 weeks ($p<0.01$) and 29 weeks to 43 weeks ($p<0.01$) (figure 5.7D). The average step length was significantly higher in exercised SH mice at 29 weeks and in comparison to exercised GH mice ($p<0.01$) and reduced significantly in exercised SH mice with age from 29 weeks to 43 weeks ($p<0.01$) (figure 5.7E).
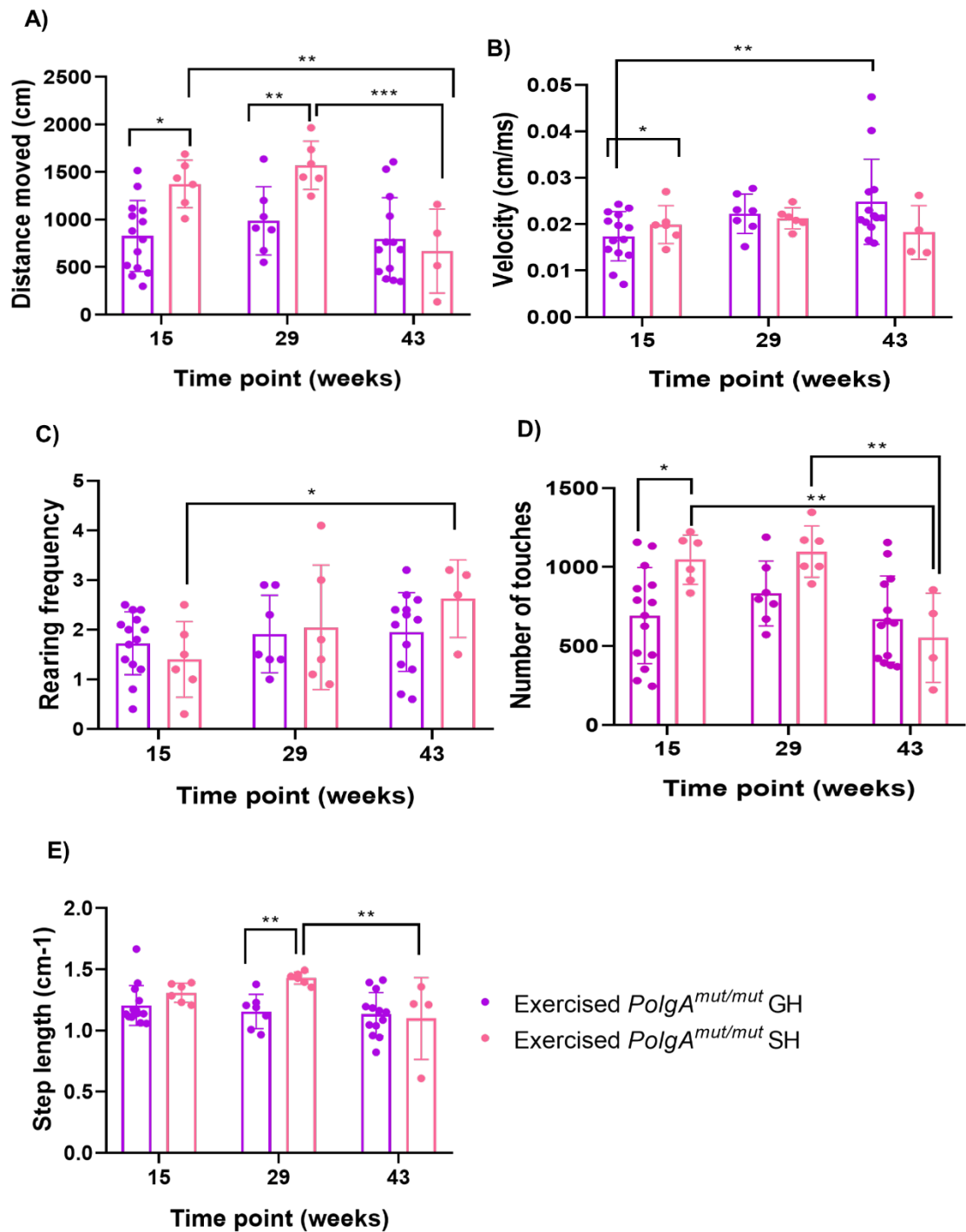
Figure 5.7. Open field testing in exercised GH and SH *PolgA^mut/mut* mice. A) Total distance moved was significantly reduced in exercised SH mice with advancing age (**p<0.01). B) Average velocity was significanty increased in exercised GH mice with advancing age (**p<0.01). C) Rearing frequency. D) Total number of touches was significanrly reduced in exercised SH mice with advancing age (**p<0.01). E) Step length. Error bars represent ±SD.

5.3.4 *Organ weights in PolgA^{mut/mut} mice*

Organ weights in sedentary *PolgA^{mut/mut}* GH (n=10), sedentary *PolgA^{mut/mut}* SH (n=5), exercised GH (n=10) and exercised SH (n=5) mice were measured after organ harvest (detailed chapter 2 section 2.17). Figures 5.8 shows organ weight comparisons between different cohorts (unpaired t-test). Figures 5.9 shows organ weights normalised to body weight (BW) (unpaired t-test). Organ weight to body weight ratio was measured in order to eliminate the effects of weight change in overall organ weight.

Pancreas weight ($p<0.003$) and pancreas: BW ratio ($p=0.004$) was significantly higher in sedentary *PolgA^{mut/mut}* SH mice in comparison to GH mice (figure 5.8A and 5.9A respectively). Liver: BW ($p=0.007$) and lung: BW ($p=0.03$) ratios were also significantly higher in sedentary *PolgA^{mut/mut}* SH mice (figure 5.9A). Considering that the body weight of Sedentary SH mice was in general lower than GH mice, it's clear that sedentary SH mice had significant hypertrophy in the stated organs. Organ hypertrophy seen in sedentary *PolgA^{mut/mut}* SH mice could be pathological or adaptation to function. There was no significant difference between the organ weights of sedentary and exercised SH mice. However left kidney and right kidney weights were significantly higher in exercised GH mice in comparison to exercised SH mice (unpaired t-test) with no significant difference in normalised organ weights between groups.
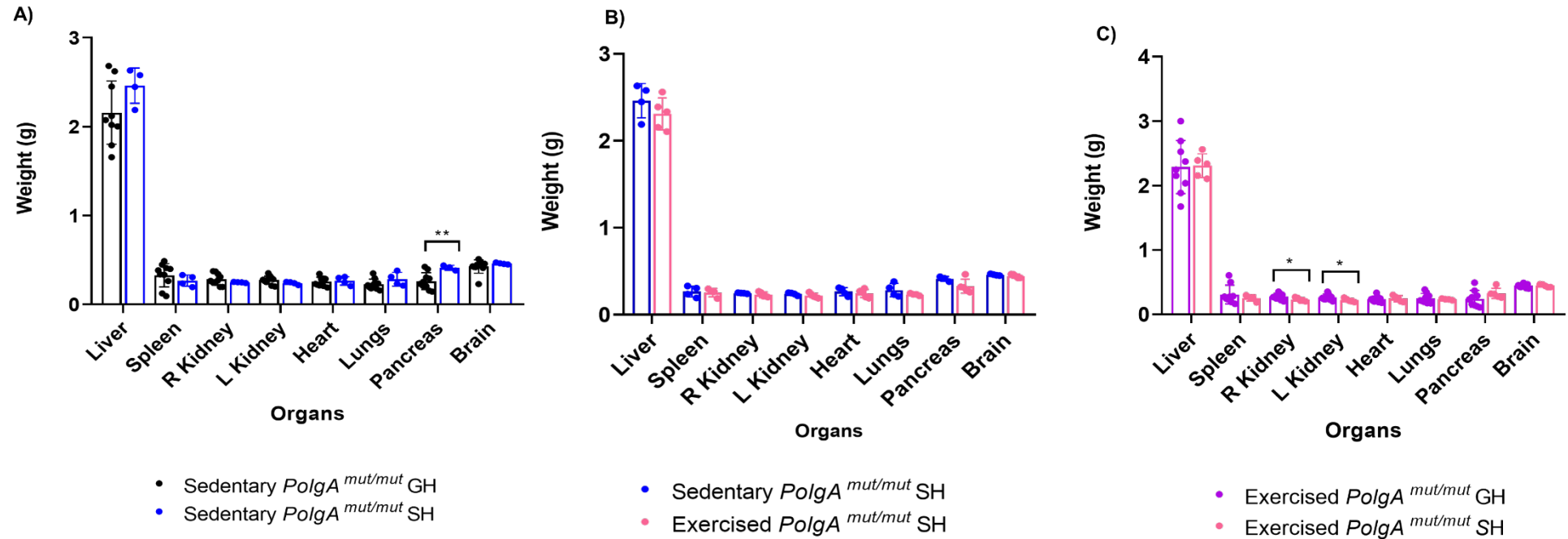
Figure 5.8. Organ weights in *PolgA^mut/mut* mice. A) Pancreas weight was significantly higher in sedentary SH mice in comparison to GH mice (**p<0.01). B) Organ weights in sedentary and exercised SH mice. C) Right kidney and left kidney weights were significantly higher in exercised GH mice in comparison to exercised SH mice (*p<0.05). (Unpaired t-test). Error bars represent mean ±SD.
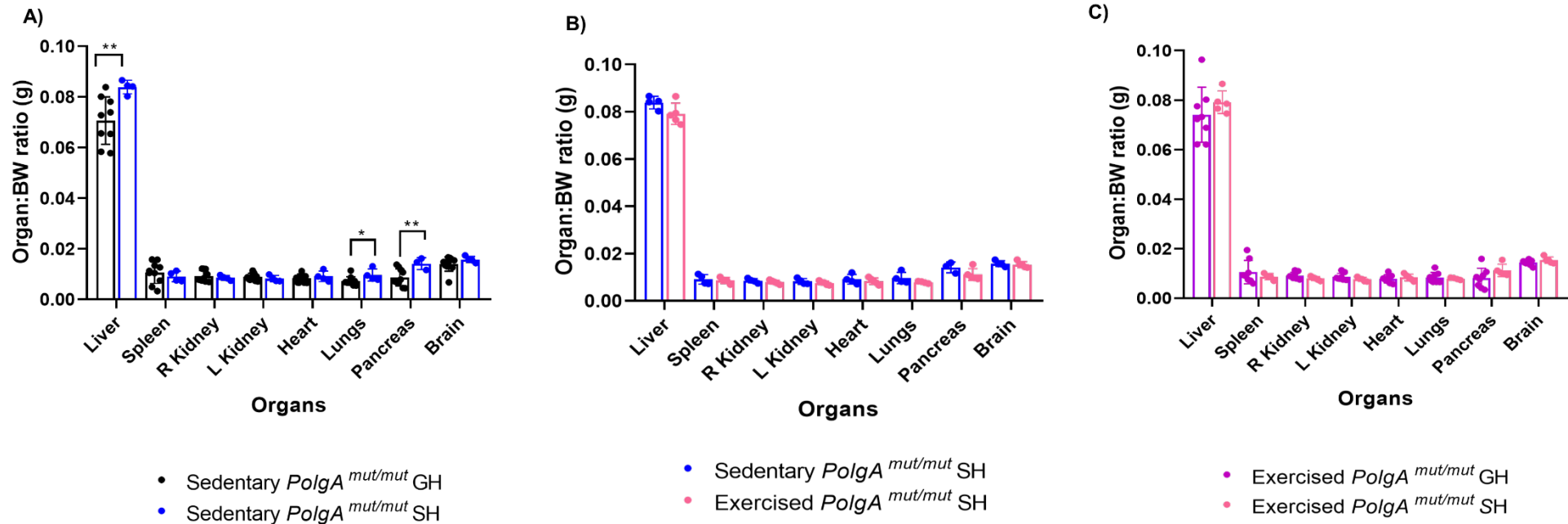
Figure 5.9. Normalised organ weights in _PolgA^{mut/mut}_ mice. A) Liver: BW (**p<0.01), lungs: BW (*p<0.05) and pancreas: BW (**p<0.01) ratios were significantly higher in sedentary SH mice in comparison to sedentary GH mice. B) Normalised organ weights in sedentary and exercised SH mice. C) Normalised organ weights in exercised GH and SH mice. Error bars represent mean ±SD.

5.3.5 *Cardiac apoptosis in PolgA$^{mut/mut}$ mice*

Cardiac apoptosis was assessed in fixed 4μm cardiac right ventricular sections (detailed chapter 2 section 2.23.2) from sedentary GH (n=10), sedentary SH (n=5), exercised GH (n=10) and exercised SH (n=5) *PolgA$^{mut/mut}$* mice by active cleaved-caspase 3 (CC3) immunohistochemistry. Images were obtained by Aperio Scanner (Leica) and the percentage of cardiac apoptosis was quantified using the nuclear v algorithm on Genie software (Leica Biosystems). Dark brown circular regions represent the expression of active form of *Caspase-3.* The percentage of apoptosis was quantified by the ratio of total nuclei count to total apoptotic nuclei count.

CC3 immunohistochemistry revealed that the percentage of apoptotic nuclei was significantly higher in the cardiac muscle of sedentary *PolgA$^{mut/mut}$* SH mice in comparison to sedentary *PolgA$^{mut/mut}$* GH mice (p=0.007, unpaired t-test) (figure 5.10A). Cardiac apoptosis has already been documented in sedentary *PolgA$^{mut/mut}$* GH mice in comparison to sedentary *PolgA$^{+/+}$* GH mice in chapter 3. This is exacerbated in the sedentary *PolgA $^{mut/mut}$* SH mice suggesting that solitary housing conditions are detrimental to the phenotype.

Cardiac apoptosis was also quantified in sedentary (n=5) and exercised (n=5) *PolgA$^{mut/mut}$* SH mice right ventricular muscle (figure 5.10B). No significant difference (unpaired t-test) between the rates of cardiac apoptosis of both groups were seen, indicating that singly-housing exacerbates cardiac apoptosis which is not rescued following endurance exercise.

Cardiac apoptosis was measured in exercised *PolgA$^{mut/mut}$* GH (n=10) and SH (n=5) mice right ventricular muscle. Figure 5.10C shows that the rate of cardiac apoptosis was significantly higher in exercised SH mice in comparison to exercised GH mice (p=0.0071, unpaired t-test), confirming that single housing is detrimental to the *PolgA$^{mut/mut}$* phenotype and is not altered with exercise.
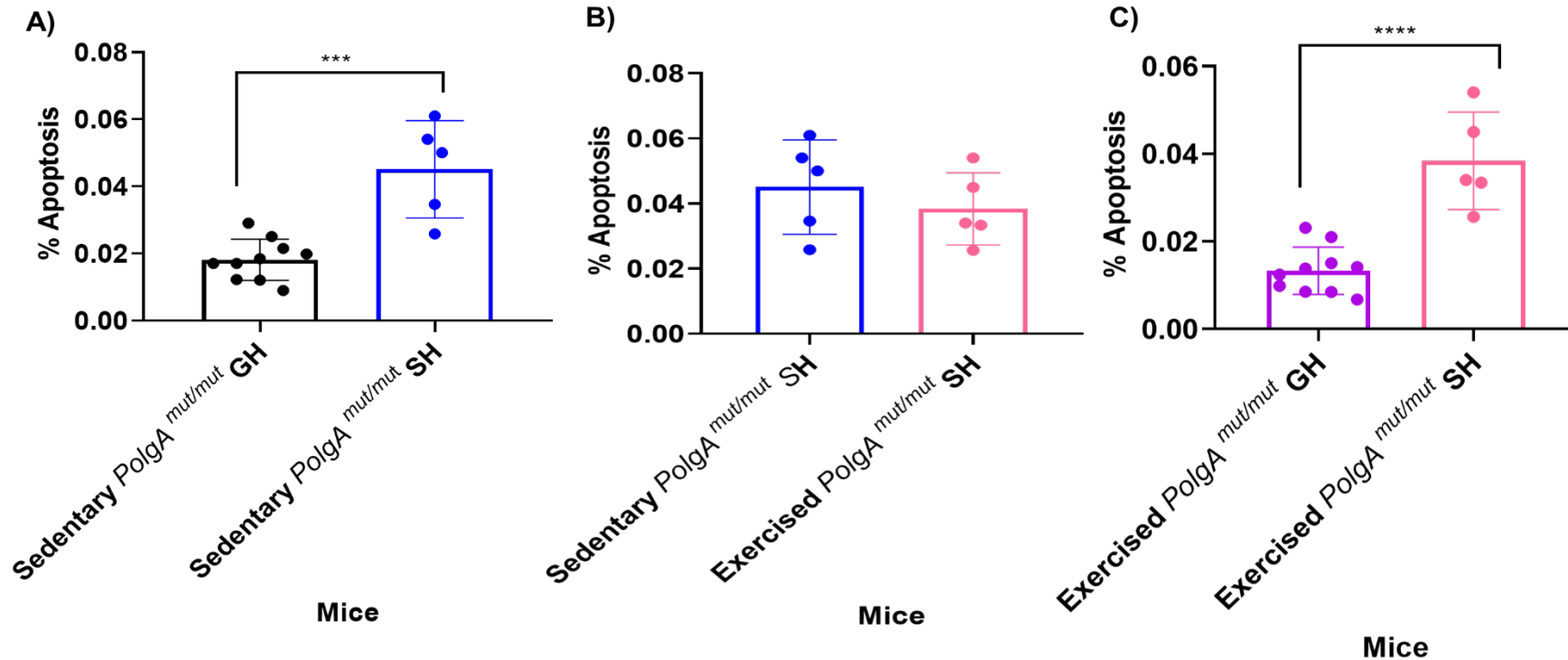
Figure 5.10. Rate of apoptosis in *PolgA^mut/mut* mice. A) Rate of cardiac apoptosis is significantly higher in sedentary *PolgA^mut/mut* SH mice in comparison to sedentary GH mice (***p=0.007). B) There was no significant difference in the percentage of apoptosis between the sedentary SH and exercised SH mice (p=0.6). C) Exercised SH mice have significantly higher rate of apoptotic nuclei than GH mice (***p=0.0071, unpaired t-test). Error bars represent mean ±SD.

5.3.6 *Cardiomyocyte width and cardiac fibrosis in PolgA$^{mut/mut}$ mice*

Cardiomyocyte width and cardiac fibrosis was assessed in 4µm fixed right ventricular cardiac muscle sections in sedentary GH (n=10), sedentary SH (n=5), exercised GH (n=10) and exercised SH (n=5) *PolgA$^{mut/mut}$* mice by Haematoxylin and Eosin (H&E) staining (detailed chapter 2 section 2.20) and Masson trichrome staining (detailed chapter 2 section 2.22) respectively.

H&E staining is used to morphologically assess the structure of cardiomyocytes and determine any alteration in their shape and size. Five random snapshots of x20 magnification images were obtained using Zeiss microscopy and the width of 50 transverse cardiomyocytes were analysed from each image to make a total of 250 fibres from each mouse. Zen (v2.5) analysis software (Zeiss) was used to measure cardiomyocyte width.

Similarly, cardiac fibrosis was assessed in both cohorts by Masson trichrome staining to assess the presence of collagenous tissue to identify cardiac fibrosis. Images were obtained from Nikon Tie widefield microscope and analysed using NIS elements software. The percentage of fibrosis was assessed by using RGB general analysis in which each dye is separated by RGB thresholding and the area of collagen to total tissue section was quantified to determine the percentage of fibrosis. Cardiomyocyte width and cardiac fibrosis micrographs are presented in figure 5.11.
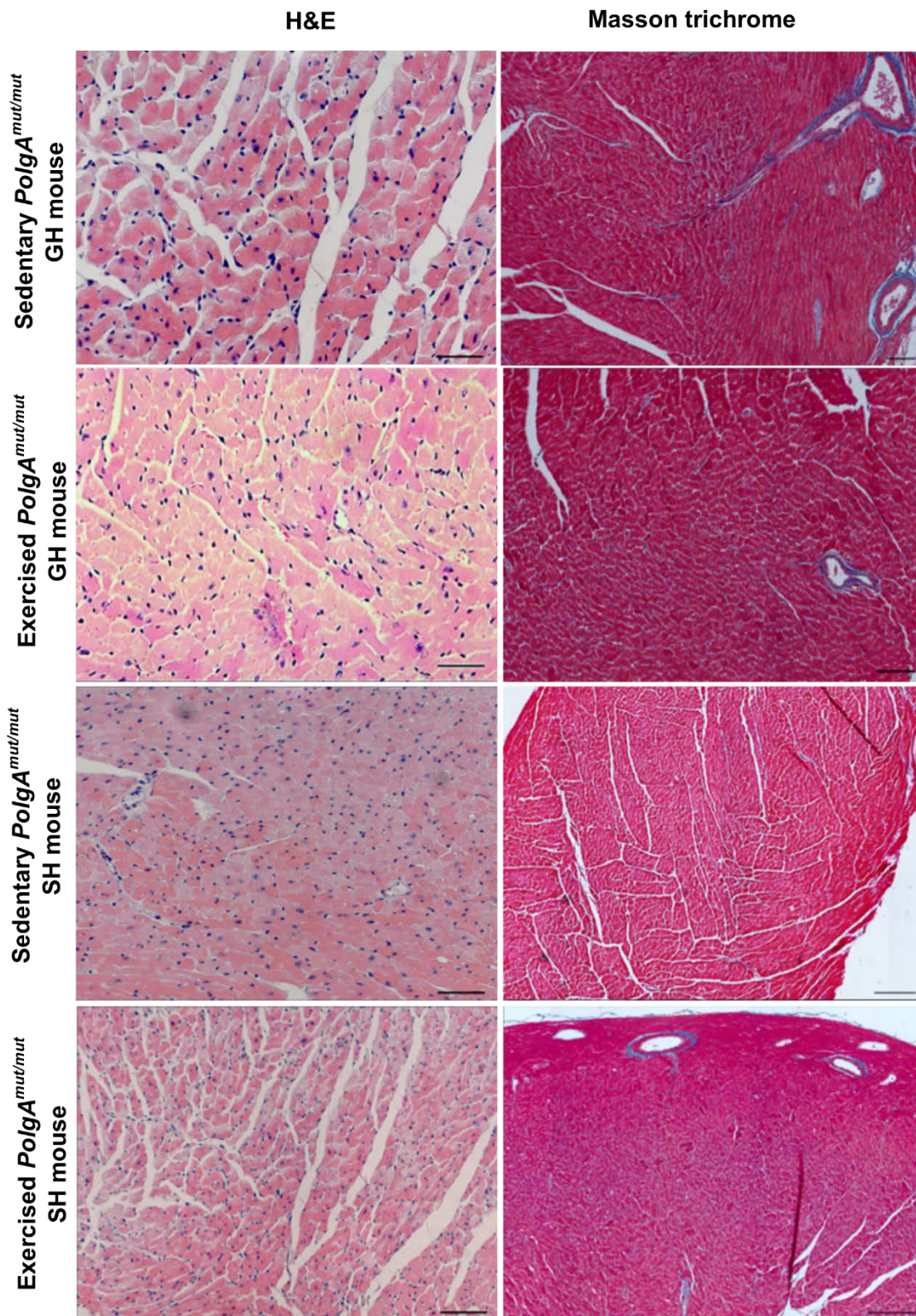
Figure 5.11. Cardiomyocyte width and cardiac fibrosis in *PolgA^{mut/mut}* mice.
H&E histochemistry was used to visualise cardiomyocyte width (magnification x20,
Scale bars=100µm) and Masson trichrome staining was carried out to visualise
cardiac fibrosis. Magnification x10. Scale bars=200µm.

Cardiomyocyte width was shown to be significantly higher in GH $PolgA^{mut/mut}$ mice from chapter 3 in comparison to $PolgA^{+/+}$ mice. Cardiomyocyte width was significantly higher (5.78µm greater in average) in the sedentary GH mice in comparison to SH mice (p=0.003, unpaired t-test) meaning that solitary housing condition alleviate enlarged cardiomyocyte width in $PolgA^{mut/mut}$ mouse (figure 5.12A). Cardiac fibrosis was proven to be significantly higher in GH $PolgA^{mut/mut}$ mice from chapter 3, but does not seem to be affected by singly-housing (figure 5.12D). Since cardiomyocytes have high density of mitochondria to allow for more efficient ATP synthesis, larger cardiomyocytes which normally lead to hypertrophy also normalises wall tension during the conditioning process. In the setting of inactive lifestyle however cardiomyocyte hypertrophy could be pathological. However the difference in the hypertrophy level could be due to the small sample size in the SH cohort.

No significant differences were seen in percentage of cardiac fibrosis and cardiomyocyte width between the sedentary and exercised SH mice (unpaired t-test), meaning that exercise in the context of single-housing has no impact on cardiomyocyte width and the level of cardiac fibrosis in $PolgA^{mut/mut}$ mice (figures 5.12B and 5.12E respectively). These findings are similar to the findings of chapter 4 figure 4.4 where exercise in the context of group-housing in $PolgA^{mut/mut}$ mice did not affect cardiomyocyte hypertrophy and cardiac fibrosis observed in $PolgA^{mut/mut}$ mice.

Similarly, exercise in the context of singly-housing in $PolgA^{mut/mut}$ SH mice did not change cardiomyocyte width and the level of cardiac fibrosis as shown in figures 5.12C and 5.12F respectively. This could simply mean that exercise and housing condition do not have an impact on the levels of cardiac fibrosis and cardiomyocyte hypertrophy in exercised cohort and only the housing condition have an impact on cardiomyocyte width in sedentary cohort. Although in comparison to $PolgA^{+/+}$ mice a significant increase in cardiac fibrosis was observed in singly-housed $PolgA^{mut/mut}$ mice.
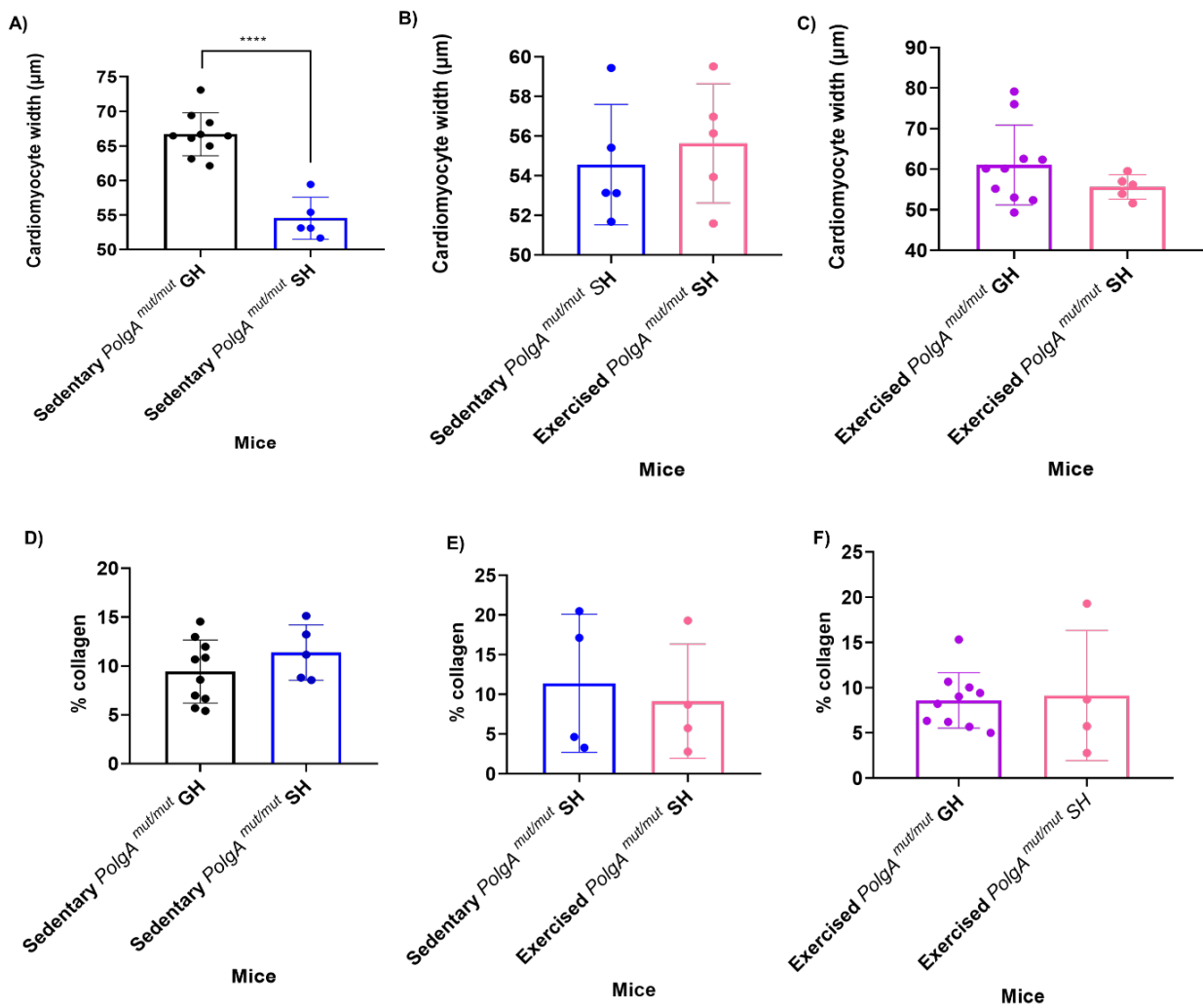
Figure 5.12. Cardiomyocyte width and cardiac fibrosis in *PolgA^mut/mut* mice. A) Cardiomyocyte width is significantly higher in sedentary GH mice in comparison to SH mice (***p=0.003, unpaired t-test). B, E) There is no significant difference in cardiomyocyte width (p=0.9) and percentage of cardiac fibrosis in SH sedentary and exercised mice. C, F) There was no significant difference between the cardiomyocyte width (p=0.3) and cardiac fibrosis in exercised GH and SH mice (unpaired t-test). Error bars represent mean ±SD.

5.3.7 *Mitochondrial complex I (NDUFB8) and complex IV (MTCOI) expression levels in PolgA*$^{mut/mut}$ *mice hearts*

Cardiac mitochondrial ETC complex I (CI) NDUFB8 subunit and complex IV (CIV) MTCOI subunit expression levels were quantified by immunofluorescence (detailed chapter 2 section 2.24.2). Paraffin fixed right ventricular cardiac sections (4µm) from sedentary GH (n=10), sedentary SH (n=5), exercised GH (n=10) and exercised SH (n=5) *PolgA*$^{mut/mut}$ mice were subjected for detection of NDUFB8, MTCOI, VDAC (mitochondrial mass marker) and laminin (myocardial basal membrane protein marker). A mitochondrial mass marker was used to confirm genuine mitochondrial signal. Images were acquired using Nikon LSM800 microscope (figure 5.13). The expression levels of two complexes were normalised to Porin levels and quantified by an in-house immuno-analyser software. Five random snapshots of x10 magnification were selected from each mouse for analysis. Laminin was used to semi-automatically detect and outline transverse cardiomyocytes for analysis. Analysed cardiomyocytes were categorised into positive, intermediate positive, intermediate negative and negative expression levels of NDUFB8 and MTCOI based on their z-scores. Mitochondrial respiratory chain graphs (MRC) were generated as shown in figures 5.14. Percentage of CI and CIV expression levels were also quantified in each group and compared in figure 5.15. Porin Z-scores were used to classify fibres into very low (Z-scores <-3SD), low (Z-scores between -3SD and -2SD), normal (Z-scores between -2SD and +2SD), high (Z-scores between +2SD and +3SD) and very high (Z-scores >+3SD) (detailed chapter 2 table 2.4). Porin expression levels as z-score values are shown in figure 5.16.
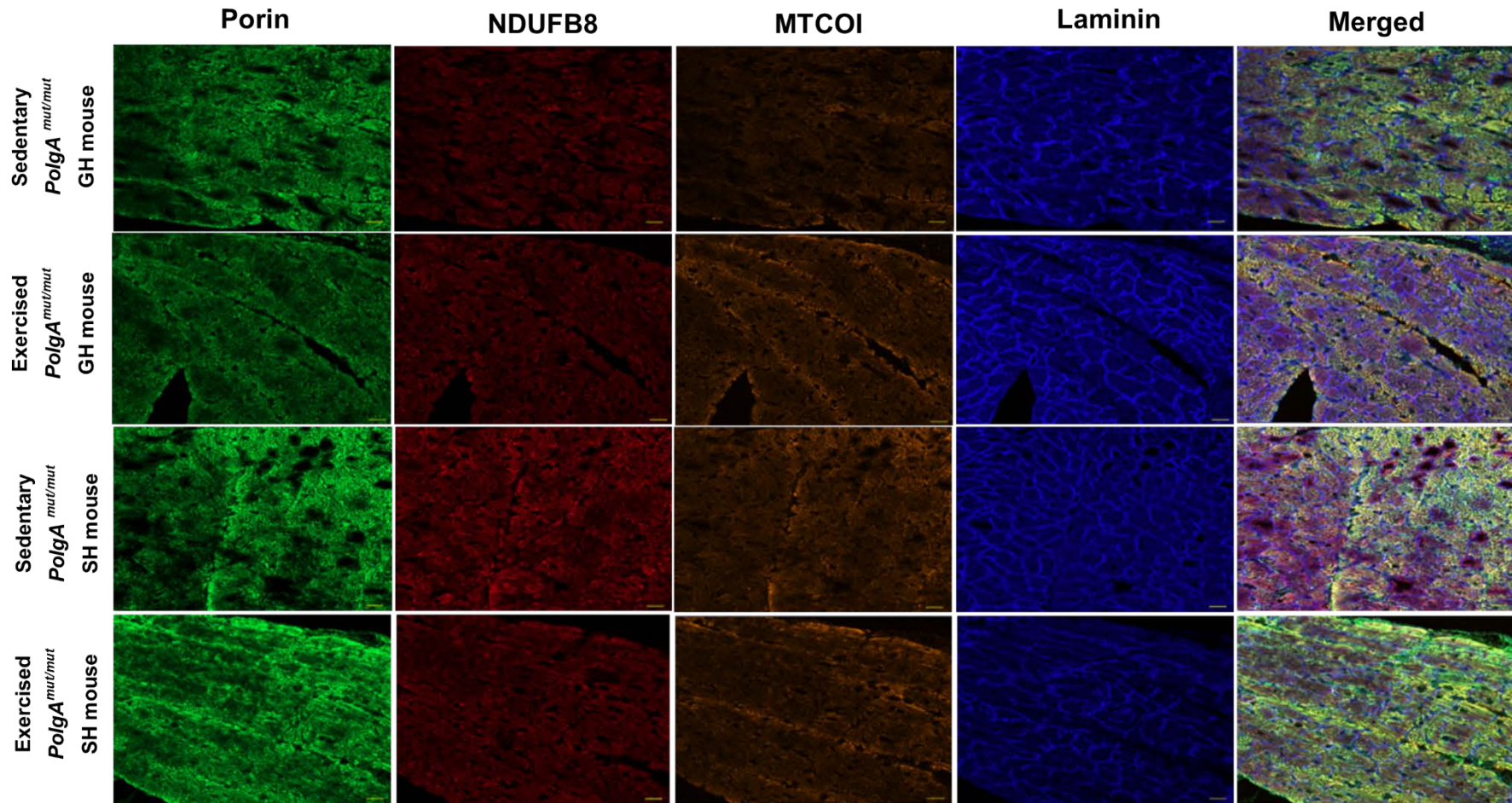
Figure 5.13. Mitochondrial NDUFB8 (CI) and MTCOI (CIV) subunit expression levels. Representative images of right ventricular cardiac muscle for immuno detection of NDUFB8 (complex I), MTCOI (complex IV), Porin (mitochondrial mass marker) and laminin (cardiomyocyte boundary marker) in *PolgA$^{mut/mut}$* mice. Magnification x10. Scale bars=100μm.
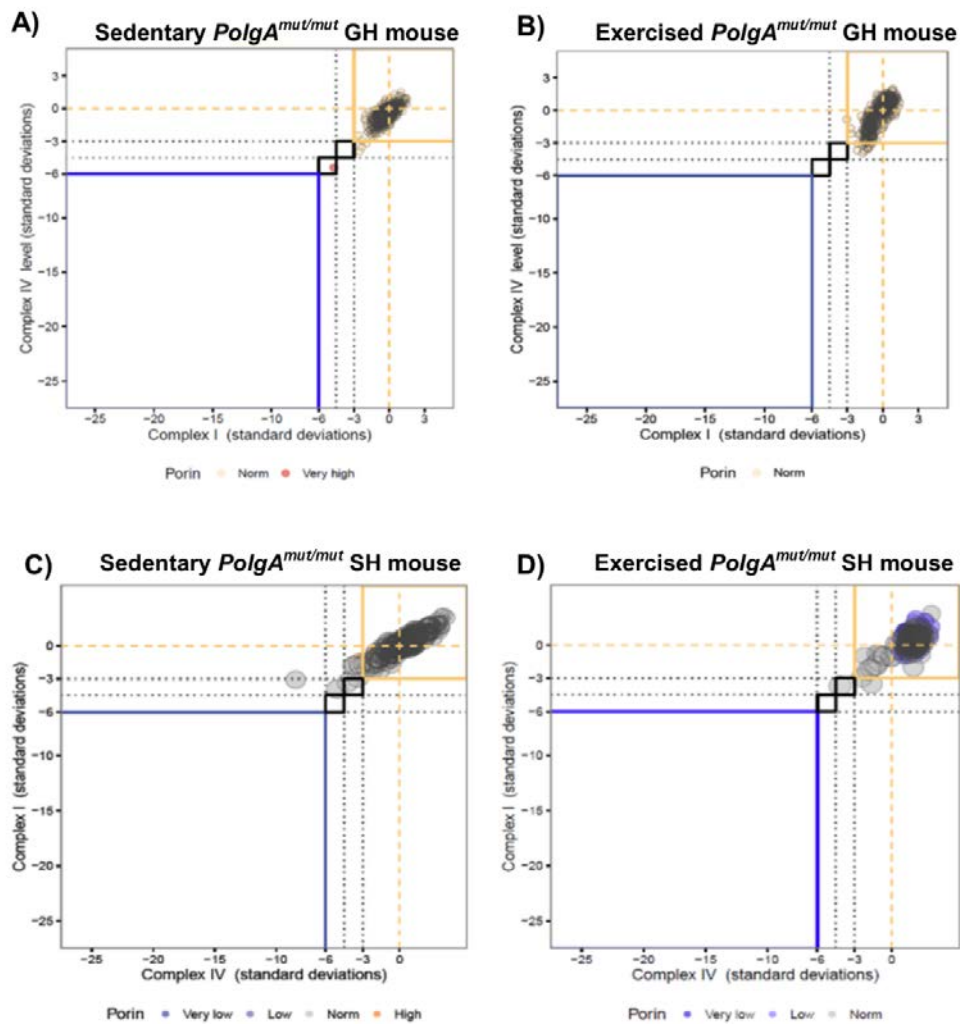
**Figure 5.14. MRC plots from sedentary and exercised, GH and SH *PolgA^mut/mut*
mice.** A) Sedentary GH. B) Exercised GH. C) Sedentary SH. D) Exercised SH mice.
Each dot represent a cardiomyocyte. Solid yellow lines represent SD limits for the
classification of cardiomyocytes. Yellow dashed lines represent mean expression
level of cardiomyocytes with normal CI and CIV. Each cardiomyocyte was colour
coded according to mitochondrial mass expression levels.
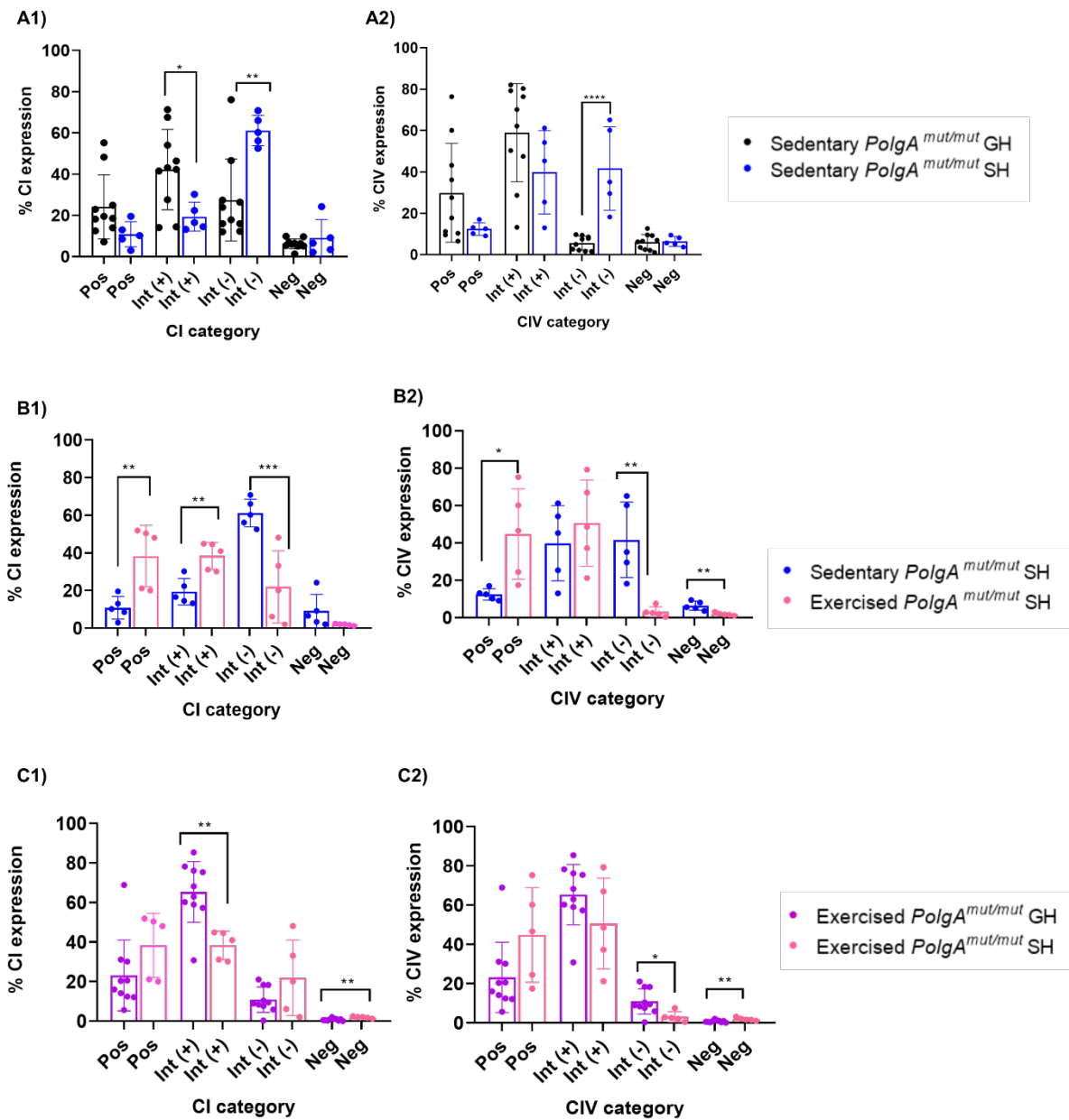
Figure 5.15. Percentage of cardiomyocytes with MTCOI and NDUFB8 expression levels (unpaired t-test). A) Sedentary GH and SH mice. B) Sedentary and exercised SH mice. C) Exercised GH and SH mice hearts. Unpaired t-test in each category between groups. Error bars represent mean ±SD.

192
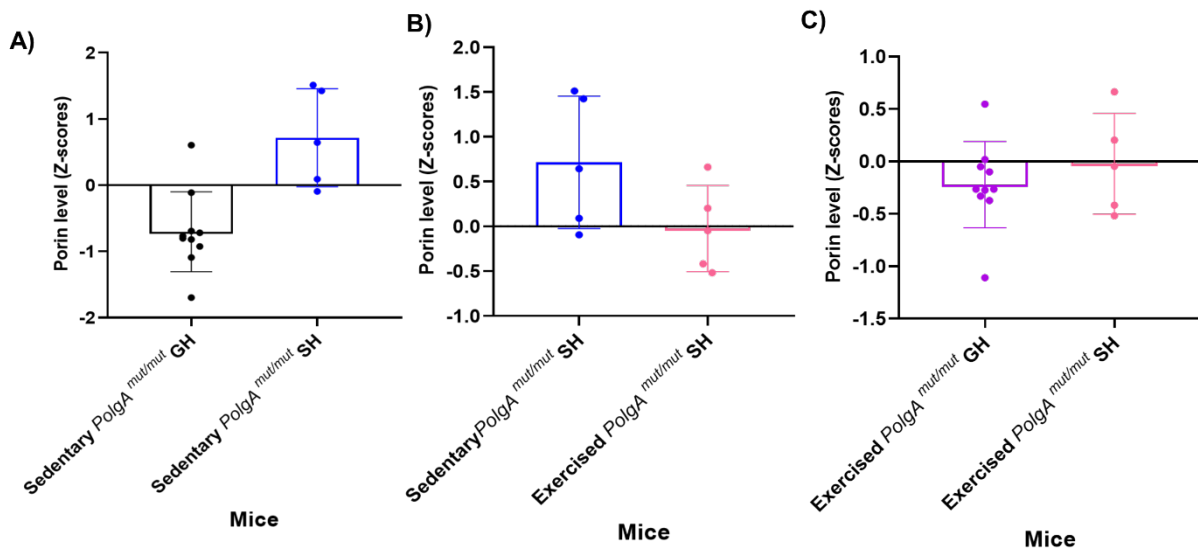
Figure 5.16. Porin Z-scores in: A) sedentary GH and SH mice. B) Sedentary and exercised SH mice. C) Exercised GH and SH mice. Error bars represent mean ±SD.

The percentage of cardiomyocytes with intermediate negative NDUFB8 and MTCOI expression levels were significantly higher in the right ventricular cardiac muscle of sedentary *PolgA^mut/mut* SH mice in comparison to sedentary *PolgA^mut/mut* GH mice ($p < 0.01$ and $p < 0.0001$ respectively) (figures 5.15A1, A2). Interestingly, the percentage of cardiomyocytes with intermediate positive expression levels of NDUFB8 was significantly higher in sedentary GH mice in comparison to SH mice ($p < 0.05$, unpaired t-test) (figure 5.15A).

Unpaired t-test between the different categories revealed that the percentage of cardiomyocytes with positive and intermediate positive expression of NDUFB8 and intermediate positive expression of MTCOI was significantly higher in exercised *PolgA^mut/mut* SH mice in comparison to sedentary *PolgA^mut/mut* SH mice ($p < 0.001$) (figure 5.15B1 and B2) Whereas percentage of cardiomyocytes with intermediate negative MTCOI and NDUFB8 as well as negative MTCOI expression was significantly higher in sedentary *PolgA^mut/mut* SH mice in comparison to exercised *PolgA^mut/mut* SH mice. The negative shift in the expression levels of MTCOI and NDUFB8 in sedentary SH cohort may be an indication of decreased cellular respiration in the cardiac muscle of sedentary SH mice. These findings although confirm the presence of enzymes but do not account for the activity of subunits.

An unpaired t-test was performed to analyse NDUFB8 and MTCOI expression in exercised *PolgA^mut/mut* GH and exercised *PolgA^mut/mut* SH mice right ventricular

cardiac muscle (figures 5.15C1, C2). Exercised *PolgA* $^{mut/mut}$ GH mice had significantly higher percentage of cardiomyocytes with intermediate positive expression levels (p<0.01) as well as intermediate negative MTCOI expression (p<0.05), whereas exercised *PolgA$^{mut/mut}$* SH mice had significantly higher percentage of cardiomyocytes with negative expression of NDUFB8 and MTCOI (p<0.01).

Figures 5.16 represent mitochondrial mass marker expression levels. Porin z-scores were generated through immunoanalyser software and were within the normal range in all four cohorts of mice, indicating that porin levels were not affected by exercise and singly-housing in mice.

5.3.8 *COX activity in PolgA$^{mut/mut}$ mice hearts*

Mitochondrial complex IV (COX) activity was quantified by COX/SDH histochemistry in left ventricular cardiac muscle sections from sedentary GH (n=10), sedentary SH (n=5), exercised GH (n=10) and exercised SH (n=5) mice. COX deficient cells stain blue by reduction of NBT, allowing for the visualisation of nuclear encoded succinate dehydrogenase. Images were acquired by Nikon Tie microscope and the percentage of blue staining was measured in comparison to total tissue area. Five random snapshots of x10 magnification per mouse was selected for analysis through NIS elements software where RGB general analysis algorithm was used to set a threshold for each channel. The percentage of COX deficiency was calculated by the ratio of total tissue area to total blue staining region. An unpaired t-test was performed to statistically analyse the difference in COX activity between groups.

In order to visualise the effects of housing condition on cardiac COX activity of sedentary *PolgA$^{mut/mut}$* mice, both sedentary GH and sedentary SH mice cardiac sections were assessed for COX/SDH histochemistry (figure 5.17). Interestingly, percentage of COX deficiency was significantly higher in sedentary SH *PolgA$^{mut/mut}$* mice hearts in comparison to sedentary GH mice (5.18A).

COX activity was also measured in sedentary and exercised *PolgA* $^{mut/mut}$ SH mice (figure 5.18B). The percentage of cardiomyocytes with COX deficiency was not significantly different between the two cohorts, indicating that exercise in the setting of singly-housed mice does not alleviate COX deficiency in *PolgA* $^{mut/mut}$ mice hearts.

194

COX activity was also determined in exercised $PolgA^{mut/mut}$ GH and SH mice in order to find out whether singly-housing has any effect on the mitochondrial function of exercised mice. There was no significant difference between the levels of COX activity between the two groups (figure 5.18C).

I have confirmed in chapter 4 section 4.3.9 that group-housed $PolgA^{mut/mut}$ mice whether sedentary or exercised had similar levels of COX activity. Similarly singly-housed $PolgA^{mut/mut}$ mice have non-significant levels of COX deficiency whether sedentary or exercised. COX deficiency analysis in all groups indicate that singly-housed inactive $PolgA^{mut/mut}$ mice, have compromised COX activity as shown in figure 5.18A. These findings purely show that the effects of singly-housing is more prominent on mitochondrial function than the state of activity of mice.
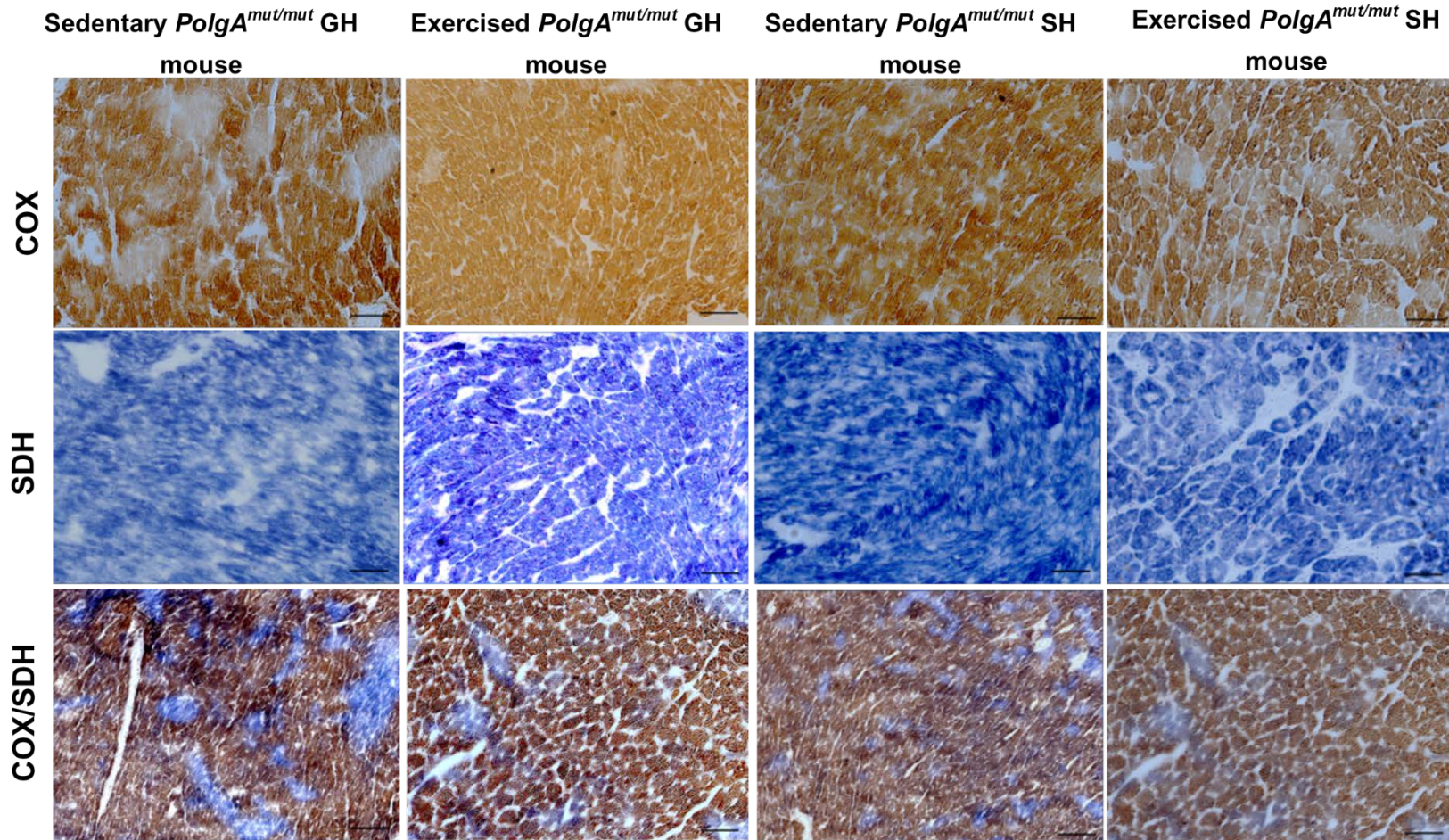
Figure 5.17. Representative micrographs of mitochondrial COX, SDH activity and COX/SDH histochemistry in *PolgA^{mut/mut}* mice. A mosaic pattern of COX deficiency is seen within the left ventricular cardiac muscle of all groups with COX/SDH histochemistry. Magnification x10. Scale bars=100µm.
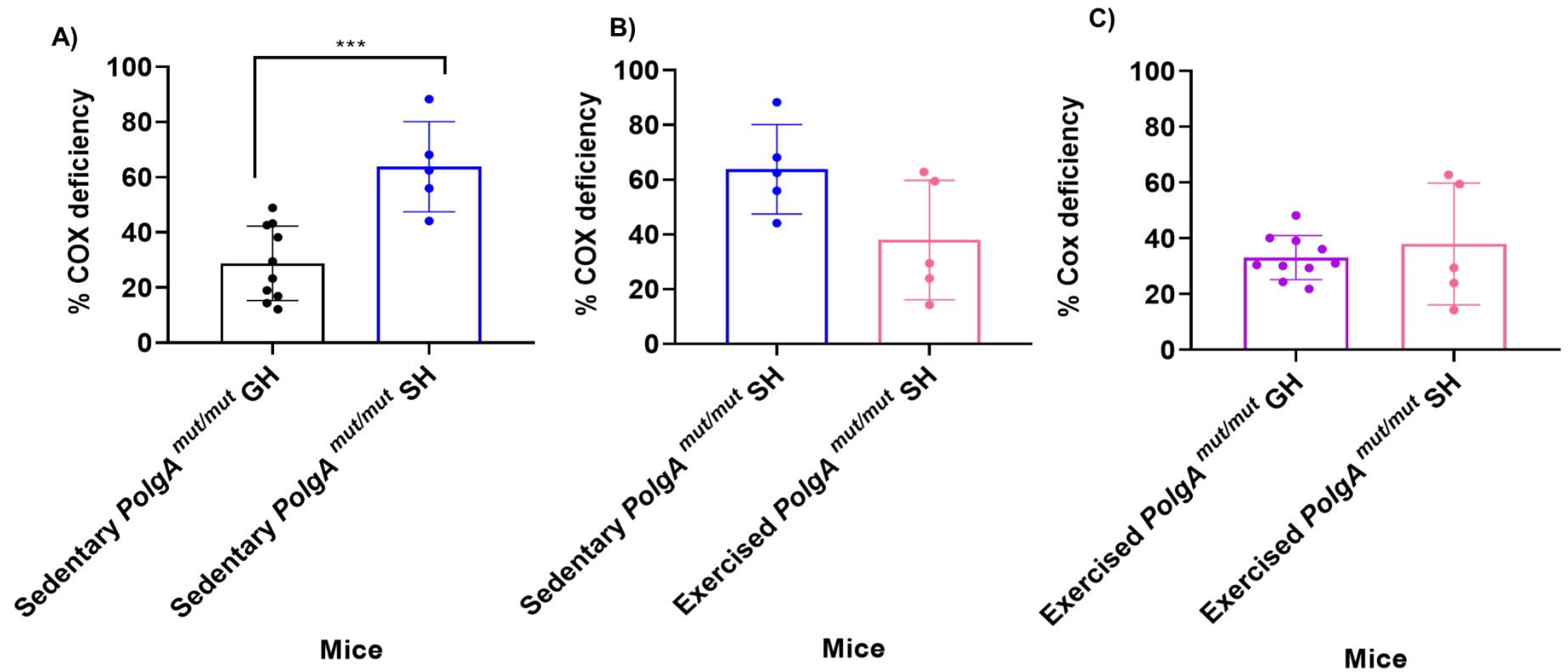
Figure 5.18. COX deficiency in *PolgA^{mut/mut}* mice hearts. A) The percentage of COX deficiency is significantly higher in the left ventricular cardiac muscle of SH cohort (***p=0.0005, unpaired t-test) in comparison to GH mice. B) There is no significant difference between the level of COX activity of sedentary and exercised SH mice (p=0.06, unpaired t-test). C) There is no significant difference in the COX activity of exercised GH and SH mice (p=0.5, unpaired t-test). Error bars represent mean± SD.

5.3.9 *NBTx and laminin immunofluorescence in PolgA$^{mut/mut}$ mice hearts*

NBTx assay and laminin immunofluorescence was performed in left ventricular cardiac muscle of sedentary *PolgA$^{mut/mut}$* GH (n=10), sedentary *PolgA$^{mut/mut}$* SH (n=5), exercised *PolgA$^{mut/mut}$* GH (n=10) and exercised *PolgA$^{mut/mut}$* SH (n=5) mice in order to visualise and quantify COX deficiency based on NBTx activity only through the technique described in chapter 3 section 3.3.10.

Left ventricular cardiac sections were stained for cytochrome *c* oxidase and NBTx activity followed by laminin immunofluorescence. COX functional cells remain transparent through NBTx assay where NBT is not reduced and deposited inside cells by SDH. COX dysfunctional cells however turn blue and the amount of blue deposition inside cells i.e. depth of blue, determines the degree of deficiency. Five random snapshots of x10 magnification Images were obtained and analysed through an in-house immunoanalyzer software. 500 transverse cardiomyocytes per mouse were semi-automatically selected through laminin immunofluorescence and analysed through the software. The darker the blue staining, the more COX deficient the cells were; however this was observed in black through the monochrome camera (figure 5.19). An arbitrary z-scoring was used (Chapter 2 section 2.24.1) to categorise cardiomyocytes into groups of positive, intermediate and negative according to the NBT activity based on COX activity of wild-type tissue.
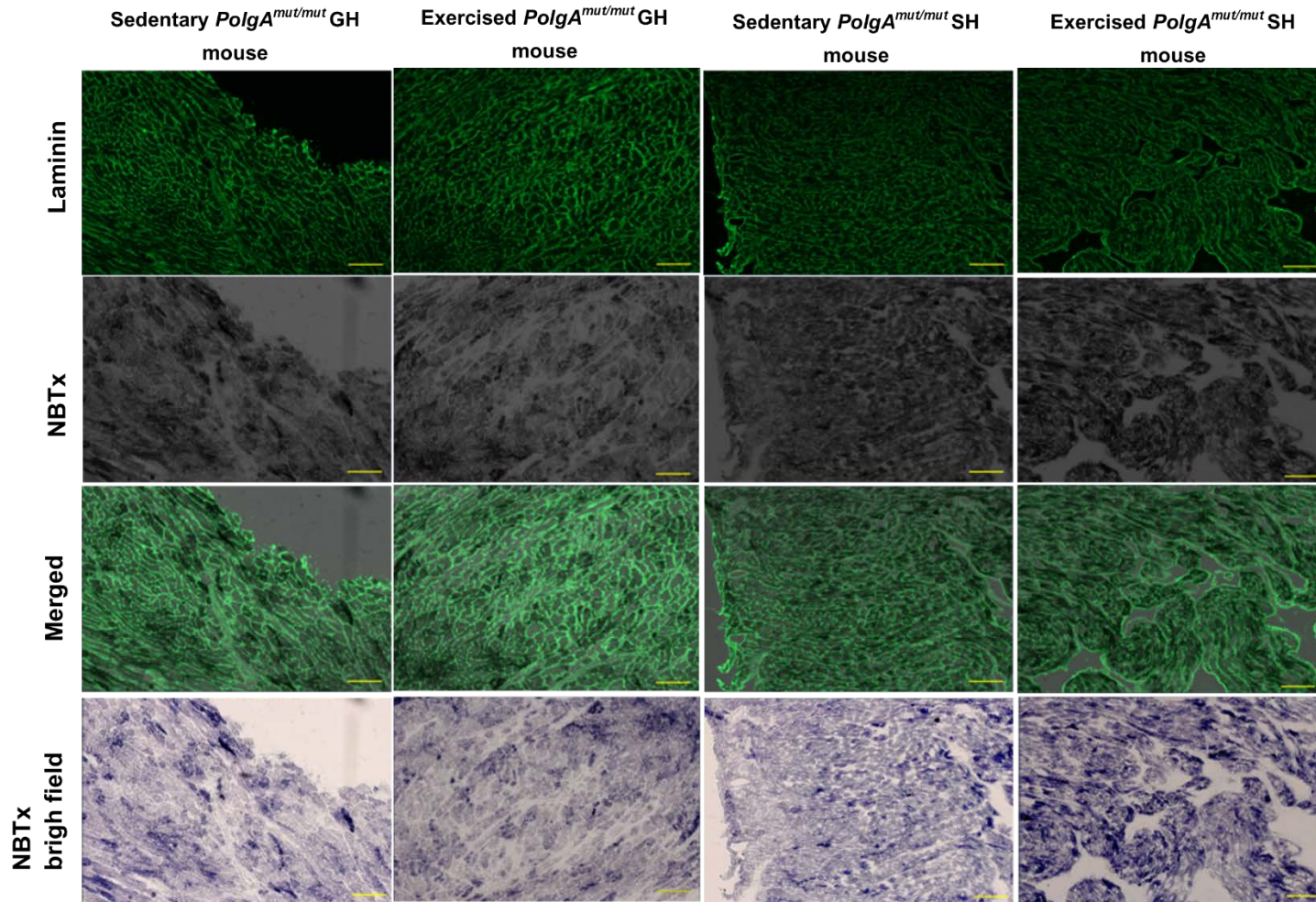
Figure 5.19. NBTx assay and laminin immunofluorescence in *PolgA^{mut/mut}* mice. Images were obtained from LSM800 microscope and analysed in immuno-analyser software. Scale bars=100μm.

In order to observe changes in COX activity of inactive mice within different housing conditions, sedentary GH (n=10) and sedentary SH (n=5) mice were compared (figure 5.20). Sedentary GH mice had significantly higher percentage of cardiomyocytes with positive and intermediate COX activity (figure 5.20A) ($p<0.001$) and sedentary SH mice had a significantly higher percentage of COX negative cardiomyocytes in comparison to GH mice. Percentage of COX intermediate cardiomyocytes were significantly higher in exercised SH mice cohort in comparison to sedentary SH group ($p<0.01$, unpaired t-test) (figure 5.20B). Exercised SH mice have significantly higher percentage of COX negative cardiomyocytes ($p<0.001$, unpaired t-test) and exercised GH mice have significantly higher COX positive cardiomyocytes (figure 5.20C) ($p<0.05$, unpaired t-test).
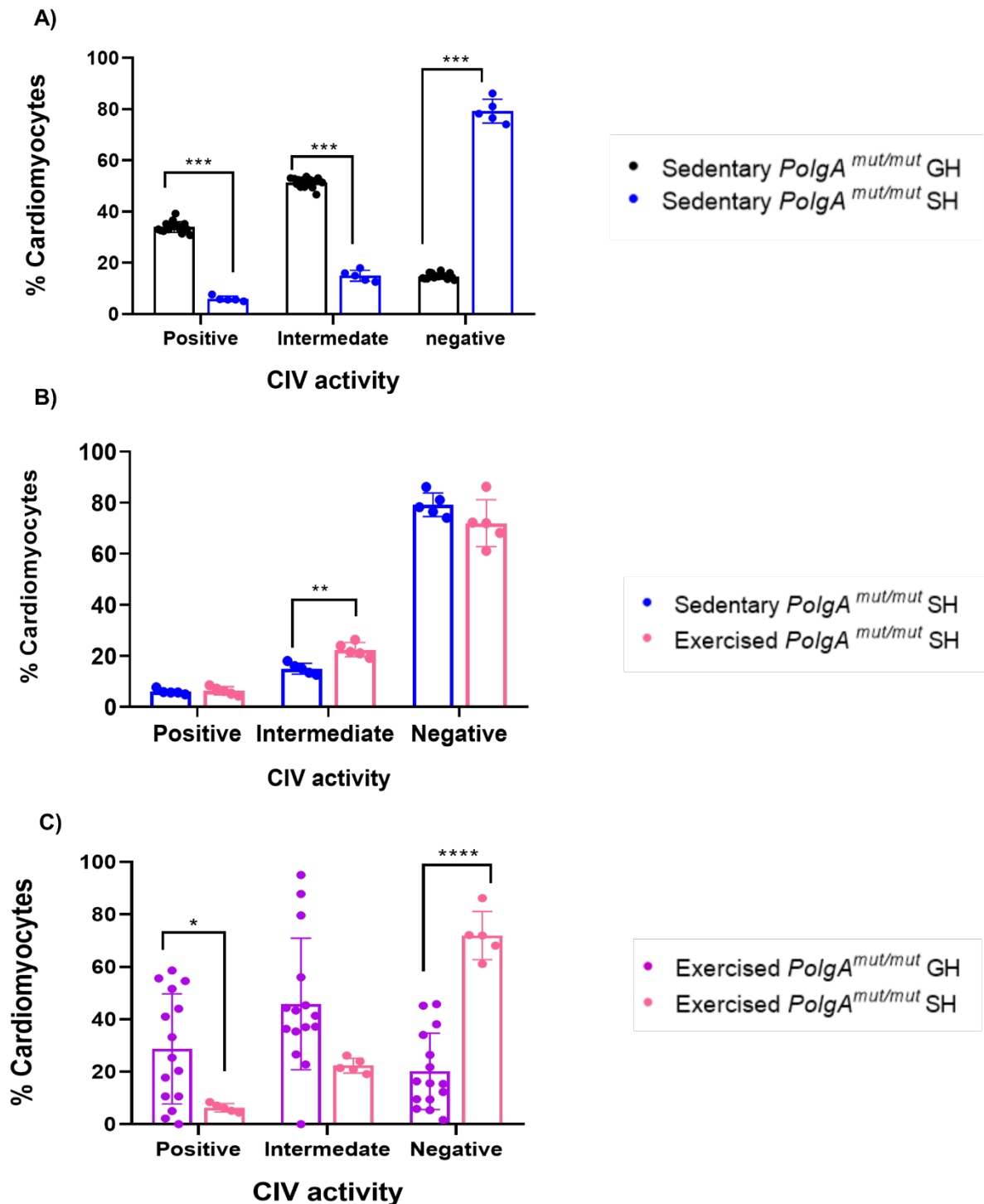
Figure 5.20. Complex IV activity by NBTx assay in *PolgA^mut/mut* GH mice. A) Sedentary GH mice had significantly higher percentage of cardiomyocytes with positive and intermediate COX activity (***$p<0.001$, unpaired t-test) however SH mice had significantly higher percentage of cardiomyocytes with negative COX activity. B) SH Exercised cohort had greater percentage of cardiomyocytes with intermediate COX activity in comparison to SH sedentary mice (**$p<0.01$, unpaired t-test). C) SH exercised mice had significantly higher percentage of cardiomyocytes with negative COX activity in comparison to exercised GH mice (*$p<0.05$) and exercised GH mice had significantly higher percentage of cardiomyocytes with COX positive activity in

comparison to exercised GH mice (****p<0.0001, unpaired t-test). Error bars represent mean± SD.

5.3.10 *MtDNA copy number in PolgA$^{mut/mut}$ mice hearts*

Mitochondrial DNA (mtDNA) copy number was quantified by qRT-PCR through amplification of genes encoding for mitochondrial encoded protein (ND1) and nuclear-encoded protein (β-actin). The ratio of ND1: B-actin ratio in the left ventricular muscle of sedentary GH (n=10), sedentary SH (n=5), exercised GH (n=10) and exercised SH (n=5) mice determined mtDNA copy number (detailed chapter 2 section 2.26).

There was no significant difference between the mtDNA copy numbers of any of the groups (unpaired t-test) confirming that different housing conditions do not have an impact on mitochondrial DNA proliferation/degradation in *PolgA$^{mut/mut}$* mice hearts (figure 5.21A-C).
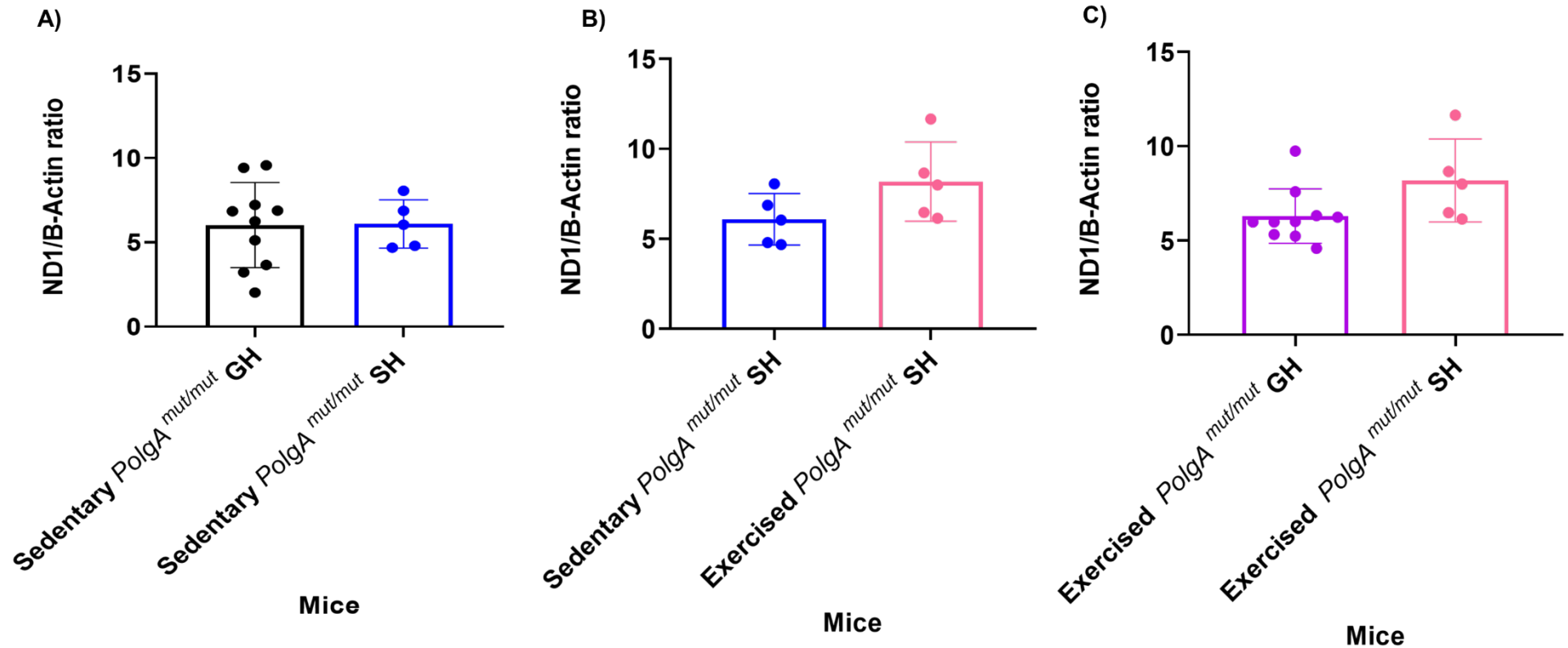
Figure 5.21. Mitochondrial DNA copy number in *PolgA^{mut/mut}* mice hearts. A) There is no significant difference between the cardiac mtDNA copy number of sedentary GH and sedentary SH cohorts (p=1, unpaired t-test). B) There is no significant difference between the mtDNA copy number of sedentary and exercised SH cohort (p=0.06). C) There is no significant difference between the mtDNA copy number of exercised GH and SH mice (p=0.06, unpaired t-test). Error bars represent mean± SD.

5.4 Discussion

I have shown in previous chapters that *PolgA^mut/mut* mice suffer from premature ageing phenotypes and that endurance exercise did not alleviate progeroid phenotypes and mitochondrial dysfunction in the setting of singly-housing. This is in stark contrast to the findings of Safdar *et al* (2011) who showed that endurance exercise was able to extend lifespan, improve mitochondrial function and completely reverse the premature ageing phenotype. To try and understand the different outcomes of the two studies, I looked in detail for any major differences in the way that the two studies had been conducted. The main difference between the studies that I discovered was the housing conditions. In my study, the mice were group-housed, whereas Safdar *et al* (2011) housed single mice in individual cages. It is well-known that housing conditions can have a significant effect on both the welfare of the animals and experimental outcomes. Kamakura *et al* (2016) showed that solitary housed C57BL/6J mice had significantly lower levels of corticosterone levels in comparison to group-housed mice. They reported that this stress inducer hormone level increases due to territory-related aggression in group-housed mice. A study by Kalliokoski *et al* (2014) reported that BALB/c mice singly-housed for three weeks showed marked hypothermia due to their altered serotonin activity. They emphasised the importance of social housing in mice and that mice with deprived social contact develop depressive-like behaviours. Leraci *et al* (2016) have also demonstrated that nine weeks old individually housed C57BL/6J male mice showed higher locomotive activity and that anxiety and depressive characteristics were induced by social isolation and downregulation of neuroplasticity-related genes.

Similar to the findings of my study and Laraci *et al* (2016), another work by Febigner *et al* (2014) also reported that C57BL/6J mice which were housed in individual cages have significantly higher locomotive activity than group-housed mice. They also showed that group-housed mice have shorter-bouts of rapid eye movement during sleep, meaning that their sleep is much more disturbed than singly-housed mice and are more alert possibly due to tension between mice within a cage. This may also have a direct effect on the level of activity of group-housed mice during the day when the open field test was performed.

The mouse model I have studied has the *PolgA ^mut/mut* genotype on a C57BL/6J background, therefore it is possible that the housing conditions are one of the factors

underling the differences between our study and that of Safdar *et al*. For this reason, I conducted a pilot study to examine the effects of single or group housing mice on the baseline *PolgA^{mut/mut}* phenotype and on their physiological, behavioural and biochemical response to exercise.

Data on previous research showed that the median lifespan of group-housed sedentary *PolgA^{mut/mut}* mice was 336 days by Trifunovic *et al* (2004) and 416 days by Kujoth *et* al (2005). Safdar *et al* (2011) found that singly-housed *PolgA^{mut/mut}* mice had a further reduction of lifespan to ~230 days. Considering they had a very small sample size and that out of 18 mice that they culled, only 4 were included in their lifespan curve with no clear reason for the selection process. They have combined the data obtained from male and female mice to draw conclusion in their study or at least they have not segregated/ specified their observations in male and female mice. Human studies reveal that females in general live longer than males due to lower cardiovascular risks from the action of endogenous estradiol levels and the differences in their chromosomal constitution and genome composition (Eskes and Haanen, 2007). However in mice there is large genetic contribution and broad distribution within strains that determine the total lifespan in males and females (The Jackson laboratory, 1964). One of the first studies by Asdell *et al* in 1967 showed that female mice lived longer, highlighting the effects of sex hormones upon longevity. Therefore, it's fair to conclude that studies on mice should not combine observations from male and female. Combination of genetic (sex-differences) and environmental (singly-housing) factors may be a reason why Safdar *et al* (2011) have detected such shortening of lifespan in *PolgA^{mut/mut}* mice. Steptoe *et al* (2013) have documented that social isolation in humans is associated with increased mortality rate. It's also reported that social relationships are crucial in maintenance of health especially during older age and is linked to mental and physical health (Holt-Lunstad, Smith and Layton, 2010). Socially isolated individuals are also at a higher risk of developing CV disease (Barth *et al,* 2010), cognitive deterioration (Bassuk *et al,* 1999) and infections (Cohen, 1997).

Safdar *et al* (2011) have shown that endurance exercise completely reversed the shortening of lifespan in *PolgA ^{mut/mut}* mice to ~500 days, whereas my data showed that exercised mice had a median lifespan of 272 days, very similar to singly-housed sedentary mice. The significant difference between the findings of the two studies on single-housing could firstly be due to great heterogeneity in mitochondrial function of

mice which directly have an impact on the energy state of most organs as mitochondria are involved in the longevity pathway. Secondly it could be the fact that male and female mice may withstand the social isolation of singly-housing differently.

My data also showed that the body weight of singly-housed *PolgA^mut/mut* mice decreased significantly with age and in comparison to group-housed mice at the end of the study. Socially-isolated wild-type mice showed significant reduction in food consumption and lower body weight in comparison to socially housed mice. Whereas in a mouse model of obesity (BRS-3 deficient mice) single-housing caused a greater body weight gain and food consumption (Yamada *et al*, 2000). Similarly wild-type mice exhibited higher social responses in isolation than the mouse model of obesity. Schiavone *et al* (2016) have identified that psychosocial stress such as cage isolation in rats is a key regulator in bone homeostasis in male Wistar rats and that social housing significantly reduces the body weight of these mice. Another study by Katsunori and Yoshitomo (2007) have reported that solitary-housing in mouse model of diabetes (KK mouse) is associated with early mortality and morbidity as well as accelerated adiposity. It's therefore crucial to bear in mind that housing conditions may affect different strain of mice in various ways. However a pre-disposed disease burden may exaggerate the environmental stress such as solitary housing.

I've also shown that the percentage of cardiac apoptosis was significantly higher in the singly-housed *PolgA^mut/mut* mice in comparison to group-housed mice. Dai *et al* (2010) and Kujoth *et al* (2005) have demonstrated cardiac apoptosis in *PolgA^mut/mut* mice hearts, but no evidence for the impact of housing condition in cardiac apoptosis.

Trifunovic *et al* (2004) have shown that 25 weeks old *PolgA^mut/mut* mouse carry marked respiratory chain deficiency in their hearts as a direct consequence of impaired respiratory chain complex activity. Similarly, Hiona *et al* (2010) have demonstrated that *PolgA^mut/mut* mice display significant reduction in OXPHOS complex expression including complexes I, III and IV. The assembly of complexes, activity and mRNA expression of all the complexes as well as the ATP content were downregulated in *PolgA^mut/mut* mice skeletal muscle. In chapter 4, I have reported that sedentary and exercised group-housed *PolgA^mut/mut* mice had similar levels of COX activity however Safdar *et al* (2011) have documented that the reduction in mitochondrial complex I and complex IV activity was rescued with exercise when mice are singly-housed. I have compared grouped- and singly-housed *PolgA ^mut/mut*

mice to observe whether that is the case and found out that COX activity, Complex I and COX expression levels were significantly higher in group-housed $PolgA^{mut/mut}$ mice. It seemed as singly-housing skewed cardiomyocytes COX activity and expression negatively, meaning that single-housing exacerbates mitochondrial dysfunction.

The second aim of this study was to understand the effects of 6 months of endurance treadmill running exercise on singly-housed $PolgA^{mut/mut}$ mice. My data showed that exercise had no major effect on the lifespan, body condition, behavioural and locomotive activity of singly-housed mice. The exercised cohort however showed significantly higher temperatures at 29 weeks of age in comparison to sedentary mice and at 29 weeks and 43 weeks of age in comparison to exercised group-housed mice which may indicate an attempt made by exercised mice to thermoregulate when they are housed in solitude. The body temperature of mice indicate their health and metabolic state (Gordon, 2017). It's also known that body temperature has a positive correlation with body weight and a negative correlation with age in C57BL/6J mice (Talan, 1984). Swoap and Gutila (2009) have investigated the thermoregulatory capacity of mice in different biological and environmental conditions. They have shown that core body temperature of mice fluctuates during ad libitum feeding and changes into hypothermic state when food is removed from the cage. This hypothermic response to calorie restriction is blocked when mice are placed in a thermoneutral environment (Koizumi *et al*, 1992).

The third aim of this study was to find out whether single-housing would influence exercised $PolgA^{mut/mut}$ mice. My data showed that SH exercised mice developed significant worsening of body condition at 29 weeks of age in comparison to GH exercised mice, however due to low number of SH animals at 43 weeks (n=3) the comparison was not the most reliable at 43 weeks. Further analysis of cardiac muscle revealed that the percentage of apoptotic cardiomyocytes were significantly higher in the sedentary and exercised SH cohort.

Since both exercised and non-exercised singly-housed $PolgA^{mut/mut}$ mice had significantly higher rate of cardiac apoptosis in comparison to group-housed mice and with no significance between the two cohorts, it's sensible to conclude that housing conditions have significant impact on the rate of programmed cell death which may indicate higher cellular turnover and possible initiation of cardiac disease

as suggested by Vanempel *et al* (2005). Sabbah (2000) reported elevated levels of active CC-3 expression in response to pressure overload in heart failure rodent models and myocardial infarction (Agosto *et al*, 2011). CC-3 overexpression is also observed in patients with right ventricular dysplasia which result in cell loss and sudden death (Mallat *at al*, 1996). Mitochondrial function as a measure of COX activity was not significantly different between the two cohorts, however further classification of cardiomyocytes by NBTx revealed that cardiomyocytes of sedentary SH mice appeared to be in COX negative region in comparison to sedentary GH mice.

Although there is no clear answer to whether *PolgA^{mut/mut}* mice are better off in groups or solitary cages and whether exercise has an impact on the progression or regression of *PolgA^{mut/mut}* phenotypes, this study has confirmed that singly-housed mice experienced an overall accelerated decline in their body condition and cardiac mitochondrial function.

5.5. Limitations and future work

In order to make the study statistically more reliable, the next step would be to increase the sample size for the singly-housed mice now that significant changes are seen with altering housing condition. The future work would be to assess each mouse independently for their exercise tolerance level and tailor the exercise programme to their individual needs based on their maximal aerobic capacity. Due to high variation in biological data, there may be significant and inevitable differences in the control group as well. Although previous research has shown that *PolgA^{mut/mut}* mice develop premature ageing phenotypes from around the age of 16 weeks onwards, it's crucial to measure cardiac mitochondrial function in younger cohort of mice before they show signs of accelerated ageing to set the baseline values for more reliable comparisons within the same colony of mice that was tested throughout the process.

Chapter 6

Chapter 6. The effects of ageing and endurance exercise on cardiovascular system and mitochondrial function of C57BL/6J mice

6.1 Introduction

6.1.1 *Age-related cardiovascular changes*

Physiological cardiovascular ageing leads to structural and functional (macroscopic and microscopic) changes in the heart and the vasculature. Age-related cardiovascular structural changes include increased arterial stiffness, left ventricular wall thickness and fibrosis (Scholz *et al,* 1988; Strait and Lakatta, 2012). These changes may lead to diastolic dysfunction and increased afterload (Lakatta and Levy, 2003). Increased left ventricular stiffness is a result of increased cardiomyocyte size and shape (elliptical to spheroid) accompanied by interventricular septum wall thickening (Hees *et al,* 2002). These age-related structural changes have crucial implications for cardiac contractile efficiency during increased cardiac workload and in development of cardiovascular disease (Strait and Lakatta, 2012).

Functional age-related changes in the cardiovascular system include a decline in end diastolic and end systolic volumes, reduced cardiac contractility, prolonged contraction and relaxation which is accompanied by reduced sympathetic signalling (Lakatta *et al,* 2009). At rest, the slower heart rate and decreased inotropic competency in the elderly is compensated by an increase in stroke volume to maintain cardiac output (Weisfeldt, 1998). The heart's repair mechanisms also become diminished with age leading to pronounced adverse remodelling and increased dysfunction (Paneni *et al,* 2017). Increased collagenous tissues in the heart and fat accumulation around the sinoatrial node (SAN) lead to a reduction in the number of pacemaker cells with age (Burgess, Mc Crea and Hedrick, 2001). Increased calcification on the fibrous cardiac skeleton also reduces the atrioventricular node (AVN) signalling and increases the risk of conduction blocking (Fleg *et al*, 2015).

6.1.2 *Age-related cardiac mitochondrial changes*

Mitochondria are proposed to play an important role in ageing due to an observed age-related decline in oxidative phosphorylation (Gomez and Hagen, 2012). Schriner *et al* (2005) investigated the effects of reactive oxygen species (ROS) on longevity and cardiac pathology. They showed that mice overexpressing mitochondrial targeted catalase (MCAT) had extended lifespan and delayed ROS damage onset in the cardiac muscle compared with controls. Mitochondrial DNA (mtDNA) deletion levels associated with ROS damage in the cardiac muscle were also found to be significantly higher in the ageing cohort and significantly lower in the aged-matched MCAT treated group. Similarly, Dai and Rabinovitch (2009) investigated the role of mitochondrial oxidative stress in cardiac ageing and determined that protein carbonylation which is an indicator of mitochondrial oxidative damage, increased with advancing age and decreased with MCAT overexpression in the mouse model. They also observed a significant increase in cardiac muscle mtDNA copy number with age due to upregulation of PGC-1α and its downstream transcription factors to increase biogenesis as a result of mitochondrial oxidative damage with age (Dai and Rabinovitch, 2009).

Further supporting evidence for the role of mitochondria in cardiac ageing stems from the study carried out on the *PolgA^{mut/mut}* mice model of accelerated ageing (detailed in chapters 3-5) (Trifunovic *et al,* 2004; Kujoth *et al,* 2005). These mice have a significantly increased mtDNA point mutation and deletion with age compared with age-matched controls, as well as increased cardiac apoptosis, increased left ventricular mass index (LVMI) and decreased systolic and diastolic function, most of which were attenuated by MCAT overexpression (Schriner et al, 2005).

Another study implicating the role of mitochondria in cardiac ageing comes from an investigation of mice with mutation of cardiac p66[shc] gene (Migliaccio *et al*, 1999). The p66 [shc] is an enzyme located in the mitochondrial intermembrane space that utilises electrons from the electron transport chain (ETC) to produce H_2O_2. Mice lacking a functional copy of p66[shc] protein have extended lifespan and attenuated ROS-mediated apoptosis. The molecular mechanism underlying the dysfunctional p66 [shc] protein is it's phosphorylation by PKC-beta and accumulation inside mitochondria to activate excessive Ca^{2+} signalling and apoptosis induction (Pinton *et al,* 2007). Francia *et al* (2009) have demonstrated that the dysfunctional p66 [shc]

protein inhibits left ventricular (LV) hypertrophy through renin-angiotensin induction and reduces ROS-mediated damage in cardiac progenitor cells in a diabetic mouse model.

6.1.3 *Age-related cardiovascular changes with exercise*

Exercise exerts an inducible form of physiological stress on the body which requires an organised response from the nervous system and cardiovascular system to increase oxygenated blood flow to the working muscle by up to 80% of the total blood flow (Roh *et al*, 2016). Disruption in any of these integrated systems leads to diminished exercise capacity and a significant decline in peak cardiac output (Milano *et al*, 2013). The functional capacity of the heart to augment HR during exercise progressively declines with advancing age (Kitzman *et al*, 1991). This is mainly due to inadequate oxygen delivery to impaired cardiac reserve and poor oxygen extraction efficiency of working muscle in the elderly. The relative increase in stroke volume (SV) in response to exercise also diminishes with age mainly due to a reduction in maximal heart rate (HR_{max}) (Gulati *et al,* 2010).

The maximal oxygen consumption (VO_2 max) or the aerobic capacity is affected by age, gender, genetics, weight, temperature and altitude of living environment (Betik and Hepple, 2008), with advancing age being the greatest driving force (Pollock *et al*, 2015). VO_2 max is a gold standard measure of cardiorespiratory fitness and is documented to reduce by 10% per decade after the age of 25 years (Robinson, 1938; Astrand, 1960) which further increases to 15% decline per decade between 50 and 70 year old individuals (Fitzgerald *et al,* 1997). The rate of VO_2 max decline accelerates further after the age of 70 in heart failure patients (Fleg and Strait, 2011). It's documented that regular endurance exercise training enhances the body's aerobic capacity (Bundy and Levaer, 2010). The intensity of exercise is also an important factor contributing to increased VO_2 max (Talbot, Metter and Fleg, 2000). A stress test is a conventional method for assessment of cardiorespiratory fitness. Data are used to improve risk stratification and to plan an exercise training (Lemond and Hom 2015). It is documented that greatest improvements in aerobic capacity are gained when intensity of exercise reaches 90% to 100% of VO_2 max (Wender and Bell, 1986; Corkery and Iversen, 2016).

Since rodents share comparable exercise physiology with humans, most short-term exercise studies are carried out in mice and rats. Healthy 24 month old C57BL/6 mice show a 28% decline in VO_2 max in comparison to their 12 month old counterparts (Schefer and Talan, 1996). Exercise-induced reduction in end-diastolic volume (preload) and exercise-induced increase in ejection fraction is less pronounced in aged rodents (Lakatta, 1990).

Epidemiological studies revealed that endurance exercise training reduces the risk of chronic diseases, extends lifespan and reduces the chances of developing physical disability in later life (Buchner D.M, 2009). Boveris and Navarro (2008) documented that moderate endurance exercise in rodents confers cellular and phenotypic protection from age-associated diseases and provides systemic metabolic benefits. A human pilot study on 538 runners revealed that over a course of 21 years the all-cause mortality and disability scores were significantly lower in the more active group (Booth and Laye, 2010).

Long term adaptations of the cardiovascular system to exercise in the elderly include physical conditioning and improved peak oxygen consumption in part through increased maximum cardiac output by augmented stroke volume (SV) and in part by increased oxygen utilisation capacity of the body (Nystoriak and Bhatnagar, 2018). The augmented SV is due to a reduction in end systolic volume and increased ejection fraction with no changes in end diastolic volume. Cardiac performance is also diminished with age, and pathological cardiac hypertrophy was suggested to be linked to a reduction in mitochondrial Ca^{2+} ATPase2a (SERCA2a) expression and excessive ROS generation. Exercise in the elderly reverses the ROS damage to mitochondria as seen with physiological aging (Roh *et al*, 2016).

6.1.4 *Impact of exercise on cardiac mitochondrial function*

Since excessive mitochondrial ROS generation is documented to reduce cardiac performance with age (Kornfeld *et al,* 2015), studies were carried out to evaluate the role of exercise in augmenting antioxidant levels such as catalase, superoxide dismutase and glutathione peroxidase as ROS scavenging enzymes to provide cardioprotective benefits of exercise (Somani, Frank and Rybak, 1995 and Linke *et al*, 2005). Interestingly an increase in PGC1-α expression, which is a regulator of

mitochondrial biogenesis, was found in the cardiac and skeletal muscle in response to endurance exercise (Little *et al*, 2010). On the other hand, aging is documented to be linked to reduced muscle specific PGC-1-α expression coincident with reduced mitochondrial function (Ling *et al*, 2004 and Dillon *et al,* 2012). A study conducted by Moraes team in 2012 showed that increased expression of PGC-1-α in the muscle of *PolgA* $^{mut/mut}$ mice increases mitochondrial biogenesis and improves mitochondrial function including mtDNA content and complex IV activity, as well as cardiac phenotypes such as improved ejection fraction, without reducing mtDNA mutation accumulation. It's believed that the cardio-protective effects of PGC-1-α are likely to be due to its ROS-lowering effects since St-Pierre *et al* (2006) have suggested that PGC-1-α induces ROS-detoxifying enzyme activation such as GP-x1 and SOD2 in mouse models of neurodegeneration.

Yoo *et al* (2019) investigated the effects of acute exercise on mitochondrial function of Fischer rats and concluded that mitochondrial ETC and Ca^{2+} retention capacity of all tissues increased significantly. No changes in H_2O_2 production of different fibre types of skeletal muscle or rate of mitophagy were seen. It's also been confirmed that decreased Ca^{2+} retention capacity leads to opening of the mitochondrial permeability transition pore (mPTP) and further release of pro-apoptotic molecules which initiate cell death (Anderson *et al*, 1981).

Another study by Menshikova and her team (2006) was performed and showed that 12 weeks of exercise increased cardiolipins and mitochondrial DNA copy number in aged individuals. They also demonstrated that mitochondrial oxidative capacity was increased as a measure of ETC complexes II-IV. Conversely, a study carried out by Gun-Soo and Seon-Rye (2013) showed adverse effects of 8 weeks of endurance exercise training that decreased mitochondrial coupling of phosphorylation and respiration due to mitochondrial damage is due to a shift in lipid metabolism.

Due to the conflicting outcomes of previous studies on the effects of endurance exercise on mitochondrial and cardiovascular health in older age, I decided to investigate the role of late-life endurance exercise training on cardiac and mitochondrial function in a mouse model of normal physiological ageing.

6.1.5 *Mouse model*

Since mice age a lot faster than humans, 14-15 month old C57BL/6J (wild-type) mice are considered as middle-aged corresponding to 38-47 years old humans. By the end of the study mice were 22 month old which corresponded to older individuals of 61-65 years old (Jackson laboratory, 2007). The C57BL/6J mouse model is one of the most common studied in the ageing field due to its well-characterised health-span and lifespan as well as having defined normal phenotypes with age (Brewer and Treuting, 2011). C57BL/6J mice have an extensively researched database of physiological changes with age that correlate closely with that in humans and a well characterised system of assessing end points (Burkholder *et al,* 2012).

6.2 Aims of study

The two aims of the present study were to understand the effects of age and endurance exercise on clinical phenotype, locomotor activity, grip strength and haemodynamic measures including maximal oxygen consumption, heart rate, blood pressure and cardiac function in wild type (C57BL/6J) male mice. For this reason, I aim to characterise the following:

- Investigate the effects of advancing age on the stated parameters of n=10 C57BL/6J mice in order to set the baseline characteristics of aged mice prior to the exercise intervention.
- Investigate the impact of six month of endurance treadmill running exercise on the stated parameters and to investigate post-mortem cardiac pathology and cardiac mitochondrial function of aged n=10 C57BL6/J mice.

6.3 Results

6.3.1 *Clinical scoring and body weight assessment with age*

14 month old sedentary C57BL/6J mice (Charles River Laboratory) were group-housed in cages of between two to four and randomly assigned to either the sedentary (n=10) or exercised (n=10) groups. Clinical scoring as a determinant of lifespan and health span was recorded from the age of 14 months to 22 months according to the method detailed in chapter 2 section 2.10. The higher clinical scores indicate the worsening of body condition in mice (figure 6.1A). Body weight is also recorded as an independent measure of health state in mice at 14, 18 and 22 months of age as shown in figure 6.1B. The body condition of mice significantly worsened with advancing age from 20 months onwards and the body weight of mice increased significantly from 14 months onwards (One way ANOVA repeated measures). Monitoring videos are attached to the appendix for observation of phenotypic and behavioural changes in mice.
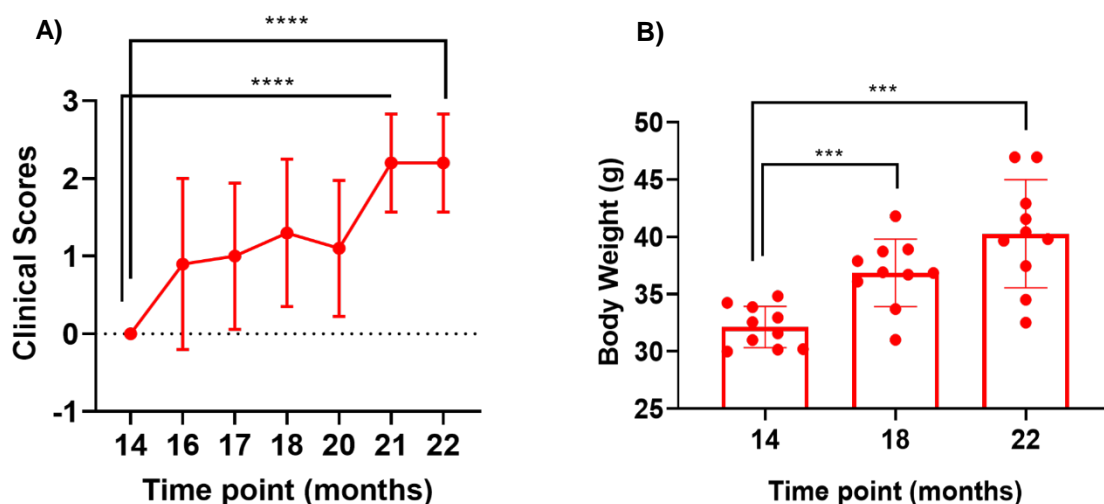
Figure 6.1. Body condition scoring and body weight with age. A) Clinical scoring from 14 months to 22 months (****p=0.0001) (One-way ANOVA repeated measures). B) Body weight at 14m, 18m and 22 months (***p<0.001) (One-way repeated measures ANOVA). Error bars represent mean ±SD.

6.3.2 *Clinical scoring and body weight assessment with exercise*

The body condition of sedentary and exercised C57BL6/J mice was compared at different time points. Two mice from each group died prior to the start of the

intervention from fight wounds. The other 10 remaining mice lived up to the end of the study (22 months).

Clinical scoring is a strong indicator of end point and was carried out in sedentary (n=10) and exercised (n=10) mice from the age of 14 months (pre-intervention) to 22 months (post-intervention) (figure 6.2A). There was no significant difference in the body condition scoring of sedentary and exercised mice up to 20 months of age. At 21 months and 22 months of age sedentary mice showed significant deterioration in body condition in comparison to exercised mice ($p<0.05$, Two way ANOVA repeated measures).

Body weight of sedentary and exercised mice was recorded as part of the clinical scoring data at 14, 18 and 22 months of age (figure 6.2B). Sedentary mice showed significantly higher body weight at 22 months of age ($p<0.05$) and also with advancing age from 14 months onwards, whereas exercised mice maintained a consistent body weight across the course of the study (Two way ANOVA repeated measures).
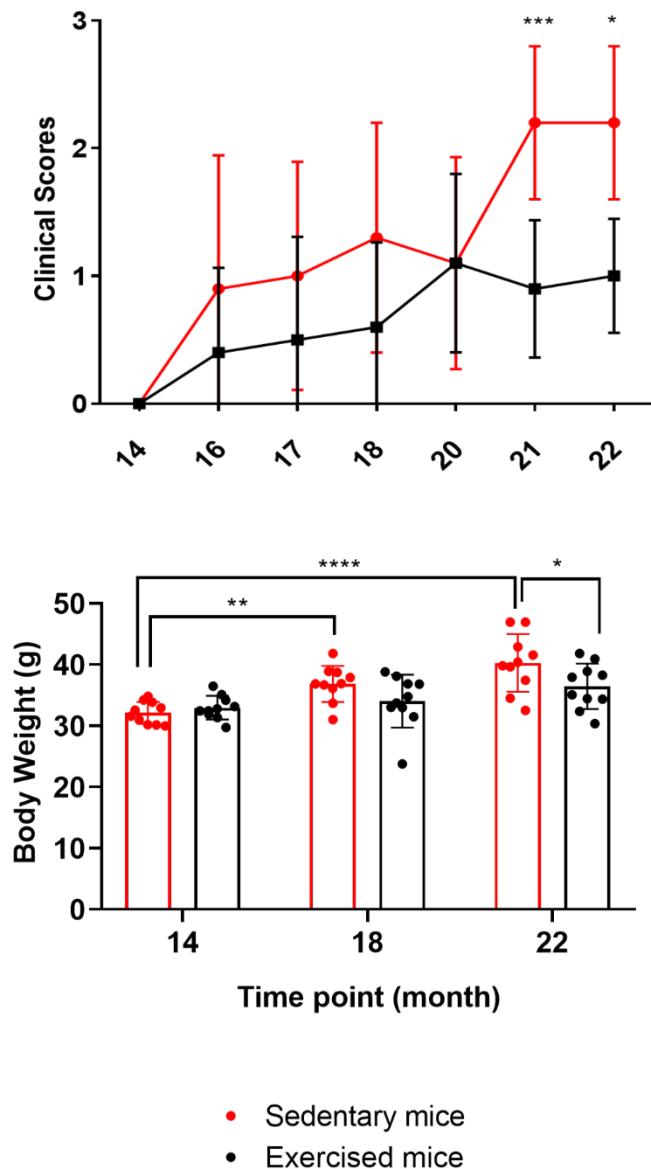
Figure 6.2. Body condition scoring and body weight in sedentary and exercised mice. A) Clinical scoring of sedentary mice was significantly higher in comparison to exercised mice at 21 months (***p<0.0003) and 22 months of age (*p<0.05). B) Body weights at 22 months (*p<0.05) (Two-way ANOVA repeated measures). Error bars represent mean ±SD.

6.3.3 *Open field testing (OFT) with age*

Open field testing (OFT) was carried out over a 5 minute period according to the technique explained in chapter 2 section 2.16.1, in order to investigate behavioural and locomotive activity of C57BL6/J mice with age from 14 months to 22 months as shown in figures 6.3A-E (One way ANOVA repeated measures).

Total distance travelled, average velocity and rearing frequencies were not significantly different with advancing age in mice (figures 6.3A, 6.3B and 6.3C). Total number of touches were significantly reduced from 14 months to 18 months ($p<0.05$) and from 14 months to 22 months of age ($p<0.001$) (figure 6.3D) which indicates a general decline in locomotive activity with advancing age. Step length was significantly decreased from 14 months to 18 months ($p<0.001$) and from 14 months to 22 months of age ($p<0001$) which indicate deterioration of coordination and balance with increasing age (figure 6.3E).
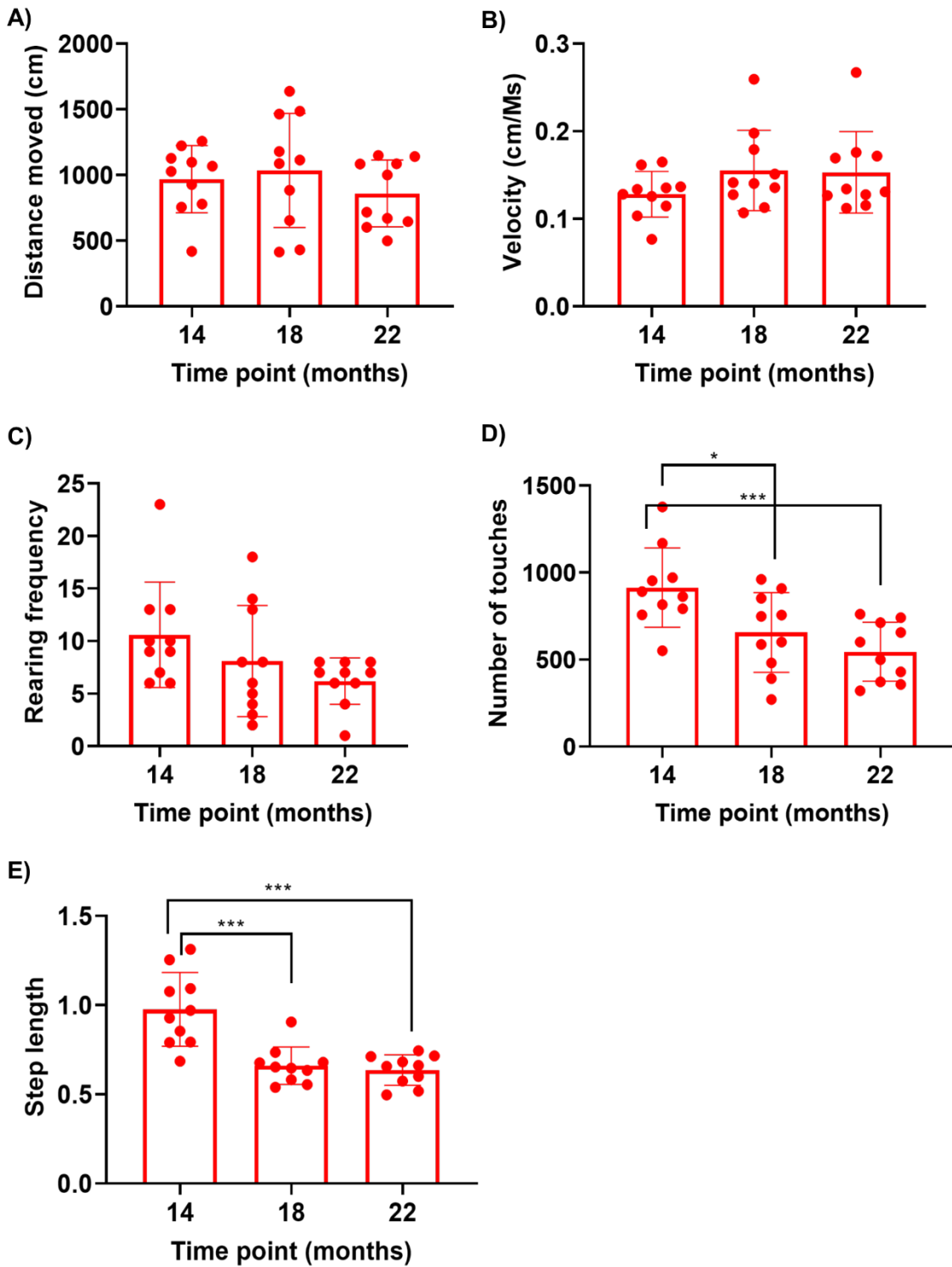
Figure 6.3. Open field testing in aged sedentary mice. A) Distance moved. B) Average velocity. C) Rearing frequency. D) Total number of touches reduced with age (***p<0.001). E) Step length reduced with age (***p<0.001) (One-way ANOVA repeated measures). Error bars represent mean ±SD.

6.3.4 *Open field testing (OFT) with exercise*

Similarly the locomotive activity and behavioural changes in C57BL6/J exercised (n=10) mice was assessed by OFT and compared to the sedentary cohort (n=10). Figures 6.4 (A-E) demonstrate quantitative measures obtained from both cohorts of mice pre-intervention (14 months), mid-intervention (18 months) and post-intervention (22 months). A two-way ANOVA repeated measures was carried out between groups.

Total distance moved (figure 6.4A) represent the overall locomotive state of mice which was not significantly different between groups pre- and post-intervention. Other parameters including average velocity and rearing frequency did not change significantly between the two cohorts at different time points. Longer step length is either an indication of having to compensate for the alteration in gait and balance or the unfamiliarity of the mouse with the open field device which decreased significantly with advancing age in both groups, however there was no difference between groups pre- and post-intervention. Since both mice have been acclimatised to the OFT device to the same extent, it seems as if the decline in step length in both groups was an indication of reduced balance and coordination of mice. Total number of touches were also reduced significantly with increasing age in both groups but not significantly between groups at any time point (figure 6.4E). Reduced step length and reduced number of touches may simply be a sign of increasing frailty and poor coordination in mice. Step length is a product of total distance moved over total number of touches.
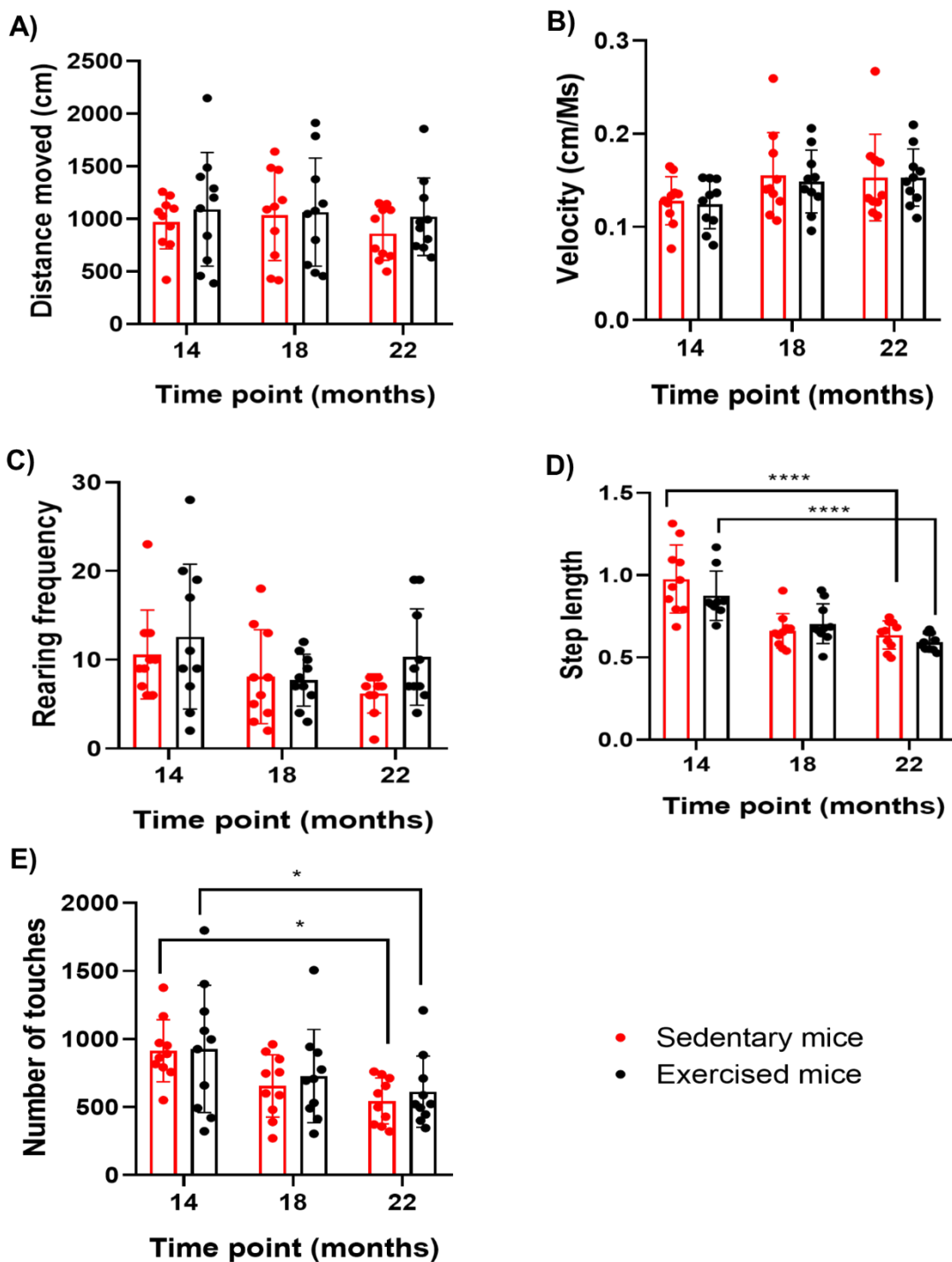
Figure 6.4. Open field testing in sedentary and exercised mice at 14, 18 and 22 months of age. A) Total distance moved at any time point (p>0.05). B) Average velocity at any time point (p>0.05). C) Rearing frequency at any time point (p>0.05). D) Step length was reduced in both groups with advancing age in both cohorts (****p<0.0001). E) Total number of touches was decreased in both groups with advancing age (*p<0.05). (Two-way ANOVA repeated measures). Error bars represent mean ±SD.

6.3.5 *Rotarod performance test with age*

The rotarod performance test was carried out in C57BL6/J mice with advancing age to assess grip strength, balance and motor coordination according to the technique explained in chapter 2 section 2.16.2. Figure 6.5A shows the time mice take to fall off the rod during three trials at three time points (14 months, 18 months and 22 months of age) known as the latency to fall. The longer the mice stay on the rotarod, the more grip strength and coordination they have to hang on the rod at higher speeds.

Figure 6.5B represent the average of all three trials at 14 month, 18 month and 22 month of age. Trials number 1 and 2 did not change significantly with advancing age, however, the time to fall off the rotating rod on trial number 3 was significantly reduced in mice by the end of 18m and 22m ($p<0.001$). Since trial 1 acts more as an acclimatisation and learning stage, most mice behave similar with changes occur in trials 2 and 3 (figure 6.5B, one way ANOVA repeated measures).
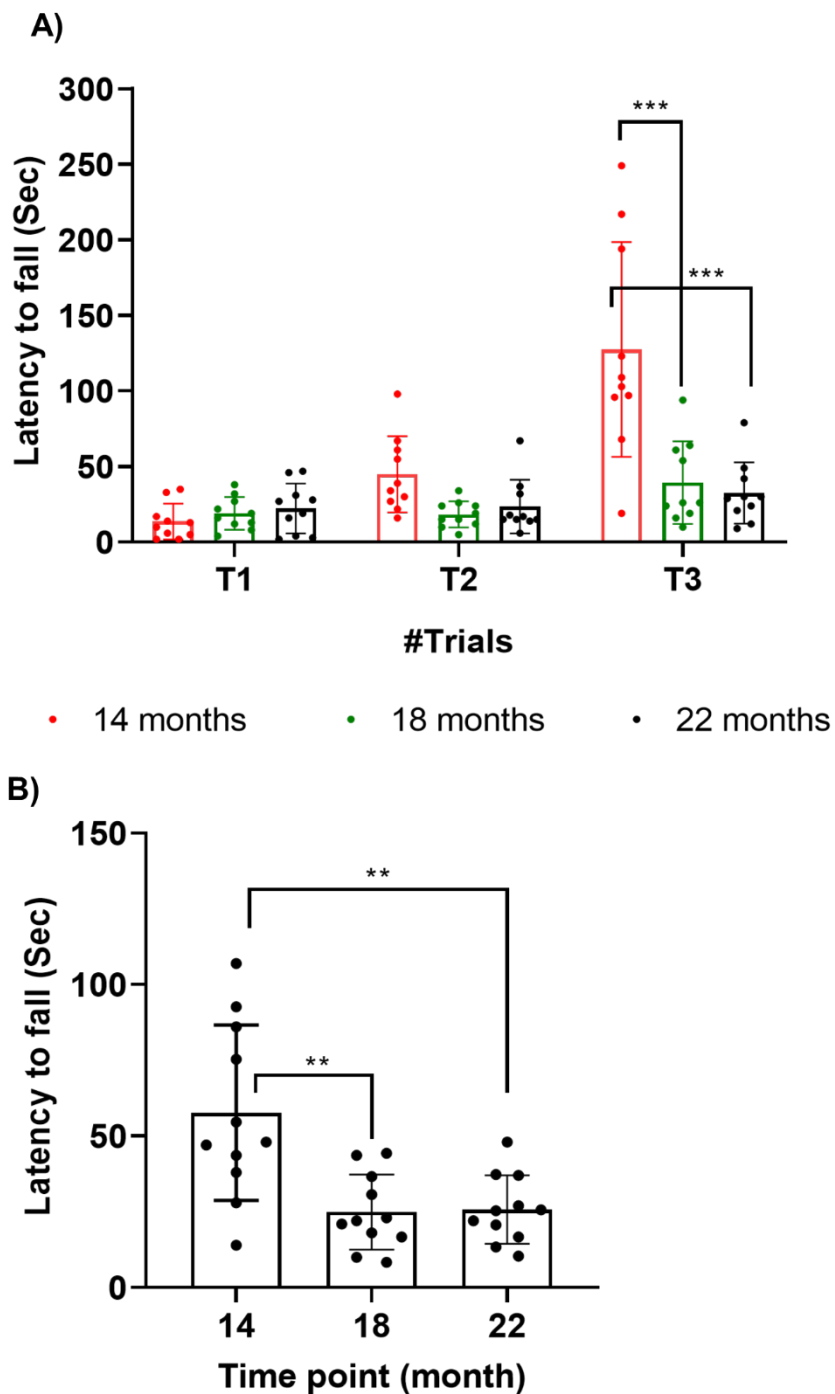
Figure 6.5. Rotarod performance in aged mice. The time to fall off the rotating rod at 14, 18, and 22 months of age. A) At T#1 and T#2 there was no significant difference between the latency to fall in sedentary and exercised mice at any time point (p>0.05). At T#3, 14 months vs 18 months (***p<0.001) and 14 months vs 22 months (***p<0.001). (One-way ANOVA repeated measures). B) Latency to fall at three time points. Trials 1-3 are averaged within each time point. Mice take longer to fall off the rotating rod at younger age (**p<0.01).Error bars represent mean ±SD.

6.3.6 *Rotarod performance test with exercise*

Similar to above, grip strength, coordination and balance was measured as the latency to fall off the accelerating rod using rotarod device in C57BL6/J sedentary (n=10) and exercised (n=10) groups at 14 months (pre-intervention), 18 months and 22 months of age according to the technique explained in chapter 2 section 2.16.2 (figure 6.6A). Two way ANOVA repeated measures was used to measure significant changes between groups pre-, mid- and post-intervention over three trials.

Sedentary mice at 22 months of age do not seem to be able to remain stable on the rod and learn through trial 1 and possibly trial 2, hence very short time to fall off the rotating rod. On trial number three, 14 months old sedentary and exercised mice did not seem to have significantly different latency to fall however at 22 months of age, exercised mice took 324 seconds longer to fall off the rotating rod (p<0.001) in comparison to the sedentary cohort who took 26 seconds to fall. This test clearly demonstrates that sedentary mice have significantly weaker muscle strength and poorer coordination and balance and/or slower learning ability by 22 months of age as they fall off the rotating rod quicker than exercised mice.

Figure 6.6B represent the average of three trials at each time point in order to observe the combined effects of all trials. At 14 months of age, the combined effects of three trials on exercised mice have a profound effect which makes exercised mice stay on the rotating rod significantly longer than sedentary mice (p<0.05, two-way ANOVA repeated measures). Although trials 1 and 2 are not significantly higher in exercised mice at 14 months of age, but the average of all three trials are significantly higher in exercised mice which skews the data in exercised mice pre-intervention.
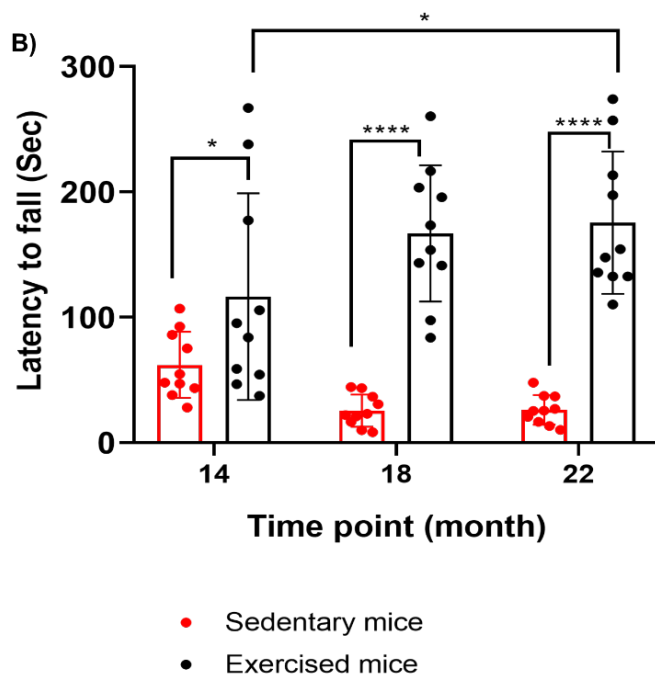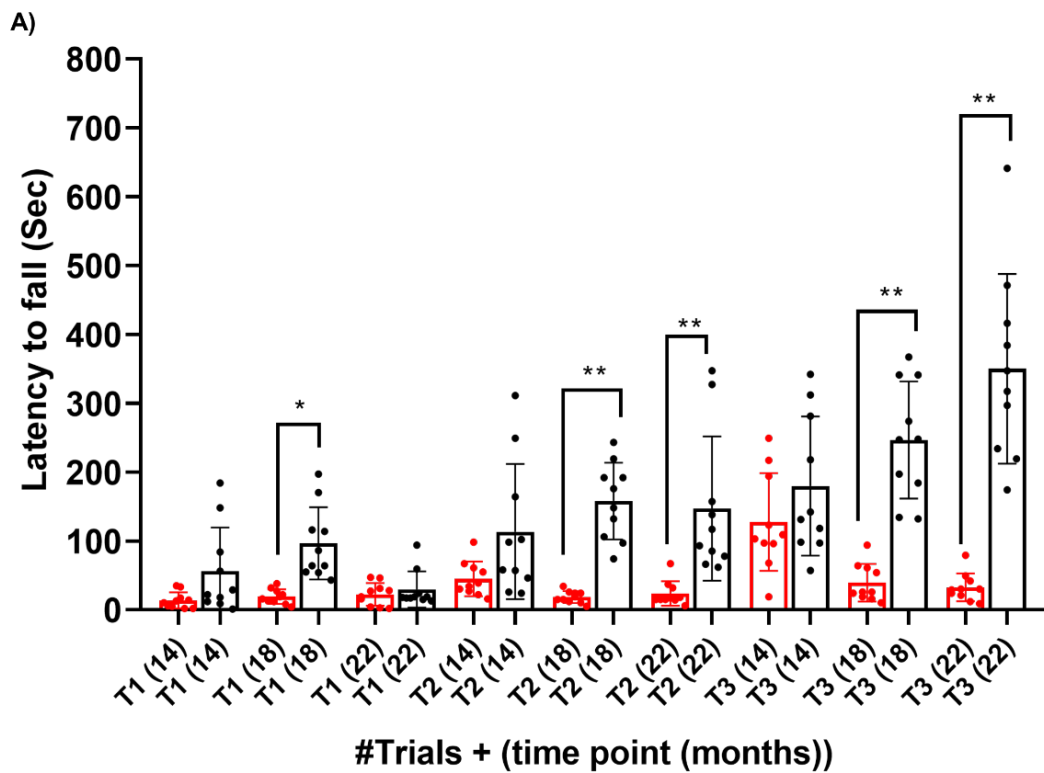
Figure 6.6. Latency to fall between sedentary and exercised mice at 14, 18 and 22 month of age. A) #T1, 14 months (p>0.05), 18 months (*p<0.05), 22 months (p>0.5). #T2, 14 months (p>0.05), 18 months (***p=0.0011), 22 months (**p=0.01). #T3, 14m (p=0.8), 18m (***p=0.0011), 22m (**p=0.0023) (Two-way ANOVA repeated measures). B) The average of three trials at 14, 18 and 22 months of age. Exercised mice took longer to fall off the rotating tod at 14 months (*p<0.05), 18 months (p<0.0001), 22 months (***p<0.0001). Error bars represent mean ±SD.

226

6.3.7 *Haemodynamics and cardiovascular changes*

6.3.8 *Cardiac function test through cardiac Magnetic Resonance Imaging (cMRI) with age*

Cardiac Magnetic Resonance Imaging (cMRI) (7-Tesla horizontal bore from Varian Inc, Palo Alto, CA, USA) was carried out in C57BL6/J sedentary mice (n=10) at 14 months and 22 months of age based on the technique described in chapter 2 section 2.10. ECG-gated cine-MRI scans were analysed in Segment v2.0 (http://segment.heiberg.se) to measure Left ventricular mass (LVM), and the LV functional parameters including the end diastolic volume (LVEDV), end systolic volume (LVESV) as well as stroke volume (SV), ejection fraction (EF) and cardiac output index (CO).

An example to illustrate analysis in Segment is included in chapter 2 section 2.12.1, figure 2.2. All parameters obtained are presented in figure 6.7. Due to variation in body weight between mice, LVM, volume measurements and CO were normalised to body weight (figure 6.8). CO was significantly increased with advancing age (p<0.05, paired t-test). LVESV was significantly decreased with advancing age (p<0.05, paired t-test). LVMI, LVEDVI and LVESVI were all unchanged with advancing age (paired t-test). Increased CO with age could partly be due to increased body weight with age.
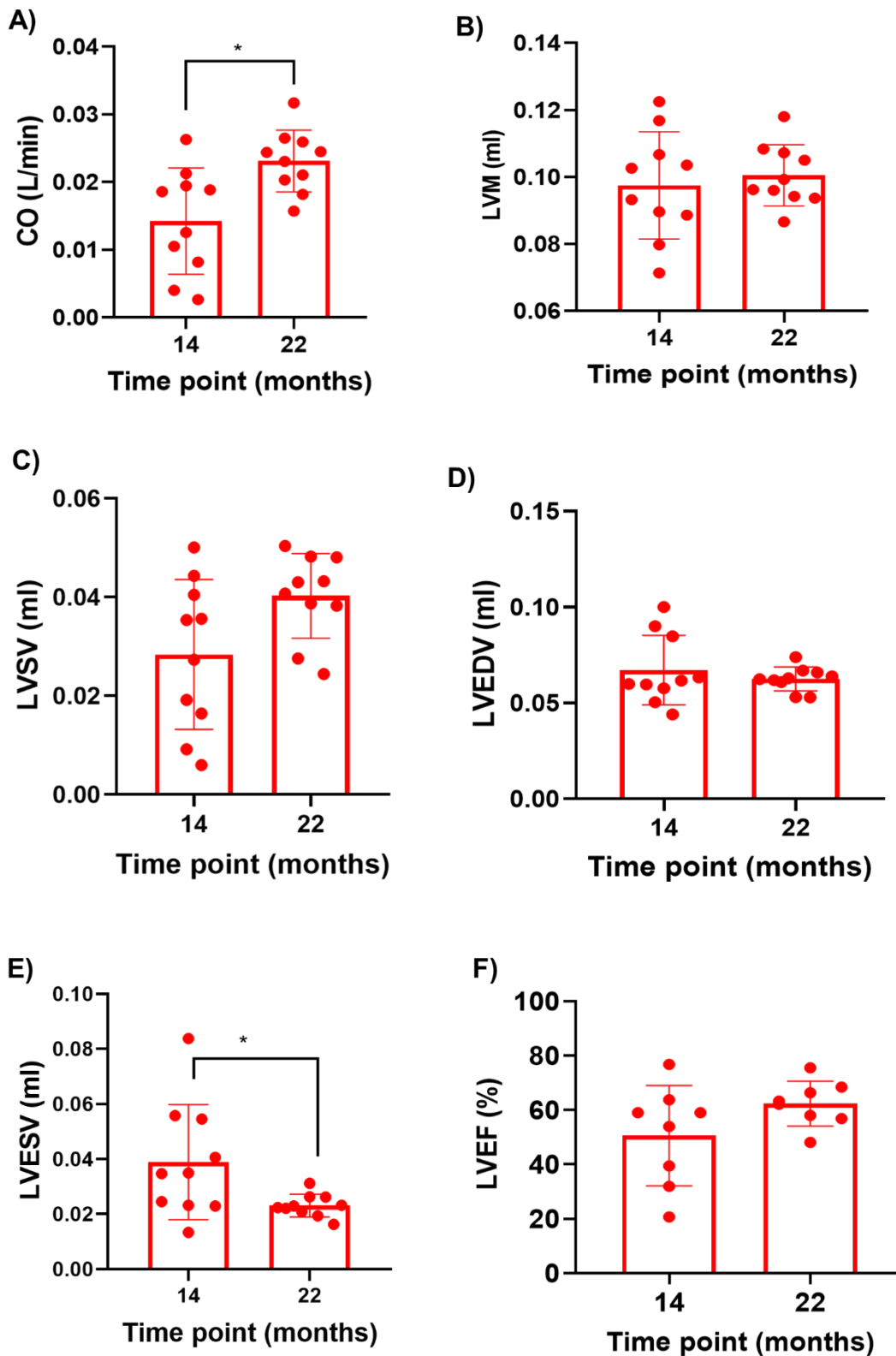
Figure 6.7. Haemodynamic measurements from cardiac MRI. Original MRI parameters (paired t-test). A) CO increased significantly with age (*p<0.05). B, C, D, E) no significant differences were seen in LVM, LVSV, LVEDV and LVEF. F) LVESV decreased significantly with increasing age (*p<0.05). Error bars represent mean ±SD.
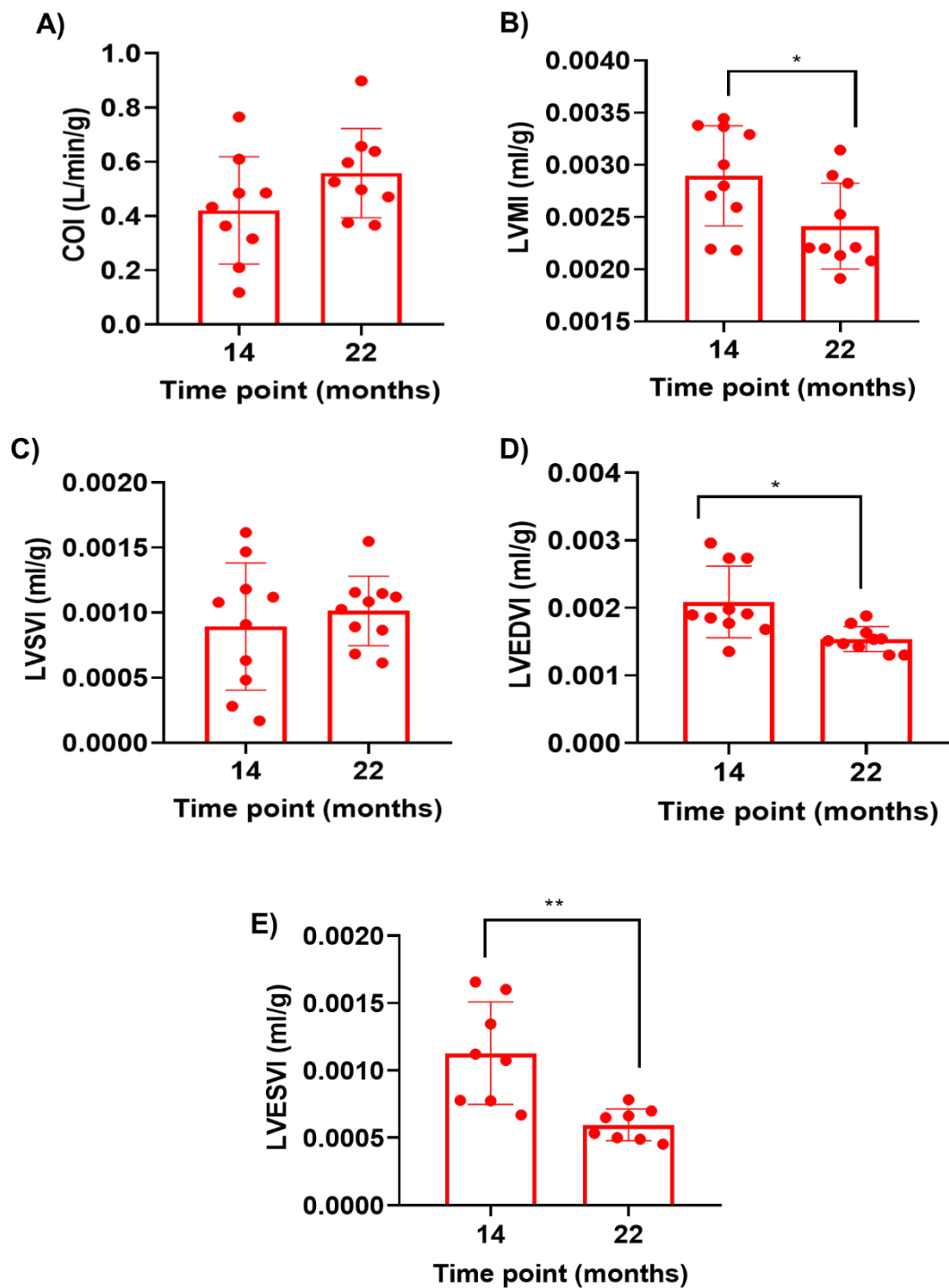
Figure 6.8. MRI parameters indexed to body weight (paired t-test). A) Cardiac output index (COI) (p=0.23), B) Left ventricular mass index (LVMI) was significantly higher in younger mice (*p=0.03). C) Left ventricular stroke volume index (LVSVI) (p=0.54). D) Left ventricular end systolic volume index (LVESVI) (*p<0.05). E) Left ventricular end diastolic volume index (LVEDVI) was significantly higher in younger mice (*p=0.05).

6.3.9 *Cardiac function test through cMRI with exercise*

Cardiac MRI was carried out pre- (14 months of age) and post-intervention (22 months of age) in C57BL6/J sedentary and exercised mice. Similarly cardiac function analysis was carried out in Segment as explained in chapter 2 section 2.12.1. Figures 6.9 A-F represent original cardiac MRI data and figures 6.10 A-E represent cardiac MRI measures normalised to body weight. There was no significant difference between cardiac output index (COI) and left ventricular stroke volume index (LVSVI) between groups pre- and post-intervention. (Two-way ANOVA repeated measures).
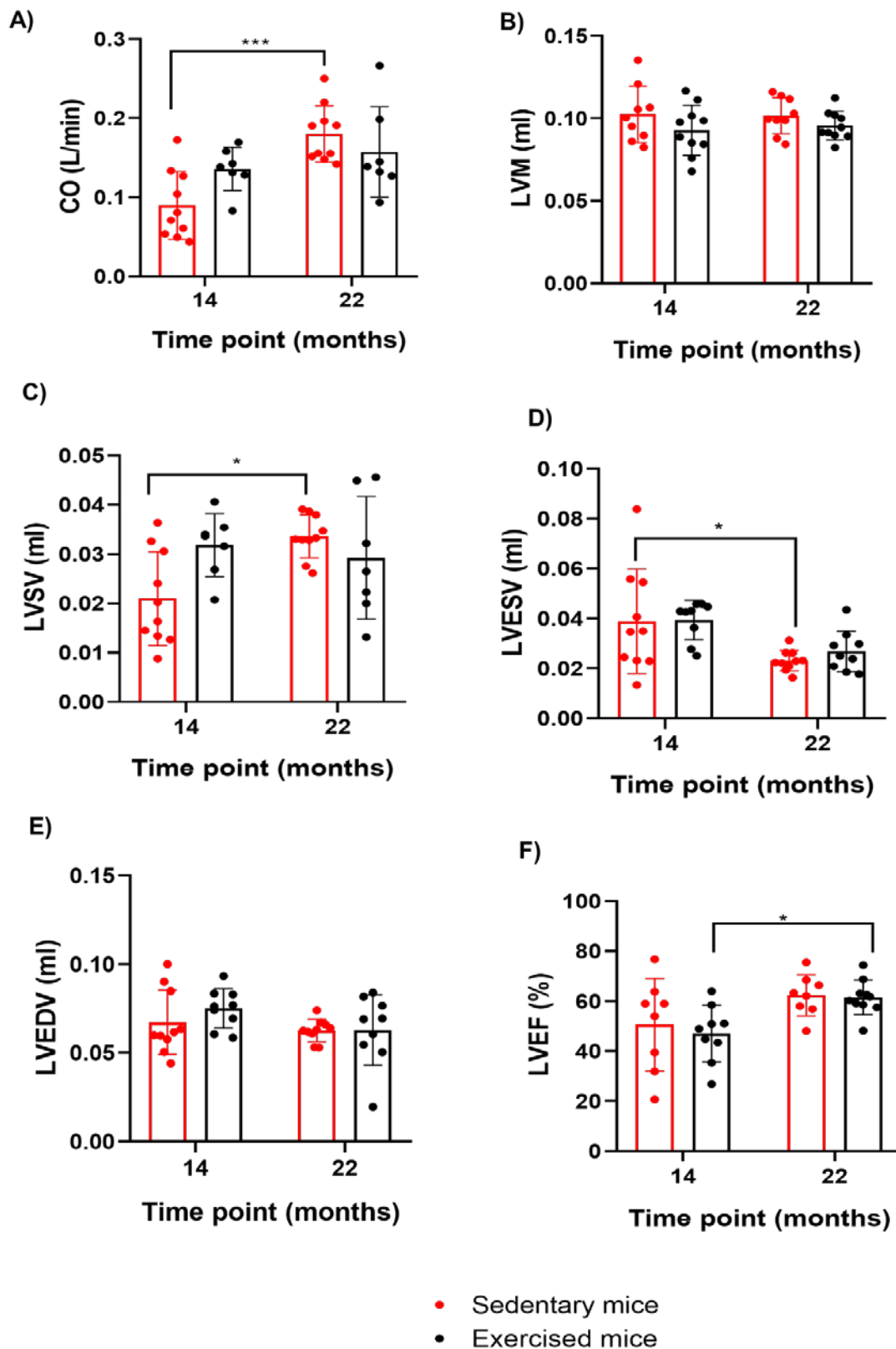
Figure 6.9. Haemodynamic cardiac function measurements in sedentary and exercised mice. LVM and LVEDV did not change in any of the cohorts with age. There was no significant difference in any cardiac function parameters between groups pre- and post-intervention with exercise (Two-way ANVOA repeated measures). Error bars represent mean ±SD.
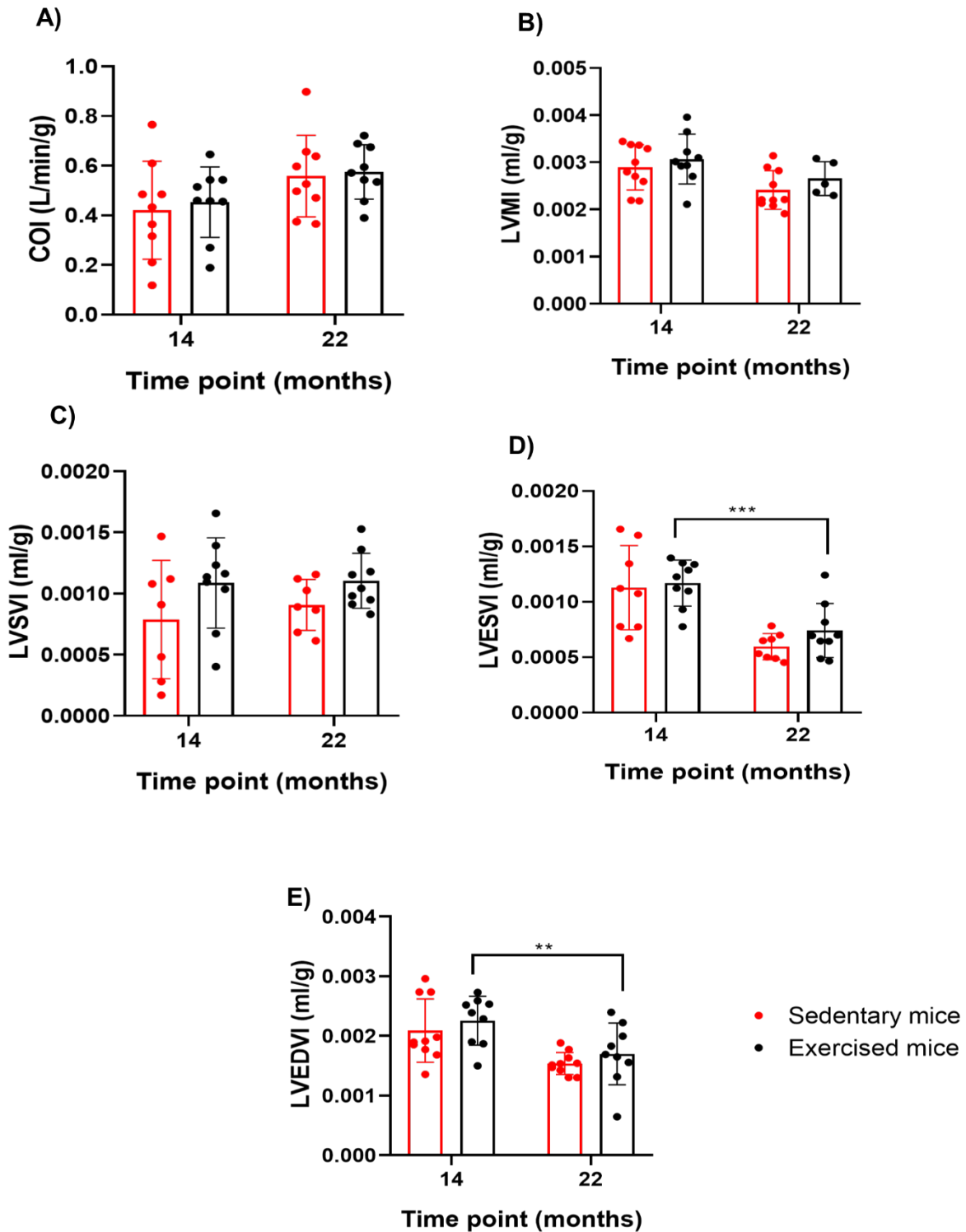
Figure 6.10. Normalised haemodynamic cardiac function measurements in sedentary and exercised mice. A) Cardiac output index (COI). B) LVMI and C) left ventricular systolic volume index (LVSVI) were not significantly different pre- and post-intervention. D, E) Left ventricular end systolic volume and end diastolic volume index reduced in exercised mice with age (***p<0.001 and **p<0.01 respectively, Two-way ANOVA repeated measures).

6.3.10 *Blood pressure with age*

Arterial blood monitoring is key to the evaluation of phenotypical changes associated with cardiovascular pathology and lifestyle interventions. A non-invasive blood pressure monitor (NIBP) (Columbus instruments, Ohio, USA) in C57BL6/J mice was used to measure blood pressure from the arterial tail and data were recorded in NIBP software (Columbus) at 14 months and 22 months of age according to the technique shown in chapter 2 section 2.15. As well as mean arterial blood pressure (MABP), systolic blood pressure (SBP) and diastolic blood pressure (DBP) were also recorded (figures 6.11A-C). Blood pressure did not change with increasing age in sedentary mice (paired t-test).
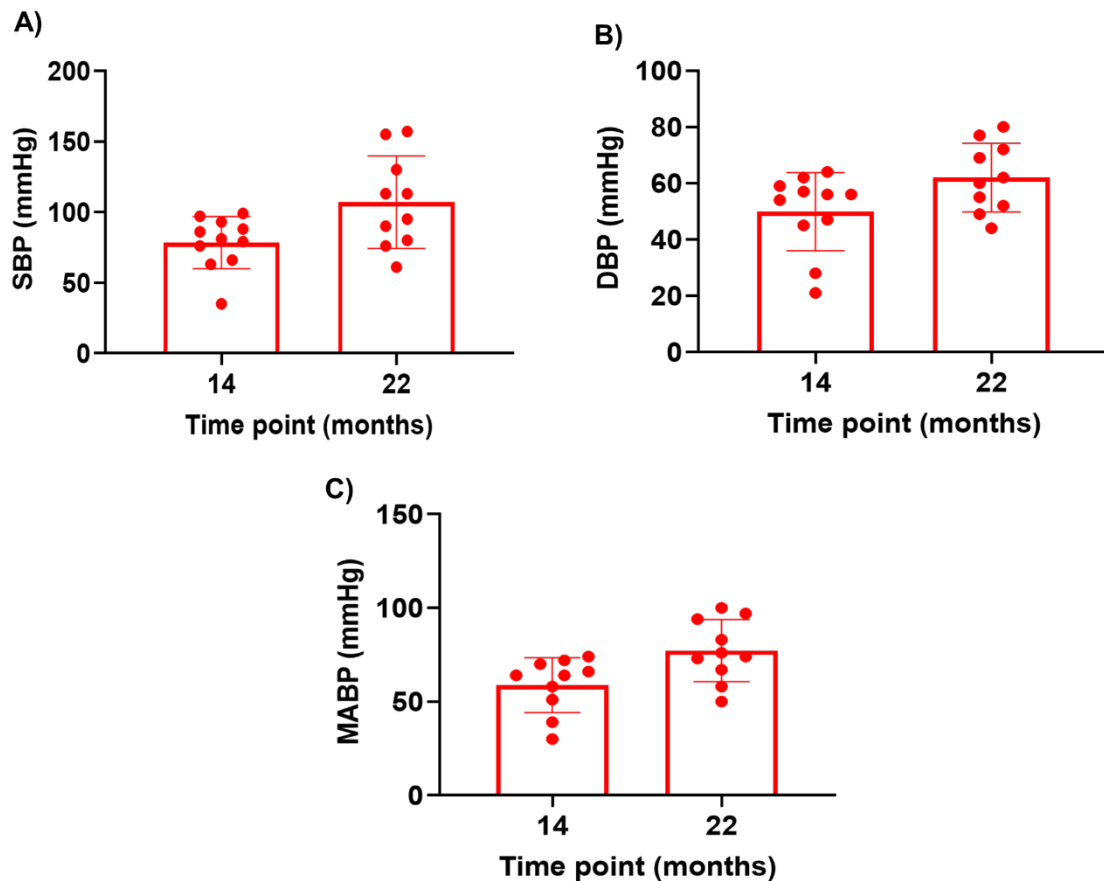
Figure 6.11. Blood pressure changes with advancing age. A) Systolic blood pressure (SBP) (p=0.077). B) Diastolic blood pressure (DBP) (p=0.05) and C) Mean arterial blood pressure (MABP) (p=0.07) (Paired t-test) did not significantly change with increasing age. Error bars represent mean ±SD.

6.3.11 *Blood pressure with exercise*

Next I evaluated the effect of exercise on MABP, SBP and DBP using an NIBP system in C57BL6/J sedentary (n=10) and exercised (n=10) mice at 14 month (pre-intervention) and 22 month (post-intervention) of age. BP measurements were averaged and plotted in figure 6.12 (A-C). There was no significant differences between any of the blood pressure measurements between the two groups at any time point.
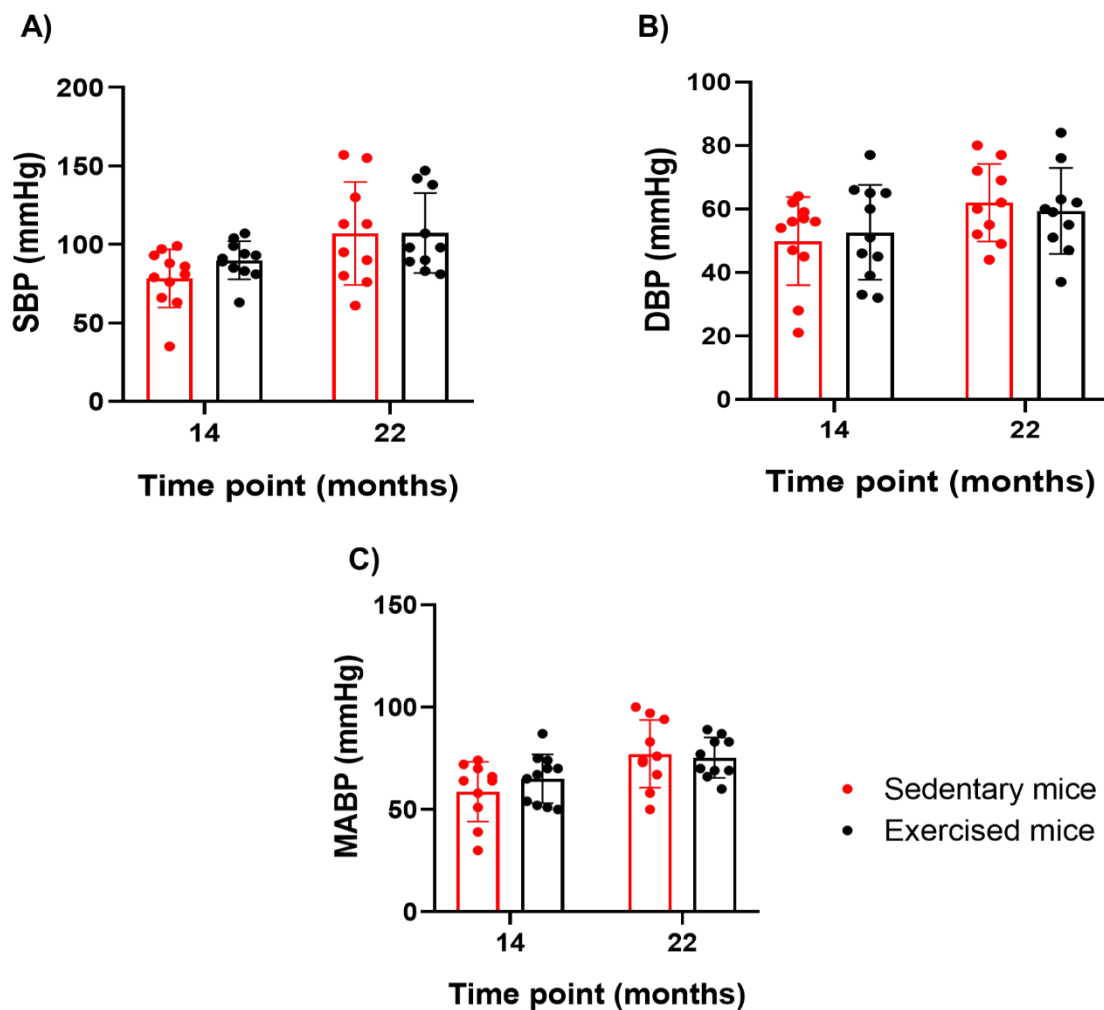
Figure 6.12. Blood pressure changes with exercise. A) Systolic blood pressure (SBP) (p>0.05) B) Diastolic blood pressure (DBP) (p>0.05) and C) Mean arterial blood pressure (MABP) were not significantly different between the two groups at any time point (p>0.05) (Two-way ANOVA repeated measures). Error bars represent mean ±SD.

6.3.12 *Heart rate changes with age*

Resting heart rate (HR) was measured during blood pressure measurements using an NIBP monitor. All C57BL6/J mice were placed in a restrainer of suitable size at the same time and same room temperature. Heart rate was calculated from measuring the BP at the peripheral site (tail artery) from each mouse at 14 months and 22 months of age in triplicates according to the technique detailed in chapter 2 section 2.15 and the mean data are presented in figure 6.13. HR was significantly reduced in mice with increasing age (p=0.004, paired t-test).
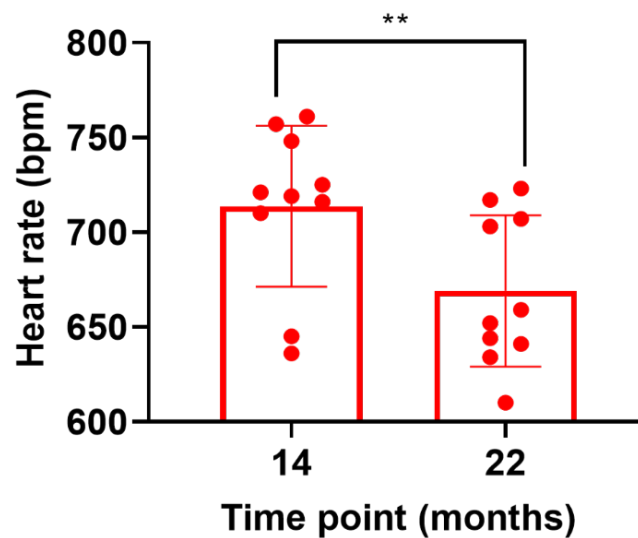
Figure 6.13. Resting heart rate at 14 and 22 months of age. Heart rate has significantly decreased in mice with increasing age (**p=0.004) (Paired t-test). Error bar represent mean ±SD.

6.3.13 *Heart rate changes with exercise*

Resting HR was also measured in C57BL6/J mice pre-intervention at 14 months and post-intervention at 22 months of age through non-invasive blood pressure monitor according to the method explained in chapter 2 section 2.15. Figure 6.14 demonstrate the changes in HR as a result of exercise training in aged mice. Exercise had no effect on the resting HR in 22 month mice in comparison with sedentary mice and no changes in HR were seen in exercised mice with increasing age.
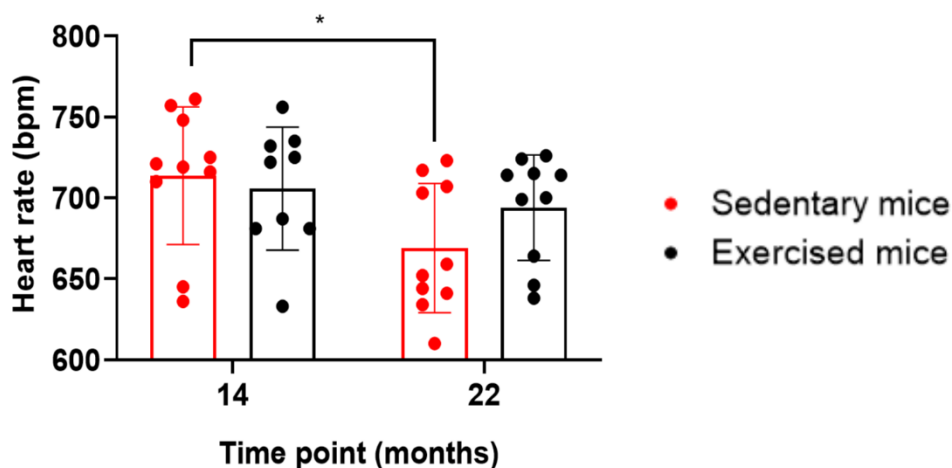
Figure 6.14. Resting heart rate in sedentary and exercised mice at 14 months and 22 months of age. HR was significant reduced in sedentary mice with advancing age (*$p < 0.05$), however no differences were seen between groups at any time point. (Two-way ANOVA repeated measures). Error bars represent mean ±SD.

6.3.14 *Aerobic capacity with age*

Aerobic capacity is measured using the Oxymax system metabolic treadmill (Columbus instruments, USA). $VO_{2\ peak}$ (peak oxygen consumption) and respiratory exchange ratio (RER) during submaximal exercise were measured at three time points; 14, 18 and 22 month of age (details in chapter 2 section 2.13). $VO_{2\ peak}$ is the highest rate of oxygen consumption during incremental exercise and RER is a product of $VCO_{2\ peak}$ (peak CO_2 production during incremental exercise) over $VO_{2\ peak}$ which is a determinant of anaerobic threshold. The $VO_{2\ peak}$ of C57BL6/J mice (n=10) declined significantly with advancing age ($p < 0.0001$) (figure 6.15A). No significant difference in the rate of RER was seen with age (figure 6.15B) (One-way ANOVA repeated measures).
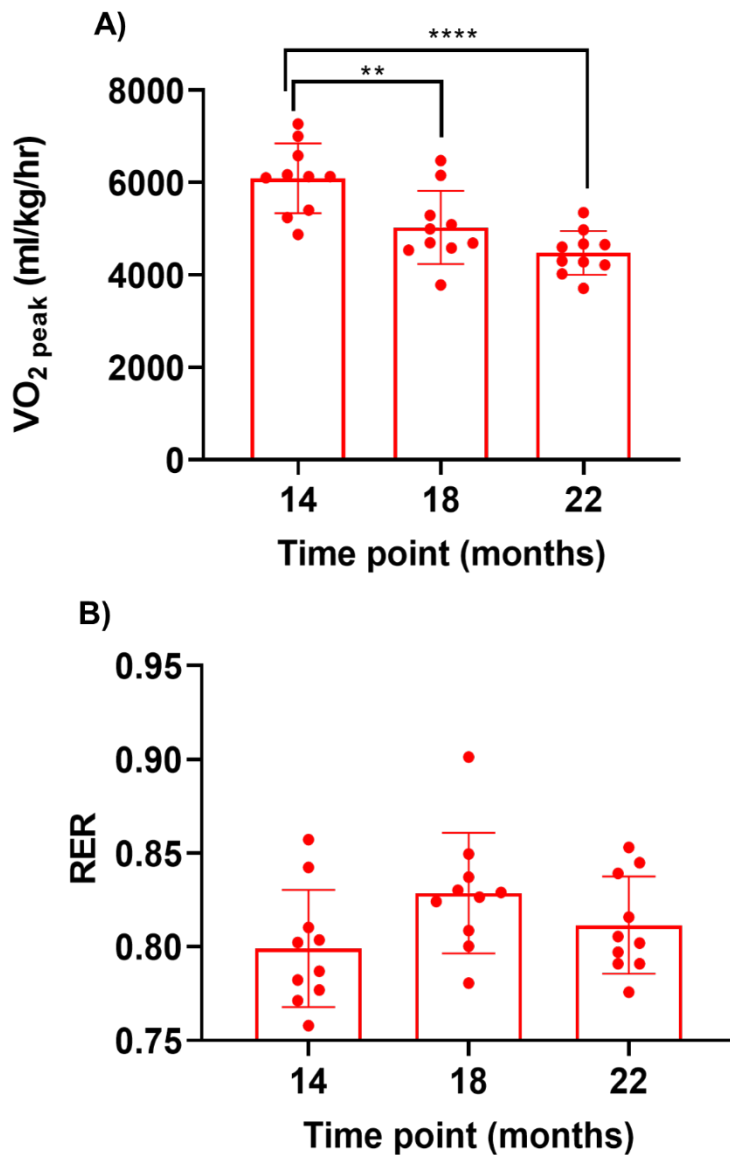
Figure 6.15.VO$_{2\ peak}$ and RER in response to exercise. A) VO$_{2\ peak}$ decreased significantly with advancing age in sedentary mice (****$p<0.0001$). B) RER at 14, 18 and 22 months ($p>0.05$). (One-way ANOVA repeated measures). Error bars represent ±SD.

6.3.15 *Aerobic capacity with exercise*

To see whether six month of endurance exercise affected cardiorespiratory fitness, VO$_{2\ peak}$ and RER were measured in C57BL6/J sedentary (n=10) and exercised (n=10) mice at three time points (14, 18 and 22 months) throughout the intervention (figure 6.16). The rate of VO$_{2\ peak}$ decline in both groups were measured (figure 6.17). Since VO$_{2\ peak}$ decreases with advancing age in both groups, the difference in rate of VO$_2$ decline determines the observed improvement. The rate of VO$_{2\ peak}$ decline in

sedentary mice was 26.45% and the rate of $VO_{2\ peak}$ decline in exercised mice was 23.84%. There was a trend towards a 2.6% increase in the rate of decline in the sedentary mice however this did not reach statistical significance (p>0.05) (figure 6.17).
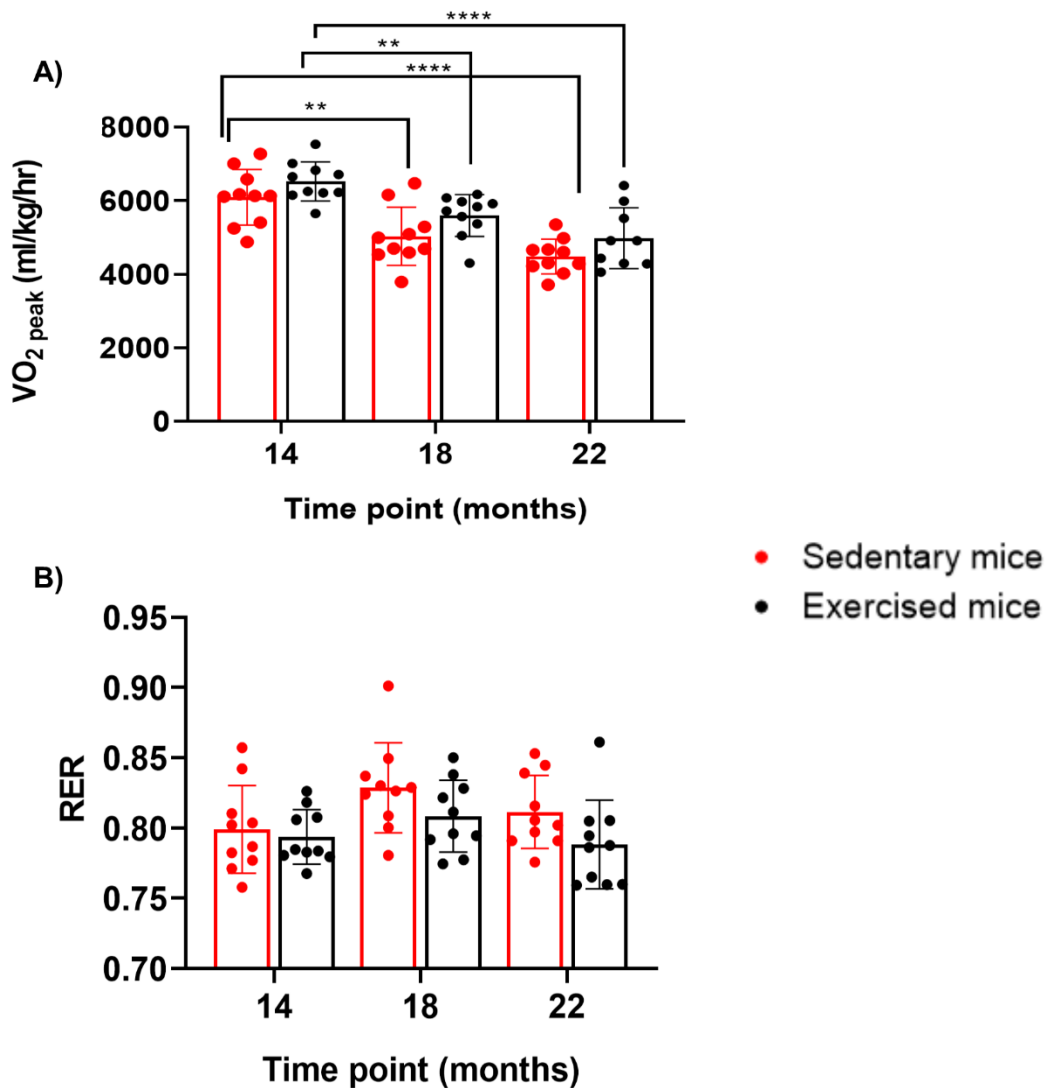
Figure 6.16. $VO_{2\ peak}$ and RER in sedentary and exercised mice at 14m, 18m and 22m of age. A) $VO_{2\ peak}$ was not significantly different between the two groups at 14, 18 and 22 months of age (p>0.05). B) RER was not significantly different between the groups at different time points (p>0.05) (Two-way ANOVA repeated measures). Error bars represent mean ±SD.
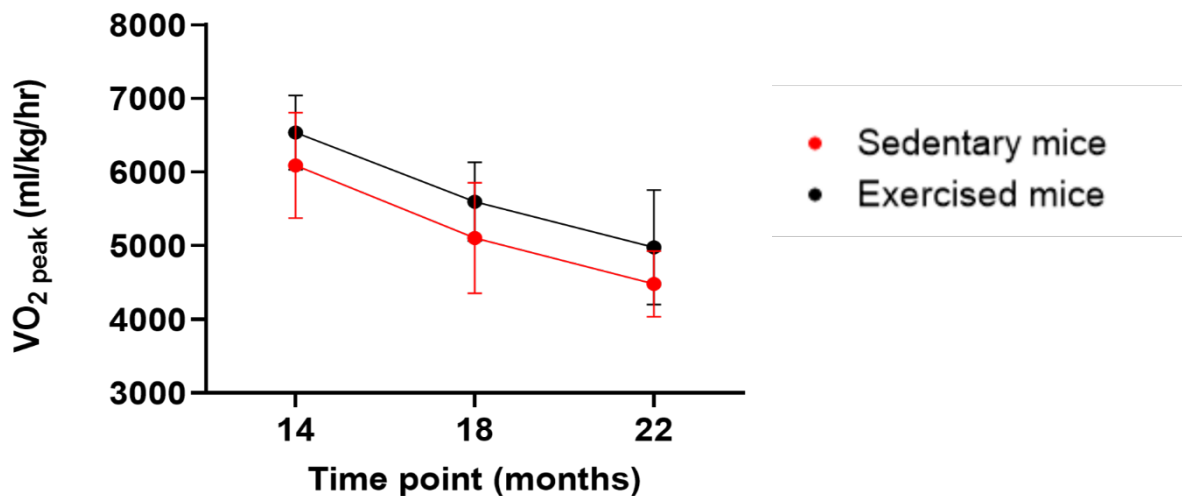
Figure 6.17. Rate of VO$_2$ $_{peak}$ decline in sedentary and exercised mice at three time points (14, 18 and 22 months). There was no significant difference between the rates of decline between the two groups.

6.3.16 *Organ weight changes with exercise*

Sedentary (n=10) and exercised (n=10) C57BL6/J mice were culled humaenly at 22 months of age post cMRI by terminal anaesthesia and organs were harvested (details in chapter 2 section 2.17) and harvesting sheet (appendix 2) for further biochemical and molecular analysis. Organ weights and normalised organ weights to body weight were measured following dissection and organ harvest as shown in figures 6.18A and 6.18B respectively. Right kidney weight was significantly higher in the exercised cohort ($p < 0.01$) regardless of the body weight. The ratio of right kidney ($p < 0.001$), left kidney ($p < 0.01$), heart ($p < 0.05$) and the brain ($p < 0.05$) to body weight was also significantly higher in the exercised cohort. Although the underlying mechanism for organ hypertrophy is not determined in this chapter, however this may be reflected on the fact that exercised mice are leaner.
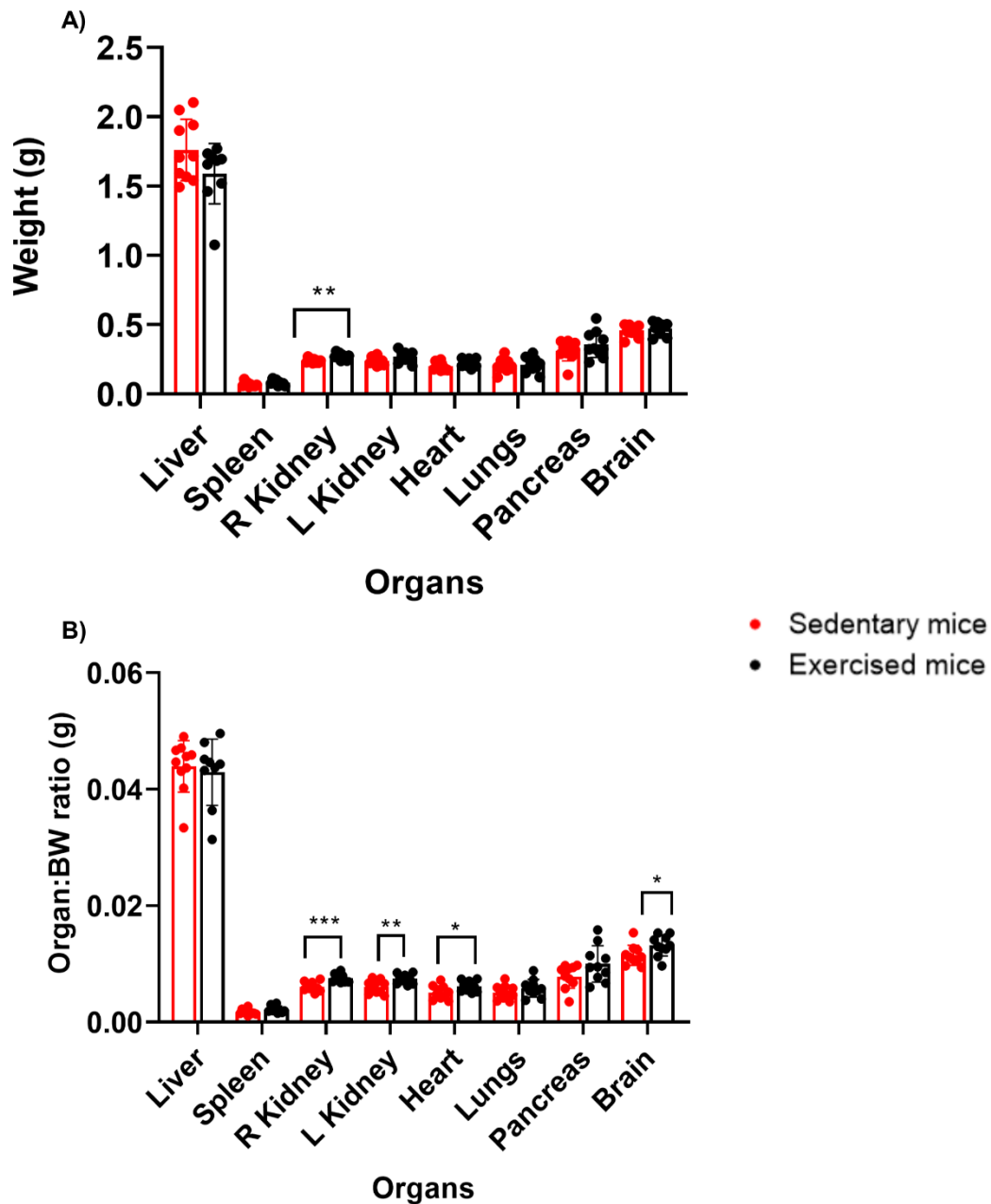
Figure 6.18.Organ weights in sedentary and exercised mice. A) Organ weight in sedentary and exercised mice. Right kidney weight is significantly higher in exercised mice (**$p<0.01$) in comparison to sedentary mice. B) Organ to body weight ratio is significantly higher in the right kidney (***$p<0.001$), left kidney (**$p=0.0043$), heart (*$p=0.02$) and the brain (*$p=0.037$) of the exercised mice in comparison to sedentary mice (unpaired t-test). Error bars represent mean ±SD.

6.3.17 *Cellular and molecular analysis in the heart following exercise*

Mouse hearts were harvested and dissected longitudinally according to table 1 in appendix 2**.** The left side of the heart (left ventricle and left atria) was snap-frozen in isopentane cooled in liquid nitrogen and the right side of the heart (right ventricle and right atria) were formalin-fixed and embedded in paraffin.

The LV is under stress in response to exercise especially with advancing age and the RV is associated with numerous cardiovascular diseases and its role in vascular and RV remodelling is well-known. COX/SDH histochemistry, NBTx analysis and mitochondrial DNA copy number were performed on the LV muscle (frozen). Haematoxylin and Eosin staining, Masson trichrome staining, cleaved caspase 3 immunohistochemistry and mitochondrial complex I and complex IV immunofluorescence were performed on the RV cardiac muscle (fixed).

6.3.18 *Cardiac fibrosis and cardiomyocyte width changes following exercise*

Haematoxylin and Eosin (H&E) staining was carried out to determine right ventricular (RV) cardiomyocyte width according to the technique explained in chapter 2 section 2.20.1. The nuclei were stained dark blue/purple by haematoxylin incubation and were subsequently stained in eosin to visualise cellular components such as cytoplasm and myocardium in pink. Images were acquired by Zeiss light microscope and analysed using Zen analysis software (see chapter 2 section 2.19.2). Five random snapshots of x20 magnification were selected from C57BL6/J sedentary (n=10) and exercised (n=10) mice and the width of 50 random transverse cardiomyocytes were measured from each image (figure 6.19). Cardiomyocyte width was significantly higher in the RV cardiac muscle of exercised mice (in average 25.22μm) in comparison to sedentary mice (in average 16.37μm) ($p < 0.0001$, unpaired t-test) (figure 6.19B).

Cardiac fibrosis was assessed in C57BL6/J sedentary (n=10) ad exercised (n=10) mice by Masson trichrome staining in which a three coloured dye was used to stain cell nuclei in purple, cytoplasm and cardiomyocytes in red and collagenous connective tissue in blue (Figure 6.19A bottom row images) according to the technique further explained in chapter 2 section 2.22. Images of x10 magnification

were acquired by Nikon Tie microscope and analysed using NIS elements software. RGB general analysis algorithm was used to create and set threshold for each RGB channel in order to find out the percentage of cardiomyocytes with blue collagenous fibrotic areas. The ratio of total tissue area to blue staining determined the percentage of cardiac fibrosis (figure 6.19C). Sedentary mice have a significantly higher percentage of cardiac fibrosis in comparison to exercised cohort (p=0.008, unpaired t-test) which may indicate abnormal thickening of the heart muscle with age due to excessive deposition of extracellular matrix in the cardiac tissue. Exercise seems to be able to attenuate the excessive accumulation of fibrotic tissues on the cardiac muscle.
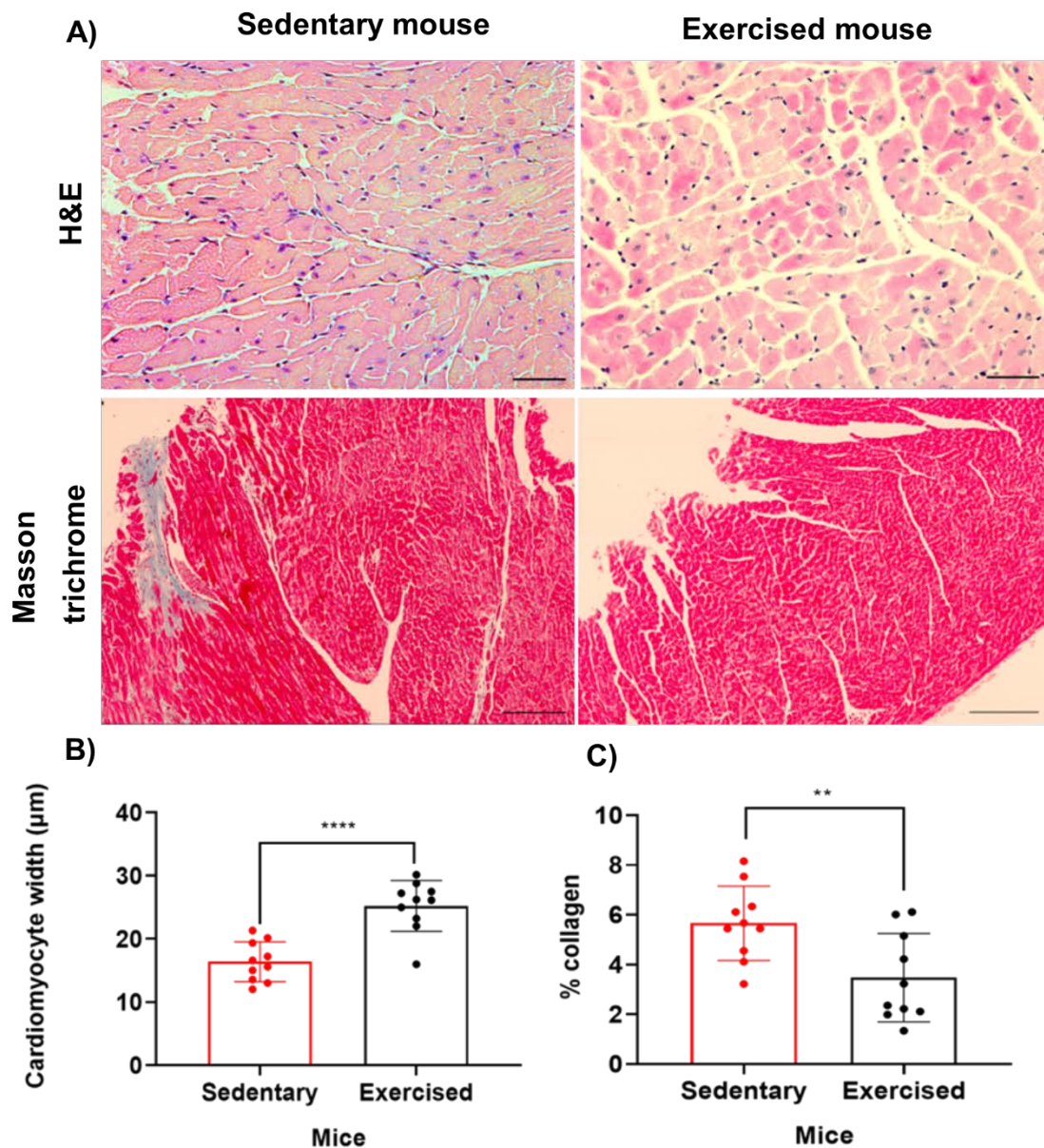
Figure 6.19. Percentage of cardiac fibrosis and cardiomyocyte width in sedentary and exercised mice. A) Top row images represent H&E staining (Magnification x20. Scale bars=100μm) and bottom row images show trichrome staining from sedentary and exercised cohort (Magnification x10. Scale bars=200μm).Cardiomyocyte width was significantly bigger in exercised mice (****p<0.0001). C) Percentage of cardiac fibrosis was significantly higher in the sedentary cohort (**p=0.008, unpaired t-test). Error bars represent mean ±SD.

6.3.19 *Cardiac Apoptosis following exercise*

Activated-cleaved caspase 3 immunohistochemistry was carried out in C57BL6/J sedentary (n=10) and exercised (n=10) mice hearts to quantify levels of apoptosis (details in chapter 2 section 2.23.2). Five random snapshots of x10 magnification

were taken by Aperio-scanner and analysed through Image-scope analysis software, nuclear staining algorithm. The total number of apoptotic nuclei as dark brown regions were calculated as the ratio of total number of nuclei (figure 6.20). Sedentary mice had significantly higher frequency of apoptotic cells compared with mice in the exercised cohort (p=0.04, unpaired t-test).
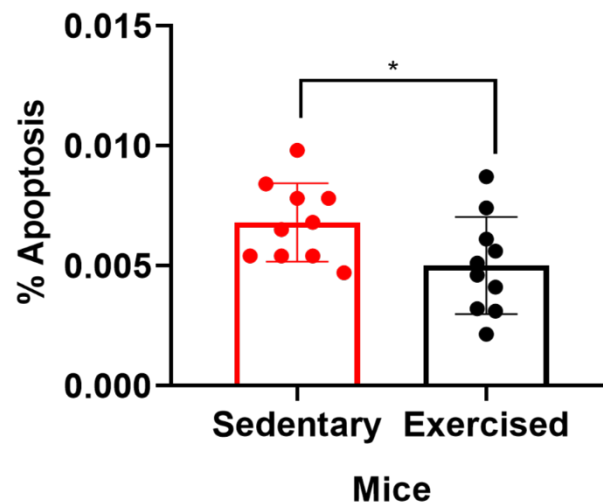
Figure 6.20. Percentage of cardiac apoptosis in sedentary and exercised mice.
The frequency of apoptotic nuclei is significantly higher in the sedentary mice in comparison to exercised mice (*p=0.04). Error bars represent mean ±SD.

6.3.20 *Cardiac mitochondrial complex I and complex IV expression levels following exercise*

Mitochondrial complex IV (MTCOI) and complex I (NDUFB8) expression levels were measured in the RV cardiac muscle of C57BL6/J sedentary (n=10) and exercised (n=10) mice using the OXPHOS immunofluorescence assay detailed in chapter 2 section 2.24.2. Images were obtained by LSM800 microscope and analysed using the in-housed immunoanalyzer software. Laminin was used to mark the cardiomyocyte boundaries and Porin to normalise complex I and complex IV protein levels to. Five random snapshots of x10 magnification were obtained from each mouse and the transverse cardiomyocytes were selected for analysis through the semi-automated software (figure 6.21). Cardiomyocytes were categorised based on their OXPHOS protein levels relative to Porin z-scores into groups of positive (z>-

3SD), intermediate positive (-4.5<z<-3 SD), intermediate negative (-6<z<-4.5 SD) and negative (z<-6 SD) expression levels. Mitochondrial respiratory chain plots (MRC) were generated and an example from each group was shown in figure 6.22 two figures on the left. Each dot represent an individual muscle fibre and is colour coded according to the Porin levels. Dotted black lines represent the SD limit for the classification of fibres. Percentage of cardiomyocytes with MTCOI (CIV) positive and intermediate positive expression levels were significantly higher in the exercised cohort (p<0.01) in comparison to sedentary cohort. There was no significant difference in any of the CI categories between the two groups (unpaired t-test). Mitochondrial mass marker (porin) z-scores were used to categorise mitochondrial mass levels. Figure 6.22C shows that porin levels in both sedentary and exercised mice are all within the normal range (between 2 and -2SD).
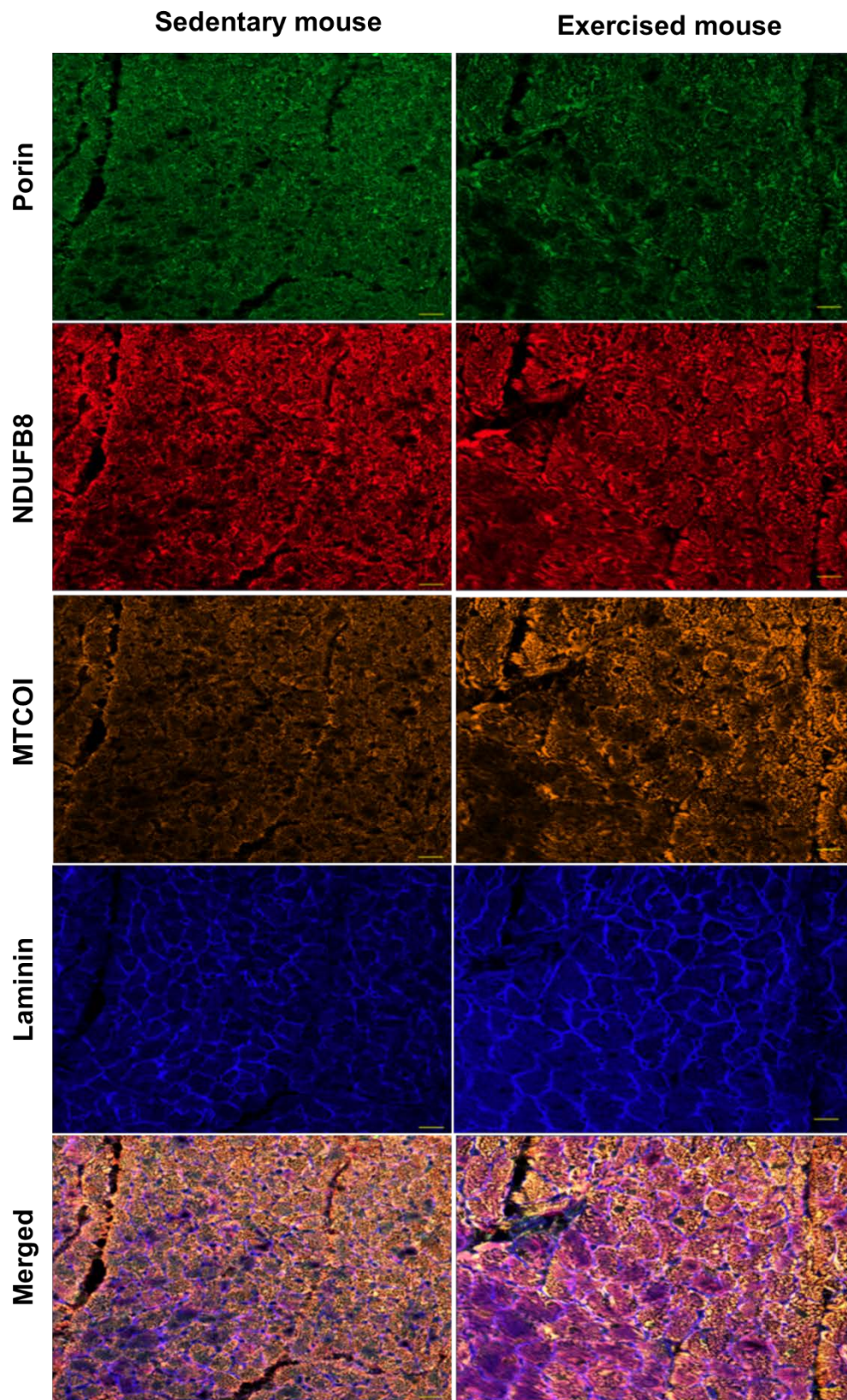
Figure 6.21. RV muscle mitochondrial complex I (NDUFB8) and complex IV (MTCOI) expression levels. Fluorescence detection visualised; Porin (mitochondrial mass)-green (488nm), complex I subunit (NDUFB8) - red (647nm), complex IV subunit (MTCOI)-orange (546nm), laminin (myocardial protein)-blue (405). Merged image represent fluorescence from all the channels combined. Magnification x10. Scale bars=100µm.
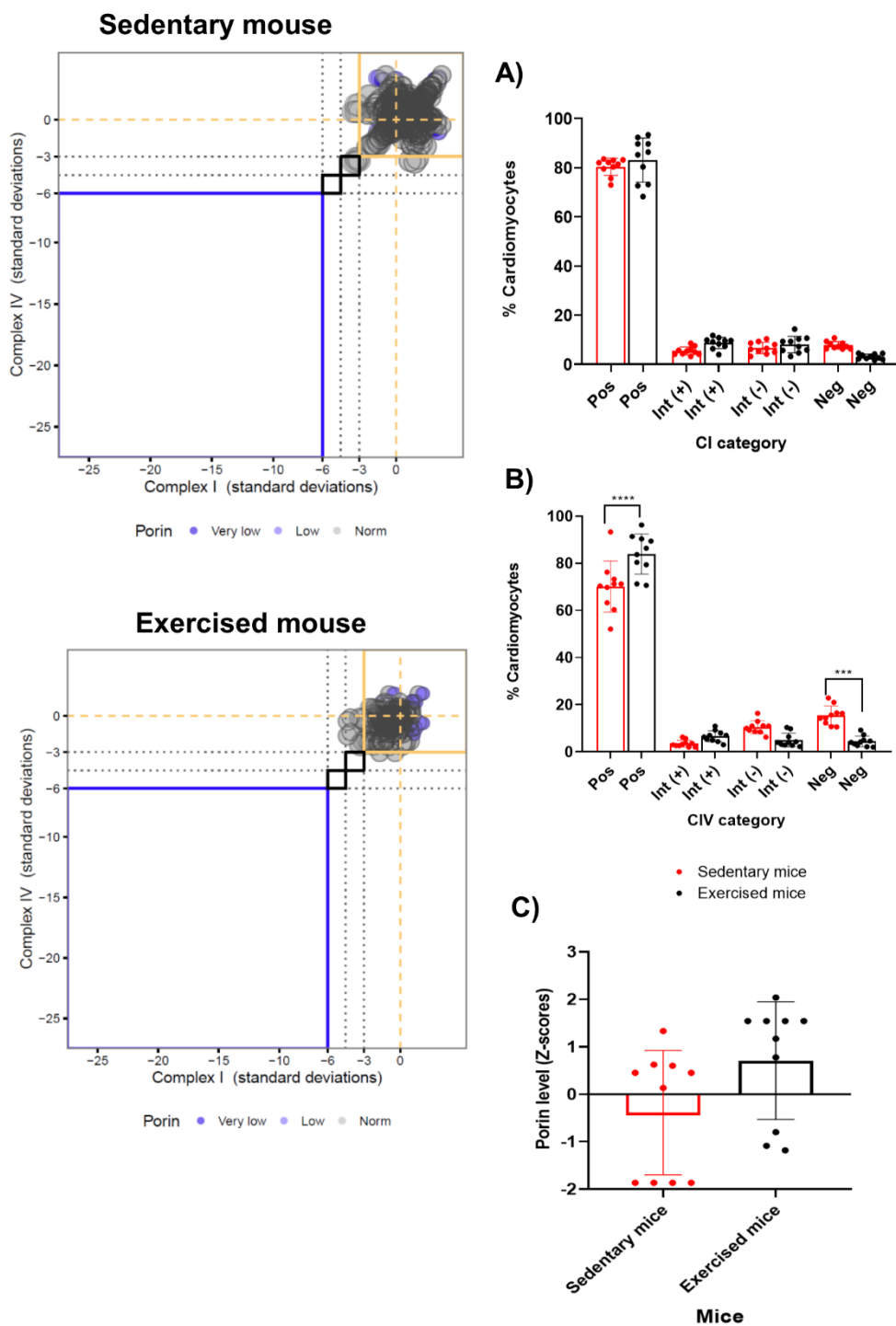
Figure 6.22. Mitochondrial respiratory chain plots (MRC), NDUFB8, MTCOI and porin expression levels. Sedentary mouse MRC plot and Exercised mouse MRC plot on the left. A) Percentage of cardiomyocytes with complex I subunit (NDUFB8) expression. B) Percentage of cardiomyocytes with complex IV (MTCOI) expression levels. (Unpaired t-test). C) Porin z-scores determine mitochondrial mass within the normal range. Error bars represent mean ±SD.

6.3.21 *Cardiac mitochondrial complex IV activity following exercise*

Mitochondrial complex IV (COX) activity was quantified by COX/SDH histochemistry in LV cardiac muscle sections from C57BL6/J sedentary (n=10) and exercised (n=10) mice (chapter 2 section 2.21). Five random fields of x10 magnification were acquired using Nikon Tie microscope and analysed using NIS elements software (figure 6.23). The RGB general analysis algorithm was used to set a threshold for different channels. The percentage of COX deficiency was determined by the ratio of total tissue area to the total blue deficient regions. Individual COX and SDH histochemistry was used to distinguish and visualise the heterogeneity of COX activity in cells. Figure 6.24 shows the percentage of COX deficiency in sedentary and exercised mice by unpaired t-test analysis. There is no significant difference in COX activity between the two groups (unpaired t-test, p=0.44).
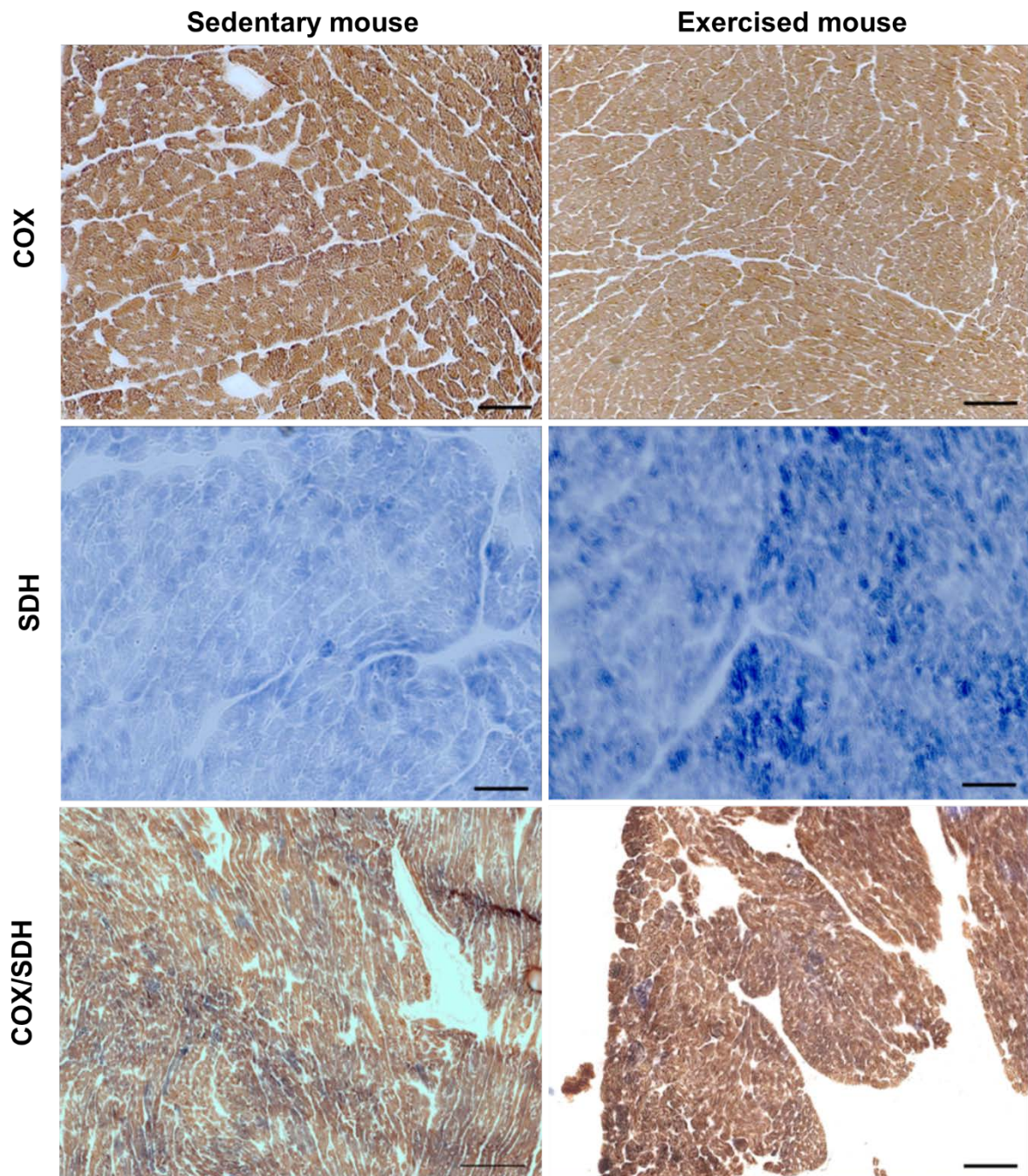
Figure 6.23. Representative COX, SDH and COX/SDH histochemistry in sedentary and exercised LV tissue. Top images represent COX staining in brown, middle row images show nuclear encoded SDH staining in blue and bottom row show combined COX/SDH to observe COX deficiency in blue. Magnification x10. Scale bars=100µm.
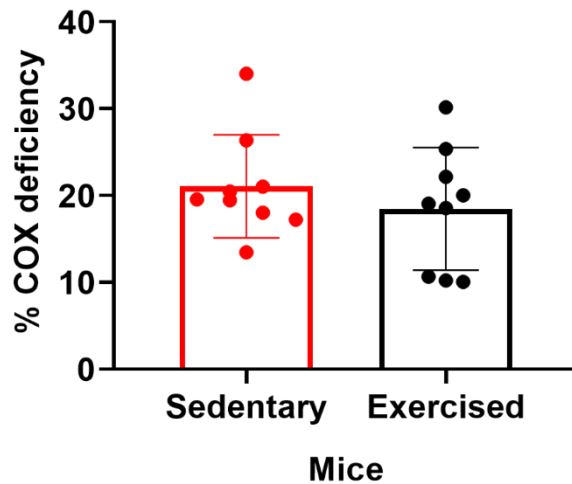
Figure 6.24. Percentage of COX deficiency through COX/SDH histochemistry.
There is no significant difference in the level of COX deficiency between groups
(unpaired t-test, p=0.44). Error bars represent mean ±SD.

6.3.22 *Cardiac COX activity through NBTx assay following exercise*

NBTx assay and laminin immunofluorescence was carried out in LV cardiac muscle
of C57BL6/J sedentary (n=10) and exercised (n=10) mice. NBTx assay relies on a
similar theory to COX/SDH in order to visualise and quantitate the degree of COX
deficiency although only through NBT activity (detailed chapter 2 section 2.24.1).
COX functional cells remain colourless as there is no NBT reduction by SDH. COX
deficient cells however stain various degrees of blue depending on the level of
deficiency. The darker the blue staining, the more deficient the cells were. Laminin
immunofluorescence was carried out following NBTx assay to allow for easy
detection and analysis of cardiomyocytes. Images were acquired on LSM800
microscope and analysed through an in-house immuno-analyser software. 500
transverse cardiomyocytes per image were analysed. A numbering system was used
to categorise cardiomyocytes into groups of COX positive, COX intermediate and
COX negative cardiomyocytes (figure 6.26) based on the activity of COX in young
C57BL/6J mice hearts. Figure 6.25 shows NBTx staining, laminin
immunofluorescence in green and merged image consisting of NBTx bright field and
laminin channel in green overlapping. Figure 6.26 demonstrates that exercised mice
seemed to have higher percentage of cardiomyocytes in COX positive category
(p<0.01) whereas sedentary mice had significantly more cardiomyocytes in COX

intermediate (P<0.001) and COX negative (p<0.05) (unpaired t-test). NBTx provided more detail of the spread of COX activity of cardiomyocytes whereas COX/SDH (figure 6.23) only demonstrated the presence or absence of COX deficiency omitting the heterogeneity of COX activity in the cardiomyocytes.
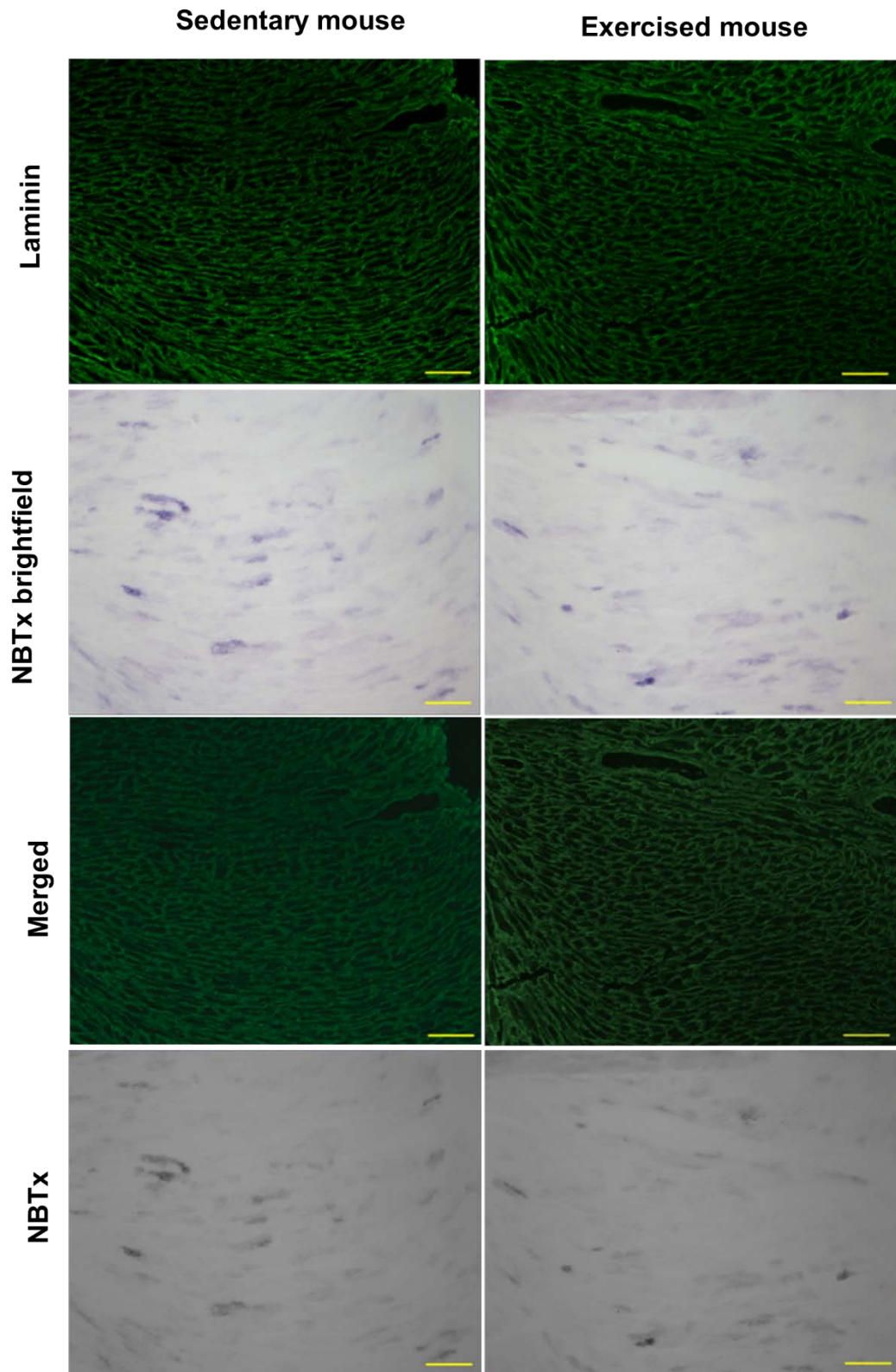
Figure 6.25. Representative immunofluorescence and bright field images of sedentary and exercised mice LV muscle. Laminin-green (488), NBTx through monochrome camera and bright field to demonstrate the blue nature of reduced NBT. Magnification x10. Scale bars=100μm.
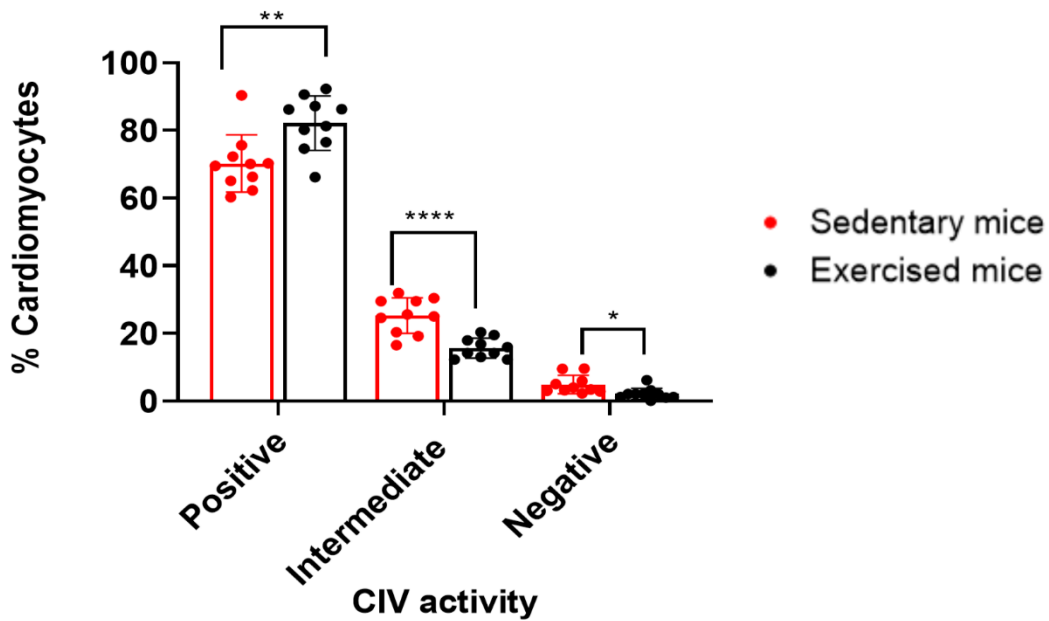
Figure 6.26.COX activity levels in sedentary and exercised mice. Percentage of cardiomyocytes with positive COX activity was significantly higher in the exercised cohort (**p<0.01). Percentage of cardiomyocytes with COX intermediate and COX negative activity was significantly higher in the sedentary cohort (****p<0.0001 and *p<0.05 respectively, unpaired t-test). Error bars represent mean ±SD.

6.3.23 *Exercise-associated skeletal muscle cytokine levels*

In order to quantify markers of inflammation, I performed total cytokine array on the skeletal muscle of both cohorts of C57BL6/J mice at the end of intervention when mice were 22 month of age. The technique requires a significant volume of tissue and since the amount of heart tissue was limited and used extensively in histochemical procedures, the skeletal muscle was used a surrogate tissue commonly affected by ageing. Total muscle homogenate cytokine levels were assessed in sedentary (n=10) and exercised (n=10) mice quadriceps using the V-PLEX mouse cytokine kit (Meso Scale Discovery, USA) as detailed in chapter 2 section 2.27. Quadriceps were homogenised and the total cytokine array was carried out from protein extracts. Skeletal muscle is an organ under strain during exercise especially with advancing age and its repair is associated with key inflammatory cytokines. The concentration of 10 cytokines (IFN-γ, IL-10, IL-12p70, IL-2, IL-4, IL-5, IL-6, KC/GRO and TNF-α) were measured post-intervention (22 months). An

unpaired t-test was carried out to discern the changes in each cytokine level between groups, pre- and post-intervention. Figures 6.27A-B demonstrate that there is no significant difference between any of the muscle cytokine in the two cohorts.
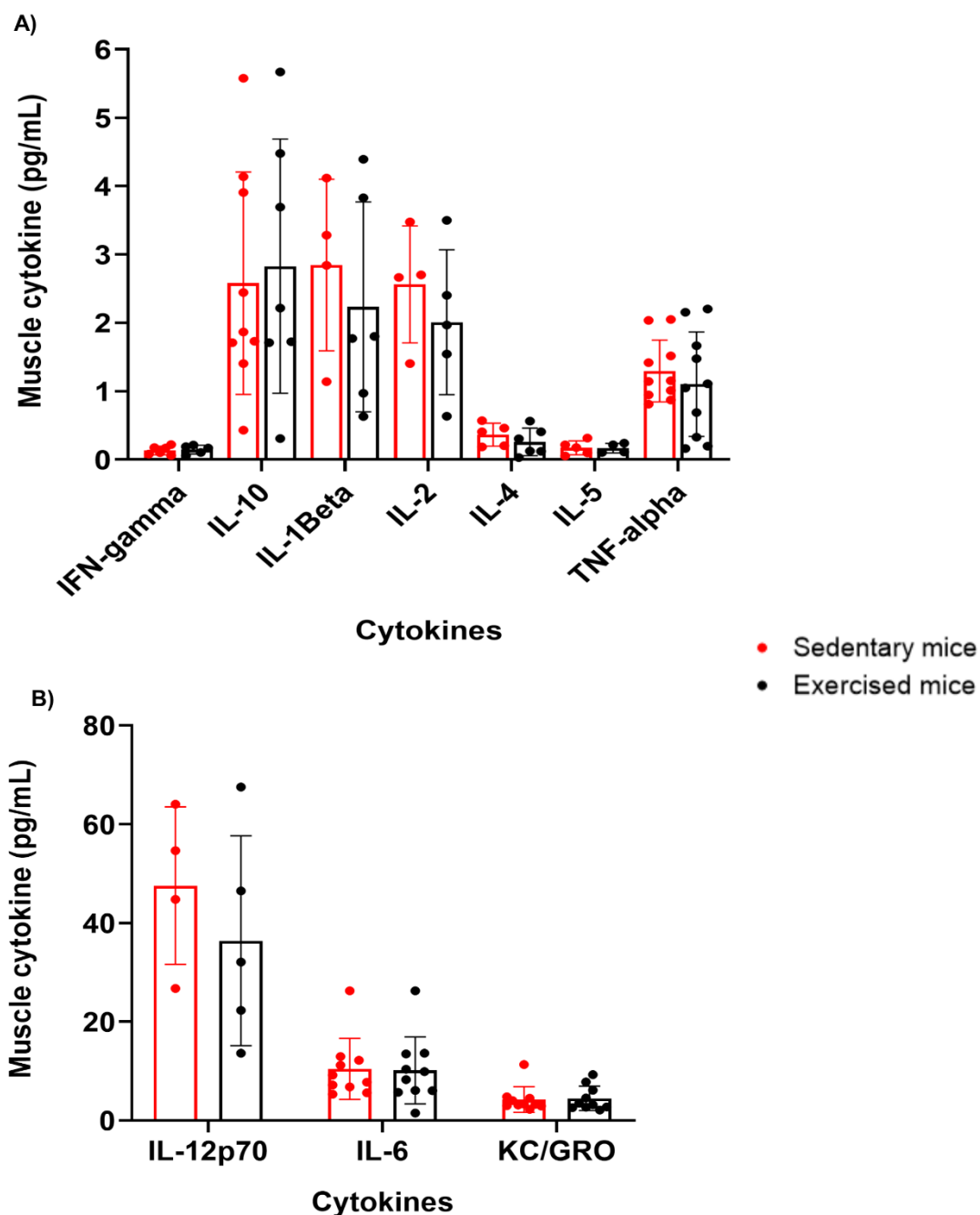
Figure 6.27. Total muscle homogenate cytokine levels in sedentary and exercised mice. No significant changes in the level of muscle cytokines were seen between groups post-intervention (unpaired t-test). Error bars represent mean ±SD.

6.3.24 *Exercise-associated cardiac mitochondrial DNA copy number*

Mitochondrial DNA (mtDNA) copy number was quantified in C57BL6/J sedentary (n=10) and exercised (n=10) mice LV cardiac muscle by the ratio of ND1 (mitochondrial OXPHOS gene) to β-actin (house-keeping nuclear encoded gene). Real-time quantitative PCR was used to amplify the genes of interest and the ratio of both genes determined the amount of mtDNA present in each cell as detailed in chapter 2 section 2.26. There was no significant difference in the cardiac mtDNA copy numbers between the two groups (figure 6.28).
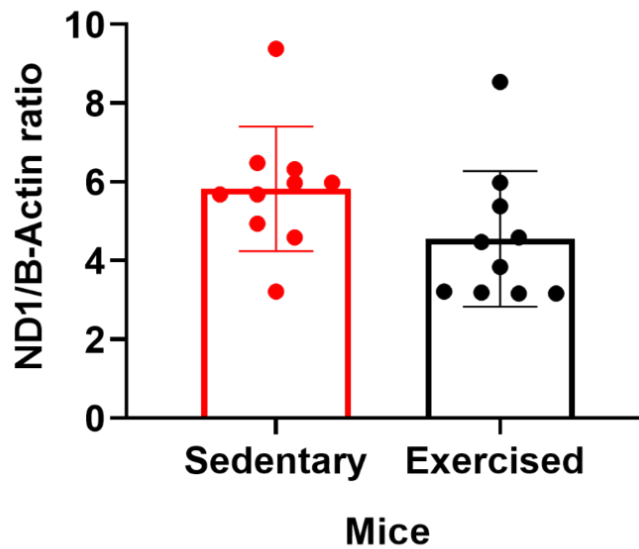
Figure 6.28. Mitochondrial DNA copy number in sedentary and exercised mice LV cardiac muscle. There is no significant difference between the mtDNA copy number of both cohorts (p=0.2) (unpaired t-test). Error bars represent mean ±SD.

6.4 Discussion

This study has shown that C57BL/6J mice undergo significant phenotypic change, worsening of body condition and significant weight gain with advancing age. Their inquisitiveness and step length reduced significantly with age indicative of lower locomotive activity. A study carried out by Shoji *et al* (2016) showed that older mice present diminished locomotive activity in novel environments. This study did not show significant reduction in locomotive activity of mice but rather an increase in

anxiety-like behaviours such as decreased step length and reduced number of touches in sedentary mice. I have also shown that sedentary mice have a significant decline in grip strength, coordination and balance as they get older. Takeshita *et al* (2017) demonstrated that lower grip strength is associated with neuromuscular dysfunction. Interestingly, Xuan *et al* (2016) showed that reduction in grip strength is a predictor of mortality. Cardiac function was assessed in young and aged C57BL6/J mice by cMRI technique in this study. There was no significant change in LVM and LVEDV with advancing age in sedentary mice. However, left ventricular mass index, left ventricular end diastolic volume index and left ventricular end systolic volume index decreased significantly with advancing age. Left ventricular mass is an independent predictor of myocardial morbidity and mortality according to Verdecchia *et al* (2001). Wiesmann *et al* (2000) have also shown that LV mass index decreases with advancing age. As body weight also increases with age, LV mass indexed to body weight would naturally be smaller than in younger counterparts unless LVM also significantly increased with age. It is largely known that aging is associated with hypertension due to decreased diastolic and increased systolic blood pressures (Pinto, 2007). Resting heart rate also decreased significantly with age. Kostis *et al* (1982) have shown that resting heart rate does not change massively with advancing age, however the maximum heart rate achieved in response to exercise is reduced with age. Aerobic capacity of mice decreased with age as predicted according to previous research (Chappell *et al*, 2003). Fitzgerald *et al* (1997) have declared that the rate of decline in VO_2 max is smaller in endurance-trained athletes than those with sedentary lifestyle. The Baltimore longitudinal study by Ades and Toth (2005) has criticised the previous cross-sectional studies on aerobic capacity where older participants selected might have been healthier than younger ones due to their selective survival.

As the baseline traits of sedentary C57BL/6J mice were characterised in the first aim of this study, the next step was to investigate the effect of 6 months of endurance exercise training on physiological and cardiovascular parameters in the second part of this study.

Since physical ability and cardiovascular plasticity that are required to perform endurance exercise becomes limited with age (Wang *et al,* 2014), it's crucial to devise an exercise regimen to target and improve the multi-organ decline seen during normal aging. A study carried out by Fujimoto *et al* (2010) reported that life-

long endurance training reversed cardiac compliance (as a measure of slop of the pressure-volume curve), increased LV mass, improved arterial stiffness and aerobic capacity by 19%. However 1 year of progressive vigorous training in sedentary men at 65 years of age had little effects on cardiac compliance. The physiological LV remodelling observed with exercise included a significant increase in LV mass, increase in cardiac output and stoke volume which was accompanied by an overall decrease in body weight and heart rate (Fujimoto *et al*, 2010). As well as improvements in aerobic capacity and cardiac function, Zampieri *et al* (20016) showed that physical exercise also increases the mitochondrial calcium uniporter and mitochondrial CIV expression levels in aged skeletal muscle. They confirmed a complete remodelling of mitochondrial structure and function by exercise training possibly due to increased expression of mitochondrial fusion protein OPA1.

My study has confirmed that cardiac hypertrophy occurred in exercised mice as measured by an increase in cardiomyocyte width in the absence of cardiac fibrosis. Marvao *et al* (2015) categorised cardiac hypertrophy without cardiac fibrosis as physiological hypertrophy which is also seen during pregnancy and chronic exercise.

Agarwal *et al* (2009) have suggested that cardiomyocyte hypertrophy in exercised mice is related to anti-inflammatory properties of exercise shown by an increase in TNF-α expression, causing reduced rate of cardiac fibrosis. Endurance exercise is not only documented to improve cardiac function in normal aging, it is cited to mediate CV risk factors in people with stroke as well. Tang *et al* (2013) suggested that high intensity exercise improves the function of right side of the heart and myocardial relaxation whereas low intensity exercise was shown to improve glucose and inflammatory markers as well as plasma lipid metabolism after stroke. Similarly, Roest *et al* (2004) have shown that exercise training in patients with atrial correction for transposition of great arteries have increased right ventricular end diastolic volume (EDV) and right ventricular end systolic volume (ESV) without significant changes in stroke volume (SV) and ejection fraction (EF). Since ejection fraction (EF) is affected by afterload, preload, contractility of the cardiac muscle and heart rate, changes in EF may arise from alteration in any of the contributing factors. My data show that EF was improved post-exercise however no other parameter was affected post-exercise. Paridon *et al* (1991) showed that a relationship between chronotropic impairment and exercise capacity was not established confirming the limited

association of afterload with increased RVEDV and RVESV in response to physical exercise.

Significant improvements in cardiac mitochondrial function were observed with endurance exercise in this study seen that the percentage of cardiomyocytes with COX positive expression levels and COX positive activity levels were significantly higher in the exercised cohort compared to non-exercised sedentary mice, demonstrating a positive shift in mitochondrial function with exercise. Bishop *et al* (2014) have suggested that physical activity increases mitochondrial function but not content as was assessed by citrate synthase activity. They have also documented that exercise training intensity in mice and rats are the most crucial determinant of improvement in mitochondrial function and exercise training repetition strongly correlate with improvements in mitochondrial content. They've observed that mitochondrial improvements were reversed immediately upon withdrawal of physical activity, highlighting the plasticity of cardiac and skeletal muscle to exercise training. My porin data suggested that mitochondrial mass was not affected with exercise since low and very low levels of porin were not detected in any of the cardiomyocytes from both groups.

Interestingly, Lundby and Jacobs (2015) reported that exercise training increases intermyofibrillar mitochondrial volume in skeletal muscle by up to 40% due to enhanced muscle cross-sectional area and growth. Jacobs *et al (*2013) have reported that six sessions of high intensity interval training in untrained male subjects enhanced skeletal muscle's respiratory capacity by increasing the expression and activity of mitochondrial enzymes that facilitate aerobic metabolism. Whereas Lundby and Jacobs (2015) demonstrated that low/moderate endurance training improved fat oxidation capacity by mitochondria and not necessarily the global respiratory capacity. Although most of the research carried out in rodent models may have implications in human research, the psychological responses in which mice experience during exercise seems to be different to humans (Lehmann and Herkenham, 2011). Since decline in mitochondrial content with age in human skeletal muscle was documented to be linked to decline in cardiorespiratory fitness (Short *et al*, 2005), Robinson *et al* (2005) investigated the effects of exercise training on isolated mitochondrial from human skeletal muscle at resting and fasting state in order to observe the impact of exercise training on the ageing process. They have reported a significant improvement in skeletal muscle gene expression levels

especially those involved in mitochondrial function, muscle growth and insulin signalling cascade in older subjects by exercise. High intensity training enabled the most robust increase in regulation of transcription and translation of skeletal muscle growth and mitochondrial function.

6.5 Conclusion

In this study, I have confirmed that 6 months of exercise intervention in C57BL/6J mice improved functional capacity such as higher locomotive activity, assumed stronger muscles and better body conditioning score. Cardiac function was also improved in exercised mice as evident by higher percentage of ejection fraction. Cardiomyocyte hypertrophy was evident in exercised mice as well as lower percentage of cardiac fibrosis and apoptosis. Mitochondrial CIV expression and activity was significantly higher in the exercised group. Therefore, this late-life exercise intervention strategy was beneficial in attenuating physiological, cardiac and mitochondrial decline with age.

6.6 Future work

Given the current baseline physical, cardiac and mitochondrial characteristics of C57BL/6J mice and the impacts of ageing observed in the first aim of this chapter, this mouse model would enable the investigation of individual VO_2 max testing to assess exercise performance and aerobic capacity in each mouse. Younger mice are more malleable to exercise training in a way that smaller and more variable training responses were observed in the old compared to young subjects (Harber *et al,* 2012). It's advantageous to perform individual exercise intolerance test for each mouse and personalise the endurance exercise regimen based on their maximal oxygen consumption rate (Wang *et al,* 2014).

Chapter 7

Chapter7. Final Discussion

The aim of this thesis was to investigate the role of endurance exercise on physical, mitochondrial and cardiovascular function of two mouse models, one of accelerated and one of normal aging. Understanding the mechanisms underlying the decline in cardiovascular and mitochondrial function in aging and whether these changes can be modulated with endurance exercise are fundamental if we are going to prescribe exercise as a lifestyle intervention in later life.

The main findings of the *PolgA^mut/mut* mouse study was that endurance exercise did not alleviate the physiological and functional decline observed in male *PolgA^mut/mut* mice with age and did not mitigate the reduction in cardiac mitochondrial function. *PolgA^mut/mut* mice had significant reduction in body condition, weight loss and diminished thermoregulatory capacity compared with age-matched WT mice. I showed significant age-related decline in physical function in comparison to *PolgA^+/+* mice confirming previous studies (Trifunovic *et al*, 2004; Kujoth *et al*, 2005). The established decline in cardiac mitochondrial function, cardiomyocyte hypertrophy, cardiomyocyte apoptosis and accumulation of cardiac fibrosis in *PolgA^mut/mut* mice was not altered with endurance exercise. Solitary-housing in general appeared to accelerate the deterioration in body condition and implement a decline in locomotive activity from a younger age regardless of the state of physical activity. In contrast with the findings of this study, Safdar *et al* (2011) reported that endurance exercise alleviates premature aging phenotypes and induces mitochondrial rejuvenation in solitary-housed *PolgA^mut/mut* mice. They have averaged their findings from male and female mice and observed significant reduction in lifespan of sedentary mice in comparison to exercised mice. This may skew their results since clinical scoring for example is influenced by aggression in males and hormonal factors in female mice. Interestingly, group-housed exercised and non-exercised *PolgA^mut/mut* mice revealed fewer apoptotic cells in the heart in comparison to exercised and non-exercised *PolgA^mut/mut* mice housed in solitude. Exercise in the setting of single-housing however did not seem to be able to alleviate cardiomyocyte apoptosis in comparison to non-exercised cohort. This may mean that housing condition, may partly play a role in cardiac apoptosis regardless of the status of physical activity of *PolgA^mut/mut* mice.

Endurance exercise had no effect on CI and CIV expression and CIV activity in the cardiac muscle of group-housed *PolgA^{mut/mut}* mice. CIV activity however was further diminished when mice were singly-housed. Again, confirming that housing condition may play a role in cardiac mitochondrial function regardless of the status of physical activity of *PolgA^{mut/mut}* mice. My study also showed that exercise and single-housing did not have an impact on mitochondrial biogenesis as demonstrated by mitochondrial mass (porin) expression levels. Mitochondrial mass in skeletal muscle was suggested to be increased with endurance exercise (Koltai *et al*, 2012) due to the higher demand on energy production machinery of working muscle. Vettor *et al* (2014) demonstrated that eNOS plays a significant role in upregulation of mitochondrial biogenesis and PGC-1α in the cardiac muscle of rodent models.

Singly-housed exercised mice appeared to have higher CI and CIV expression levels in comparison to singly-housed sedentary mice, however the activity of CIV was non-significant between the groups. The presence of non-active CIV protein is not enough to improve mitochondrial function. Safdar *et al* (2011) suggested that 6 months of endurance exercise attenuated all the symptoms of pre-mature aging previously described by Trifunovic *et al* (2004) and Kujoth *et al* (2005). They have also found that exercise restored mtDNA depletion, reduced the frequency of mtDNA point mutations, maintained mitochondrial morphology and increased mitochondrial biogenesis by an increase in mitochondrial ETC subunits and CIV activity. The methodology by which this research group had conducted their study was unclear. For instance, 18 mice from each gender was selected, however molecular data was conducted on <5 mice while gender was not stated, which raises the question of whether those mice were selected randomly or not. If only four mice lived until 72 weeks as they have suggested, then statistics will not be as reliable for such strong claims.

In the normal aging C57BL6/J mouse study, I have confirmed that the body condition, physical function and muscle strength of mice deteriorates with normal aging. I have also observed reduction in LVMI, LVEDVI and LVESVI with age in agreement with a study carried out by Fiechter *et al* (2013). The cardiovascular changes which occur with increasing age are suggested to play a major role in the response of the CV system to disease. The significant decline in ventricular chamber volume and dimension with age could be a compensatory response to the decline in LV muscle mass in an attempt to maintain normal EF. Since body weight was increased in the

mice with advancing age, normalisation of cardiac volumes and mass data may at least in part mask the changes observed in ventricular volumes observed with aging. With increasing body weight, both blood volume and cardiac output increases to meet the body's increased metabolic rate. Therefore, it was necessary to normalise cardiac function measurements to each mouse's body weight as previously described (Maceira *et al*, 2006; fuchs *et al*, 2016) in order to visualise changes that occur as a result of exercise and age and not weight gain. Moreover, I presented evidence of decreased resting HR with age. Previous studies have reported an age-related decline in maximal HR (Fuchi *et al*, 1989; Hagberg *et al*, 1985; Rivera *et al*, 1989), but not a significant change in resting HR. One of the limitations of obtaining haemodynamic measures in this study was a lack of data on the impact of animal handling, restraining during the measurements and no alternative method for measuring BP and HR. There was a significant animal-to-animal and time-dependent variation in tail-cuff method of obtaining BP and HR in mice which may bias the results if they're not taken over many trials. A study published by Wilde *et al* in 2017 compared the telemetry method of obtaining BP non-invasively and the tail-cuff method and concluded that the latter underestimates the core blood pressure changes during handling and restraining of mice which directly affects cardiovascular parameters such as the heart rate and core body temperature. Core body temperature can ultimately affect blood pressure i.e. lower temperatures can cause dilation of blood vessels to increase blood pressure (Mayo clinic, 2019).

My study showed a significant reduction in peak oxygen consumption rate ($VO_{2\ peak}$) with age in agreement with previous research (Chow *et al,* 2007). A number of studies have reported a 10% decline in $VO_{2\ max}$ per decade after the age of 25 which increases up to 15% from the age of 50 onwards in non-active healthy individuals (Robinson, 1938; Astrand, 1960; Hawkins and Wiswell, 2003). A general decline in $VO_{2\ max}$ with age is suggested to be a result of declined cardiac output and therefore reduced blood supply to the active muscle (Kim *et al,* 2016).

In the late-life endurance exercise intervention study, I demonstrated that exercised mice had a significantly slower decline in their body condition and significantly lower body weight post-intervention in comparison to the sedentary group. The body weight of exercised mice remained steady throughout the intervention. Improvements in the muscle strength of exercised mice was also observed post-intervention. This finding is parallel to the study carried out by Joanisse *et al* (2016) where the skeletal muscle

strength was assessed through rotarod testing in old C57BL6/J mice. The authors have reported that 8 weeks of progressive exercise training improved the regenerative capacity of skeletal muscle in aged male mice. There is also evidence that late-life exercise may improve physical function and reduce disability in developed countries (Ettinger *et al*, 1997; Jette *et al,* 1999; Minor *et al*, 1989). My study suggested there may be a potential improvements in aerobic capacity of exercised mice as shown by slower rate of $VO_{2\ peak}$ decline with age. A slow decline in $VO_{2\ max}$ has also been observed in athletes of low-impact sports such as rowing with increasing age (Reaburn and Dascombe, 2008). In addition the rate of age-related $VO_{2\ max}$ decline in male master athletes is documented to be approximately one-half the rate of decline observed in non-exercised age-matched males (Rogers *et al,* 1990). $VO_{2\ peak}$ as a measure of oxidative function was used in this study as an important factor in assessing the improvements in the rate of aerobic capacity decline with age.

In agreement with this study, a study carried out by a group of scientists in University of Texas on more than 50 participants of between the age of 45-64 have showed that moderate aerobic exercise for two years restores LV elasticity and compliance by 25% and improves VO_2 max by 18%, reducing the chances of developing heart failure in later life (Erin *et al*, 2018). They also found that LVEDV was increased with exercise, contributing to greater stroke volume for any filling pressure. A study by Hawkins and Wiswell (2003) reported that it is harder to reduce VO_2 max loss with regular exercise in older men and women rather than middle-aged individuals, due to both central and peripheral adaptations with age.

Another study conducted by Zhao and Ma (2016) revealed that a swimming intervention in male C57BL6/J mice for 8 weeks developed cardioprotection against apoptosis by reducing the apoptosis-related microRNAs (miRNAs) and enhancing Bcl-2/Bax ratio in the cardiac muscle of exercised mice. Similarly, 4 weeks of swimming exercise in an $AMPK^{-/-}$ mouse model revealed attenuation of isoproterenol-induced cardiac fibrosis by inhibiting NADPH oxidase-ROS pathway mediated AMPK activation (Ma *et al*, 2015). Isoproterenol was used as a non-selective β-AR agonist to induce cardiac fibrosis. One study suggests that miRNAs respond to exercise by inhibiting excessive collagen formation, increasing angiogenesis and regulating the renin-angiotensin system (Fernandes *et al,* 2015). The increase in angiogenesis and

cardiomyocyte size growth was found to be associated with a series of miRNAs with cardioprotective roles.

I have also observed a significant reduction in cardiac apoptosis in exercised mice in comparison to sedentary mice. Interestingly, a study by Kwak, Song and Lawler (2006) reported an age-related increase in mitochondrial Bax/Bcl-2 ratio and exercise-induced amelioration of mitochondrial mediated apoptosis with age, leading to diminished DNA fragmentation. A study by Nakajima *et al* (2010) showed that chronic endurance exercise in older people increases the methylation of pro-inflammatory apoptosis-related speck-like protein caspase (ASC) genes in circulatory blood which otherwise decrease with advancing age. These group of ASC proteins are responsible for modulating IL-18 and IL-1B cytokines. Nakajima *et al* (2010) reported that exercise is associated with attenuation of the age-related increase in pro-inflammatory cytokines. However, no significant exercise-induced changes in the level of muscle cytokines were observed in my study. Also, the balance in the number and distribution of cardiomyocytes and fibroblasts is disturbed with age, leading to inflammation and cardiac fibrosis (Kyselvic and Leddy, 2017). I have demonstrated that endurance exercise in a normal ageing mouse model reduces cardiac fibrosis in agreement with the study carried out Kyselvic and Leddy in 2017. Fibroblasts secrete extracellular collagen chains under physiological conditions which assemble into cross-links of fibrils in the interstitium. The authors concluded that cardiac remodelling through exercise is beneficial, decreasing cardiac fibrosis, increasing PI3K activity, improving calcium handling and endothelial function from increases in nitric oxide (NO) production. Similarly, Xu *et al* (2008) have shown that the levels of angiotensin-II were significantly reduced in ischaemic patients that underwent exercise training. This resulted in reduced fibrogenesis as a measure of decreased expression of tissue inhibitor of metalloproteinase-1 (TIMP-1) which promotes accumulation of myocardial fibrosis (Takawale *et al*, 2017) with unchanged expression of matrix metalloproteinase-1 which attenuates the development of myocardial fibrosis (Foronjy *et al*, 2008). Xu *et al* (2008) have also documented a significant reduction in collagenous tissue in LV cross-sections of exercised mice in comparison to non-active mice suggesting that myocardial fibrosis is attenuated in infarcted hearts with endurance exercise. Giannuzzi *et al* (2003) have shown that long-term moderate exercise training in 90 patients with chronic stable heart failure

attenuated abnormal cardiac remodelling and improved exercise tolerance and quality of life.

The effects of endurance exercise on mitochondrial OXPHOS function has also been extensively researched in the past. Lundby and Jacos (2015) have shown that with exercise training, the population of intermyofibrillar mitochondrial volume density increases significantly as well as mitochondrial proteins that facilitate aerobic metabolism. These adaptations and the magnitude of change was suggested to be dependent on both exercise intensity and duration. In my study, the proportion of cardiomyocytes with positive mitochondrial OXPHOS complex IV expression and activity was significantly higher in the exercised mice, demonstrating a positive shift in the expression and activity of complex IV with endurance exercise.

7.1 Use of mouse models

The premature mouse model of ageing known as *PolgA^mut/mut* mice was used in the first part of this study to investigate the effects of the accumulation of mitochondrial dysfunction on the ageing phenotype with a particular focus on the CV system, and whether endurance exercise could ameliorate this phenotype. One advantage of this mouse model was the development of early ageing phenotypes for a relatively quick study with large number of samples. In addition, humans are known to accumulate mtDNA mutations with age whereas C57BL6 mice do not to the same extent so it is a good model to use to see if exercise can improve mitochondrial function due to somatic mutations.

An advantage of using C57BL6/J mouse model of normal healthy ageing is that the maturation phase of mice is 45 times faster over the age of 5 months in comparison to human ageing which enables studies to be carried out in short period of time. A disadvantage of using mice as subjects of this study is the fact that mice do not live in their natural environment therefore their mental and physiological state may not reflect that of seen in humans.

7.2 Implications of this research on human interventions

Now that the beneficial effects of exercise in aged mouse heart have been characterised, clinical trials on human studies would be carried out more confidently. Although there are still large unknown areas, an obvious finding is that the later the endurance exercise begins in the lifetime of a healthy individual, the less the beneficial effects will be. There are obvious differences in the environmental conditions and physiology of mice and humans therefore care should be taken when designing an appropriate clinical intervention study and human subjects should be closely monitored.

7.3 Future work

An advantage of the *PolgA$^{mut/mut}$* mouse study was recruitment of a large number of samples. However, due to limited procedures that could be carried out on mice under the license of which the two studies were part of, mice were not allowed to perform an exercise intolerance test to reach their maximal aerobic capacity (VO$_{2\ max}$) for a more tailored exercise regime. Since the molecular mechanism underlying normal age-related changes vary to that of premature age-related changes, I have observed no improvements in *PolgA$^{mut/mut}$* mitochondrial and cardiac function but promising improvements in mouse model of normal ageing with exercise (C57BL6/J mice).

Future work would include taking into account the external factors such as microenvironment, diet, housing conditions, thermoregulation, stress, social interactions, and genetics of mice whom respond better to exercise interventions. Using an optimal ageing systems where exercise may be more beneficial on long term interventions is also an important point to consider. There is more control in rodent models over genetics, external factors such as housing, diet and level of exercise they undergo. However, in humans there is more control over how much one can tolerate exercise and that communication makes interventions easier both for the researcher and the subjects. A downfall of performing a research on rodents is that monitoring and scoring of clinical conditions are assessed using a human-based scoring system. Mice are tested throughout the intervention without them having any understanding of the procedure and that may exert extra stress on mice which should also be considered.

7.4 Final conclusion

This research has successfully assessed the baseline characteristics, cardiac pathology and mitochondrial function in accelerated ageing *PolgA^{mut/mut}* mouse model and normal ageing C57BL6/J mouse model.
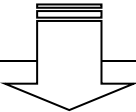
The normal aging process has an impact on ventricular ESV and EDV as well as LV mass in healthy aged mice. Exercise in part has managed to alleviate the cardiac fibrosis and apoptosis that is normally seen within aged heart. C57BL6/J mice as normal ageing mouse model were more successful in benefiting from the exercise regime than the *PolgA^{mut/mut}* mice. This could be due to the fact that mutator mice experience higher mtDNA mutation burden from younger age. Single-housing in these subset of mice seems to be able to shift the manifestation of disease to younger age since solitary housed mice show accelerated decline in body condition straight after their cage separation pre-intervention at 14 weeks of age. My data suggest that wherever possible male mice should be group housed.

Appendices

Chapter 8. Appendices

Appendix 1. Mouse monitoring criteria, used to assess clinical phenotypes of
PolgA^{mut/mut} and C57BL/6J mice for severity and progression of body condition states
based on known clinical features of stated mice (Richardson and Greaves, 2015).

Table 8.1. Mouse monitoring recording sheet for _PolgA^{mut/mut}_ mice. One score of three, three scores of two, 20% body weight loss or temperatures below 30⁰C in one observation is an indication of ill health and mice should be monitored closely.

Mouse ID	RFID transponder		Notch	Cage	DOB		Harvest Date						
Observation	Date	Weight (g)	Weight	Coat	Skin Tone	Behaviour	Posture and Mobility	Abdominal distension	Foot colour	Faeces	Total Score	RFID Temp	Notes
1													
2													
3													

271

Table 8.2. Mouse monitoring recording sheet for C57BL6/J mice.

Mouse ID		Notch		Cage		DOB		Harvest Date					
Observation	Date	Weight (g)	Weight	Coat	Skin Tone	Behaviour	Posture and Mobility	Abdominal distension	Foot colour	Faeces	Total Score	Notes
1												
2												
3												

272

Appendix 2. Mouse Harvesting sheet. Used for *PolgA^mut/mut* and C57BL6/J mice.

Cage:	**Date:**
Mouse No:	**Storage Location:**
Harvest Number:	**Final Urine & Faeces location:**

Weighing and Measurements:

Remove any fat from tissue before weighing

Body weight	g
Liver	g
Spleen	g
Kidney R	g
Kidney L	g
Heart	g
Lung	g
Pancreas	g
Skeletal Muscle	g
Fat	g
Brain	g
S. Intestine	cm
Colon	cm

Equipment:

1. Dissection kit:

2. Scalpels

3. Formalin

4. Liquid nitrogen

5. 70% Ethanol spray

6. Labelled tubes and cassettes (blue and white)

7. Needles and syringes for blood collection and pinning the mouse

8. Ice

9. Dry ice for transport

10. PBS for perfusion of organs

11. Gloves, blue roll, yellow bag for body disposal

12. Ruler

13. Petri dishes for small intestine pinning

14. Scales

15. Weighing boats

16. Isopentane

17. Isoflurane

18. Dissection sheet guidelines

19. Body/Organ harvest sheet

20. Biopsy pads

21. Microscope

Dissection Protocol:

1. Weigh the mouse.
2. Spray the mouse with 70% EtOH, and cut open from the tail to the neck.
3. Aspirate blood from the heart and place it in ice (serum is collected from the supernatant after centrifugation at 8000rpm for 10mins).
4. Weigh each mouse tissue prior to dividing for fixing or freezing.
   a. Fixing 10% formalin
   b. Freezing in liquid N_2

Mouse Tissue
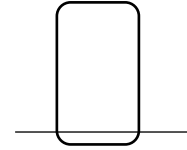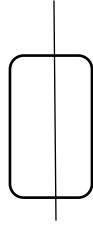
1. **Right Kidney** – Cut longitudinal, half is fixed, half is frozen.
2. **Left Kidney** – Cut transverse, half is fixed, half is frozen.
3. **Skin** – Shave skin from back, use paper towel to cut 2 slivers. One is fixed, the other is frozen
4. **Brain** – Cut between hemispheres. Left hemisphere is fixed, the right hemisphere is frozen.
5. **Fat** – follow the protocol for fat dissection (fat dissolves in formalin).
6. **Muscle** –Muscle is dunked in isopentane first. The isolated skeletal muscles include quadriceps, EDL, TA, gastrocnemius and soleus muscles from both legs. The left leg muscles were fixed, and the right leg muscle was frozen. Quadriceps of right leg was homogenised for protein extraction.
7. **Lung** – Left lung (2lobes) is fixed, the right lung is frozen.
8. **Heart** – Cut longitudinal, right side is fixed and left side is slowly cooled in isopentane.

9. **Spleen** - Half the spleen goes into the tissue cassette with the Liver. The other half of the spleen gets frozen.
10. **Liver**– Triangular lobe of liver goes into tissue cassette. Cut a capsule off the bilobulated lobe and discard. Cut a sliver from the exposed capsule and place into tissue cassette. Cut a capsule off the large lobe and discard. Cut a sliver from the exposed capsule. Cut two squares from this sliver, one gets frozen for RNA, the other gets frozen for protein. The rest of the liver gets frozen.
11. **Pancreas** – This is located wrapped around the proximal SI next to the stomach. It is hard to distinguish from fat, however, if required, the pancreas sinks and fat floats in water. Half the pancreas is fixed, the other half is frozen.
12. **SI** – Measure the SI its contents are then collected. 2 ends of the SI are frozen. The rest is rolled up into a coil and fixed

13. **Colon** – The contents of the colon is collected. 2 ends of the colon are frozen. The rest is fixed.

14. **Caecum** – The contents of the caecum is collected.

15. **Stomach** – The contents of the stomach is emptied. The stomach is rolled up. A sliver is cut to be frozen. The rest is fixed.

Appendix 3. Expanded RM3 chow diet composition. Used for *PolgA^mut/mut* and C57BL6/J mice (Special Diet Services, LSB Biotech).

Calculated Analysis

Rat and Mouse No.3 Breeding (E)

NUTRIENTS		Total	Supp (9)
Proximate Analysis			
Moisture (1)	%	10.00	
Crude Oil	%	4.25	
Crude Protein	%	22.39	
Crude Fibre	%	4.21	
Ash	%	7.56	
Nitrogen Free Extract	%	51.20	
Digestibility Co-Efficients (7)			
Digestible Crude Oil	%	3.86	
Digestible Crude Protein	%	20.21	
Carbohydrates, Fibre and Non Starch Polysaccharides (NSP)			
Total Dietary Fibre	%	15.43	
Pectin	%	1.43	
Hemicellulose	%	9.20	
Cellulose	%	3.93	
Lignin	%	1.50	
Starch	%	33.92	
Sugar	%	5.75	
Energy (5)			
Gross Energy	MJ/kg	15.21	
Digestible Energy (15)	MJ/kg	12.42	
Metabolisable Energy (15)	MJ/kg	11.36	
Atwater Fuel Energy (AFE) (8)	MJ/kg	13.90	
AFE from Oil	%	11.50	
AFE from Protein	%	26.93	
AFE from Carbohydrate	%	61.57	
Fatty Acids			
Saturated Fatty Acids			
C12:0 Lauric	%	0.05	
C14:0 Myristic	%	0.20	
C16:0 Palmitic	%	0.36	
C18:0 Stearic	%	0.09	
Monounsaturated Fatty Acids			
C14:1 Myristoleic	%	0.01	
C16:1 Palmitoleic	%	0.13	
C18:1 Oleic	%	1.03	
Polyunsaturated Fatty Acids			
C18:2(ω6) Linoleic	%	1.15	
C18:3(ω3) Linolenic	%	0.17	
C20:4(ω6) Arachidonic	%	0.22	
C22:5(ω3) Clupanodonic	%	0.04	
Amino Acids			
Arginine	%	1.54	
Lysine (6)	%	1.33	0.09
Methionine	%	0.34	
Cystine	%	0.34	
Tryptophan	%	0.27	
Histidine	%	0.57	
Threonine	%	0.86	
Isoleucine	%	0.98	
Leucine	%	1.68	
Phenylalanine	%	1.03	
Valine	%	1.10	
Tyrosine	%	0.80	
Taurine	%		
Glycine	%	1.88	
Aspartic Acid	%	1.43	

NUTRIENTS		Total	Supp (9)
Glutamic Acid	%	4.07	
Proline	%	1.38	
Serine	%	0.97	
Hydroxyproline	%	0.06	
Hydroxylysine	%		
Alanine	%	0.14	
Macro Minerals			
Calcium	%	1.15	0.56
Total Phosphorus	%	0.82	0.09
Phytate Phosphorus	%	0.25	
Available Phosphorus	%	0.58	0.09
Sodium	%	0.32	0.19
Chloride	%	0.43	0.31
Potassium	%	0.81	
Magnesium	%	0.29	0.04
Micro Minerals			
Iron	mg/kg	188.17	82.50
Copper	mg/kg	20.28	8.75
Manganese	mg/kg	102.01	52.70
Zinc	mg/kg	51.34	8.64
Cobalt	µg/kg	617.02	525.00
Iodine	µg/kg	1395.12	775.00
Selenium	µg/kg	497.70	200.00
Fluorine	mg/kg	9.24	
Vitamins			
β-Carotene (2)	mg/kg	0.15	
Retinol (2)	µg/kg	5977.24	5812.50
Vitamin A (2)	iu/kg	19923.60	19375.00
Cholecalciferol (3)	µg/kg	102.22	72.50
Vitamin D (3)	iu/kg	4088.65	2900.00
α-Tocopherol (4)	mg/kg	100.35	81.14
Vitamin E (4)	iu/kg	110.39	89.25
Vitamin B₁ (Thiamine)	mg/kg	27.08	19.11
Vitamin B₂ (Riboflavin)	mg/kg	10.60	7.60
Vitamin B₆ (Pyridoxine)	mg/kg	19.54	14.46
Vitamin B₁₂ (Cyanocobalamine)	µg/kg	26.78	17.75
Vitamin C (Ascorbic Acid)	mg/kg	1.33	
Vitamin K (Menadione)	mg/kg	4.15	3.72
Folic Acid (Vitamin B₉)	mg/kg	2.73	0.49
Nicotinic Acid (Vitamin PP) (6)	mg/kg	85.00	19.11
Pantothenic Acid (Vitamin B₃₅)	mg/kg	40.27	23.80
Choline (Vitamin B₄₇)	mg/kg	1641.65	366.60
Inositol	mg/kg	1903.20	
Biotin (Vitamin H) (6)	µg/kg	322.87	

Notes
1. All values are calculated using a moisture basis of 10%.
   Typical moisture levels will range between 9.5 - 11.5%.
2. a. Vitamin A includes Retinol and the Retinol equivalents of β-carotene
   b. Retinol includes the Retinol equivalents of β-Carotene.
   c. 0.48 µg Retinol = 1 µg β-carotene = 1.6 iu Vitamin A activity
   d. 1 µg Retinol = 3.33* iu Vitamin A activity
   e. 1 iu Vitamin A = 0.3 µg Retinol = 0.6 µg β-carotene
   f. The standard analysis for Vitamin A does not detect β-carotene
3. 1µg Cholecalciferol (D₃) = 40.0 iu Vitamin D
4. 1 mg all-rac-α-tocopherol = 1.1 iu Vitamin E activity
   1 mg all-rac-α-tocopherol acetate = 1.0 iu Vitamin E activity
5. 1 MJ = 239.23 Kcalories = 239.23 Calories = 239,230 calories
6. These nutrients coming from natural raw materials such as cereals may have low availabilities due to the interactions with other compounds.
7. Based on in-vitro digestibility analysis.
8. AF Energy = Atwater Fuel Energy = ((CO%/100)*9000}+
   ((CP%/100)*4000)+((NFE%/100)*4000)/239.23
9. Supplemented nutrients from manufactured and mined sources.
15. Calculated.

References

Chapter 9. References

Ades, E. (2019). *Species Specific Information: Mouse.* [online] Web.jhu.edu. Available at: http://web.jhu.edu/animalcare/procedures/mouse.html [Accessed 18 Mar. 2019].

Agosto, M, Azrin, M, Singh, K, Jaffe, A. and Liang, B. (2011). Serum Caspase-3 p17 Fragment Is Elevated in Patients With ST-Segment Elevation Myocardial Infarction. Journal of the American College of Cardiology, 57(2), pp.220-221.

Ahlqvist, K, Hämäläinen, R, Yatsuga, S, Uutela, M, Terzioglu, M, Götz, A, Forsström, S, Salven, P, Angers-Loustau, A, Kopra, O, Tyynismaa, H, Larsson, N, Wartiovaara, K, Prolla, T, Trifunovic, A. and Suomalainen, A. (2012). Somatic Progenitor Cell Vulnerability to Mitochondrial DNA Mutagenesis Underlies Progeroid Phenotypes in Polg Mutator Mice. Cell Metabolism, 15(1), pp.100-109.

Akasheva, D, Plokhova, E, Tkacheva, O, Strazhesko, I, Dudinskaya, E, Kruglikova, A, Pykhtina, V, Brailova, N, Pokshubina, I, Sharashkina, N, Agaltsov, M, Skvortsov, D. and Boytsov, S. (2015). Age-Related Left Ventricular Changes and Their Association with Leukocyte Telomere Length in Healthy People. PLOS ONE, 10(8), p.e0135883.

Al Rawi, S, Louvet-Vallee, S, Djeddi, A, Sachse, M, Culetto, E, Hajjar, C, Boyd, L, Legouis, R. and Galy, V. (2011). Postfertilization Autophagy of Sperm Organelles Prevents Paternal Mitochondrial DNA Transmission. *Science,* 334(6059), pp.1144-1147.

Alberts, B, Bray, D, Lewis, J, Raff, M, Roberts, K. and Watson, J. (1994). *Molecular biology of the cell.* 3rd ed. New York: Garland.

Alberts, B, Johnson, A, Lewis, J, Raff, M, Roberts, K. and Walter, P. (2002). Molecular Biology of the Cell. 4th ed. New York: Garland Science.

Anderson, S, Bankier, A, Barrell, B, de Bruijn, M, Coulson, A, Drouin, J, Eperon, I, Nierlich, D, Roe, B, Sanger, F, Schreier, P, Smith, A, Staden, R. and Young, I.

(1981). Sequence and organization of the human mitochondrial genome. Nature, 290(5806), pp.457-465.

Andziak, B. and Buffenstein, R. (2006). Disparate patterns of age-related changes in lipid peroxidation in long-lived naked mole-rats and shorter-lived mice. Aging Cell, 5(6), pp.525-532. 316 Antico Arciuch, V, Elguero, M, Poderoso, J. and Carreras, M. (2012). Mitochondrial Regulation of Cell Cycle and Proliferation.

Antico Arciuch, V, Elguero, M, Poderoso, J. and Carreras, M. (2012). Mitochondrial Regulation of Cell Cycle and Proliferation. *Antioxidants & Redox Signaling*, 16(10), pp.1150-1180.

Aragonés, J, Schneider, M, Van Geyte, K, Fraisl, P, Dresselaers, T, Mazzone, M, Dirkx, R, Zacchigna, S, Lemieux, H, Jeoung, N, Lambrechts, D, Bishop, T, Lafuste, P, Diez-Juan, A, Harten, S, Van Noten, P, De Bock, K, Willam, C, Tjwa, M, Grosfeld, A, Navet, R, Moons, L, Vandendriessche, T, Deroose, C, Wijeyekoon, B, Nuyts, J, Jordan, B, Silasi-Mansat, R, Lupu, F, Dewerchin, M, Pugh, C, Salmon, P, Mortelmans, L, Gallez, B, Gorus, F, Buyse, J, Sluse, F, Harris, R, Gnaiger, E, Hespel, P, Van Hecke, P, Schuit, F, Van Veldhoven, P, Ratcliffe, P, Baes, M, Maxwell, P. and Carmeliet, P. (2008). Deficiency or inhibition of oxygen sensor Phd1 induces hypoxia tolerance by reprogramming basal metabolism. Nature Genetics, 40(2), pp.170-180.

Archer, S. (2013). Mitochondrial Dynamics — Mitochondrial Fission and Fusion in Human Diseases. New England Journal of Medicine, 369(23), pp.2236-2251.

Asdell, S, Doornenbal, H, Joshi, S. and Sperling, G. (1967). The effects of sex steroid hormones upon longevity in rats. Reproduction, 14(1), pp.113-120.

Ashley, M, Laipis, P. and Hauswirth, W. (1989). Rapid segregation of heteroplasmic bovine mitodiondria. *Nucleic Acids Research*, 17(18), pp.7325-7331.

Astrand I. Aerobic work capacity in men and women with special reference to age. Acta Physiol Scand Suppl. 1960; 49: 1–92. 3.

Athanasiou, L, Fotiadis, D. and Michalis, L. (2017). Introduction. Atherosclerotic Plaque Characterization Methods Based on Coronary Imaging, pp.1-21. Athanasiou,

L, Fotiadis, D. and Michalis, L. (2017). Introduction. Atherosclerotic Plaque Characterization Methods Based on Coronary Imaging, pp.1-21.

Attanasio, C. and Netti, P. (2017). Bioreactors for Cell Culture Systems and Organ Bioengineering. Kidney Transplantation, Bioengineering and Regeneration, pp.889-899. 317 Attardi, G. and Montoya, J. (1983). [41] Analysis of human mitochondrial RNA.

Attardi, G. and Montoya, J. (1983). [41] Analysis of human mitochondrial RNA. Biomembranes Part K: Membrane Biogenesis: Assembly and Targeting (Prokaryotes, Mitochondria, and Chloroplasts), pp.435-469.

Aubert, G, Vega, R. and Kelly, D. (2013). Perturbations in the gene regulatory pathways controlling mitochondrial energy production in the failing heart. Biochimica et Biophysica Acta (BBA) - Molecular Cell Research, 1833(4), pp.840-847.

Austad, S. and Fischer, K. (2016). Sex Differences in Lifespan. *Cell Metabolism*, 23(6), pp.1022-1033.

Austin, S. and St-Pierre, J. (2012). PGC1 and mitochondrial metabolism - emerging concepts and relevance in ageing and neurodegenerative disorders. Journal of Cell Science, 125(21), pp.4963-4971.

Avila, J., Kim, S. and Massett, M. (2017). Differences in Exercise Capacity and Responses to Training in 24 Inbred Mouse Strains. *Frontiers in Physiology*, 8.

Balaban, R. (2012). Metabolic homeostasis of the heart: Figure 1. The Journal of General Physiology, 139(6), pp.407-414.

Balaban, R, Nemoto, S. and Finkel, T. (2005). Mitochondria, Oxidants, and Aging. *Cell*, 120(4), pp.483-495.

Baloh, R, Schmidt, R, Pestronk, A. and Milbrandt, J. (2007). Altered Axonal Mitochondrial Transport in the Pathogenesis of Charcot-Marie-Tooth Disease from Mitofusin 2 Mutations. Journal of Neuroscience, 27(2), pp.422-430.

Bandy, B. and Davison, A. (1990). Mitochondrial mutations may increase oxidative stress: Implications for carcinogenesis and aging?. *Free Radical Biology and Medicine*, 8(6), pp.523-539.

Barja, G. (2002). Rate of generation of oxidative stress-related damage and animal longevity. Free Radical Biology and Medicine, 33(9), pp.1167-1172.

Barth, J, Schneider, S. and von Känel, R. (2010). Lack of Social Support in the Etiology and the Prognosis of Coronary Heart Disease: A Systematic Review and Meta-Analysis. *Psychosomatic Medicine*, 72(3), pp.229-238.

Bartolomucci, A, Palanza, P. and Parmigiani, S. (2002). Group housed mice: are they really stressed? *Ethology Ecology & Evolution*, 14(4), pp.341-350.

Bassuk, S, Glass, T. and Berkman, L. (1999). Social Disengagement and Incident Cognitive Decline in Community-Dwelling Elderly Persons. *Annals of Internal Medicine*, 131(3), p.165.

Bayod, S, del Valle, J, Lalanza, J, Sanchez-Roige, S, de Luxán-Delgado, B, CotoMontes, A, Canudas, A, Camins, A, Escorihuela, R. and Pallàs, M. (2012). Longterm physical exercise induces changes in sirtuin 1 pathway and oxidative parameters in adult rat tissues. Experimental Gerontology, 47(12), pp.925-935. 318

Beer, M, Seyfarth, T, Sandstede, J, Landschütz, W, Lipke, C, Köstler, H, von Kienlin, M, Harre, K, Hahn, D. and Neubauer, S. (2002). Absolute concentrations of high-energy phosphate metabolites in normal, hypertrophied, and failing human myocardium measured noninvasively with 31P-SLOOP magnetic resonance spectroscopy. Journal of the American College of Cardiology, 40(7), pp.1267-1274.

Bender, A, Krishnan, K, Morris, C, Taylor, G, Reeve, A, Perry, R, Jaros, E, Hersheson, J, Betts, J, Klopstock, T, Taylor, R. and Turnbull, D. (2006). High levels of mitochondrial DNA deletions in substantia nigra neurons in aging and Parkinson disease. Nature Genetics, 38(5), pp.515-517.

Bénit, P, Lebon, S. and Rustin, P. (2009). Respiratory-chain diseases related to complex III deficiency. Biochimica et Biophysica Acta (BBA) - Molecular Cell Research, 1793(1), pp.181-185.

Bergman, O. and Ben-Shachar, D. (2016). Mitochondrial Oxidative Phosphorylation System (OXPHOS) Deficits in Schizophrenia. The Canadian Journal of Psychiatry, 61(8), pp.457-469.

Berliner, J, Navab, M, Fogelman, A, Frank, J, Demer, L, Edwards, P, Watson, A. and Lusis, A. (1995). Atherosclerosis: Basic Mechanisms. Circulation, 91(9), pp.2488-2496.

Bernal, G, Wahlstrom, J, Crawley, C, Cahill, K, Pytel, P, Liang, H, Kang, S, Weichselbaum, R. and Yamini, B. (2014). Loss of <i>Nfkb1</i> leads to early onset aging. *Aging*, 6(11), pp.931-942.

Bers, D. (2002). Cardiac excitation–contraction coupling. *Nature*, 415(6868), pp.198-205. Image

Betik, A. and Hepple, R. (2008). Determinants of VO2 max decline with aging: an integrated perspective. Applied Physiology, Nutrition, and Metabolism, 33(1), pp.130-140.

Betts, J. (2013). Anatomy & physiology. Bhatnagar, P, Wickramasinghe, K, Williams, J, Rayner, M. and Townsend, N. (2015). The epidemiology of cardiovascular disease in the UK 2014. Heart, 101(15), pp.1182-1189.

Bhf.org.uk. (2019). Cardiovascular Disease Statistics 2018. [online] Available at: https://www.bhf.org.uk/what-we-do/our-research/heart-statistics/heart-statisticspublications/cardiovascular-disease-statistics-2018 [Accessed 18 Jul. 2019].

Bhf.org.uk. (2019). How your heart works. [Online] Available at: https://www.bhf.org.uk/informationsupport/how-a-healthy-heart-works [Accessed 1 May 2019].

Bhf.org.uk. (2019). *Heart and Circulatory Diseases Statistics 2018*. [online] Available at: https://www.bhf.org.uk/what-we-do/our-research/heart-statistics/heart-statistics-publications/cardiovascular-disease-statistics-2018 [Accessed 7 Jan. 2019].

Bibb, M, Van Etten, R, Wright, C, Walberg, M. and Clayton, D. (1981). Sequence and gene organization of mouse mitochondrial DNA. Cell, 26(2), pp.167-180.

Biomembranes Part K: Membrane Biogenesis: Assembly and Targeting (Prokaryotes, Mitochondria, and Chloroplasts), pp.435-469.

Bishop, D, Granata, C. and Eynon, N. (2014). Can we optimise the exercise training prescription to maximise improvements in mitochondria function and content?. Biochimica et Biophysica Acta (BBA) - General Subjects, 1840(4), pp.1266- 1275.

Bjorksten, J. and Tenhu, H. (1990). The crosslinking theory of aging — Added evidence. Experimental Gerontology, 25(2), pp.91-95.

Blasiak, J., Glowacki, S., Kauppinen, A. and Kaarniranta, K. (2013). Mitochondrial and Nuclear DNA Damage and Repair in Age-Related Macular Degeneration. *International Journal of Molecular Sciences*, 14(2), pp.2996-3010.

Blomqvist, C. and Saltin, B. (1983). Cardiovascular Adaptations to Physical Training. Annual Review of Physiology, 45(1), pp.169-189. 320

Boczonadi, V. and Horvath, R. (2014). Mitochondria: Impaired mitochondrial translation in human disease. The International Journal of Biochemistry & Cell Biology, 48, pp.77-84.

Boczonadi, V, Ricci, G. and Horvath, R. (2018). Mitochondrial DNA transcription and translation: clinical syndromes. Essays In Biochemistry, 62(3), pp.321-340.

Bogenhagen, D. and Clayton, D. (1977). Mouse L cell mitochondrial DNA molecules are selected randomly for replication throughout the cell cycle. Cell, 11(4), pp.719-727.

Bonora, M., Patergnani, S., Rimessi, A., De Marchi, E., Suski, J., Bononi, A., Giorgi, C., Marchi, S., Missiroli, S., Poletti, F., Wieckowski, M. and Pinton, P. (2012). ATP synthesis and storage. *Purinergic Signalling*, 8(3), pp.343-357.

Borta, A, Schwarting, R. K. Inhibitory avoidance, pain reactivity, and plus-maze behavior in Wistar rats with high versus low rearing activity. J. Phys. Behav. 84, 387-396 (2005).

Boulet, L, Karpati, G. & Shoubridge, E. A. Distribution and threshold expression of the tRNALys mutation in skeletal muscle of patients with myoclonic epilepsy and ragged-red fibers (MERRF). Am. J. Hum. Genet. 51, 1187–1200 (1992).

Boushel, R, Gnaiger, E, Schjerling, P, Skovbro, M, Kraunsøe, R. and Dela, F. (2007). Patients with type 2 diabetes have normal mitochondrial function in skeletal muscle. Diabetologia, 50(4), pp.790-796.

Bowmaker, M, Yang, M, Yasukawa, T, Reyes, A, Jacobs, H, Huberman, J. and Holt, I. (2003). Mammalian Mitochondrial DNA Replicates Bidirectionally from an Initiation Zone. Journal of Biological Chemistry, 278(51), pp.50961-50969.

Boengler, K., Kosiol, M., Mayr, M., Schulz, R. and Rohrbach, S. (2017). Mitochondria and ageing: role in heart, skeletal muscle and adipose tissue. *Journal of Cachexia, Sarcopenia and Muscle*, 8(3), pp.349-369.

Bras, M, Queenan, B. and Susin, S. (2005). Programmed cell death via mitochondria: Different modes of dying. Biochemistry (Moscow), 70(2), pp.231-239.

Brierley, E, Johnson, M, Lightowlers, R, James, O. and Turnbull, D. (1998). Role of mitochondrial DNA mutations in human aging: Implications for the central nervous system and muscle. Annals of Neurology, 43(2), pp.217-223.

Bressenot, A., Marchal, S., Bezdetnaya, L., Garrier, J., Guillemin, F. and Plénat, F. (2008). Assessment of Apoptosis by Immunohistochemistry to Active Caspase-3, Active Caspase-7, or Cleaved PARP in Monolayer Cells and Spheroid and Subcutaneous Xenografts of Human Carcinoma. *Journal of Histochemistry & Cytochemistry*, 57(4), pp.289-300.

Brown, D, Perry, J, Allen, M, Sabbah, H, Stauffer, B, Shaikh, S, Cleland, J, Colucci, W, Butler, J, Voors, A, Anker, S, Pitt, B, Pieske, B, Filippatos, G, Greene, S. and Gheorghiade, M. (2016). Mitochondrial function as a therapeutic target in heart failure. Nature Reviews Cardiology, 14(4), pp.238-250. 321

Brubaker, P. and Kitzman, D. (2011). Chronotropic Incompetence. *Circulation*, 123(9), pp.1010-1020.

Bua, E, Johnson, J, Herbst, A, Delong, B, McKenzie, D, Salamat, S. and Aiken, J. (2006). Mitochondrial DNA–Deletion Mutations Accumulate Intracellularly to Detrimental Levels in Aged Human Skeletal Muscle Fibers. *The American Journal of Human Genetics*, 79(3), pp.469-480.

Bundy, M. and Leaver, A. (2010). Training and conditioning. A Guide to Sports and Injury Management, pp.1-9.

Burgess, M, McCrea, J. and Hedrick, H. (2001). Age-associated changes in cardiac matrix and integrins. Mechanisms of Ageing and Development, 122(15), pp.1739-1756.

Burri, L, Vascotto, K, Gentle, I, Chan, N, Beilharz, T, Stapleton, D, Ramage, L. and Lithgow, T. (2006). Integral membrane proteins in the mitochondrial outer membrane of Saccharomyces cerevisiae. FEBS Journal, 273(7), pp.1507-1515.

Cai, Y, Bullard, J, Thompson, N. and Spremulli, L. (2000). Interaction of Mitochondrial Elongation Factor Tu with Aminoacyl-tRNA and Elongation Factor Ts. Journal of Biological Chemistry, 275(27), pp.20308-20314.

Cain, P, Ahl, R, Hedstrom, E, Ugander, M, Allansdotter-Johnsson, A, Friberg, P, Marild, S. and Arheden, H. (2007). Physiological determinants of the variation in left ventricular mass from early adolescence to late adulthood in healthy subjects. Clinical Physiology and Functional Imaging, 27(4), pp.254-262.

Cain, P, Ahl, R, Hedstrom, E, Ugander, M, Allansdotter-Johnsson, A, Friberg, P. and Arheden, H. (2009). Age and gender specific normal values of left ventricular mass,

volume and function for gradient echo magnetic resonance imaging: a cross sectional study. BMC Medical Imaging, 9(1).

Calvert, J. and Lefer, D. (2012). Overview of Cardiac Muscle Physiology. *Muscle*, pp.57-66.

Calvert, J. and Lefer, D. (2013). Role of β-Adrenergic Receptors and Nitric Oxide Signaling in Exercise-Mediated Cardioprotection. *Physiology*, 28(4), pp.216-224.

Calvo, S, Clauser, K. and Mootha, V. (2015). MitoCarta2.0: an updated inventory of mammalian mitochondrial proteins. Nucleic Acids Research, 44(D1), pp.D1251-D1257.

Campbell, G, Krishnan, K, Deschauer, M, Taylor, R. and Turnbull, D. (2014). Dissecting the mechanisms underlying the accumulation of mitochondrial DNA deletions in human skeletal muscle. Human Molecular Genetics, 23(17), pp.4612-4620.

Campisi, J. (2000). Cellular senescence, ageing and cancer. Innovation in Aging, 2(suppl.1), pp.798-798.

Cao, L, Shitara, H, Sugimoto, M, Hayashi, J, Abe, K. and Yonekawa, H. (2009). New Evidence Confirms That the Mitochondrial Bottleneck Is Generated without Reduction of Mitochondrial DNA Content in Early Primordial Germ Cells of Mice. PLoS Genetics, 5(12), p.e1000756.

Carreiro, J. (2009). The cardiovascular system. *An Osteopathic Approach to Children*, pp.73-83.

Case, J. and Wallace, D. (1981). Maternal inheritance of mitochondrial DNA polymorphisms in cultured human fibroblasts. *Somatic Cell Genetics*, 7(1), pp.103-108.

Chaban, Y, Boekema, E. and Dudkina, N. (2012). Structures of mitochondrial oxidative phosphorylation supercomplexes and mechanisms for their stabilisation. Biochimica et Biophysica Acta (BBA) - Bioenergetics, 1837(4), pp.418- 426.

Chang, D. and Clayton, D. (1984). Precise identification of individual promoters for transcription of each strand of human mitochondrial DNA. Cell, 36(3), pp.635-643.

Cheeseman, K. and Slater, T. (1993). An introduction to free radical biochemistry. British Medical Bulletin, 49(3), pp.481-493.

Chen, H. and Chan, D. (2009). Mitochondrial dynamics-fusion, fission, movement, and mitophagy-in neurodegenerative diseases. Human Molecular Genetics, 18(R2), pp.R169-R176.

Chen, H, Detmer, S, Ewald, A, Griffin, E, Fraser, S. and Chan, D. (2003). Mitofusins Mfn1 and Mfn2 coordinately regulate mitochondrial fusion and are 323 essential for embryonic development. The Journal of Cell Biology, 160(2), pp.189- 200.

Chen, M, Logan, T, Hochberg, M, Shelat, S, Yu, X, Wilding, G, Tan, W, Kujoth, G, Prolla, T, Selak, M, Kundu, M, Carroll, M. and Thompson, J. (2009). Erythroid dysplasia, megaloblastic anemia, and impaired lymphopoiesis arising from mitochondrial dysfunction. *Blood*, 114(19), pp.4045-4053.

Chen, Q, Vazquez, E, Moghaddas, S, Hoppel, C. and Lesnefsky, E. (2003). Production of Reactive Oxygen Species by Mitochondria. Journal of Biological Chemistry, 278(38), pp.36027-36031.

Chial, H. and Craig, J. (2008) mtDNA and mitochondrial diseases. Nature Education 1(1):217 Chinnery, P. and Samuels, D. (1999). Relaxed Replication of mtDNA: A Model with Implications for the Expression of Disease. The American Journal of Human Genetics, 64(4), pp.1158-1165.

Chinnery, P. and Samuels, D. (1999). Relaxed Replication of mtDNA: A Model with Implications for the Expression of Disease. *The American Journal of Human Genetics*, 64(4), pp.1158-1165.

Chinnery, P, Johnson, M, Wardell, T, Singh-Kler, R, Hayes, C, Brown, D, Taylor, R, Bindoff, L. and Turnbull, D. (2000). The epidemiology of pathogenic mitochondrial DNA mutations. Annals of Neurology, 48(2), pp.188-193.

Chow, L, Greenlund, L, Asmann, Y, Short, K, McCrady, S, Levine, J. and Nair, K. (2007). Impact of endurance training on murine spontaneous activity, muscle mitochondrial DNA abundance, gene transcripts, and function. Journal of Applied Physiology, 102(3), pp.1078-1089.

Clark-Matott, J, Saleem, A, Dai, Y, Shurubor, Y, Ma, X, Safdar, A, Beal, M, Tarnopolsky, M. and Simon, D. (2015). Metabolomic analysis of exercise effects in the POLG mitochondrial DNA mutator mouse brain. *Neurobiology of Aging*, 36(11), pp.2972-2983.

Clayton, D. (1982). Replication of animal mitochondrial DNA. Cell, 28(4), pp.693-705.

Clayton, D. (2000). Transcription and replication of mitochondrial DNA. Human Reproduction, 15(suppl 2), pp.11-17.

Clayton, D. A, Doda, J. N. and Friedberg, E. C. (1974). The absence of a pyrimidine dimer repair mechanism in mammalian mitochondria. Proc. Natl. Acad. Sci. U.S.A. 71, 2777–2781

Cohen, S. (1997). Social Ties and Susceptibility to the Common Cold. *JAMA: The Journal of the American Medical Association*, 277(24), p.1940.

Coller H.A, Bodyak N.D, Khrapko K. In: Increasing Healthy Life Span: Conventional Measures and Slowing the Innate Aging Process. Harman D, editor. Vol. 959. New York: New York Acad Sciences; 2002. pp. 434–447

Collins, F. and Tabak, L. (2014). Policy: NIH plans to enhance reproducibility. *Nature*, 505(7485), pp.612-613.

Conley, K. (2016). Mitochondria to motion: optimizing oxidative phosphorylation to improve exercise performance. The Journal of Experimental Biology, 219(2), pp.243-249.

Cook, L, Hillhouse, A, Myles, M, Lubahn, D, Bryda, E, Davis, J. and Franklin, C. (2014). The Role of Estrogen Signaling in a Mouse Model of Inflammatory Bowel Disease: A Helicobacter Hepaticus Model. PLoS ONE, 9(4), p.e94209.

Cornelius, E. (1972). Increased incidence of lymphomas in thymectomized Mice - evidence for an immunological theory of aging. Experientia, 28(4), pp.459-459.

Costall, B, Jones, B. J, Kelly, M. E, Naylor, R. J, Tomkins, D. M. Exploration of mice in a black and white test box: validation as a model of anxiety. Pharmacol. Biochem. Behav. 32, 777-785 (1989).

Cottrell, D, Blakely, E, Johnson, M, Ince, P, Borthwick, G. and Turnbull, D. (2001). Cytochrome c oxidase deficient cells accumulate in the hippocampus and choroid plexus with age. Neurobiology of Aging, 22(2), pp.265-272.

Courses.lumenlearning.com. (2019). *Heart Anatomy | Anatomy and Physiology*. [online] Available at: https://courses.lumenlearning.com/nemcc-ap/chapter/heart-anatomy/ [Accessed 23 Aug. 2019].

Croston, T, Thapa, D, Holden, A, Tveter, K, Lewis, S, Shepherd, D, Nichols, C, Long, D, Olfert, I, Jagannathan, R. and Hollander, J. (2014). Functional deficiencies of subsarcolemmal mitochondria in the type 2 diabetic human heart. American Journal of Physiology-Heart and Circulatory Physiology, 307(1), pp.H54-H65.

Cuervo, A. and Dice, J. (2000). Age-related Decline in Chaperone-mediated Autophagy. *Journal of Biological Chemistry*, 275(40), pp.31505-31513.

D'Souza, A. and Minczuk, M. (2018). Mitochondrial transcription and translation: overview. *Essays In Biochemistry*, 62(3), pp.309-320.

Dabkowski, E, Baseler, W, Williamson, C, Powell, M, Razunguzwa, T, Frisbee, J. and Hollander, J. (2010). Mitochondrial dysfunction in the type 2 diabetic heart is associated with alterations in spatially distinct mitochondrial proteomes. *American Journal of Physiology-Heart and Circulatory Physiology*, 299(2), pp.H529-H540.

Dai DF, Santana LF, Vermulst M, Tomazela DM, Emond MJ, MacCoss MJ, Gollahon K, Martin GM, Loeb LA, Ladiges WC, Rabinovitch PS. Overexpression of catalase targeted to mitochondria attenuates murine cardiac aging. Circulation. 2009 Jun 2; 119(21):2789-97.

Dai, D. and Rabinovitch, P. (2009). Cardiac Aging in Mice and Humans: The Role of Mitochondrial Oxidative Stress. *Trends in Cardiovascular Medicine*, 19(7), pp.213-220.

Dai, D, Chen, T, Wanagat, J, Laflamme, M, Marcinek, D, Emond, M, Ngo, C, Prolla, T. and Rabinovitch, P. (2010). Age-dependent cardiomyopathy in mitochondrial mutator mice is attenuated by overexpression of catalase targeted to mitochondria. Aging Cell, 9(4), pp.536-544.

Dai, D, Rabinovitch, P. and Ungvari, Z. (2012). Mitochondria and Cardiovascular Aging. *Circulation Research*, 110(8), pp.1109-1124.

Dai, Y, Clark, J, Zheng, K, Kujoth, G, Prolla, T. and Simon, D. (2014). Somatic mitochondrial DNA mutations do not increase neuronal vulnerability to MPTP in young POLG mutator mice. *Neurotoxicology and Teratology*, 46, pp.62-67.

Dai, Y, Kiselak, T, Clark, J, Clore, E, Zheng, K, Cheng, A, Kujoth, G, Prolla, T, Maratos-Flier, E. and Simon, D. (2013). Behavioral and metabolic characterization of heterozygous and homozygous POLG mutator mice. *Mitochondrion*, 13(4), pp.282-291.

Dairaghi, D, Shadel, G. and Clayton, D. (1995). Addition of a 29 Residue Carboxyl-terminal Tail Converts a Simple HMG Box-containing Protein into a Transcriptional Activator. *Journal of Molecular Biology*, 249(1), pp.11-28.

Dalla Rosa, I, Zhang, H, Khiati, S, Wu, X. and Pommier, Y. (2017). Transcription profiling suggests that mitochondrial topoisomerase IB acts as a topological barrier and regulator of mitochondrial DNA transcription. Journal of Biological Chemistry, 292(49), pp.20162-20172.

Darling, R, Dingess, P, Schlidt, K, Smith, E. and Brown, T. (2016). Incubation of food craving is independent of macronutrient composition. Scientific Reports, 6(1).

Davidovic, M, Erceg, P, Trailov, D, Djurica, S, Milosevic, D. and Stevic, R. (2010). The Privilege to Be Old. Gerontology, 49(5), pp.335-339.

Davies, K, Quintanilha, A, Brooks, G. and Packer, L. (1982). Free radicals and tissue damage produced by exercise. Biochemical and Biophysical Research Communications, 107(4), pp.1198-1205.

De Biase, C, De Rosa, R, Luciano, R, De Luca, S, Capuano, E, Trimarco, B. and Galasso, G. (2014). Effects of physical activity on endothelial progenitor cells (EPCs). *Frontiers in Physiology*, 4.

De Grey, A. (1997). A proposed refinement of the mitochondrial free radical theory of aging. BioEssays, 19(2), pp.161-166.

De Meirleir, L, Seneca, S, Lissens, W, Clercq, D, Eyskens, F, Gerlo, E, Smet, J. and Coster, R. (2004). Respiratory chain complex V deficiency due to a mutation in the assembly gene ATP12. [online] Available at: https://jmg.bmj.com/content/41/2/120 [Accessed 16 Jul. 2019].

Del Giacco, S, Scorcu, M, Argiolas, F, Firinu, D. and Del Giacco, G. (2014). Exercise Training, Lymphocyte Subsets and Their Cytokines Production: Experience of an Italian Professional Football Team and Their Impact on Allergy. BioMed Research International, 2014, pp.1-6.

DeLuca, S. and O'Farrell, P. (2012). Barriers to Male Transmission of Mitochondrial DNA in Sperm Development. *Developmental Cell*, 22(3), pp.660-668.

Deram, S. and Villares, S. (2009). Genetic variants influencing effectiveness of weight loss strategies. *Arquivos Brasileiros de Endocrinologia & Metabologia*, 53(2), pp.129-138.

Detmer, S. and Chan, D. (2007). Functions and dysfunctions of mitochondrial dynamics. *Nature Reviews Molecular Cell Biology*, 8(11), pp.870-879.

Dhingra, R. and Vasan, R. (2012). Age As a Risk Factor. *Medical Clinics of North America*, 96(1), pp.87-91.

Dillon, L, Williams, S, Hida, A, Peacock, J, Prolla, T, Lincoln, J. and Moraes, C. (2012). Increased mitochondrial biogenesis in muscle improves aging phenotypes in the mtDNA mutator mouse. Human Molecular Genetics, 21(10), pp.2288-2297.

Dröge, W. (2002). Free Radicals in the Physiological Control of Cell Function. Physiological Reviews, 82(1), pp.47-95.

Dufour, E, Boulay, J, Rincheval, V. and Sainsard-Chanet, A. (2000). A causal link between respiration and senescence in Podospora anserina. Proceedings of the National Academy of Sciences, 97(8), pp.4138-4143.

Dufour, E, Terzioglu, M, Sterky, F, Sorensen, L, Galter, D, Olson, L, Wilbertz, J. and Larsson, N. (2008). Age-associated mosaic respiratory chain deficiency causes trans-neuronal degeneration. Human Molecular Genetics, 17(10), pp.1418-1426.

Echols, H. and Goodman, M. (1991). Fidelity Mechanisms in DNA Replication. Annual Review of Biochemistry, 60(1), pp.477-511. 327

Edgar, D, Shabalina, I, Camara, Y, Wredenberg, A, Calvaruso, M, Nijtmans, L, Nedergaard, J, Cannon, B, Larsson, N. and Trifunovic, A. (2009). Random Point Mutations with Major Effects on Protein-Coding Genes Are the Driving Force behind Premature Aging in mtDNA Mutator Mice. *Cell Metabolism*, 10(2), pp.131-138.

Eisele, J, Schaefer, I, Randel Nyengaard, J, Post, H, Liebetanz, D, Brüel, A. and Mühlfeld, C. (2007). Effect of voluntary exercise on number and volume of cardiomyocytes and their mitochondria in the mouse left ventricle. Basic Research in Cardiology, 103(1), pp.12-21.

Ekstrand, M. (2004). Mitochondrial transcription factor A regulates mtDNA copy number in mammals. Human Molecular Genetics, 13(9), pp.935-944.

Elson, J., Andrews, R., Chinnery, P., Lightowlers, R., Turnbull, D. and Howell, N. (2001). Analysis of European mtDNAs for Recombination. *The American Journal of Human Genetics*, 68(1), pp.145-153.

Ekstrand, M, Terzioglu, M, Galter, D, Zhu, S, Hofstetter, C, Lindqvist, E, Thams, S, Bergstrand, A, Hansson, F, Trifunovic, A, Hoffer, B, Cullheim, S, Mohammed, A, Olson, L. and Larsson, N. (2007). Progressive Parkinsonism in mice with respiratory-chain-deficient dopamine neurons. *Proceedings of the National Academy of Sciences*, 104(4), pp.1325-1330.

Elson, J, Samuels, D, Turnbull, D. and Chinnery, P. (2001). Random Intracellular Drift Explains the Clonal Expansion of Mitochondrial DNA Mutations with Age. The American Journal of Human Genetics, 68(3), pp.802-806.

Eluamai, A. and Brooks, K. (2013). Effect of aerobic exercise on mitochondrial DNA and aging. *Journal of Exercise Science & Fitness*, 11(1), pp.1-5.

Eskes, T. and Haanen, C. (2007). Why do women live longer than men?. *European Journal of Obstetrics & Gynecology and Reproductive Biology*, 133(2), pp.126-133.

Ettinger, W. (1997). A Randomized Trial Comparing Aerobic Exercise and Resistance Exercise With a Health Education Program in Older Adults With Knee Osteoarthritis. JAMA, 277(1), p.25-31.

Eura, Y, Ishihara, N, Yokota, S. and Mihara, K. (2003). Two Mitofusin Proteins, Mammalian Homologues of FZO, with Distinct Functions Are Both Required for Mitochondrial Fusion. *Journal of Biochemistry*, 134(3), pp.333-344.

Eurek Alert!. (2019). One way social isolation changes the mouse brain. [Online] Available at: https://www.eurekalert.org/pub_releases/2018-05/cp-ows051018.php [Accessed 1 May 2019].

Fabian, D. & Flatt, T. (2011) the Evolution of Aging. Nature Education Knowledge 3(10):9 Falkenberg, M. (2018). Mitochondrial DNA replication in mammalian cells: overview of the pathway. Essays in Biochemistry, 62(3), pp.287-296. 328

Fabian, D. & Flatt, T. (2011) the Evolution of Aging. Nature Education Knowledge 3(10):9

Falkenberg, M. (2018). Mitochondrial DNA replication in mammalian cells: overview of the pathway. *Essays In Biochemistry*, 62(3), pp.287-296.

Falkenberg, M, Gaspari, M, Rantanen, A, Trifunovic, A, Larsson, N. and Gustafsson, C. (2002). Mitochondrial transcription factors B1 and B2 activate transcription of human mtDNA. Nature Genetics, 31(3), pp.289-294.

Falkenberg, M, Larsson, N. and Gustafsson, C. (2007). DNA Replication and Transcription in Mammalian Mitochondria. Annual Review of Biochemistry, 76(1), pp.679-699.

Fayet, G, Jansson, M, Sternberg, D, Moslemi, A, Blondy, P, Lombès, A, Fardeau, M. and Oldfors, A. (2002). Ageing muscle: clonal expansions of mitochondrial DNA point mutations and deletions cause focal impairment of mitochondrial function. *Neuromuscular Disorders*, 12(5), pp.484-493.

Fellous, T. G, S. A. McDonald, J. Burkert, A. Humphries, S. Islam, N. M. De-Alwis, L. Gutierrez-Gonzalez, P. J. Tadrous, G. Elia, H. M. Kocher, S. Bhattacharya, L. Mears, M. El-Bahrawy, D. M. Turnbull, R. W. Taylor, L. C. Greaves, P. F. Chinnery, C. P. Day, N. A. Wright and M. R. Alison (2009). "A methodological approach to tracing cell lineage in human epithelial tissues." Stem Cells 27(6): 1410-1420.

Fernandes, T, Baraúna, V, Negrão, C, Phillips, M. and Oliveira, E. (2015). Aerobic exercise training promotes physiological cardiac remodeling involving a set of microRNAs. American Journal of Physiology-Heart and Circulatory Physiology, 309(4), pp.H543-H552.

Fernandes, T, Soci, U. and Oliveira, E. (2011). Eccentric and concentric cardiac hypertrophy induced by exercise training: microRNAs and molecular determinants. Brazilian Journal of Medical and Biological Research, 44(9), pp.836- 847.

Ferrari, R, Cargnoni, A. and Ceconi, C. (2006). Anti-ischaemic effect of ivabradine. Pharmacological Research, 53(5), pp.435-439.

Fiechter, M, Fuchs, T, Gebhard, C, Stehli, J, Klaeser, B, Stähli, B, Manka, R, Manes, C, Tanner, F, Gaemperli, O. and Kaufmann, P. (2013). Age-related normal structural

and functional ventricular values in cardiac function assessed by magnetic resonance. *BMC Medical Imaging*, 13(1).

Filler, K, Lyon, D, Bennett, J, McCain, N, Elswick, R, Lukkahatai, N. and Saligan, L. (2014). Association of mitochondrial dysfunction and fatigue: A review of the literature. BBA Clinical, 1, pp.12-23.

Filosto, M, Mancuso, M, Vives-Bauza, C, Vilà, M, Shanske, S, Hirano, M, Andreu, A. and DiMauro, S. (2003). Lack of paternal inheritance of muscle mitochondrial DNA in sporadic mitochondrial myopathies. *Annals of Neurology*, 54(4), pp.524-526.

Finkbeiner, S. and Greenberg, M. (1998). Ca2 channel-regulated neuronal gene expression. *Journal of Neurobiology*, 37(1), pp.171-189.

Fischer, A, Cannon, B. and Nedergaard, J. (2018). Optimal housing temperatures for mice to mimic the thermal environment of humans: An experimental study. *Molecular Metabolism*, 7, pp.161-170.

Fisher, R.P. and Clayton, D.A. (1988) Purification and characterization of human mitochondrial transcription factor 1. Mol Cell Biol 8, 3496-509.

Fitzgerald, M, Tanaka, H, Tran, Z. and Seals, D. (1997). Age-related declines in maximal aerobic capacity in regularly exercising vs. sedentary women: a metaanalysis. Journal of Applied Physiology, 83(1), pp.160-165.

Fleg, J. and Strait, J. (2011). Age-associated changes in cardiovascular structure and function: a fertile milieu for future disease. Heart Failure Reviews, 17(4-5), pp.545-554.

Fleg, J, Morrell, C, Bos, A, Brant, L, Talbot, L, Wright, J. and Lakatta, E. (2005). Accelerated Longitudinal Decline of Aerobic Capacity in Healthy Older Adults. Circulation, 112(5), pp.674-682.

Fleg, J, O'Connor, F, Gerstenblith, G, Becker, L, Clulow, J, Schulman, S. and Lakatta, E. (1995). Impact of age on the cardiovascular response to dynamic upright

exercise in healthy men and women. Journal of Applied Physiology, 78(3), pp.890-900.

Flis, V. and Daum, G. (2013). Lipid Transport between the Endoplasmic Reticulum and Mitochondria. *Cold Spring Harbor Perspectives in Biology*, 5(6), pp.a013235-a013235.

Flores, I, Cayuela, M. and Blasco, M. (2005). Effects of Telomerase and Telomere Length on Epidermal Stem Cell Behavior. *Science*, 309(5738), pp.1253-1256.

Fluck, H. HoppelerMolecular basis of skeletal muscle plasticity—from gene to form and function

Foronjy, R, Sun, J, Lemaitre, V. and D'armiento, J. (2008). Transgenic Expression of Matrix Metalloproteinase-1 Inhibits Myocardial Fibrosis and Prevents the Transition to Heart Failure in a Pressure Overload Mouse Model. Hypertension Research, 31(4), pp.725-735.

Franchi, M., Reeves, N. and Narici, M. (2017). Skeletal Muscle Remodeling in Response to Eccentric vs. Concentric Loading: Morphological, Molecular, and Metabolic Adaptations. *Frontiers in Physiology*, 8.

Frangogiannis, N. (2012). Regulation of the Inflammatory Response in Cardiac Repair. Circulation Research, 110(1), pp.159-173.

Frey, T. and Mannella, C. (2000). The internal structure of mitochondria. *Trends in Biochemical Sciences*, 25(7), pp.319-324.

Friedman, D. B. & Johnson, T. E. *A mutation in the age-1 gene in Caenorhabditis elegans lengthens life and reduces hermaphrodite fertility*. *Genetics* **118**, 75–86 (1988)

Frolova, L, Tsivkovskii, R, Sivolobova, G, Oparina, N, Serpinsky, O, Blinov, V, Tatkov, S. and Kisselev, L. (1999). Mutations in the highly conserved GGQ motif of class 1 polypeptide release factors abolish ability of human eRF1 to trigger peptidyl-tRNA hydrolysis. RNA, 5(8), pp.1014-1020.

Fukai, T. and Ushio-Fukai, M. (2011). Superoxide Dismutases: Role in Redox Signaling, Vascular Function, and Diseases. Antioxidants & Redox Signaling, 15(6), pp.1583-1606.

Fuke, S., Kametani, M., Yamada, K., Kasahara, T., Kubota-Sakashita, M., Kujoth, G., Prolla, T., Hitoshi, S. and Kato, T. (2014). HeterozygousPolgmutation causes motor dysfunction due to mtDNA deletions. *Annals of Clinical and Translational Neurology*, 1(11), pp.909-920.

Fulop, T, Witkowski, J, Pawelec, G, Alan, C. and Larbi, A. (2014). On the Immunological Theory of Aging. *Aging*, pp.163-176.

Galomov, E. (2010). The Role of p66shc in Oxidative Stress and Apoptosis. *Acta Naturae*, 2(4), pp.44-51.

Ganesh, J, Wong, L. and Gorman, E. (2012). Mitochondrial Respiratory Chain Complex II. *Mitochondrial Disorders Caused by Nuclear Genes*, pp.203-218.

Gao, X, Jakovljevic, D. and Beard, D. (2019). Cardiac Metabolic Limitations Contribute to Diminished Performance of the Heart in Aging. *Biophysical Journal*.

Gaur, R, Grasso, D, Datta, P, Krishna, P, Das, G, Spencer, A, Agrawal, R, Spremulli, L. and Varshney, U. (2008). A Single Mammalian Mitochondrial Translation Initiation Factor Functionally Replaces Two Bacterial Factors. Molecular Cell, 29(2), pp.180-190.

Gavrilov, L. and Gavrilova, N. (2002). Evolutionary Theories of Aging and Longevity. *The Scientific World JOURNAL*, 2, pp.339-356.

Gebhard, C. (2019). [online] http://spo.escardio.org/eslides/view.aspx?eevtid=54&fp=P3356. Available at: http://spo.escardio.org/eslides/view.aspx?eevtid=54&fp=P3356 [Accessed 8 May 2019].

Gems, D. and Doonan, R. (2009). Antioxidant defense and aging inC. elegans: Is the oxidative damage theory of aging wrong?. *Cell Cycle*, 8(11), pp.1681-1687.

Gems, D. and Partridge, L. (2013). Genetics of Longevity in Model Organisms: Debates and Paradigm Shifts. Annual Review of Physiology, 75(1), pp.621-644.

Giannuzzi, P, Temporelli, P, Corrà, U. and Tavazzi, L. (2003). Antiremodeling Effect of Long-Term Exercise Training in Patients with Stable Chronic Heart Failure. Circulation, 108(5), pp.554-559. 331

Gilde, A. and Van Bilsen, M. (2003). Peroxisome proliferator-activated receptors (PPARS): regulators of gene expression in heart and skeletal muscle. Acta Physiologica Scandinavica, 178(4), pp.425-434.

Giorgi, C, Agnoletto, C, Bononi, A, Bonora, M, De Marchi, E, Marchi, S, Missiroli, S, Patergnani, S, Poletti, F, Rimessi, A, Suski, J, Wieckowski, M. and Pinton, P. (2012). Mitochondrial calcium homeostasis as potential target for mitochondrial medicine. *Mitochondrion*, 12(1), pp.77-85.

Giorgio, M, Migliaccio, E, Orsini, F, Paolucci, D, Moroni, M, Contursi, C, Pelliccia, G, Luzi, L, Minucci, S, Marcaccio, M, Pinton, P, Rizzuto, R, Bernardi, P, Paolucci, F. and Pelicci, P. (2005). Electron Transfer between Cytochrome c and p66Shc Generates Reactive Oxygen Species that Trigger Mitochondrial Apoptosis. Cell, 122(2), pp.221-233.

Glennon, P, Sugden, P. and Poole-Wilson, P. (1995). Cellular mechanisms of cardiac hypertrophy. Heart, 73(6), pp.496-499.

Gómez, L. and Hagen, T. (2012). Age-related decline in mitochondrial bioenergetics: Does supercomplex destabilization determine lower oxidative capacity and higher superoxide production?. Seminars in Cell & Developmental Biology, 23(7), pp.758-767.

Good, C, Hoffman, A, Hoffer, B, Chefer, V, Shippenberg, T, Bäckman, C, Larsson, N, Olson, L, Gellhaar, S, Galter, D. and Lupica, C. (2011). Impaired nigrostriatal function precedes behavioral deficits in a genetic mitochondrial model of Parkinson's disease. The FASEB Journal, 25(4), pp.1333-1344.

Gordon, C. (2017). The mouse thermoregulatory system: Its impact on translating biomedical data to humans. Physiology & Behavior, 179, pp.55-66.

Goto, Y, Nonaka, I. and Horai, S. (1990). A mutation in the tRNALeu(UUR) gene associated with the MELAS subgroup of mitochondrial encephalomyopathies. Nature, 348(6302), pp.651-653.

Gouliaeva, N, Kuznetsova, E. and Gaziev, A. (2006). Proteins associated with mitochondrial DNA protect it against X-rays and hydrogen peroxide. Biophysics, 51(4), pp.620-623. 332

Greaves, L, Elson, J, Nooteboom, M, Grady, J, Taylor, G, Taylor, R, Mathers, J, Kirkwood, T. and Turnbull, D. (2012). Comparison of Mitochondrial Mutation Spectra in Ageing Human Colonic Epithelium and Disease: Absence of Evidence for Purifying Selection in Somatic Mitochondrial DNA Point Mutations. PLoS Genetics, 8(11), p.e1003082.

Greaves, L, Nooteboom, M, Elson, J, Tuppen, H, Taylor, G, Commane, D, Arasaradnam, R, Khrapko, K, Taylor, R, Kirkwood, T, Mathers, J. and Turnbull, D. (2014). Clonal Expansion of Early to Mid-Life Mitochondrial DNA Point Mutations Drives Mitochondrial Dysfunction during Human Ageing. PLoS Genetics, 10(9), p.e1004620.

Gredilla, R, Garm, C. and Stevnsner, T. (2012). Nuclear and Mitochondrial DNA Repair in Selected Eukaryotic Aging Model Systems. *Oxidative Medicine and Cellular Longevity*, 2012, pp.1-12.

Green, E.L. [6th ed.] 1964. *Handbook on Genetically Standardized Jax Mice.* The Jackson Laboratory, Bar Harbor, Maine. 82 p.

Gronau, T, Krüger, K, Prein, C, Aszodi, A, Gronau, I, Iozzo, R, Mooren, F, Clausen-Schaumann, H, Bertrand, J, Pap, T, Bruckner, P. and Dreier, R. (2016). Forced exercise-induced osteoarthritis is attenuated in mice lacking the small leucine-rich proteoglycan decorin. *Annals of the Rheumatic Diseases*, 76(2), pp.442-449.

Gu, C, Zhang, J, Chen, Y. and Lei, J. (2011). A trigger model of apoptosis induced by tumor necrosis factor signaling. *BMC Systems Biology*, 5(Suppl 1), p.S13.

Gulati, M, Shaw, L, Thisted, R, Black, H, Bairey Merz, C. and Arnsdorf, M. (2010). Heart Rate Response to Exercise Stress Testing in Asymptomatic Women. Circulation, 122(2), pp.130-137.

Gusdon, A, Callio, J, Distefano, G, O'Doherty, R, Goodpaster, B, Coen, P. and Chu, C. (2017). Exercise increases mitochondrial complex I activity and DRP1 expression in the brains of aged mice. *Experimental Gerontology*, 90, pp.1-13.

Hagan, C. (2007). When are mice considered old? [Blog] JAX Blog. Available at: https://www.jax.org/news-and-insights/jax-blog/2017/november/whenare-mice-considered-old# [Accessed 1 May 2019].

Haller, R. (2015). Exercise and mitochondrial function in health and disease. *Neuromuscular Disorders*, 25, p.S184.

Han, G. and Kim, S. (2013). Effects of Endurance Exercise on Mitochondrial Function in Mice. Journal of Physical Therapy Science, 25(10), pp.1317-1319.

Hansen, M, Taubert, S, Crawford, D, Libina, N, Lee, S. and Kenyon, C. (2007). Lifespan extension by conditions that inhibit translation in Caenorhabditis elegans. *Aging Cell*, 6(1), pp.95-110.

Hansson, G. (2005). Inflammation, Atherosclerosis, and Coronary Artery Disease. New England Journal of Medicine, 352(16), pp.1685-1695.

Harman, D. (1956). Aging: A Theory Based on Free Radical and Radiation Chemistry. *Journal of Gerontology*, 11(3), pp.298-300.

Hashimura, Y, Morioka, I, Hisamatsu, C, Yokoyama, N, Taniguchi-Ikeda, M, Yokozaki, H, Murayama, K, Ohtake, A, Itoh, K, Takeshima, Y. and Iijima, K. (2016). Mitochondrial respiratory chain complex IV deficiency complicated with chronic intestinal pseudo-obstruction in a neonate. Pediatrics International, 58(7), pp.651-655.

301

Hatefi, Y. (1985). The Mitochondrial Electron Transport and Oxidative Phosphorylation System. Annual Review of Biochemistry, 54(1), pp.1015-1069.

Hattori, R, Otani, H, Uchiyama, T, Imamura, H, Cui, J, Maulik, N, Cordis, G, Zhu, L. and Das, D. (2001). Src tyrosine kinase is the trigger but not the mediator of ischemic preconditioning. American Journal of Physiology-Heart and Circulatory Physiology, 281(3), pp.H1066-H1074.

Hauswirth, W. and Laipis, P. (1982). Mitochondrial DNA polymorphism in a maternal lineage of Holstein cows. *Proceedings of the National Academy of Sciences*, 79(15), pp.4686-4690.

Hawkins, S. and Wiswell, R. (2003). Rate and Mechanism of Maximal Oxygen Consumption Decline with Aging. Sports Medicine, 33(12), pp.877-888.

Heemst, V. (2010). Insulin, IGF-1 and longevity. Aging Dis, 1(2).

Hees, P, Fleg, J, Lakatta, E. and Shapiro, E. (2002). Left ventricular remodeling with age in normal men versus women. The American Journal of Cardiology, 90(11), pp.1231-1236.

Hedegard, W. (2019). *Anatomy & Physiology: Support and Movement.* 2nd ed.

Herrmann, J. and Neupert, W. (2000). Protein transport into mitochondria. Current Opinion in Microbiology, 3(2), pp.210-214.

Higginbotham, M, Morris, K, Williams, R, Coleman, R. and Cobb, F. (1986). Physiologic basis for the age-related decline in aerobic work capacity. The American Journal of Cardiology, 57(15), pp.1374-1379.

Hiona, A and Leeuwenburgh, C. (2008). The role of mitochondrial DNA mutations in aging and sarcopenia: Implications for the mitochondrial vicious cycle theory of aging. Experimental Gerontology, 43(1), pp.24-33.

Hiona, A, Sanz, A, Kujoth, G, Pamplona, R, Seo, A, Hofer, T, Someya, S, Miyakawa, T, Nakayama, C, Samhan-Arias, A, Servais, S, Barger, J, Portero-Otín, M, Tanokura,

M, Prolla, T. and Leeuwenburgh, C. (2010). Mitochondrial DNA Mutations Induce Mitochondrial Dysfunction, Apoptosis and Sarcopenia in Skeletal Muscle of Mitochondrial DNA Mutator Mice. *PLoS ONE*, 5(7), p.e11468.

Holt I.J, Lorimer, H.E, and Jacobs, H.T. 2000. Coupled leading- and lagging-strand synthesis of mammalian mitochondrial DNA. Cell 100: 515-524 Holt, I. and Reyes, A. (2012). Human Mitochondrial DNA Replication. Cold Spring Harbor Perspectives in Biology, 4(12), pp.a012971-a012971.

Holt, I, Harding, A. and Morgan-Hughes, J. (1988). Deletions of muscle mitochondrial DNA in patients with mitochondrial myopathies. *Nature*, 331(6158), pp.717-719.

Holt-Lunstad, J, Smith, T. and Layton, J. (2010). Social Relationships and Mortality Risk: A Meta-analytic Review. *PLoS Medicine*, 7(7), p.e1000316.

Hong, T. and Shaw, R. (2016). Ion Channel Trafficking. Ion Channels in Health and Disease, pp.25-51.

Hood, D. (2009). Mechanisms of exercise-induced mitochondrial biogenesis in skeletal muscleThis paper is one of a selection of papers published in this Special Issue, entitled 14th International Biochemistry of Exercise Conference – Muscles as Molecular and Metabolic Machines, and has undergone the Journal's usual peer review process. Applied Physiology, Nutrition, and Metabolism, 34(3), pp.465-472.

Howden, E, Sarma, S, Lawley, J, Opondo, M, Cornwell, W, Stoller, D, Urey, M, Adams-Huet, B. and Levine, B. (2018). Reversing the Cardiac Effects of Sedentary Aging in Middle Age—A Randomized Controlled Trial. *Circulation*, 137(15), pp.1549-1560.

Huang, C, Yang, A, Lin, Y, Wu, F, Lin, J, Chan, Y, Tsai, F, Tsai, C, Kuo, C. and Lee, S. (2012). Anti-apoptotic and pro-survival effects of exercise training on hypertensive hearts. Journal of Applied Physiology, 112(5), pp.883-891.

Hudson, G. and Chinnery, P. (2006). Mitochondrial DNA polymerase-γ and human disease. Human Molecular Genetics, 15(suppl_2), pp.R244-R252.

Huss, J, Imahashi, K, Dufour, C, Weinheimer, C, Courtois, M, Kovacs, A, Giguère, V, Murphy, E. and Kelly, D. (2007). The Nuclear Receptor ERRα Is Required for the Bioenergetic and Functional Adaptation to Cardiac Pressure Overload. Cell Metabolism, 6(1), pp.25-37.

Huynh, K, McMullen, J, Julius, T, Tan, J, Love, J, Cemerlang, N, Kiriazis, H, Du, X. and Ritchie, R. (2010). Cardiac-Specific IGF-1 Receptor Transgenic Expression Protects Against Cardiac Fibrosis and Diastolic Dysfunction in a Mouse Model of Diabetic Cardiomyopathy. *Diabetes*, 59(6), pp.1512-1520.

Ieraci, A, Mallei, A. and Popoli, M. (2019). *Social Isolation Stress Induces Anxious-Depressive-Like Behavior and Alterations of Neuroplasticity-Related Genes in Adult Male Mice.*

Irrcher, I, Adhihetty, P, Joseph, A, Ljubicic, V. and Hood, D. (2003). Regulation of Mitochondrial Biogenesis in Muscle by Endurance Exercise. Sports Medicine, 33(11), pp.783-793.

Ishihara, N, Nomura, M, Jofuku, A, Kato, H, Suzuki, S, Masuda, K, Otera, H, Nakanishi, Y, Nonaka, I, Goto, Y, Taguchi, N, Morinaga, H, Maeda, M, Takayanagi, R, Yokota, S. and Mihara, K. (2009). Mitochondrial fission factor Drp1 is essential for embryonic development and synapse formation in mice. Nature Cell Biology, 11(8), pp.958-966.

Iwata, S, LEe, J, Okada, K, Iwata, M, Rasmussen, B, Link, T, Ramaswamy, S. and Jap, B. (1998). Complete Structure of the 11-Subunit Bovine Mitochondrial Cytochrome bc1 Complex. *Science*, 281(5373), pp.64-71.

Jacobs, R, Flück, D, Bonne, T, Bürgi, S, Christensen, P, Toigo, M. and Lundby, C. (2013). Improvements in exercise performance with high-intensity interval training coincide with an increase in skeletal muscle mitochondrial content and function. Journal of Applied Physiology, 115(6), pp.785-793. 336

Jänicke, R, Sprengart, M, Wati, M. and Porter, A. (1998). Caspase-3 Is Required for DNA Fragmentation and Morphological Changes Associated with Apoptosis. Journal of Biological Chemistry, 273(16), pp.9357-9360.

Jansen-Durr, P. (2002). Healthy ageing: a question of stress, damage and repair: Meeting on mechanisms of biological ageing. EMBO Reports, 3(12), pp.1127-1132.

Jenuth, J, Peterson, A, Fu, K. and Shoubridge, E. (1996). Random genetic drift in the female germline explains the rapid segregation of mammalian mitochondrial DNA. *Nature Genetics*, 14(2), pp.146-151.

Jette, A, Lachman, M, Giorgetti, M, Assmann, S, Harris, B, Levenson, C, Wernick, M. and Krebs, D. (1999). Exercise--it's never too late: the strong-for-life program. *American Journal of Public Health*, 89(1), pp.66-72.

Jiang, M, Kauppila, T, Motori, E, Li, X, Atanassov, I, Folz-Donahue, K, Bonekamp, N, Albarran-Gutierrez, S, Stewart, J. and Larsson, N. (2017). Increased Total mtDNA Copy Number Cures Male Infertility despite Unaltered mtDNA Mutation Load. *Cell Metabolism*, 26(2), pp.429-436.e4.

Jiménez-Menéndez, N, Fernández-Millán, P, Rubio-Cosials, A, Arnan, C, Montoya, J, Jacobs, H, Bernadó, P, Coll, M, Usón, I. and Solà, M. (2010). Human mitochondrial mTERF wraps around DNA through a left-handed superhelical tandem repeat. Nature Structural & Molecular Biology, 17(7), pp.891-893.

Jin, K. (2019). Modern Biological Theories of Aging. *Aging and disease*, 1(2), pp.72-74.

Joanisse, S, Nederveen, J, Baker, J, Snijders, T, Iacono, C. and Parise, G. (2016). Exercise conditioning in old mice improves skeletal muscle regeneration. The FASEB Journal, 30(9), pp.3256-3268.

Johnson, D, Dean, D, Smith, A. and Johnson, M. (2005). Structure, function and formation of biological iron-sulphur clusters. Annual Review of Biochemistry, 74(1), pp.247-281.

Johnson, K. (1993). Conformational Coupling in DNA polymerase Fidelity. *Annual Review of Biochemistry*, 62(1), pp.685-713.

Jornayvaz, F. and Shulman, G. (2010). Regulation of mitochondrial biogenesis. Essays In Biochemistry, 47, pp.69-84. Kaguni, L. (2004). DNA polymerase γ, The Mitochondrial Replicase. Annual Review of Biochemistry, 73(1), pp.293-320. 337

Jornayvaz, F. and Shulman, G. (2010). Regulation of mitochondrial biogenesis. *Essays in Biochemistry*, 47, pp.69-84.

Kalliokoski, O, Jacobsen, K, Darusman, H, Henriksen, T, Weimann, A, Poulsen, H, Hau, J. and Abelson, K. (2013). Mice Do Not Habituate to Metabolism Cage Housing–A Three Week Study of Male BALB/c Mice. *PLoS ONE*, 8(3), p.e58460.

Kalliokoski, O, Teilmann, A, Jacobsen, K, Abelson, K. and Hau, J. (2014). The Lonely Mouse – Single Housing Affects Serotonergic Signaling Integrity Measured by 8-OH-DPAT-Induced Hypothermia in Male Mice. *PLoS ONE*, 9(12), p.e111065.

Kaguni, L. (2004). DNA Polymerase γ, The Mitochondrial Replicase. *Annual Review of Biochemistry*, 73(1), pp.293-320.

Kamakura, R, Kovalainen, M, Leppäluoto, J, Herzig, K. and Mäkelä, K. (2016). The effects of group and single housing and automated animal monitoring on urinary corticosterone levels in male C57BL/6 mice. Physiological Reports, 4(3), p.e12703.

Kaneda, H, Hayashi, J, Takahama, S, Taya, C, Lindahl, K. and Yonekawa, H. (1995). Elimination of paternal mitochondrial DNA in intraspecific crosses during early mouse embryogenesis. *Proceedings of the National Academy of Sciences*, 92(10), pp.4542-4546.

Kang, C, Chung, E, Diffee, G. and Ji, L. (2013). Exercise training attenuates aging-associated mitochondrial dysfunction in rat skeletal muscle: Role of PGC-1α. *Experimental Gerontology*, 48(11), pp.1343-1350.

Kang, I, Chu, C. and Kaufman, B. (2018). The mitochondrial transcription factor TFAM in neurodegeneration: emerging evidence and mechanisms. FEBS Letters, 592(5), pp.793-811.

Kanki, T, Nakayama, H, Sasaki, N, Takio, K, Alam, T, Hamasaki, N. and Kang, D. (2004). Mitochondrial Nucleoid and Transcription Factor A. Mitochondrial Pathogenesis, pp.61-68.

Kanki, T, Ohgaki, K, Gaspari, M, Gustafsson, C, Fukuoh, A, Sasaki, N, Hamasaki, N. and Kang, D. (2004). Architectural Role of Mitochondrial Transcription Factor A in Maintenance of Human Mitochondrial DNA. Molecular and Cellular Biology, 24(22), pp.9823-9834.

Kauppila, J. and Stewart, J. (2015). Mitochondrial DNA: Radically free of free-radical driven mutations. *Biochimica et Biophysica Acta (BBA) - Bioenergetics*, 1847(11), pp.1354-1361.

Kauppila, T, Kauppila, J. and Larsson, N. (2017). Mammalian Mitochondria and Aging: An Update. *Cell Metabolism*, 25(1), pp.57-71.

Kemi, O., Loennechen, J., Wisløff, U. and Ellingsen, Ø. (2002). Intensity-controlled treadmill running in mice: cardiac and skeletal muscle hypertrophy. *Journal of Applied Physiology*, 93(4), pp.1301-1309.

Kenyon, C. (2005). The Plasticity of Aging: Insights from Long-Lived Mutants. Cell, 120(4), pp.449-460.

Kenyon, C, Chang, J, Gensch, E, Rudner, A. and Tabtiang, R. (1993). A C. elegans mutant that lives twice as long as wild type. *Nature*, 366(6454), pp.461-464.

Kim, C, Wheatley, C, Behnia, M. and Johnson, B. (2016). The Effect of Aging on Relationships between Lean Body Mass and VO2max in Rowers. PLOS ONE, 11(8), p.e0160275.

Kim, Y, Triolo, M. and Hood, D. (2017). Impact of Aging and Exercise on Mitochondrial Quality Control in Skeletal Muscle. Oxidative Medicine and Cellular Longevity, 2017, pp.1-16.

King, M. P. & Attardi, G. Human cells lacking mtDNA: repopulation with exogenous mitochondria by complementation. Science 246, 500–503 (1989).

Kirkwood, T. (1996). Human senescence. *BioEssays*, 18(12), pp.1009-1016.

Kirkwood, T. (2005). Understanding the Odd Science of Aging. Cell, 120(4), pp.437-447.

Kirkwood, T. (2008). Understanding ageing from an evolutionary perspective. Journal of Internal Medicine, 263(2), pp.117-127.

Kitzman, D, Higginbotham, M, Cobb, F, Sheikh, K. and Sullivan, M. (1991). Exercise intolerance in patients with heart failure and preserved left ventricular systolic function: Failure of the Frank-Starling mechanism. Journal of the American College of Cardiology, 17(5), pp.1065-1072.

Klass, M. R. A method for the isolation of longevity mutants in the nematode Caenorhabditis elegans and initial results. Mech. Ageing Dev. 22, 279– 286 (1983)

Koch, A. (2004). Peroxisome elongation and constriction but not fission can occur independently of dynamin-like protein 1. Journal of Cell Science, 117(17), pp.3995-4006.

Koizumi, A, Tsukada, M, Wada, Y, Masuda, H. and Weindruch, R. (1992). Mitotic Activity in Mice is suppressed by Energy Restriction-Induced Torpor. The Journal of Nutrition, 122(7), pp.1446-1453.

Kõks, S, Dogan, S, Tuna, B, González-Navarro, H, Potter, P. and Vandenbroucke, R. (2016). Mouse models of ageing and their relevance to disease. *Mechanisms of Ageing and Development*, 160, pp.41-53.

Kolesar, J, Safdar, A, Abadi, A, MacNeil, L, Crane, J, Tarnopolsky, M. and Kaufman, B. (2014). Defects in mitochondrial DNA replication and oxidative damage in muscle of mtDNA mutator mice. Free Radical Biology and Medicine, 75, pp.241- 251.

Koltai, E, Hart, N, Taylor, A, Goto, S, Ngo, J, Davies, K. and Radak, Z. (2012). Age-associated declines in mitochondrial biogenesis and protein quality control factors are minimized by exercise training. *American Journal of Physiology-Regulatory, Integrative and Comparative Physiology*, 303(2), pp.R127-R134.

Korhonen, J, Gaspari, M. and Falkenberg, M. (2003). TWINKLE Has 5′ → 3′ DNA Helicase Activity and Is Specifically Stimulated by Mitochondrial Single-stranded DNA-binding Protein. Journal of Biological Chemistry, 278(49), pp.48627-48632.

Kornfeld, O, Hwang, S, Disatnik, M, Chen, C, Qvit, N. and Mochly-Rosen, D. (2015). Mitochondrial Reactive Oxygen Species at the Heart of the Matter. *Circulation Research*, 116(11), pp.1783-1799.

Kostis, J, Moreyra, A, Amendo, M, Di Pietro, J, Cosgrove, N. and Kuo, P. (1982). The effect of age on heart rate in subjects free of heart disease. Studies by ambulatory electrocardiography and maximal exercise stress test. Circulation, 65(1), pp.141-145.

Kowald, A. and Kirkwood, T. (1996). A network theory of ageing: the interactions of defective mitochondria, aberrant proteins, free radicals and scavengers in the ageing process. Mutation Research/DNAging, 316(5-6), pp.209-236.

Kowald, A. and Kirkwood, T. (2011). The evolution and role of mitochondrial fusion and fission in aging and disease. *Communicative and intergrative biology*, 4(5).

Kowald, A. and Kirkwood, T. (2018). Resolving the Enigma of the Clonal Expansion of mtDNA Deletions. *Genes*, 9(3), p.126.

Krishnan, K, Greaves, L, Reeve, A. and Turnbull, D. (2007). The ageing mitochondrial genome. *Nucleic Acids Research*, 35(22), pp.7399-7405.

Kruithof, B, van den Hoff, M, Wessels, A. and Moorman, A. (2003). Cardiac muscle cell formation after development of the linear heart tube. Developmental Dynamics, 227(1), pp.1-13.

Kühlbrandt, W. (2015). Structure and function of mitochondrial membrane protein complexes. BMC Biology, 13(1).

Kujoth, G, Hiona, A, Pugh, T, Someya, S, Panzer, K, Wohlgemuth, S, Hofer, T, Seo, A, Sullivan, R, Jobling, W, Morrow, J, Van Remmen, H, Sedivy, M, Yamasoba, T, Tanokura, M, Weinduch, R, Leeuwenburgh, C. and Prolla, T. (2005). Mitochondrial

DNA Mutations, Oxidative Stress, and Apoptosis in Mammalian Aging. *Science*, 309(5733), pp.481-484.

Kujoth, G, Bradshaw, P, Haroon, S. and Prolla, T. (2007). The Role of Mitochondrial DNA Mutations in Mammalian Aging. *PLoS Genetics*, 3(2), p.e24.

Kwak, H, Song, W. and Lawler, J. (2006). Exercise training attenuates age-induced elevation in Bax/Bcl-2 ratio, apoptosis, and remodeling in the rat heart. *The FASEB Journal*, 20(6), pp.791-793.

Labunskyy, V. and Gladyshev, V. (2013). Role of Reactive Oxygen SpeciesMediated Signaling in Aging. Antioxidants & Redox Signaling, 19(12), pp.1362-1372.

Lakatta, E. and Sollott, S. (2002). Perspectives on mammalian cardiovascular aging: humans to molecules. *Comparative Biochemistry and Physiology Part A: Molecular & Integrative Physiology*, 132(4), pp.699-721.

Lakes, E. and Allen, K. (2016). Gait analysis methods for rodent models of arthritic disorders: reviews and recommendations. *Osteoarthritis and Cartilage*, 24(11), pp.1837-1849.

Larsson, N. (2010). Somatic Mitochondrial DNA Mutations in Mammalian Aging. Annual Review of Biochemistry, 79(1), pp.683-706.

Larsson, N. and Clayton, D. (1995). Molecular Genetic Aspects of Human Mitochondrial Disorders. Annual Review of Genetics, 29(1), pp.151-178.

Larsson, N, Wang, J, Wilhelmsson, H, Oldfors, A, Rustin, P, Lewandoski, M, Barsh, G. and Clayton, D. (1998). Mitochondrial transcription factor A is necessary for mtDNA maintance and embryogenesis in mice. Nature Genetics, 18(3), pp.231-236.

Lauber, K, Bohn, E, Kröber, S, Xiao, Y, Blumenthal, S, Lindemann, R, Marini, P, Wiedig, C, Zobywalski, A, Baksh, S, Xu, Y, Autenrieth, I, Schulze-Osthoff, K, Belka, C, Stuhler, G. and Wesselborg, S. (2003). Apoptotic Cells Induce Migration of Phagocytes via Caspase-3-Mediated Release of a Lipid Attraction Signal. *Cell*, 113(6), pp.717-730.

Lee, S, Kaya, A, Avanesov, A, Podolskiy, D, Song, E, Go, D, Jin, G, Hwang, J, Kim, E, Kim, D. and Gladyshev, V. (2017). Age-associated molecular changes are deleterious and may modulate life span through diet. Science Advances, 3(2), p.e1601833.

Lee, Y, Kwon, I, Jang, Y, Song, W, Cosio-Lima, L. and Roltsch, M. (2017). Potential signaling pathways of acute endurance exercise-induced cardiac autophagy and mitophagy and its possible role in cardioprotection. The Journal of Physiological Sciences, 67(6), pp.639-654.

Lehmann, M. and Herkenham, M. (2011). Environmental Enrichment Confers Stress Resiliency to Social Defeat through an Infralimbic Cortex-Dependent Neuroanatomical Pathway. Journal of Neuroscience, 31(16), pp.6159-6173. 341

Lemieux, H. and Hoppel, C. (2009). Mitochondria in the human heart. *Journal of Bioenergetics and Biomembranes*, 41(2), pp.99-106.

LeMond, G. and Hom, M. (2015). Gauging Fitness. *The Science of Fitness*, pp.117-143.

Lenaz, G. (2001). The Mitochondrial Production of Reactive Oxygen Species: Mechanisms and Implications in Human Pathology. *IUBMB Life (International Union of Biochemistry and Molecular Biology: Life)*, 52(3-5), pp.159-164.

Lenaz, G, Fato, R, Genova, M, Bergamini, C, Bianchi, C. and Biondi, A. (2006). Mitochondrial Complex I: Structural and functional aspects. Biochimica et Biophysica Acta (BBA) - Bioenergetics, 1757(9-10), pp.1406-1420.

Lenhart, P, Broselid, S, Barrick, C, Leeb-Lundberg, L. and Caron, K. (2013). Gprotein-coupled receptor 30 interacts with receptor activity-modifying protein 3 and confers sex-dependent cardioprotection. Journal of Molecular Endocrinology, 51(1), pp.191-202.

Leońska-Duniec, A, Ahmetov, I. and Zmijewski, P. (2016). Genetic variants influencing effectiveness of exercise training programmes in obesity – an overview of human studies. *Biology of Sport*, 33(3), pp.207-214.

Leraci, A, Mallei, A. and Popoli, M. (2019). Social Isolation Stress Induces AnxiousDepressive-Like Behavior and Alterations of Neuroplasticity-Related Genes in Adult Male Mice.

Levy, M, Allsopp, R, Futcher, A, Greider, C. and Harley, C. (1992). Telomere endreplication problem and cell aging. Journal of Molecular Biology, 225(4), pp.951-960.

Li, J. and Yuan, J. (2008). Caspases in apoptosis and beyond. Oncogene, 27(48), pp.6194-6206. Liao, H. and Spremulli, L. (1990). Identification and Initial Characterization of Translational Initiation Factor 2 from Bovine Mitochondria". The journal of biological chemistry, 265(23), pp.13618-13622.

Liao, H. and Spremulli, L. (1990). Identification and Initial Characterization of Translational Initiation Factor 2 from Bovine Mitochondria". *The journal of biological chemistry*, 265(23), pp.13618-13622.

Lieber, M. (2010). The Mechanism of Double-Strand DNA Break Repair by the Nonhomologous DNA End-Joining Pathway. Annual Review of Biochemistry, 79(1), pp.181-211.

Lim, S, Longley, M. and Copeland, W. (1999). The Mitochondrial p55 Accessory Subunit of Human DNA Polymerase γ Enhances DNA Binding, Promotes Processive DNA Synthesis, and ConfersN-Ethylmaleimide Resistance. Journal of Biological Chemistry, 274(53), pp.38197-38203. 342

Lin, X, Zhang, X, Guo, J, Roberts, C, McKenzie, S, Wu, W, Liu, S. and Song, Y. (2015). Effects of Exercise Training on Cardiorespiratory Fitness and Biomarkers of Cardiometabolic Health: A Systematic Review and Meta-Analysis of Randomized Controlled Trials. Journal of the American Heart Association, 4(7).

Lindenmayer, G, Sordahl, L, Harigaya, S, Allen, J, Besch, H. and Schwartz, A. (1971). Some biochemical studies on subcellular systems isolated from fresh recipient human cardiac tissue obtained during transplantation. The American Journal of Cardiology, 27(3), pp.277-283.

Linke, A, Adams, V, Schulze, P, Erbs, S, Gielen, S, Fiehn, E, Möbius-Winkler, S, Schubert, A, Schuler, G. and Hambrecht, R. (2005). Antioxidative Effects of Exercise Training in Patients With Chronic Heart Failure. Circulation, 111(14), pp.1763-1770.

Little, J, Safdar, A, Cermak, N, Tarnopolsky, M. and Gibala, M. (2010). Acute endurance exercise increases the nuclear abundance of PGC-1α in trained human skeletal muscle. American Journal of Physiology-Regulatory, Integrative and Comparative Physiology, 298(4), pp.R912-R917.

Liu, P, Qian, L, Sung, J, de Souza-Pinto, N, Zheng, L, Bogenhagen, D, Bohr, V, Wilson, D, Shen, B. and Demple, B. (2008). Removal of Oxidative DNA Damage via FEN1-Dependent Long-Patch Base Excision Repair in Human Cell Mitochondria. Molecular and Cellular Biology, 28(16), pp.4975-4987.

Liu, P. and Demple, B. (2010). DNA repair in mammalian mitochondria: Much more than we thought?. *Environmental and Molecular Mutagenesis*, p.NA-NA.

Ljubicic and D. A. Hood (2009). Diminished contraction-induced intracellular signaling towards mitochondrial biogenesis in aged skeletal muscle," Aging Cell, vol. 8, no. 4, pp. 394–404.

Ljubicic, V., Joseph, A., Adhihetty, P., Huang, J., Saleem, A., Uguccioni, G. and Hood, D. (2009). Molecular basis for an attenuated mitochondrial adaptive plasticity in aged skeletal muscle. *Aging*, 1(9), pp.818-830.

Logan, A, Shabalina, I, Prime, T, Rogatti, S, Kalinovich, A, Hartley, R, Budd, R, Cannon, B. and Murphy, M. (2014). In vivolevels of mitochondrial hydrogen peroxide increase with age in mtDNA mutator mice. *Aging Cell*, 13(4), pp.765-768.

Londhe, P. and Guttridge, D. (2015). Inflammation induced loss of skeletal muscle. *Bone*, 80, pp.131-142.

Lowery, D. and King, J. (2019). *Physiology, Cardiac Output*. Cleveland: StatPearls.

Lucchetti, B, Zanluqui, N, de Ataides Raquel, H, Lovo-Martins, M, Tatakihara, V, de Oliveira Belém, M, Michelini, L, de Almeida Araújo, E, Pinge-Filho, P. and Martins-

Pinge, M. (2017). Moderate Treadmill Exercise Training Improves Cardiovascular and Nitrergic Response and Resistance to Trypanosoma cruzi Infection in Mice. Frontiers in Physiology, 8.

Lundby, C. and Jacobs, R. (2015). Adaptations of skeletal muscle mitochondria to exercise training. Experimental Physiology, 101(1), pp.17-22.

Luo, S, Ge, Z, Wang, Z, Jiang, Z, Wang, Z, Ouyang, Y, Hou, Y, Schatten, H. and Sun, Q. (2013). Unique insights into maternal mitochondrial inheritance in mice. *Proceedings of the National Academy of Sciences*, 110(32), pp.13038-13043.

Luo, S, Valencia, C, Zhang, J, Lee, N, Slone, J, Gui, B, Wang, X, Li, Z, Dell, S, Brown, J, Chen, S, Chien, Y, Hwu, W, Fan, P, Wong, L, Atwal, P. and Huang, T. (2018). Biparental Inheritance of Mitochondrial DNA in Humans. *Proceedings of the National Academy of Sciences*, 115(51), pp.13039-13044.

Luoma, P, Melberg, A, Rinne, J, Kaukonen, J, Nupponen, N, Chalmers, R, Oldfors, A, Rautakorpi, I, Peltonen, L, Majamaa, K, Somer, H. and Suomalainen, A. (2004). Parkinsonism, premature menopause, and mitochondrial DNA polymerase γ mutations: clinical and molecular genetic study. The Lancet, 364(9437), pp.875- 882.

Lyons, C., Mathieu-Costello, O. and Moyes, C. (2006). Regulation of Skeletal Muscle Mitochondrial Content During Aging. *The Journals of Gerontology Series A: Biological Sciences and Medical Sciences*, 61(1), pp.3-13.

M. Mikhelson, V. and A. Gamaley, I. (2013). Telomere Shortening Is a Sole Mechanism of Aging in Mammals. *Current Aging Science*, 5(3), pp.203-208.

Ma, X, Fu, Y, Xiao, H, Song, Y, Chen, R, Shen, J, An, X, Shen, Q, Li, Z. and Zhang, Y. (2015). Cardiac Fibrosis Alleviated by Exercise Training Is AMPKDependent. PLOS ONE, 10(6), p.e0129971.

Maceira, A, Prasad, S, Khan, M. and Pennell, D. (2006). Reference right ventricular systolic and diastolic function normalized to age, gender and body surface area from steady-state free precession cardiovascular magnetic resonance. European Heart Journal, 27(23), pp.2879-2888.

Maklakov, A. and Lummaa, V. (2013). Evolution of sex differences in lifespan and aging: Causes and constraints. *BioEssays*, 35(8), pp.717-724.

Malanga, C. (2007). Structure and Function of the Heart. xPharm: The Comprehensive Pharmacology Reference, pp.1-5.

Manivannan, A, Soundararajan, P. and Jeong, B. (2017). Role of Reactive Oxygen Species Signaling in Cell Proliferation and Differentiation. Reactive Oxygen Species in Plants, pp.319-329. 344

Mallat, Z, Tedgui, A, Fontaliran, F, Frank, R, Durigon, M. and Fontaine, G. (1996). Evidence of Apoptosis in Arrhythmogenic Right Ventricular Dysplasia. *New England Journal of Medicine*, 335(16), pp.1190-1197.

Manivannan, A, Soundararajan, P. and Jeong, B. (2017). Role of Reactive Oxygen Species Signaling in Cell Proliferation and Differentiation. *Reactive Oxygen Species in Plants*, pp.319-329.

Manouze, H, Ghestem, A, Poillerat, V, Bennis, M, Ba-M'hamed, S, Benoliel, J, Becker, C. and Bernard, C. (2019). Effects of single cage housing in the rat and mouse pilocarpine models of epilepsy.

Margulis, L. and D. Bermudes, 1985. Symbiosis as a mechanism of evolution: Status of cell symbiosis theory. Symbiosis 1:101–124.

Marriott, B. and Carlson-Newberry, S. (1996). *Nutritional needs in cold and in high-altitude environments*. Washington, D.C.: National Academy Press.

Martin, M, Cho, J, Cesare, A, Griffith, J. and Attardi, G. (2005). Termination Factor-Mediated DNA Loop between Termination and Initiation Sites Drives Mitochondrial rRNA Synthesis. *Cell*, 123(7), pp.1227-1240.

Mayorga, M., Bahi, N., Ballester, M., Comella, J. and Sanchis, D. (2004). Bcl-2 Is a Key Factor for Cardiac Fibroblast Resistance to Programmed Cell Death. *Journal of Biological Chemistry*, 279(33), pp.34882-34889.

315

Mc Auley, M, Guimera, A, Hodgson, D, Mcdonald, N, Mooney, K, Morgan, A. and Proctor, C. (2017). Modelling the molecular mechanisms of aging. Bioscience Reports, 37(1), p.BSR20160177.

McDonald, S. A, L. C. Greaves, L. Gutierrez-Gonzalez, M. Rodriguez-Justo, M. Deheragoda, S. J. Leedham, R. W. Taylor, C. Y. Lee, S. L. Preston, M. Lovell, T. Hunt, G. Elia, D. Oukrif, R. Harrison, M. R. Novelli, I. Mitchell, D. L. Stoker, D. M. Turnbull, J. A. Jankowski and N. A. Wright (2008). "Mechanisms of field cancerization in the human stomach: the expansion and spread of mutated gastric stem cells." Gastroenterology 134(2): 500-510.

Media.cellsignal.com. (2019). [online] Available at: https://media.cellsignal.com/www/pdfs/science/pathways/Apoptosis_Mitochondrial.pdf [Accessed 1 May 2019].

Mella, J, Chiswick, E, King, E. and Remick, D. (2014). Location, Location, Location. *Shock*, 42(4), pp.337-342.

Menshikova, E, Ritov, V, Fairfull, L, Ferrell, R, Kelley, D. and Goodpaster, B. (2006). Effects of Exercise on Mitochondrial Content and Function in Aging Human Skeletal Muscle. The Journals of Gerontology Series A: Biological Sciences and Medical Sciences, 61(6), pp.534-540.

Mesoscale.com. (2019). *V-PLEX Mouse Cytokine 29-Plex Kit | Meso Scale Discovery*. [online] Available at: https://www.mesoscale.com/en/products/v-plex-mouse-cytokine-29-plex-kit-k15267d/ [Accessed 1 May 2019].

Mihl, C, Dassen, W. and Kuipers, H. (2008). Cardiac remodelling: concentric versus eccentric hypertrophy in strength and endurance athletes. *Netherlands Heart Journal*, 16(4), pp.129-133.

Mikkelsen, U, Couppé, C, Karlsen, A, Grosset, J, Schjerling, P, Mackey, A, Klausen, H, Magnusson, S. and Kjær, M. (2013). Life-long endurance exercise in humans: Circulating levels of inflammatory markers and leg muscle size. *Mechanisms of Ageing and Development*, 134(11-12), pp.531-540.

M. Mikhelson, V. and A. Gamaley, I. (2013). Telomere Shortening Is a Sole Mechanism of Aging in Mammals. *Current Aging Science*, 5(3), pp.203-208.

Milenkovic, D, Matic, S, Kuhl, I, Ruzzenente, B, Freyer, C, Jemt, E, Park, C, Falkenberg, M. and Larsson, N. (2013). TWINKLE is an essential mitochondrial helicase required for synthesis of nascent D-loop strands and complete mtDNA replication. Human Molecular Genetics, 22(10), pp.1983-1993.

Minczuk, M, He, J, Duch, A, Ettema, T, Chlebowski, A, Dzionek, K, Nijtmans, L, Huynen, M. and Holt, I. (2011). TEFM (c17orf42) is necessary for transcription of human mtDNA. Nucleic Acids Research, 39(10), pp.4284-4299.

Minor, M, Webel, R, Kay, D, Hewett, J. and Anderson, S. (1989). Efficacy of physical conditioning exercise in patients with rheumatoid arthritis and osteoarthritis. Arthritis & Rheumatism, 32(11), pp.1396-1405.

Miquel, J, A. C. Economos, J. Fleming and J. E. Johnson, Jr. (1980). "Mitochondrial role in cell aging." Exp Gerontol 15(6): 575-591.

Mita, S, Schmidt, B, Schon, E, DiMauro, S. and Bonilla, E. (1989). Detection of "deleted" mitochondrial genomes in cytochrome-c oxidase-deficient muscle fibers of a patient with Kearns-Sayre syndrome. Proceedings of the National Academy of Sciences, 86(23), pp.9509-9513.

Mittler, R. (2017). ROS Are Good. Trends in Plant Science, 22(1), pp.11-19. Miyaki, M, Yatagai, K. and Ono, T. (1977) Strand breaks of mammalian mitochondrial DNA induced by carcinogens. Chem. Biol. Interact. 17, 321–329

Miyaki, M, Yatagai, K. and Ono, T. (1977) Strand breaks of mammalian mitochondrial DNA induced by carcinogens. Chem. Biol. Interact. 17, 321–329

Molina, D. and DiMaio, V. (2015). Normal Organ Weights in Women. The American Journal of Forensic Medicine and Pathology, 36(3), pp.176-181.

Montoya, J, Christianson, T, Levens, D, Rabinowitz, M. and Attardi, G. (1982). Identification of initiation sites for heavy-strand and light-strand transcription in

human mitochondrial DNA. *Proceedings of the National Academy of Sciences*, 79(23), pp.7195-7199.

Moreira-Gonçalves, D, Ferreira, R, Fonseca, H, Padrão, A, Moreno, N, Silva, A, Vasques-Nóvoa, F, Gonçalves, N, Vieira, S, Santos, M, Amado, F, Duarte, J, Leite-Moreira, A. and Henriques-Coelho, T. (2015). Cardioprotective effects of early and late aerobic exercise training in experimental pulmonary arterial hypertension. Basic Research in Cardiology, 110(6).

Müller-Höcker, J. (1990). Cytochrome c oxidase deficient fibres in the limb muscle and diaphragm of man without muscular disease: An age-related alteration. Journal of the Neurological Sciences, 100(1-2), pp.14-21.

Müller-Höcker, J, Johannes, A, Droste, M, Kadenbach, B, Pongratz, D. and Hühner, G. (1986). Fatal mitochondrial cardiomyopathy in Kearns-Sayre syndrome with deficiency of cytochrome-c-oxidase in cardiac and skeletal muscle. *Virchows Archiv B Cell Pathology Including Molecular Pathology*, 52(1), pp.353-367.

Müller-Höcker, J, Schäfer, S, Weis, S, Münscher, C. and Strowitzki, T. (1996). Morphological-cytochemical and molecular genetic analyses of mitochondria in isolated human oocytes in the reproductive age. Molecular Human Reproduction, 2(12), pp.951-958.

Müller-Höcker, J, Seibel, P, Schneiderbanger, K. and Kadenbach, B. (1993). Different in situ hybridization patterns of mitochondrial DNA in cytochrome c oxidasedeficient extraocular muscle fibres in the elderly. Virchows Archiv A Pathological Anatomy and Histopathology, 422(1), pp.7-15.

Munukka, E, Ahtiainen, J, Puigbó, P, Jalkanen, S, Pahkala, K, Keskitalo, A, Kujala, U, Pietilä, S, Hollmén, M, Elo, L, Huovinen, P, D'Auria, G. and Pekkala, S. (2018). Six-Week Endurance Exercise Alters Gut Metagenome That Is not reflected in Systemic Metabolism in Over-weight Women. Frontiers in Microbiology, 9.

Murphy, E. (2017). The blood-brain barrier and protein-mediated fatty acid uptake: role of the blood-brain barrier as a metabolic barrier. Journal of Neurochemistry, 141(3), pp.324-329.

Murphy, M. (2009). How mitochondria produce reactive oxygen species. *Biochemical Journal*, 417(1), pp.1-13.

Nagy, P, Griesenbeck, J, Kornberg, R. and Cleary, M. (2001). A trithorax-group complex purified from Saccharomyces cerevisiae is required for methylation of histone H3. *Proceedings of the National Academy of Sciences*, 99(1), pp.90-94.

Narath, E, Skalicky, M. and Viidik, A. (2001). Voluntary and forced exercise influence the survival and body composition of ageing male rats differently. Experimental Gerontology, 36(10), pp.1699-1711.

Neubauer, S, Horn, M, Cramer, M, Harre, K, Newell, J, Peters, W, Pabst, T, Ertl, G, Hahn, D, Ingwall, J. and Kochsiek, K. (1997). Myocardial Phosphocreatine-toATP Ratio Is a Predictor of Mortality in Patients With Dilated Cardiomyopathy. Circulation, 96(7), pp.2190-2196.

Niu, X, Trifunovic, A, Larsson, N. and Canlon, B. (2007). Somatic mtDNA mutations cause progressive hearing loss in the mouse. *Experimental Cell Research*, 313(18), pp.3924-3934.

Nonogaki, K, Nozue, K. and Oka, Y. (2007). Social Isolation Affects the Development of Obesity and Type 2 Diabetes in Mice. *Endocrinology*, 148(10), pp.4658-4666.

Ojala, D, Montoya, J. and Attardi, G. (1981). tRNA punctuation model of RNA processing in human mitochondria. *Nature*, 290(5806), pp.470-474.

Olivo, P, Van de Walle, M, Laipis, P. and Hauswirth, W. (1983). Nucleotide sequence evidence for rapid genotypic shifts in the bovine mitochondrial DNA D-loop. *Nature*, 306(5941), pp.400-402.

Olovnikov, A. (1996). Telomeres, telomerase, and aging: Origin of the theory. Experimental Gerontology, 31(4), pp.443-448.

Olsson, I. and Dahlborn, K. (2002). Improving housing conditions for laboratory mice: a review of 'environmental enrichment'. *Laboratory Animals*, 36(3), pp.243-270.

Olver, T, Ferguson, B. and Laughlin, M. (2015). Molecular Mechanisms for Exercise Training-Induced Changes in Vascular Structure and Function. Progress in Molecular Biology and Translational Science, pp.227-257.

Omar García-Lepe, U. and Ma Bermúdez-Cruz, R. (2019). Mitochondrial Genome Maintenance: Damage and Repair Pathways. *DNA Repair- An Update*.

Ono, K. and Iijima, T. (2010). Cardiac T-type Ca2+ channels in the heart. Journal of Molecular and Cellular Cardiology, 48(1), pp.65-70.

Palmer, J, Tandler, B. and Hoppel, C. (1985). Biochemical differences between subsarcolemmal and interfibrillar mitochondria from rat cardiac muscle: Effects of procedural manipulations. Archives of Biochemistry and Biophysics, 236(2), pp.691-702.

Paneni, F, Diaz Cañestro, C, Libby, P, Lüscher, T. and Camici, G. (2017). The Aging Cardiovascular System. Journal of the American College of Cardiology, 69(15), pp.1952-1967.

Papaharalambus, C. and Griendling, K. (2007). Basic Mechanisms of Oxidative Stress and Reactive Oxygen Species in Cardiovascular Injury. *Trends in Cardiovascular Medicine*, 17(2), pp.48-54.

Paradies, G, Paradies, V, De Benedictis, V, Ruggiero, F. and Petrosillo, G. (2014). Functional role of cardiolipin in mitochondrial bioenergetics. Biochimica et Biophysica Acta (BBA) - Bioenergetics, 1837(4), pp.408-417.

Pekkala, S, Lensu, S, Nokia, M, Vanhatalo, S, Koch, L. G, Britton, S. L. (2017). Intrinsic aerobic capacity governs the associations between gut microbiota composition and fat metabolism age-dependently in rat siblings. *Physiol. Genomics* 49, 733–746. doi: 10.1152/physiolgenomics.00081.2017

Perier, C, Bender, A, García-Arumí, E, Melià, M, Bové, J, Laub, C, Klopstock, T, Elstner, M, Mounsey, R, Teismann, P, Prolla, T, Andreu, A. and Vila, M. (2013). Accumulation of mitochondrial DNA deletions within dopaminergic neurons triggers neuroprotective mechanisms. *Brain*, 136(8), pp.2369-2378.

Pham, A, Meng, S, Chu, Q. and Chan, D. (2012). Loss of Mfn2 results in progressive, retrograde degeneration of dopaminergic neurons in the nigrostriatal circuit. Human Molecular Genetics, 21(22), pp.4817-4826.

Philschatz.com. (2019). Heart Anatomy · Anatomy and Physiology. [online] Available at: https://philschatz.com/anatomy-book/contents/m46676.html [Accessed 1 May 2019].

Picca, A, Lezza, A, Leeuwenburgh, C, Pesce, V, Calvani, R, Bossola, M, Manes-Gravina, E, Landi, F, Bernabei, R. and Marzetti, E. (2018). Circulating Mitochondrial DNA at the Crossroads of Mitochondrial Dysfunction and Inflammation During Aging and Muscle Wasting Disorders. *Rejuvenation Research*, 21(4), pp.350-359.

Picard, M, Vincent, A. and Turnbull, D. (2016). Expanding Our Understanding of mtDNA Deletions. Cell Metabolism, 24(1), pp.3-4.

Pilegaard, H, Saltin, B. and Neufer, P. (2003). Exercise induces transient transcriptional activation of the PGC-1α gene in human skeletal muscle. The Journal of Physiology, 546(3), pp.851-858.

Pinnell, J, Turner, S. and Howell, S. (2007). Cardiac muscle physiology. Continuing Education in Anaesthesia Critical Care & Pain, 7(3), pp.85-88.

Pinto, E. (2007). Blood pressure and ageing. Postgraduate Medical Journal, 83(976), pp.109-114.

Pinton P, Rimessi A, Marchi S, Orsini F, Migliaccio E, Giorgio M, Contursi C, Minucci S, Mantovani F, Wieckowski MR, Del Sal G, Pelicci PG, Rizzuto R. Protein kinase C beta and prolyl isomerase 1 regulate mitochondrial effects of the life-span determinant p66Shc. Science. 2007 Feb 2; 315(5812):659-63.

Piquereau, J, Caffin, F, Novotova, M, Lemaire, C, Veksler, V, Garnier, A, Ventura-Clapier, R. and Joubert, F. (2013). Mitochondrial dynamics in the adult cardiomyocytes: which roles for a highly specialized cell?. *Frontiers in Physiology*, 4.

Poljsak, B, Šuput, D. and Milisav, I. (2013). Achieving the Balance between ROS and Antioxidants: When to Use the Synthetic Antioxidants. Oxidative Medicine and Cellular Longevity, 2013, pp.1-11. 349

Pollock, R, Carter, S, Velloso, C, Duggal, N, Lord, J, Lazarus, N. and Harridge, S. (2015). An investigation into the relationship between age and physiological function in highly active older adults. *The Journal of Physiology*, 593(3), pp.657-680.

Ponamarev, M, Longley, M, Nguyen, D, Kunkel, T. and Copeland, W. (2002). Active Site Mutation in DNA Polymerase γ Associated with Progressive External Ophthalmoplegia Causes Error-prone DNA Synthesis. Journal of Biological Chemistry, 277(18), pp.15225-15228.

Poole, D, Hirai, D, Copp, S. and Musch, T. (2012). Muscle oxygen transport and utilization in heart failure: implications for exercise (in)tolerance. American Journal of Physiology-Heart and Circulatory Physiology, 302(5), pp.H1050-H1063. Porter, A. and Jänicke, R. (1999). Emerging roles of caspase-3 in apoptosis. Cell Death & Differentiation, 6(2), pp.99-104.

Porter, A. and Jänicke, R. (1999). Emerging roles of caspase-3 in apoptosis. *Cell Death & Differentiation*, 6(2), pp.99-104.

Posse, V. and Gustafsson, C. (2016). Human Mitochondrial Transcription Factor B2 Is Required for Promoter Melting during Initiation of Transcription. Journal of Biological Chemistry, 292(7), pp.2637-2645.

Posttranslational Targeting of Proteins. (2017). *Cell Biology*, pp.303-315.

Rand, D. (2008). Mitigating Mutational Meltdown in Mammalian Mitochondria. *PLoS Biology*, 6(2), p.e35.

Reaburn, P. and Dascombe, B. (2008). Endurance performance in masters athletes. European Review of Aging and Physical Activity, 5(1), pp.31-42.

Regis, F. (2007). Albert | Learn by doing | Grades 5-12 reading, writing, math, science, and test prep. [online] Albert.io. Available at:

https://www.albert.io/learn/apbiology/biological-processes-ek-2a2/topic-summary [Accessed 16 Jul. 2019].

Reyes, A, Yang, M, Bowmaker, M. and Holt, I. (2004). Bidirectional Replication Initiates at Sites Throughout the Mitochondrial Genome of Birds. Journal of Biological Chemistry, 280(5), pp.3242-3250.

Richter, R, Pajak, A, Dennerlein, S, Rozanska, A, Lightowlers, R. and Chrzanowska-Lightowlers, Z. (2010). Translation termination in human mitochondrial ribosomes. *Biochemical Society Transactions*, 38(6), pp.1523-1526.

Ringel, R, Sologub, M, Morozov, Y, Litonin, D, Cramer, P. and Temiakov, D. (2011). Structure of human mitochondrial RNA polymerase. *Nature*, 478(7368), pp.269-273.

Robberson, D, Kasamatsu, H. and Vinograd, J. (1972). Replication of Mitochondrial DNA. Circular Replicative Intermediates in Mouse L Cells. Proceedings of the National Academy of Sciences, 69(3), pp.737-741.

Robinson S. Experimental studies of physical fitness in relation to age. Arbeitsphysiologie. 1938; 10: 251–323. 2.

Robinson, M, Dasari, S, Konopka, A, Johnson, M, Manjunatha, S, Esponda, R, Carter, R, Lanza, I. and Nair, K. (2017). Enhanced Protein Translation Underlies Improved Metabolic and Physical Adaptations to Different Exercise Training Modes in Young and Old Humans. Cell Metabolism, 25(3), pp.581-592.

Rocha, L, Oliveira, K, Migliolo, L. and Franco, O. (2015). Effect of Moderate Exercise on Mitochondrial Proteome in Heart Tissue of Spontaneous Hypertensive Rats. American Journal of Hypertension, 29(6), pp.696-704.

Roh, J, Rhee, J, Chaudhari, V. and Rosenzweig, A. (2016). The Role of Exercise in Cardiac Aging. Circulation Research, 118(2), pp.279-295.

Rosenzweig, A. (2016). The Role of Exercise in Cardiac Aging. Circulation Research, 118(2), pp.279-295.

Rossignol, R, Gilkerson, R, Aggeler, R, Yamagata, K, Remington, S. and Capaldi, R. (2004). Energy Substrate Modulates Mitochondrial Structure and Oxidative Capacity in Cancer Cells. Cancer Research, 64(3), pp.985-993.

Rossignol, R, Faustin, B, Rocher, C, Malgat, M, Mazat, J. and Letellier, T. (2003). Mitochondrial threshold effects. *Biochemical Journal*, 370(3), pp.751-762.

Rottbauer, W, Baker, K, Wo, Z, Mohideen, M, Cantiello, H. and Fishman, M. (2001). Growth and Function of the Embryonic Heart Depend upon the CardiacSpecific L-Type Calcium Channel α1 Subunit. Developmental Cell, 1(2), pp.265-275.

Rowe, G, El-Khoury, R, Patten, I, Rustin, P. and Arany, Z. (2012). PGC-1α is Dispensable for Exercise-Induced Mitochondrial Biogenesis in Skeletal Muscle. *PLoS ONE*, 7(7), p.e41817.

Rusecka, J, Kaliszewska, M, Bartnik, E. and Tońska, K. (2018). Nuclear genes involved in mitochondrial diseases caused by instability of mitochondrial DNA. *Journal of Applied Genetics*, 59(1), pp.43-57.

Sabbah, H. (2000). Apoptotic cell death in heart failure. *Cardiovascular Research*, 45(3), pp.704-712.

Safdar, A, Bourgeois, J, Ogborn, D, Little, J, Hettinga, B, Akhtar, M, Thompson, J, Melov, S, Mocellin, N, Kujoth, G, Prolla, T. and Tarnopolsky, M. (2011). Endurance exercise rescues progeroid aging and induces systemic mitochondrial rejuvenation in mtDNA mutator mice. *Proceedings of the National Academy of Sciences*, 108(10), pp.4135-4140.

Safdar, A, Annis, S, Kraytsberg, Y, Laverack, C, Saleem, A, Popadin, K, Woods, D, Tilly, J. and Khrapko, K. (2016). Amelioration of premature aging in mtDNA mutator mouse by exercise: the interplay of oxidative stress, PGC-1α, p53, and DNA damage. A hypothesis. *Current Opinion in Genetics & Development*, 38, pp.127-132.

Safdar, A, Khrapko, K, Flynn, J, Saleem, A, De Lisio, M, Johnston, A, Kratysberg, Y, Samjoo, I, Kitaoka, Y, Ogborn, D, Little, J, Raha, S, Parise, G, Akhtar, M, Hettinga, B,

Rowe, G, Arany, Z, Prolla, T. and Tarnopolsky, M. (2015). Exercise-induced mitochondrial p53 repairs mtDNA mutations in mutator mice. *Skeletal Muscle*, 6(1).

Sandoiu, A. (2019). *How endurance exercise affects your gut bacteria*. [online] Medical News Today. Available at: https://www.medicalnewstoday.com/articles/323351.php [Accessed 12 Jul. 2019].

Sarcopenia, obesity, and natural killer cell immune senescence in aging: altered cytokine levels as a common mechanism

Sato, M. and Sato, K. (2013). Maternal inheritance of mitochondrial DNA by diverse mechanisms to eliminate paternal mitochondrial DNA. Biochimica et Biophysica Acta (BBA) - Molecular Cell Research, 1833(8), pp.1979-1984.

Saxton, A. and Bordoni, B. (2018). Anatomy, Thorax, Cardiac Muscle. Miami: Treasure Island (FL): StatPearls Publishing.

Scarpulla, R, Vega, R. and Kelly, D. (2012). Transcriptional integration of mitochondrial biogenesis. Trends in Endocrinology & Metabolism, 23(9), pp.459-466. Scheuer, J. and Tipton, C. (1977). Cardiovascular Adaptations to Physical Training. Annual Review of Physiology, 39(1), pp.221-251.

Scheuer, J. and Tipton, C. (1977). Cardiovascular Adaptations to Physical Training. *Annual Review of Physiology*, 39(1), pp.221-251.

Schiavone, S, Morgese, M, Mhillaj, E, Bove, M, De Giorgi, A, Cantatore, F, Camerino, C, Tucci, P, Maffulli, N, Cuomo, V. and Trabace, L. (2016). Chronic Psychosocial Stress Impairs Bone Homeostasis: A Study in the Social Isolation Reared Rat. *Frontiers in Pharmacology*, 7.

Schriner, S. (2005). Extension of Murine Life Span by Overexpression of Catalase Targeted to Mitochondria. Science, 308(5730), pp.1909-1911.

Schriner, S. and Linford, N. (2006). Extension of mouse lifespan by overexpression of catalase. Age, 28(2), pp.209-218.

Schultz, B. and Chan, S. (2001). Structures and Proton-Pumping Strategies of Mitochondrial Respiratory Enzymes. Annual Review of Biophysics and Biomolecular Structure, 30(1), pp.23-65.

Schulz, T, Zarse, K, Voigt, A, Urban, N, Birringer, M. and Ristow, M. (2007). Glucose Restriction Extends Caenorhabditis elegans Life Span by Inducing Mitochondrial Respiration and Increasing Oxidative Stress. Cell Metabolism, 6(4), pp.280-293.

Schwartz, M. and Vissing, J. (2002). Paternal Inheritance of Mitochondrial DNA. *New England Journal of Medicine*, 347(8), pp.576-580.

Scott, I. and Youle, R. (2010). Mitochondrial fission and fusion. Essays In Biochemistry, 47, pp.85-98. Seibenhener, M. and Wooten, M. (2015). Use of the Open Field Maze to Measure Locomotor and Anxiety-like Behavior in Mice. Journal of Visualized Experiments, (96).

Scott, I. and Youle, R. (2010). Mitochondrial fission and fusion. *Essays In Biochemistry*, 47, pp.85-98.

Seibenhener, M. and Wooten, M. (2015). Use of the Open Field Maze to Measure Locomotor and Anxiety-like Behavior in Mice. *Journal of Visualized Experiments*, (96).

Sergiev, P, Dontsova, O. and Berezkin, G. (2015). Theories of Aging: An Ever-Evolving Field. *Acta Naturae*, 7(1), pp.9-18.

Sesaki, H, Southard, S, Yaffe, M. and Jensen, R. (2003). Mgm1p, a Dynaminrelated GTPase, Is Essential for Fusion of the Mitochondrial Outer Membrane. Molecular Biology of the Cell, 14(6), pp.2342-2356.

Simard, S., Coppola, G., Rudyk, C., Hayley, S., McQuaid, R. and Salmaso, N. (2018). Profiling changes in cortical astroglial cells following chronic stress. *Neuropsychopharmacology*, 43(9), pp.1961-1971.

Shabalina, I, Vyssokikh, M, Gibanova, N, Csikasz, R, Edgar, D, HalldenWaldemarson, A, Rozhdestvenskaya, Z, Bakeeva, L, Vays, V, Pustovidko, A,

Skulachev, M, Cannon, B, Skulachev, V. and Nedergaard, J. (2017). Improved health-span and lifespan in mtDNA mutator mice treated with the mitochondrially targeted antioxidant SkQ1. Aging, 9(2), pp.315-339.

Shadel, G. and Clayton, D. (1997). Mitochondrial DNA maintenance in vertebrates. Annual Review of Biochemistry, 66(1), pp.409-435.

Sharma, L, Lu, J. and Bai, Y. (2009). Mitochondrial Respiratory Complex I: Structure, Function and Implication in Human Diseases. Current Medicinal Chemistry, 16(10), pp.1266-1277.

Sheps, S. (2019). *How cold weather affects your blood pressure.* [online] Mayo Clinic. Available at: https://www.mayoclinic.org/diseases-conditions/high-blood-pressure/expert-answers/blood-pressure/faq-20058250 [Accessed 12 Jul. 2019].

Shi, Y, Posse, V, Zhu, X, Hyvärinen, A, Jacobs, H, Falkenberg, M. and Gustafsson, C. (2016). Mitochondrial transcription termination factor 1 directs polar replication fork pausing. *Nucleic Acids Research*, 44(12), pp.5732-5742.

Short, K, Bigelow, M, Kahl, J, Singh, R, Coenen-Schimke, J, Raghavakaimal, S. and Nair, K. (2005). Decline in skeletal muscle mitochondrial function with aging in humans. Proceedings of the National Academy of Sciences, 102(15), pp.5618-5623. 353

Sigurðardóttir, S, Helgason, A, Gulcher, J, Stefansson, K. and Donnelly, P. (2000). The Mutation Rate in the Human mtDNA Control Region. The American Journal of Human Genetics, 66(5), pp.1599-1609.

Silva, J, Köhler, M, Graff, C, Oldfors, A, Magnuson, M, Berggren, P. and Larsson, N. (2000). Impaired insulin secretion and β-cell loss in tissue-specific knockout mice with mitochondrial diabetes. *Nature Genetics*, 26(3), pp.336-340.

Singh, R, Mengi, S, Xu, Y, Arneja, A. and Dhalla, N. (2002). Pathogenesis of atherosclerosis: A multifactorial process. *Experimental Clinical Cardiology*, 7(1).

Skinner, J. (2005). Influence of genetic factors on exercise and training. [online] 40, pp.121-128. Available at: http://file:///H:/Downloads/2005-40-3-121-128-eng.pdf [Accessed 27 Aug. 2019].

Skulachev, V. (2007). A biochemical approach to the problem of aging: "Megaproject" on membrane-penetrating ions. The first results and prospects. Biochemistry (Moscow), 72(12), pp.1385-1396.

Smits, P, Smeitink, J. and van den Heuvel, L. (2019). Mitochondrial Translation and Beyond: Processes Implicated in Combined Oxidative Phosphorylation Deficiencies.

Sohal, R. and Weindruch, R. (1996). Oxidative Stress, Caloric Restriction, and Aging. *Science*, 273(5271), pp.59-63.

Somani, S, Frank, S. and Rybak, L. (1995). Responses of antioxidant system to acute and trained exercise in rat heart subcellular fractions. Pharmacology Biochemistry and Behavior, 51(4), pp.627-634.

Song, D, Park, J, Maurer, L, Lu, W, Philbert, M. and Sastry, A. (2013). Biophysical significance of the inner mitochondrial membrane structure on the electrochemical potential of mitochondria. Physical Review E, 88(6).

Sörensen, L, Ekstrand, M, Silva, J, Lindqvist, E, Xu, B, Rustin, P, Olson, L. and Larsson, N. (2001). Late-Onset Corticohippocampal Neurodepletion Attributable to Catastrophic Failure of Oxidative Phosphorylation in MILON Mice. The Journal of Neuroscience, 21(20), pp.8082-8090.

Späni, D, Arras, M, König, B. and Rülicke, T. (2003). Higher heart rate of laboratory mice housed individually vs in pairs. *Laboratory Animals*, 37(1), pp.54-62.

Stamp, C, Zupanic, A, Sachdeva, A, Stoll, E, Shanley, D, Mathers, J, Kirkwood, T, Heer, R, Simons, B, Turnbull, D. and Greaves, L. (2018). Predominant Asymmetrical Stem Cell Fate Outcome Limits the Rate of Niche Succession in Human Colonic Crypts. *EBioMedicine*, 31, pp.166-173.

Stehling, O. and Lill, R. (2013). The Role of Mitochondria in Cellular Iron-Sulfur Protein Biogenesis: Mechanisms, Connected Processes, and Diseases. *Cold Spring Harbor Perspectives in Biology*, 5(8), pp.a011312-a011312.

Steptoe, A, Shankar, A, Demakakos, P. and Wardle, J. (2013). Social isolation, loneliness, and all-cause mortality in older men and women. *Proceedings of the National Academy of Sciences*, 110(15), pp.5797-5801.

St-Pierre, J, Drori, S, Uldry, M, Silvaggi, J, Rhee, J, Jäger, S, Handschin, C, Zheng, K, Lin, J, Yang, W, Simon, D, Bachoo, R. and Spiegelman, B. (2006). Suppression of Reactive Oxygen Species and Neurodegeneration by the PGC-1 Transcriptional Coactivators. Cell, 127(2), pp.397-408.

Strait, J. and Lakatta, E. (2012). Aging-Associated Cardiovascular Changes and Their Relationship to Heart Failure. *Heart Failure Clinics*, 8(1), pp.143-164.

Stumpf, J, Saneto, R. and Copeland, W. (2013). Clinical and Molecular Features of POLG-Related Mitochondrial Disease. Cold Spring Harbor Perspectives in Biology, 5(4), pp.a011395-a011395.

Sugiura, A, McLelland, G, Fon, E. and McBride, H. (2014). A new pathway for mitochondrial quality control: mitochondrial-derived vesicles. The EMBO Journal, 33(19), pp.2142-2156.

Sun, J. and Tower, J. (1999). FLP Recombinase-Mediated Induction of Cu/ZnSuperoxide Dismutase Transgene Expression Can Extend the Life Span of AdultDrosophila melanogasterFlies. Molecular and Cellular Biology, 19(1), pp.216-228.

Sun, X. and St. John, J. (2016). The role of the mtDNA set point in differentiation, development and tumorigenesis. Biochemical Journal, [online] 473(19), pp.2955-2971. Available at: http://www.biochemj.org/content/473/19/2955.figures-only [Accessed 16 Jul. 2019].

Sutovsky, P, Moreno, R, Ramalho-Santos, J, Dominko, T, Simerly, C. and Schatten, G. (2000). Ubiquitinated Sperm Mitochondria, Selective Proteolysis, and the

Regulation of Mitochondrial Inheritance in Mammalian Embryos1. *Biology of Reproduction*, 63(2), pp.582-590.

Svensson, M., Rosvall, P., Boza-Serrano, A., Andersson, E., Lexell, J. and Deierborg, T. (2016). Forced treadmill exercise can induce stress and increase neuronal damage in a mouse model of global cerebral ischemia. *Neurobiology of Stress*, 5, pp.8-18.

Swerdlow, R, Parks, J, Miller, S, Davis, R, Tuttle, J, Trimmer, P, Sheehan, J, Bennett, J. and Parker, W. (1996). Origin and functional consequences of the complex I defect in Parkinson's disease. Annals of Neurology, 40(4), pp.663-671.

Swoap, S. and Gutilla, M. (2009). Cardiovascular changes during daily torpor in the laboratory mouse. *American Journal of Physiology-Regulatory, Integrative and Comparative Physiology*, 297(3), pp.R769-R774.

Szczepanowska, K. and Trifunovic, A. (2017). Origins of mtDNA mutations in ageing. *Essays In Biochemistry*, 61(3), pp.325-337.

Taanman, J. (1999). The mitochondrial genome: structure, transcription, translation and replication. *Biochimica et Biophysica Acta (BBA) - Bioenergetics*, 1410(2), pp.103-123.

Tadaishi, M, Miura, S, Kai, Y, Kano, Y, Oishi, Y. and Ezaki, O. (2011). Skeletal Muscle-Specific Expression of PGC-1α-b, an Exercise-Responsive Isoform, Increases Exercise Capacity and Peak Oxygen Uptake. PLoS ONE, 6(12), p.e28290.

Taivassalo, T. (2003). The spectrum of exercise tolerance in mitochondrial myopathies: a study of 40 patients. Brain, 126(2), pp.413-423.

Taivassalo, T. and Haller, R. (2019). Implications of exercise training in mtDNA defects—use it or lose it?. Biochimica et Biophysica Acta (BBA) - Bioenergetics, 1659(2-3), pp.221-231.

Takawale, A, Zhang, P, Patel, V, Wang, X, Oudit, G. and Kassiri, Z. (2017). Tissue Inhibitor of Matrix Metalloproteinase-1 Promotes Myocardial Fibrosis by Mediating CD63–Integrin β1 Interaction. Hypertension, 69(6), pp.1092-1103.

Taki, A, Kermani, A, Ranjbarnavazi, S. and Pourmodheji, A. (2017). Overview of Different Medical Imaging Techniques for the Identification of Coronary Atherosclerotic Plaques. *Computing and Visualization for Intravascular Imaging and Computer-Assisted Stenting*, pp.79-106.

Talan, M. (1984). Body temperature of C57BL/6J mice with age. *Experimental Gerontology*, 19(1), pp.25-29.

Talbot, L, Metter, E. and Fleg, J. (2000). Leisure-time physical activities and their relationship to cardiorespiratory fitness in healthy men and women 18???95 years old. *Medicine & Science in Sports & Exercise*, 32(2), p.417.

Tang, A, Eng, J, Krassioukov, A, Madden, K, Mohammadi, A, Tsang, M. and Tsang, T. (2013). Exercise-Induced Changes in Cardiovascular Function after Stroke: A Randomized Controlled Trial. International Journal of Stroke, 9(7), pp.883- 889.

Tarasov, A, Griffiths, E. and Rutter, G. (2012). Regulation of ATP production by mitochondrial Ca2+. Cell Calcium, 52(1), pp.28-35.

Taverne, Y, Bogers, A, Duncker, D. and Merkus, D. (2013). Reactive Oxygen Species and the Cardiovascular System. Oxidative Medicine and Cellular Longevity, 2013, pp.1-15.

Taverne, Y, Bogers, A, Duncker, D. and Merkus, D. (2019). *Reactive Oxygen Species and the Cardiovascular System*.

Taylor, R, Barron, M, Borthwick, G, Gospel, A, Chinnery, P, Samuels, D, Taylor, G, Plusa, S, Needham, S, Greaves, L, Kirkwood, T. and Turnbull, D. (2003). Mitochondrial DNA mutations in human colonic crypt stem cells. Journal of Clinical Investigation, 112(9), pp.1351-1360.

Taylor, R, McDonnell, M, Blakely, E, Chinnery, P, Taylor, G, Howell, N, Zeviani, M, Briem, E, Carrara, F. and Turnbull, D. (2003). Genotypes from patients indicate no paternal mitochondrial DNA contribution. *Annals of Neurology*, 54(4), pp.521-524.

Tegtbur, U, Busse, M. and Kubis, H. (2009). Körperliches Training und zelluläre Anpassung des Muskels. Der Unfallchirurg, 112(4), pp.365-372.

Terman, A. (2001). Garbage catastrophe theory of aging: imperfect removal of oxidative damage?. *Redox Report*, 6(1), pp.15-26.

Terman, A. and Brunk, U. (2006). Oxidative Stress, Accumulation of Biological 'Garbage', and Aging. Antioxidants & Redox Signaling, 8(1-2), pp.197-204.

Terzioglu, M, Ruzzenente, B, Harmel, J, Mourier, A, Jemt, E, López, M, Kukat, C, Stewart, J, Wibom, R, Meharg, C, Habermann, B, Falkenberg, M, Gustafsson, C, Park, C. and Larsson, N. (2013). MTERF1 Binds mtDNA to Prevent Transcriptional Interference at the Light-Strand Promoter but Is Dispensable for rRNA Gene Transcription Regulation. *Cell Metabolism*, 17(4), pp.618-626.

Thanassoulis, G. and Vasan, R. (2010). Genetic Cardiovascular Risk Prediction. Circulation, 122(22), pp.2323-2334.

The Jackson Laboratory. (2019). *Body Weight Information for Aged C57BL/6J (000664)*. [online] Available at: https://www.jax.org/jax-mice-and-services/strain-data-sheet-pages/body-weight-chart-aged-b6 [Accessed 7 Feb. 2019].

Tilokani, L, Nagashima, S, Paupe, V. and Prudent, J. (2018). Mitochondrial dynamics: overview of molecular mechanisms. Essays In Biochemistry, 62(3), pp.341-360.

Tomkinson, A. and Mackey, Z. (1998). Structure and function of mammalian DNA ligases. Mutation Research/DNA Repair, 407(1), pp.1-9.

Trifunov, S, Pyle, A, Valentino, M, Liguori, R, Yu-Wai-Man, P, Burté, F, Duff, J, Kleinle, S, Diebold, I, Rugolo, M, Horvath, R. and Carelli, V. (2018). Clonal expansion

of mtDNA deletions: different disease models assessed by digital droplet PCR in single muscle cells. Scientific Reports, 8(1).

Trifunovic, A, Wredenberg, A, Falkenberg, M, Spelbrink, J, Rovio, A, Bruder, C, Bohlooly-Y, M, Gidlöf, S, Oldfors, A, Wibom, R, Törnell, J, Jacobs, H. and Larsson, N. (2004). Premature ageing in mice expressing defective mitochondrial DNA polymerase. Nature, 429(6990), pp.417-423.

Tung, V, Burton, T, Dababneh, E, Quail, S. and Camp, A. (2014). Behavioral Assessment of the Aging Mouse Vestibular System. Journal of Visualized Experiments, (89). Turrens, J. (2003). Mitochondrial formation of reactive oxygen species. The Journal of Physiology, 552(2), pp.335-344.

Tung, V, Burton, T, Dababneh, E, Quail, S. and Camp, A. (2014). Behavioral Assessment of the Aging Mouse Vestibular System. *Journal of Visualized Experiments*, (89).

Turrens, J. and Boveris, A. (1980). Generation of superoxide anion by the NADH dehydrogenase of bovine heart mitochondria. Biochemical Journal, 191(2), pp.421-427. 358

Turrens, J. (2003). Mitochondrial formation of reactive oxygen species. *The Journal of Physiology*, 552(2), pp.335-344.

Twig, G, Elorza, A, Molina, A, Mohamed, H, Wikstrom, J, Walzer, G, Stiles, L, Haigh, S, Katz, S, Las, G, Alroy, J, Wu, M, Py, B, Yuan, J, Deeney, J, Corkey, B. and Shirihai, O. (2008). Fission and selective fusion govern mitochondrial segregation and elimination by autophagy. The EMBO Journal, 27(2), pp.433-446.

UT Southwestern Medical Center. "Proper exercise can reverse damage from heart aging." ScienceDaily. ScienceDaily, 8 January 2018. <www.sciencedaily.com/releases/2018/01/180108090132.htm>.

Van der Bliek, A, Shen, Q. and Kawajiri, S. (2013). Mechanisms of Mitochondrial Fission and Fusion. Cold Spring Harbor Perspectives in Biology, 5(6), pp.a011072-a011072.

Vanempel, V, Bertrand, A, Hofstra, L, Crijns, H, Doevendans, P. and Dewindt, L. (2005). Myocyte apoptosis in heart failure. *Cardiovascular Research*, 67(1), pp.21-29.

Venditti, P, Napolitano, G, Barone, D. and Di Meo, S. (2013). Effect of training and vitamin E administration on rat liver oxidative metabolism. Free Radical Research, 48(3), pp.322-332.

Vermulst, M, Bielas, J, Kujoth, G, Ladiges, W, Rabinovitch, P, Prolla, T. and Loeb, L. (2007). Mitochondrial point mutations do not limit the natural lifespan of mice. Nature Genetics, 39(4), pp.540-543.

Vermulst, M, Wanagat, J, Kujoth, G, Bielas, J, Rabinovitch, P, Prolla, T. and Loeb, L. (2008). DNA deletions and clonal mutations drive premature aging in mitochondrial mutator mice. *Nature Genetics*, 40(4), pp.392-394.

Vijg, J. and Campisi, J. (2008). Puzzles, promises and a cure for ageing. *Nature*, 454(7208), pp.1065-1071.

Villani, G. and Attardi, G. (1997). In vivo control of respiration by cytochrome c oxidase in wild-type and mitochondrial DNA mutation-carrying human cells. Proceedings of the National Academy of Sciences, 94(4), pp.1166-1171.

Vogel, F, Bornhövd, C, Neupert, W. and Reichert, A. (2006). Dynamic subcompartmentalization of the mitochondrial inner membrane. The Journal of Cell Biology, 175(2), pp.237-247. 359

Wajant, H. (2002). The Fas Signaling Pathway: More Than a Paradigm. Science, 296(5573), pp.1635-1636.

Wakabayashi, J, Zhang, Z, Wakabayashi, N, Tamura, Y, Fukaya, M, Kensler, T, Iijima, M. and Sesaki, H. (2009). The dynamin-related GTPase Drp1 is required for embryonic and brain development in mice. The Journal of Cell Biology, 186(6), pp.805-816.

Wallace, D. (1992). Mitochondrial genetics: a paradigm for aging and degenerative diseases?. *Science*, 256(5057), pp.628-632.

Wallace, D. and Chalkia, D. (2013). Mitochondrial DNA Genetics and the Heteroplasmy Conundrum in Evolution and Disease. Cold Spring Harbor Perspectives in Biology, 5(11), pp.a021220-a021220.

Wallace, D, Singh, G, Lott, M, Hodge, J, Schurr, T, Lezza, A, Elsas, L. and Nikoskelainen, E. (1988). Mitochondrial DNA mutation associated with Leber's hereditary optic neuropathy. *Science*, 242(4884), pp.1427-1430.

Wallace, D, Zheng, X, Lott, M, Shoffner, J, Hodge, J, Kelley, R, Epstein, C. and Hopkins, L. (1988). Familial mitochondrial encephalomyopathy (MERRF): Genetic, pathophysiological, and biochemical characterization of a mitochondrial DNA disease. Cell, 55(4), pp.601-610.

Wang, C. and Youle, R. (2009). The Role of Mitochondria in Apoptosis. Annual Review of Genetics, 43(1), pp.95-118.

Wang, J. and Pantopoulos, K. (2011). Regulation of cellular iron metabolism. Biochemical Journal, 434(3), pp.365-381.

Wang, X, Wang, W, Li, L, Perry, G, Lee, H. and Zhu, X. (2014). Oxidative stress and mitochondrial dysfunction in Alzheimer's disease. Biochimica et Biophysica Acta (BBA) - Molecular Basis of Disease, 1842(8), pp.1240-1247.

Wanrooij, P. and Chabes, A. (2019). Ribonucleotides in mitochondrial DNA. FEBS Letters. Wan-Teng, L. (2016). Regular Exercise And Resveratrol Attenuates Oxidative Damage And Ameliorates In Aging Mouse Heart. Medicine & Science in Sports & Exercise, 48, p.906.

Wan-Teng, L. (2016). Regular Exercise And Resveratrol Attenuates Oxidative Damage And Ameliorates In Aging Mouse Heart. *Medicine & Science in Sports & Exercise*, 48, p.906.

Ward, J. (2001). *Cardiac muscle*. New York: Oxford University.

Watt, I, Montgomery, M, Runswick, M, Leslie, A. and Walker, J. (2010). Bioenergetic cost of making an adenosine triphosphate molecule in animal mitochondria. *Proceedings of the National Academy of Sciences*, 107(39), pp.16823-16827.

Webb, S, Brown, N. and Anderson, R. (1996). The structure of the mouse heart in late fetal stages. Anatomy and Embryology, 194(1).

Weichbrod RH, T. (2018). Management of Animal Care and Use Programs in Research, Education, and Testing. 2nd edition. [Place of publication not identified]: CRC Press/Taylor & Francis.

Weisfeldt, M. (1998). Aging, Changes in the Cardiovascular System, and Responses to Stress. American Journal of Hypertension, 11(3), pp.41S-45S.

Weismann A. Uber die Dauer des Lebens. Jena, Germany: Verlag von Gustav Fisher; 1882.

Weiss, J. (1934). Reaction Mechanism of Oxidation-Reduction Processes. Nature, 133(3365), pp.648-649.

Welchen, E, García, L, Mansilla, N. and Gonzalez, D. (2014). Coordination of plant mitochondrial biogenesis: keeping pace with cellular requirements. Frontiers in Plant Science, 4.

Wenger, H. and Bell, G. (1986). The Interactions of Intensity, Frequency and Duration of Exercise Training in Altering Cardiorespiratory Fitness. *Sports Medicine*, 3(5), pp.346-356.

Wessels, A. and Sedmera, D. (2003). Developmental anatomy of the heart: a tale of mice and man. Physiological Genomics, 15(3), pp.165-176.

West, A, Shadel, G. and Ghosh, S. (2011). Mitochondria in innate immune responses. *Nature Reviews Immunology*, 11(6), pp.389-402.

Who.int. (2019). Cardiovascular diseases. [Online] Available at: https://www.who.int/health-topics/cardiovascular-diseases/ [Accessed 18 Jul. 2019].

Who.int. (2019). *Cardiovascular diseases (CVDs)*. [online] Available at: https://www.who.int/news-room/fact-sheets/detail/cardiovascular-diseases-(cvds) [Accessed 7 Jan. 2019].

Wiesmann, F, Ruff, J, Hiller, K, Rommel, E, Haase, A. and Neubauer, S. (2000). Developmental changes of cardiac function and mass assessed with MRI in neonatal, juvenile, and adult mice. *American Journal of Physiology-Heart and Circulatory Physiology*, 278(2), pp.H652-H657.

Wilde, E, Aubdool, A, Thakore, P, Baldissera, L, Alawi, K, Keeble, J, Nandi, M. and Brain, S. (2017). Tail-Cuff Technique and Its Influence on Central Blood Pressure in the Mouse. Journal of the American Heart Association, 6(6).

Willett, W. (2006). The Mediterranean diet: science and practice. Public Health Nutrition, 9(1a), pp.105-110.

Wisløff, U. (2002). Aerobic exercise reduces cardiomyocyte hypertrophy and increases contractility, Ca2+ sensitivity and SERCA-2 in rat after myocardial infarction. Cardiovascular Research, 54(1), pp.162-174.

Wohlgemuth, S, Seo, A, Marzetti, E, Lees, H. and Leeuwenburgh, C. (2010). Skeletal muscle autophagy and apoptosis during aging: Effects of calorie restriction and life-long exercise. *Experimental Gerontology*, 45(2), pp.138-148.

mortality while voluntary wheel training is protective in a mouse model of colitis. *Brain, Behavior, and Immunity*, 33, pp.46-56.

Woodward, D. (2015). Energy III - Cellular Respiration (Krebs Cycle and Electron Transport Chain) - BIOL110SUMMERTEST - Confluence. [Online] Wikispaces.psu.edu. Available at: https://wikispaces.psu.edu/pages/viewpage.action?pageId=272728892 [Accessed 16 Jul. 2019].

Wooley, C., Xing, S., Burgess, R., Cox, G. and Seburn, K. (2009). Age, experience and genetic background influence treadmill walking in mice. *Physiology & Behavior*, 96(2), pp.350-361.

World Health Organization. (2019). World Health Statistics 2018: Monitoring health for the SDGs. [online] Available at: https://www.who.int/gho/publications/world_health_statistics/2018/en/ [Accessed 18 Jul. 2019].

Wredenberg, A, Freyer, C, Sandström, M, Katz, A, Wibom, R, Westerblad, H. and Larsson, N. (2006). Respiratory chain dysfunction in skeletal muscle does not cause insulin resistance. *Biochemical and Biophysical Research Communications*, 350(1), pp.202-207.

Wu, F, Zhang, J. and Beard, D. (2009). Experimentally observed phenomena on cardiac energetics in heart failure emerge from simulations of cardiac metabolism. *Proceedings of the National Academy of Sciences*, 106(17), pp.7143-7148.

Xia, Y, McClelland, J, Gupta, R, Qin, D, Zhao, X, Sohn, L, Celotta, R. and Whitesides, G. (1997). Replica molding using polymeric materials: A practical step toward nanomanufacturing. Advanced Materials, 9(2), pp.147-149.

Xu, X, Duan, S, Yi, F, Ocampo, A, Liu, G. and Izpisua Belmonte, J. (2013). Mitochondrial Regulation in Pluripotent Stem Cells. *Cell Metabolism*, 18(3), pp.325-332.

Xu, X, Wan, W, Powers, A, Li, J, Ji, L, Lao, S, Wilson, B, Erikson, J. and Zhang, J. (2008). Effects of exercise training on cardiac function and myocardial remodeling in post myocardial infarction rats. Journal of Molecular and Cellular Cardiology, 44(1), pp.114-122.

Yamada, K, Ohkihamazaki, H. and Wada, K. (2000). Differential effects of social isolation upon body weight, food consumption, and responsiveness to novel and social environment in bombesin receptor subtype-3 (BRS-3) deficient mice. *Physiology & Behavior*, 68(4), pp.555-561.

Yan, Z, Kronemberger, A, Blomme, J, Call, J, Caster, H, Pereira, R, Zhao, H, de Melo, V, Laker, R, Zhang, M. and Lira, V. (2017). Exercise leads to unfavourable cardiac remodelling and enhanced metabolic homeostasis in obese mice with cardiac and skeletal muscle autophagy deficiency. *Scientific Reports*, 7(1).

Yarosz, E. and Chang, C. (2018). The Role of Reactive Oxygen Species in Regulating T Cell-mediated Immunity and Disease. Immune Network, 18(1).

Yasukawa, T, Reyes, A, Cluett, T, Yang, M, Bowmaker, M, Jacobs, H. and Holt, I. (2006). Replication of vertebrate mitochondrial DNA entails transient ribonucleotide incorporation throughout the lagging strand. The EMBO Journal, 25(22), pp.5358-5371.

Yeagle, P. (2016). Membrane Transport. The Membranes of Cells, pp.335-378.

Yen, T, Chen, Y, King, K, Yeh, S. and Wei, Y. (1989). Liver mitochondrial respiratory functions decline with age. *Biochemical and Biophysical Research Communications*, 165(3), pp.994-1003.

Yu, P. H, Lu, L. X, Fan, H, Kazachkov, M, Jiang, Z. J, Jalkanen, S. (2006). Involvement of semicarbazide-sensitive amine oxidase-mediated deamination in lipopolysaccharide-induced pulmonary inflammation. *Am. J. Pathol.* 168, 718–726. doi: 10.2353/ajpath.2006.050970

Yue, P, Jing, S, Liu, L, Ma, F, Zhang, Y, Wang, C, Duan, H, Zhou, K, Hua, Y, Wu, G. and Li, Y. (2018). Association between mitochondrial DNA copy number and cardiovascular disease: Current evidence based on a systematic review and metaanalysis. PLOS ONE, 13(11), p.e0206003.

Zahn, J., Sonu, R., Vogel, H., Crane, E., Mazan-Mamczarz, K., Rabkin, R., Davis, R., Becker, K., Owen, A. and Kim, S. (2006). Transcriptional Profiling of Aging in Human Muscle Reveals a Common Aging Signature. *PLoS Genetics*, 2(7), p.e115.

Zeviani, M. and Donato, D. (2004). Mitochondrial disorders. *Brain*, 127(10), pp.2153-2172.

Zhang, H, Burr, S. and Chinnery, P. (2018). The mitochondrial DNA genetic bottleneck: inheritance and beyond. *Essays In Biochemistry*, 62(3), pp.225-234.

Zhao, Y. and Ma, Z. (2016). Swimming training affects apoptosis-related microRNAs and reduces cardiac apoptosis in mice. *General physiology and biophysics*, 35(04), pp.443-450.

Zheng, L, Zhou, M, Chai, Q, Parrish, J, Xue, D, Patrick, S, Turchi, J, Yannone, S, Chen, D. and Shen, B. (2005). Novel function of the flap endonuclease 1 complex in processing stalled DNA replication forks. *EMBO reports*, 6(1), pp.83-89.

Zheng, L, Zhou, M, Guo, Z, Lu, H, Qian, L, Dai, H, Qiu, J, Yakubovskaya, E, Bogenhagen, D, Demple, B. and Shen, B. (2008). Human DNA2 Is a Mitochondrial 363 Nuclease/Helicase for Efficient Processing of DNA Replication and Repair Intermediates. Molecular Cell, 32(3), pp.325-336.

Zhou, Q, Li, H. and Xue, D. (2011). Elimination of paternal mitochondria through the lysosomal degradation pathway in C. elegans. *Cell Research*, 21(12), pp.1662-1669.

Zhu, Yu, Akatsuka, Cooper and Anasetti (1999). Role of mitogen-activated protein kinases in activation-induced apoptosis of T cells. Immunology, 97(1), pp.26- 35.

Zimmerman, J, von Saint André-von Arnim, A. and McLaughlin, J. (2011). Cellular Respiration. *Pediatric Critical Care*, pp.1058-1072.

Zinovkina, L. (2018). Mechanisms of Mitochondrial DNA Repair in Mammals. Biochemistry (Moscow), 83(3), pp.233-249. Zipes, D. and Jalife, J. (2013). Cardiac electrophysiology. 6th ed. Elsevier.